Numerical Solution of Multicomponent Population Balance Systems with Applications to Particulate Processes

by

Darren Donald Obrigkeit

B.S.E. Chemical Engineering
University of Michigan, 1995

M.S. Chemical Engineering Practice
Massachusetts Institute of Technology, 1997

Submitted to the Department of Chemical Engineering
in Partial Fulfillment of the Requirements for the Degree of

Doctor of Philosophy in Chemical Engineering
at the
Massachusetts Institute of Technology

June 2001

Signature of Author .....
Department of Chemical Engineering
May 8, 2001

Certified by .....
Gregory J. McRae
Bayer Professor of Chemical Engineering
Thesis Supervisor

Accepted by .....
Robert E. Cohen
St. Laurent Professor of Chemical Engineering
Chairman, Committee for Graduate Students

Numerical Solution of Multicomponent Population Balance Systems with Applications to Particulate Processes

by
Darren Donald Obrigkeit
Submitted to the Department of Chemical Engineering on May 8, 2001
in Partial Fulfillment of the Requirements for the Degree of
Doctor of Philosophy in Chemical Engineering

Abstract

Population balances describe a wide variety of processes in the chemical industry and environment ranging from crystallization to atmospheric aerosols, yet the dynamics of these processes are poorly understood. A number of different mechanisms, including growth, nucleation, coagulation, and fragmentation typically drive the dynamics of population balance systems. Measurement methods are not capable of collecting data at resolutions which can explain the interactions of these processes.

In order to better understand particle formation mechanisms, numerical solutions could be employed, however current numerical solutions are generally restricted to a either a limited selection of growth laws or a limited solution range. This lack of modeling ability precludes the accurate and/or fast solution of the entire class of problems involving simultaneous nucleation and growth. Using insights into the numerical stability limits of the governing equations for growth, it is possible to develop new methods which reduce solution times while expanding the solution range to include many orders of magnitude in particle size.

Rigorous derivation of the representations and governing equations is presented for both single and multi-component population balance systems involving growth, coagulation, fragmentation, and nucleation sources. A survey of the representations used in numerical implementations is followed by an analysis of model complexity as new components are added. The numerical implementation of a split composition distribution method for multicomponent systems is presented, and the solution is verified against analytical results.

Numerical stability requirements under varying growth rate laws are used to develop new scaling methods which enable the description of particles over many orders of magnitude in size. Numerous examples are presented to illustrate the utility of these methods and to familiarize the reader with the development and manipulations of the representations, governing equations, and numerical implementations of population balance systems.

Thesis Supervisor: Gregory J. McRae
Title: Bayer Professor of Chemical Engineering

Acknowledgements

I would like to thank my parents and grandparents for their enduring support of my endeavors. Without their lifelong efforts, I would never have made it to MIT, much less completed a Ph.D. I thank my brothers Matthew and Kevin for their lifelong friendship; I valued the time spent with them more than anything else during my studies and I dedicate this thesis to them.

I gratefully acknowledge the support of my thesis advisor, Greg McRae. His incredible depth of knowledge lead me to new horizons I would never have known otherwise. I also thank my thesis committees, Professors Paul Barton, Klavs Jensen, and Greg Rutledge for the time they contributed towards my growth and development and for their insightful advice.

I would like to thank the members of the McRae group, especially Jose Jiminez, Cheng Wang, Gary Adamkiewicz, Gene Lin, Aleks Engel, Enrique Guinand, Betty Pun, Mort Webster, Alejandro Cano Ruiz, Jose Ortega, Volker Hoffman, Patric Bieler, and Natalia Duchini. Not only was their companionship and exchange of ideas very helpful, but they provided me the unique opportunity to practice my language skills in German and learn Spanish. Special thanks go out to Federico San Martini for his proofreading efforts for this thesis as well as other documents.

As intense and focused as MIT often is, I will always warmly remember time spent "getting away from it all" with the MIT Scuba Club and at the MIT Sailing Pavilion. MIT provided an unique opportunity for me to meet an incredible group of people from everywhere, including Behrang Noohi, Zhonghui Xu, Dave Quiram, Jim Czarnowski, Jose Cervantes, Glen Bolton, Alex Andalis and many others. I will never forget the value of their friendships.

Finally, I would like to thank all of the brothers of Delta Tau Delta, where I was Resident Advisor during my final years of study. Living in an environment full of more than 40 energetic young men has provided numerous social and athletic diversions and helped me to maintain a balanced lifestyle with my academic pursuits.

The National Science Foundation is gratefully acknowledged for providing financial support during the first three years of my graduate program. Their support made me realize that the advancement of science and technology are both national and global priorities which benefit all of mankind. I also thank the NCSA (National Center for Supercomputing Applications) for their support of my graduate research, as well as Aerodyne Research for their generous collaboration efforts.

Table of Contents

List of Figures

List of Tables

Chapter 1: Introduction to Population Balance Systems

1.1 Background

Population balance systems encompass a wide range of processes and natural phenomena and are ubiquitous in the world around us - including everything from the aerosol processes of cloud formation that help govern our climate to inhaled drug delivery systems as well as the powder and crystallization processes used in the manufacture of pharmaceuticals.

Unfortunately, current understanding of these population balance processes is limited by the ability to implement accurate and detailed models of these systems and compare them with experimental data. In addition, analytical models describe only a very limited number of systems under heavily restricted conditions. Although numerical models are necessary to solve population balance systems, a number of key modeling challenges exist, as detailed in the following sections, starting off with some examples of population balance systems.

1.2 Population Balance Process Examples

There are so many natural and man-made examples of population balance processes that it would be impossible to list even a tiny fraction of these processes. Similarly, these processes are found in so many different types of physical systems that they defy categorization. However, in order to demonstrate the wide variety of these systems, a few processes will be given as examples in this section.

1.2.1 Aerosols

Aerosol processes are essentially present in all sprays and emissions. Aerosols are generated from numerous sources ranging from hair spray and cigarette smoke to natural processes such as cloud formation and spray from ocean waves. While many of the processes have obvious impact on the environment and air quality, there are numerous important transport processes. To briefly name just a few examples, aerosols are used to deliver medications to asthmatics who use inhalers, to deliver paint to car bodies in automotive paint shops, and to deliver pesticides to crops by crop dusting.

1.2.2 Chemical and pharmaceutical processes

In the chemical industry, any process which deals with a powder, slurry, bubbles, or spray falls under the umbrella of a population balance system. Because of their large surface-to-volume ratio, particle systems are often used in mass transfer and separations operations. Examples of this include purification by crystallization; scrubbers, where a liquid spray is used to remove gas-phase vapors; and heterogeneous catalysis, where the high surface area of the particles offers a large number of reaction sites.

1.2.3 Powder and particulate processes

A number of industries largely unrelated to the chemical industry also use population balance systems in their powder and particulate processes - which includes grinding, milling, and sintering operations. Relevant examples range from the production of toner for laser printers and copiers to the milling and grinding operations used in the mining industry.

1.2.4 Other processes

Population processes have important functions in risk assessment and disaster scenarios. Many experts consider the "sarcophagus" surrounding the destroyed Chernobyl reactor to be a considerable risk - not because of the reactor but because of the amount of radioactive dust left in the building. The potential impact of an event where the sarcophagus collapsed can be modeled by a population balance problem describing the transport of radioactive dust particles in the atmosphere. Similar risk assessment studies would be equally applicable to determining the potential effects of aerosol-delivered biological weapons released over a city or against military targets.

1.3 Physical Processes

In the wide range of physical systems described by population balances the particles are subjected to a number of different processes which create, destroy, and transform the particles. As a result, population balance models must be able to describe these processes, including particle growth, nucleation, coagulation, precipitation, fragmentation, and other mechanisms. Figure 1-1 illustrates a few of these mechanisms.

1.3.1 Growth

Particle growth is often dominated by condensation and evaporation in the case of atmo-

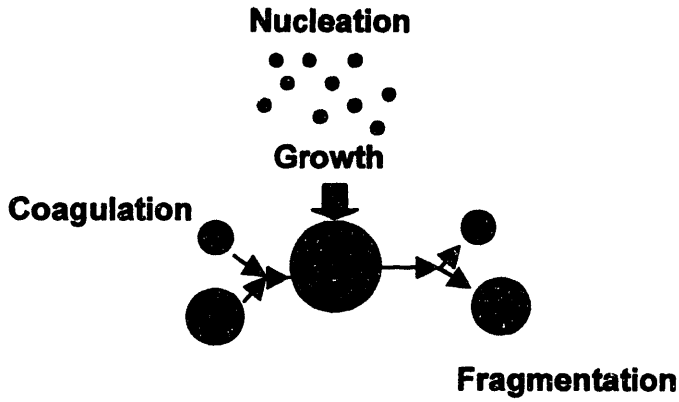

Figure 1-1: Population balance system physical processes.

spheric aerosols, although analogous mechanisms in other systems might include addition of monomers to polymers in a condensation polymerization reaction, the growth of nanoparticles in an emulsion, crystallization, or precipitation.

1.3.2 Nucleation and precipitation

Nucleation and precipitation act respectively to introduce and remove particles from a system. In nucleation, new particles of a minimum size are formed while precipitation occurs when particles become so large that they no longer remain suspended. Nucleation is a critical mechanism for both crystallization and atmospheric processes. In general, nucleation mechanisms are divided into two categories: homogeneous and heterogeneous nucleation.

1.3.3 Coagulation and fragmentation

Coagulation is the process where two particles combine to form a larger particle, where fragmentation is the opposite process which occurs when a large particle breaks apart to form two or more smaller particles. While coagulation could also include processes where three or more particles simultaneously collide to form a larger particle, in most systems these events are so rare that only two-particle (binary) collisions, are considered.

1.4 Challenges in Solving Population Balance Systems

In spite of the importance and prevalence of population balance processes, there is a notable lack of effective computer simulations and process modeling tools. In fact, developing models which describe the diversity of applications and physical processes of population balance systems

is a formidable task. Several key challenges, outlined in the following sections, explain the lack of effective population balance models.

1.4.1 Mathematical complexity of models

Typical chemical engineering process models involve the solution of a set of differential equations (DE) or differential algebraic equations (DAE). Most numerical solution engines (ABACUSS, DASSL) are specifically adapted for these classes of problems. Particle processes, however, require the solution of partial integro-differential algebraic equations (PIDAEs). A considerable body of algorithms are available to solve conventional systems of differential equations; however, the solution of DAE systems is much more difficult and is a topic of ongoing research. Partial integro-differential algebraic equation (PIDAE) systems, which result from population balance models and are much more difficult to solve than DAE systems, have not yet been addressed by any numerical algorithms.

1.4.2 Representations

The wide range of systems described by particle processes requires that a correspondingly large number of representations must be used to describe the attributes of the particles in these systems. Choosing the representation not only defines the model system and its resolution, but also directly determines which solution methods may be used as well as the amount of time required to solve the problem numerically. Typically, the representations used in these systems suffer from either 1) prohibitive solution times as more components are added to the system, or 2) an incomplete representation of the system.

1.4.3 Lack of data from experimental systems

In general, particle systems are difficult to measure. Often, as with aerosols, key characteristics such as particle size cannot be measured directly and must be inferred. Often, measuring equipment cannot measure the large number of particles in a system rapidly enough and resolution is lost. Measurement systems are often also limited by their range and unable to measure data over the full range of interest. For example, the lower size detection limit for aerosol systems is often much larger than the size of nucleating particles. In addition, many experimental systems provide data that is too complex to analyze or was generated under poorly controlled conditions, which limits efforts to properly bound the problem and validate assumptions.

1.4.4 Competing physical processes

Often multiple physical processes which have a similar effect on particles occur at the same time, making experimental and model results difficult to interpret. For example, both growth and coagulation have the effect of increasing particle size, making the two processes difficult to distinguish when interpreting results. In addition, both nucleation and fragmentation create new particles, making it difficult to determine the relative contributions of these mechanisms to particle generation.

1.5 Numerical Simulation of Chemical Engineering Systems

1.5.1 Differential equations

Often, simple mixed or uniform systems are modeled by a set of differential equations describing the states of the system. An elementary example of this might be a kinetic model describing the set of reactions given in Equation (1.1)

$$\begin{aligned} A + B &\xrightarrow{k_1} C \\ C + C &\xrightarrow{k_2} D \end{aligned} \tag{1.1}$$

This system would be modeled by a system of ordinary differential equations (ODEs) and solved using a traditional numerical integration algorithm.

$$\begin{aligned} \frac{d[A]}{dt} &= -k_1[A][B] \\ \frac{d[B]}{dt} &= -k_1[A][B] \\ \frac{d[C]}{dt} &= k_1[A][B] - 2k_2[C]^2 \\ \frac{d[D]}{dt} &= k_2[C]^2 \end{aligned} \tag{1.2}$$

Before this ODE system can be numerically integrated, two sets of specifications must be made.

1. parameter values (k_1 and k_2).

2. initial values completely describing the state of the system ([A], [B], [C], [D]).

The problem of *stiffness* arises when $k_1 << k_2$ (Shampine and Gear, 1979). From a physical standpoint, this means that the processes occuring in the system occur at very different rates.

Mathematically, this means that the Jacobian matrix representing the derivative of the linearized system around its current state vector has eigenvalues which are orders of magnitude apart.

$$\begin{aligned}
\frac{d[A]}{dt} &= -k_1[A][B] \\
\frac{d[B]}{dt} &= -k_1[A][B] \\
\frac{d[C]}{dt} &= k_1[A][B]-2k_2[C]^2 \\
\frac{d[D]}{dt} &= k_2[C]^2
\end{aligned} \rightarrow \frac{d\mathbf{Y}}{dt} = \mathbf{f}(\mathbf{Y}, t) \tag{1.3}$$

Equation (1.3) gives an example of how the equations in an ODE system can be expressed in matrix form, using the sample system given in Equation (1.2). Note that $f(\mathbf{Y},t)$ is a vector function with four components in this example. The Jacobian matrix, **J**, is calculated by taking the derivative of $f(\mathbf{Y},t)$ with respect to **Y**, as shown in Equations (1.4) and (1.5).

$$\mathbf{f}(\mathbf{Y}, t) = \begin{aligned}
f_1(\mathbf{Y}) &= -k_1[A][B] \\
f_2(\mathbf{Y}) &= -k_1[A][B] \\
f_3(\mathbf{Y}) &= k_1[A][B]-2k_2[C]^2 \\
f_4(\mathbf{Y}) &= k_2[C]^2
\end{aligned} \rightarrow \frac{d\mathbf{f}(\mathbf{Y}, t)}{d\mathbf{Y}} \rightarrow \mathbf{J} \tag{1.4}$$

$$\mathbf{J}_{i,j} = \frac{df_i(\mathbf{Y})}{dy_j} \rightarrow \begin{bmatrix} -k_1[B] & -k_1[A] & 0 & 0 \\ -k_1[B] & -k_1[A] & 0 & 0 \\ k_1[B] & k_1[A] & -4k_2[C] & 0 \\ 0 & 0 & 2k_2[C] & 0 \end{bmatrix} \tag{1.5}$$

The Jacobian matrix now represents the linearization of the system around a specific state of the system. Table 1-1 summarizes one set of initial conditions and values for the reaction rate param-

eters with the corresponding eigenvalues, λ_i, of the system.

Table 1-1: Eigenvalue calculation example

Variable	Value	Units
k_1	10	$cm^3/mol{\cdot}s$
k_2	0.01	$cm^3/mol{\cdot}s$
$[A]$	10	mol/cm^3
$[B]$	100	mol/cm^3
$[C]$	1	mol/cm^3
$[D]$	1	mol/cm^3
λ_1	-1100	eigenvalue #1
λ_2	-0.04	eigenvalue #2
λ_3	0	eigenvalue #3
λ_4	0	eigenvalue #4

Note that the nonzero eigenvalues in this system are roughly 5 orders of magnitude apart, leading to a difficult solution for the system of differential equations.

1.5.2 Partial differential equations

Unlike well-mixed systems, the solution of distributed systems is typically described by a partial differential equation (PDE). The convection-diffusion equation is a classic example of a PDE, given in its one-dimensional form here:

$$\frac{\partial c}{\partial t} = \nabla \cdot D\nabla c - (\nabla \cdot \mathbf{u}c) + R \tag{1.6}$$

Numerical PDEs solutions are implemented by some method which converts the PDEs into a system of simultaneous ordinary differential equations (see Appendix B). Common methods for implementing PDE systems include the method of lines, finite differences (FDM), finite element method (FEM), and finite volume method. Please refer to Villadsen and Michelsen (1978) or Finlayson (1972) for more information on the implementation of these methods. Essentially all of these methods utilize an interpolation scheme to create a *representation* of the solution over the

domain of the system based on values at a specific set of node points in the solution domain. Depending on the method, various techniques are then used to both determine node point placement and a linear combination of values at these node points which reproduces the original PDE. Writing all of the node point equations together, the ODE conversion of the PDE system might can be written in matrix form, as shown in Equation (1.7).

$$\frac{d\mathbf{M}}{dt} = -u\mathbf{B}\mathbf{A}^{-1} \cdot \mathbf{M} + D\mathbf{C}\mathbf{A}^{-1} \cdot \mathbf{M} \tag{1.7}$$

The converted system of ODEs is solved using one of the widely available numerical ODE algorithms, such as the popular DASSL (Petzold, 1982) solver. Like most ODE solvers, DASSL provides a convenient interface for the user through a *residual function* which is given the values of dM/dt and **M** and returns the difference between the right and left hand sides of Equation (1.7).

$$\begin{aligned} \text{residual} &= \text{right hand side - left hand side} \\ &= (-v\mathbf{B}\mathbf{A}^{-1} \cdot \mathbf{M} + D\mathbf{C}\mathbf{A}^{-1} \cdot \mathbf{M}) - \frac{d\mathbf{M}}{dt} \end{aligned} \tag{1.8}$$

The vector **M** is generally referred to as the *state vector* of the system because its members completely specify the system at any given point in time. The ODE solver uses the initial values of the state vector and the residual function to numerically solve the model. Use of an ODE solver, however, does not guarantee accurate solution of the system. In addition to the usual problem of stiffness, PDE systems have additional requirements which are necessary to reach a stable and accurate solution. These requirements are dependent on many factors, including:

- the class of PDE being solved (hyperbolic, parabolic, etc.)
- parameter values of the PDE
- the representation of the solution

Depending on these factors, the difficulty of solving the PDE and the resulting accuracty vary widely. Often, meticulous analysis of numerical error must be performed to ensure that an algorithm will result in an accurate, stable answer (Morton, 1996).

1.5.3 Differential algebraic equations

Many systems are not entirely described by ordinary differential equations but also a set of algebraic equations which govern the system. When an additional set of algebraic constraints is

applied to a system of ordinary differential equations, a set of differential algebraic equations (DAEs) results. Just as with ODEs, DAEs often describe a well-mixed or uniform system. In the case where both a PDE and a set of algebraic equations define a model, a set of partial differential algebraic equations (PDAEs) result. These PDAE systems are much more versatile and powerful than either PDEs or DAEs and can be employed to model multi-unit systems in multiple dimensions.

An example of a PDAE system is presented in the pressure swing adsorption (PSA) model given in Appendix A. Just as with ODE systems, DAEs require specification of parameters and initial conditions. However, the initialization of these systems is not arbitrary as with ODEs. Subtle issues regarding the *index* of the system restrain the set of initial conditions that may be used for some DAE systems. Specifically, systems of index 1 or more require special treatment of initial conditions. In addition, DAE systems are affected by the same problems regarding stiffness as are PDEs and ODEs.

In order to address the specific demands in solving DAE systems, new algorithms are being developed (Tolsma and Barton, 2000) which ensure proper initialization of the DAE systems. Of course, systems involving PDAEs are subject to stiffness and index initialization problems of DAEs in addition to the error analysis requirements of PDE systems.

1.5.4 Partial integro-differential equations

As in the PDE example given above, population balances typically also describe distributed systems. However, in population balance systems the distributed values are generally some characteristics of the particles in the system - mass, diameter, composition, etc. Unlike PDE systems commonly found in transport problems, the population balance formulation often includes an integral term. For example, the model describing the population of particles in a system undergoing coagulation is:

$$\frac{\partial n(m)}{\partial t} = \int_0^{m/2} \beta(m-x,x)n(m-x)n(x)dx - n(m)\int_0^{\infty}\beta(m,x)n(x)dx \qquad (1.9)$$

These partial integro-differential equations (PIDEs) add a considerable amount of computational overhead to the residual evaluation required for the numerical integration algorithm. Instead of merely multiplying two matrices by the state vector to evaluate the residual as in Equa-

tion (1.8), the algorithm now requires evaluation of two *integrals* for each member of the state vector. In many population balance systems, the limits of these integrals may be evaluated over a domain stretching over several orders of magnitude, which adds even more computational cost to solving the PIDE system. PIDE systems which are also subject to a set of algebraic constraints belong to a larger class of problems known as PIDAEs (partial integro-differential algebraic equations). While current research on the numerical solution of mathematical models is focused primarily on PDAEs and similar systems, scant work has been made on PIDAEs, which represent the most diffucult and challenging class of problems. The key challenges in solving PIDAEs include:

- computational intensity of evaluating integral terms
- lack of available numerical solution packages
- poor understanding of requirements for stability and accuracy of solution
- stiffness and index problems.

Figure 1-2 attempts to summarize some of the characteristics, applications and solution pack-

Problem	Systems	Solver	
ODE *Ordinary Differential Equation* -stiffness	•well-mixed •uniform	•ode45 •Maple	•Matlab •DASSL
PDE *Partial Differential Equation* -stiffness -stability and accuracy	•distributed •multiple dimensions	•ABACUSS •FLUENT	
PDAE *Partial Differential Algebraic Equation* -stiffness -stability and accuracy -index/consistent initialization	•distributed •multiple dimensions •multiple subsystems	•DAEPACK	
PIDAE *Partial Integro-Differential Algebraic Equation* -stiffness -stability and accuracy -index/consistent initialization -integral evaluation	•distributed •multiple dimensions •multiple subsystems •population balance processes	•none	

Figure 1-2: Numerical solution methods summary.

ages available for the various classes of mathematical problems.

1.6 Applications of Population Balance Models

The general lack of understanding of population balance processes coupled with their prevalence provides a rich area for research. In particular, there are several key areas where the development of population balance models will have significant impact.

1.6.1 Insight into physical processes

As mentioned before, many population balance processes include competing mechanisms - such as coagulation and growth or nucleation and fragmentation. Experimental data often produces little insight as to which of these mechanisms are dominant, however models have the advantage of transparency. Unlike experimental results where only the collected data is available, models are transparent in the sense that any and all of the intermediate data can be observed. This provides a great tool for interpreting the results of the model by comparing the relative contributions of nucleation, fragmentation, coagulation, and growth under varying conditions. Furthermore, these results form the basis for understanding the results of experiments and guide the design of new experiments.

1.6.2 Development of measurement systems

The nature of population balance processes makes it virtually impossible to tabulate direct measurements of population balance systems. Several challenges exist which prohibit instantaneous measurement of all population characteristics:

1. *large number of particles to measure* - by nature, population balance systems include a large number of population members or particles. Individually counting and measuring each population member is impossible; thus inference methods must be employed to estimate the population characteristics. Even using sampling methods, it is often impossible to make sampling-based population measurements fast enough to track the evolution of a dynamic system.

2. *simultaneous measurement of population characteristics* - in systems where more than one population characteristic is of interest, it is often difficult to obtain simultaneous measurements of these characteristics. For instance, measuring both aerosol size and composition can be accomplished by first passing the aerosol through a differential mobility analyzer (DMA) and then a mass spectrometer. However, when sampling a system with a large number of particles, it is difficult to determine the pairing between DMA and mass spectrometer measurements.

3. *scaling of particle characteristics* - even accurately measuring a single population characteristic can present significant challenges. For instance, particle mass typically varies over several orders of magnitude in an aerosol system, requiring that the measurement system be able to quickly measure both very tiny and very large particles with high accuracy.

In order to test the accuracy of the measurement systems, there must be some way of accurately determining what data the measurement systems *should* produce as the result of a given particle input. Implementing population balance models to reproduce the internal physics of the measurement systems provides test data against which the measurement process itself can be verified, tested, and calibrated.

1.6.3 Model discrimination and refinement

Model discrimination is a tool which enables the evaluation of a number of models against experimental data to determine which model most accurately represents the system. The ability to incorporate different physical mechanisms into a model enables comparison and testing of these mechanisms against one another. For instance, several different coagulation mechanisms exist which describe the coagulation process over different particle size ranges and operating conditions. The data generated by population balance models based on different coagulation mechanisms can be used with experimental data to determine which coagulation mechanism is active in a given system.

By varying the operating conditions and observing which mechanisms have increased and diminished effects, it is possible to begin establishing common standards and rules of thumb for population balance systems - and add to the general body of knowledge for these systems. Furthermore, model discrimination will reveal ranges where none of the current mechanisms work particularly well. In this way model discrimination will also provide motivation for refinement in areas where current models have failed to adequately describe the physics of the system.

1.6.4 Parameter estimation

Parameter estimation is the complement of model discrimination. While model discrimination answers the question, "Which model do I use?" parameter estimation answers the question, "What are the parameter values for this model?" Both of these processes are necessary to provide an accurate and optimized model for a given system.

The parameter values currently used in population balance models are derived from the theory of the underlying physical mechanisms of coagulation, growth, nucleation, fragmentation, etc. Parameter estimation determines experimental values of these parameters by data assimilation. In this way, experimental parameter values can be compared with theoretical parameter values. For instance, in an application where detailed experimental data is available in the form of $n^*(m)$ for a system governed by Equation (1.9), the population parameter esimation problem would seek to reduce the error norm between the model results and experimental results by varying the parameter β.

$$\min_{\beta} = \left\| n(m) - n^*(m) \right\| \tag{1.10}$$

This may require many model iterations to produce reliable results, and therefore a fast and accurate solution of the population balance model is needed. For more on advanced techniques for parameter estimation and data assimilation, please refer to Papoulis (1991).

1.6.5 Parametric uncertainty analysis

In many respects, parametric uncertainty analysis is the opposite process of parameter estimation. Parameter estimation take noisy data and predicts the values of the model parameters, while parametric uncertainty analysis takes a select subset of model parameters and projects the variation expected in the output (see Figure 1-3). Chapter 11 presents an example of parametric uncer-

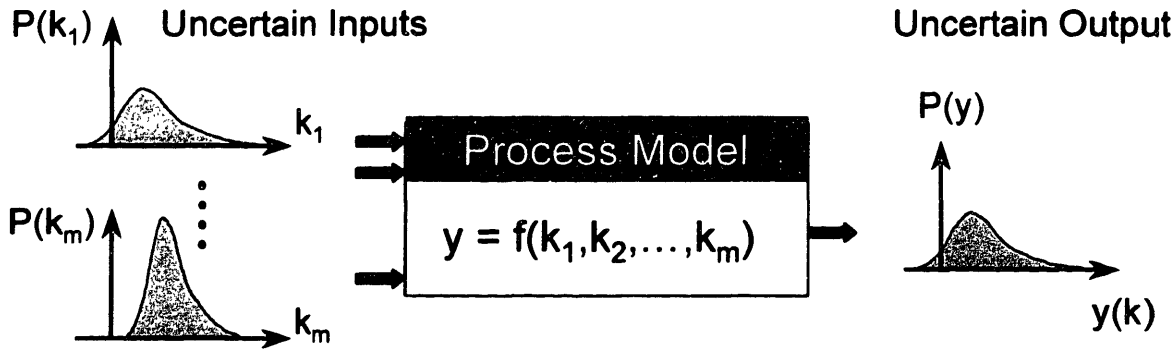

Figure 1-3: Parametric uncertainty analysis problem summary.

tainty analysis performed by the Deterministic Equivalent Modeling Method (DEMM) developed by Tatang (1994) on a population balance model with coagulation and growth.

Uncertainty analysis aids the development and understanding of population balance models in three key ways:

1. uncertainty analysis reveals which parameters have the largest and smallest affect on the solution.

2. by comparing the uncertainty in the input parameters and the resulting uncertainty in the solution, uncertainty analysis gives an estimate of how accurately model parameters can be determined based on experimental data.

3. performing uncertainty analysis at different time points in a dynamic system provides insight into which stages of the process are most sensitive to the system parameters.

1.7 Summary

In summary, the current understanding of population balances is very limited due to the lack of available experimental data and viable models to describe these processes. Experimental data is difficult to gather because a large number of indirect measurements must made very rapidly by different instruments in order to estimate population properties. Modeling these systems has suffered from the lack of ability to develop fast and accurate models, and results of existing models has been left with scant experimental data for verification.

1.8 Structure and Outline of This Work

This work starts off by introducing the concept of a number density distribution (Chapter 2), drawing analogies with probability density functions. Chapter 3 uses the definition of number density functions to derive the transformations between the various forms of the number density distribution. Using the number density function as the underlying representation of the population, Chapters 4 and 5 derive single- and multi-component forms of the population balance equation for the mechanisms of coagulation, fragmentation, growth, and sources/sinks. Chapter 6 performs an analysis of the growth rate under the varying mechanisms for particle growth, generating insights into the solution of the population balance. Chapters 7 and 8 develop the methods for solving multicomponent systems, while Chapters 9 and 10 present a case study of a physical system, illustrating how optimal scaling methods can be used to drastically reduce solution times. Finally, Chapter 11 presents conclusions as well as a discussion of directions for future research.

References

[1] Brenan, K. E.; Campbell, S. L.; and Petzold, Linda R. *Numerical Solution of Initial-Value Problems in Differential Algebraic Equations*, North-Holland, 1996.

[2] Gear, C. W. *Numerical Initial Value Problems in Ordinary Differential Equations*, Prentice Hall, 1971.

[3] Finlayson, Bruce A. *The Method of Weighted Residuals and Variational Principles, with Applications in Fluid Mechanics, Heat and Mass Transfer*, Academic Press, 1972.

[4] International Atomic Energy Commission, *Highlights of Conclusions and Recommendations*, proceedings from International Conference: One Decade After Chernobyl. Vienna, Austria, April 1996.

[5] Morton, K. W. *Numerical Solution of Convection-Diffusion Problems*, Chapman & Hall, 1996.

[6] Papoulis, Athanasios *Probability, Random Variables, and Stochastic Processes*, 3rd Ed., McGraw-Hill, 1991.

[7] Petzold, Linda R. *A Description of DASSL: A Differential/Algebraic System Solver*, SAND82-8637, Sandia National Laboratories, September 1982.

[8] Press, William H.; Teukolsky, Saul A. Vetterling, William T.; and Flannery, Brian P. *Numerical Recipies in C: The Art of Scientific Computing*, 2nd Ed., Cambridge University Press, 1993.

[9] Shampine, L. F.; and Gear, C. W. *A User's View of Solving Stiff Ordinary Differential Equations*, SIAM Review, **21**, 1-17, 1979.

[10] Tatang, Menner A. *Direct Incorporation of Uncertainty in Chemical and Environmental Systems*, Ph. D. Thesis, Massachusetts Institute of Technology, 1994.

[11] Tolsma, John. E.; and Barton, Paul I. *DAEPACK: An open modeling environment for legacy models*, Industrial and Engineering Chemistry Research, **39**(6), 1826-1839, 2000.

[12] Villadsen, John; and Michelsen, Michael L. *Solution of Differential Equation Models by Polynomial Approximation*, Prentice-Hall, 1978.

Chapter 2: Representation of Populations

2.1 Distribution Functions Introduction

In order to implement models of particle systems, some framework is needed to describe how all the particles in the system are distributed over the properties of interest. To accomplish this, we use distribution functions which take the form $n(\phi)$, where ϕ represents some attribute of the particles in the system. Table 2-1 summarizes some of the common attributes used as ϕ.

Table 2-1: Common distribution functions $n(\phi)$

ϕ - *symbol*	ϕ - *meaning*	$n(\phi)$
D_p	particle diameter	$n(D_p)$
m	particle mass	$n(m)$
l	crystal length	$n(l)$
v	particle volume	$n(v)$

Distribution functions describing populations act much like probability density functions, and are similar in the fact that they can be either discrete or continuous.

2.2 Discrete Representations of Discrete Systems

If we wanted to calculate the probabilities of the outcome of rolling two dice at a time and recording the sum, we might start by writing out all of the possible outcomes in a 2×2 matrix.

Table 2-2: Listing of outcomes from the sum of rolling two dice

Die Result	1	2	3	4	5	6
1	2	3	4	5	6	7
2	3	4	5	6	7	8
3	4	5	6	7	8	9
4	5	6	7	8	9	10
5	6	7	8	9	10	11
6	7	8	9	10	11	12

By counting the number of outcomes that lead to each given result, we obtain the frequency of results among the outcomes. In Table 2-2, the sums 2 and 12 are the least frequent with only one outcome each, while the sum 7 is the most frequent occurring in 6 outcomes. For this problem, tabulating the frequency of outcomes is a trivial task, as summarized in Table 2-3.

Table 2-3: Frequency of outcomes from rolling two dice

Sum (outcome)	*Frequency*
2	1
3	2
4	3
5	4
6	5
7	6
8	5
9	4
10	3
11	2
12	1

Figure 2-1 plots the number of outcomes as a function of the sum. If the outcomes are considered as a population, then Figure 2-1 can be interpreted as a representation for the population of outcomes. Simply changing the axes reveals that this representation is equally well-suited for representing the number of crystals in a population as a function of the number of defects. Figure 2-2 tells us that this population contains three crystals with no defects, four crystals with one defect,

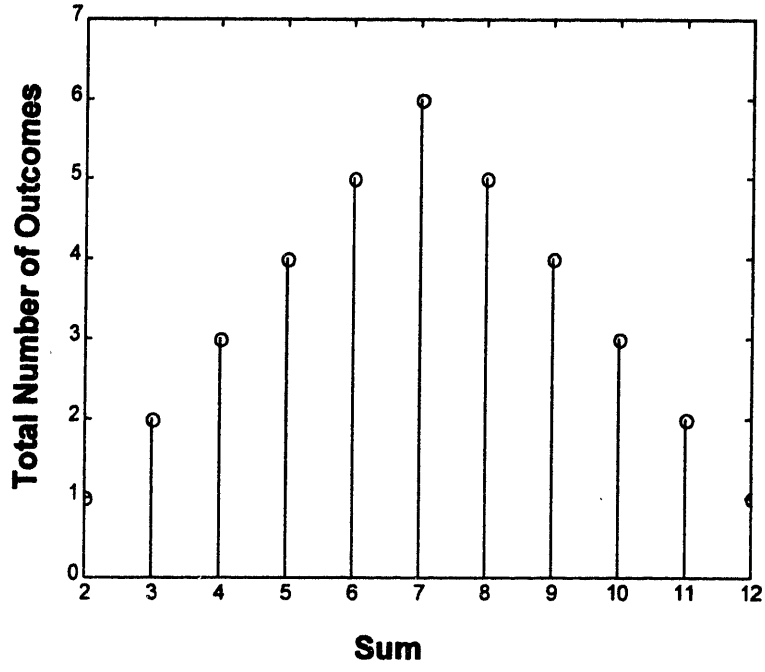

Figure 2-1: Discrete frequency plot describing the number of outcomes for each possible sum of rolling two dice.

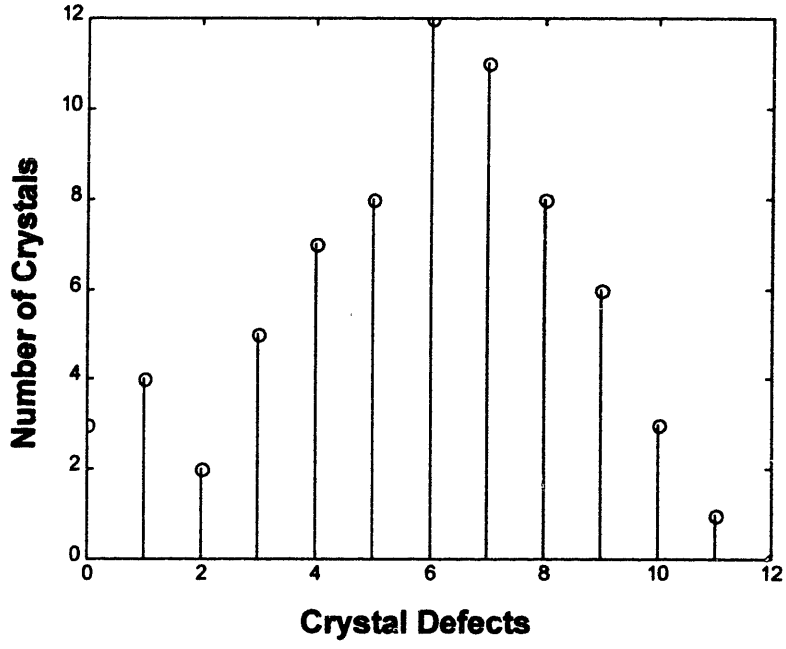

Figure 2-2: Discrete frequency plot describing the number of crystals as a function of the number of defects on each crystal.

two crystals with two defects each, etc., as shown in Table 2-9.

Table 2-4: Crystal population as a function of defects

Defects	*Number of Crystals*
0	3
1	4
2	2
3	5
4	7
5	8
6	12
7	11
8	8
9	6
10	3
11	1
12	0

Note that both of these processes are inherently discrete - it is impossible to have a crystal with 2.3 defects, just as it is impossible for a die roll to yield a non-integer result. Likewise, the graphs representing these two populations are presented as discrete graphs where the points are delta functions of varying magnitude. Thus, integrating the appropriate distribution function over the entire domain in both systems will result in the total number of outcomes and particles, respec-

tively.

Table 2-5: Comparison of probability outcomes and particle populations

Property	Probability	Particles
System	Two dice	Crystals
Attribute	Sum of outcomes from rolling	Number of defects
Defining Function	Probability mass function	Discrete population distribution
Total number	36	70

Note one distinct difference between probabilistic systems and particle processes: frequency of outcomes is *not* the standard notation for expressing probability mass functions. Rather, the relative frequency compared to the other outcomes is used to represent the probability p_i of that individual outcome.

$$p_i = \frac{\text{Outcomes of } i}{\text{Total outcomes}} \tag{2.1}$$

Calculating the probability mass function requires dividing the number of outcomes at each point by the total number of possible outcomes. This procedure normalizes the sum of all probabilities to one; for particle systems no such normalizing procedure is used or desired.

2.3 Bins: Discrete Representations of Continuous Systems

Often, practical limitations produce discrete data sets of continuous processes. A classic example of this occurs when sieves are used to sort objects by size or differential mobility analyzers are used to classify aerosol particles. As an example, an intermediate step in the production of pharmaceutical tablets involves the granulation of a recipe including starch and the active ingredient. The resulting granules may be classified by size using sieves. This sieve data typically records the amount of granules caught between sieves; mesh opening sizes in the sieves dictate the bounds of the "bins" in which these particles are classified, as shown in Figure 2-3.

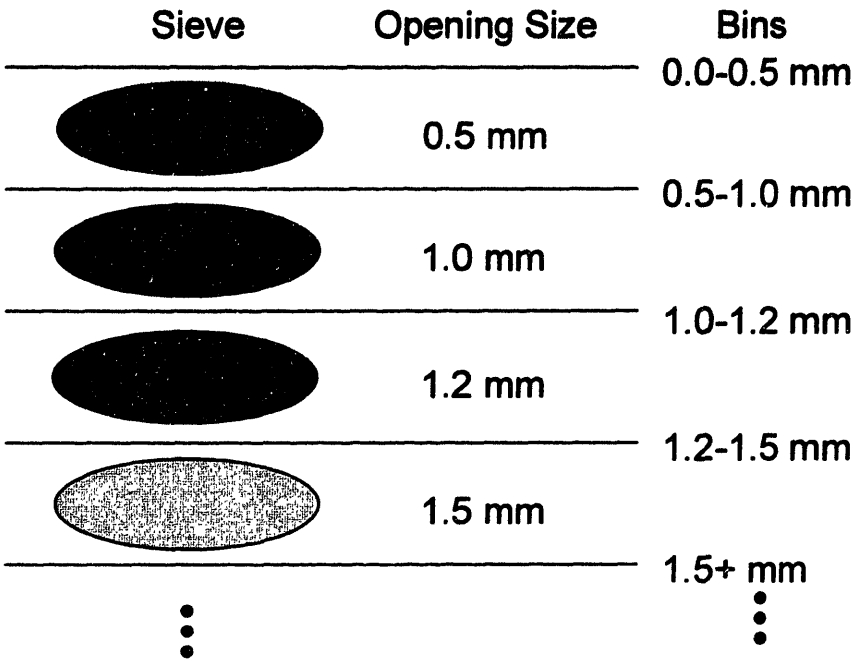

Figure 2-3: Arrangement of sieves and the resulting "bins" into which particles are collected.

Sample data for this system could be expected to as given in Table 2-6.

Table 2-6: Sample sieve data

Lower Bin Size (mm)	*Upper Bin Size (mm)*	*Mass in Bin (g)*
0	0.5	0.22
0.5	1.0	0.40
1.0	1.2	0.23
1.2	1.5	0.31
1.5	1.7	0.24
1.7	2.0	0.32
2.0	2.5	0.47
2.5	3.0	0.32
3.0	3.2	0.084
3.2	3.5	0.071
3.5	4.0	0.053

Note that the mass in each bin is no longer centered at one point within the bin, but rather spread across the entire range of the bin. Plotting the mass contained in each bin over the bin ranges yields Figure 2-4.

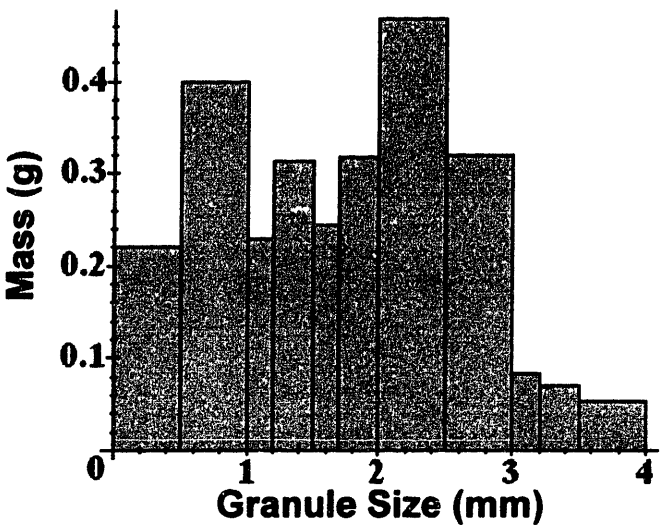

Figure 2-4: Bin plot of granule data gathered by sieves.

Just as with the systems in the previous examples, integrating this distribution function over the domain should yield the total mass of the system, 2.72 g. However, there are two problems:

- the integral of the distribution (sum of the areas of all the columns) is equal to 1.05, *not* 2.72
- the area of each column - and thus the total integral - has units of g·mm, not g.

To address these issues, it is necessary to adjust the distribution so that the area of each column is equal to the mass in that specific bin. Because the x axis is already defined by sieve spacing, it cannot be changed. The only other component of the area - the height - is thus defined by Equation (2.2).

$$\begin{aligned} \text{Mass}_i &= \text{Column Height}_i \cdot \text{Bin Width}_i \\ \text{Column Height}_i &= \frac{\text{Mass}_i}{\text{Bin Width}_i} \end{aligned} \tag{2.2}$$

Thus, column height has units of g/mm and we can now add a column to Table 2-6 which represents the distribution value, referred to as the *mass density* in this case because it represents the

amount of mass per unit length of the x axis.

Table 2-7: Sieve data with distribution

Lower Bin Size (mm)	*Upper Bin Size (mm)*	*Mass in Bin (g)*	*Mass Density (g/mm)*
0	0.5	0.22	0.44
0.5	1.0	0.40	0.80
1.0	1.2	0.23	1.15
1.2	1.5	0.31	1.05
1.5	1.7	0.24	1.22
1.7	2.0	0.32	1.06
2.0	2.5	0.47	0.93
2.5	3.0	0.32	0.64
3.0	3.2	0.084	0.42
3.2	3.5	0.071	0.24
3.5	4.0	0.053	0.11

Of course, this is a *mass* distribution; if we want to know the *number* distribution, then we would need some way of inferring particle number based on bin width and the total mass in each bin (see Chapter 3 for information on estimation techniques). Graphing the corrected mass density function results in Figure 2-5. Note the profound contrast of distribution shape when compared with Figure 2-4. Before being correctly normalized, the data appears irregular and bimodal; after normalization the distribution clearly has one mode and is relatively smooth. This is an example of a continuous process with a discrete measurement system, which in turn leads to the bin-type representation. The agglomeration process of creating the granules is continuous because the granules can take on a continuous range of values. The sieve measurement system, however, restricts the data to a much coarser bin-based representation, a common problem with measurement systems which is addressed through sophisticated statistical techniques such as the kernel function estimator (Press et al., 1993).

2.4 Continuous Population Representations

In some systems, it is possible to collect data in a very large number of bins. Consider a sys-

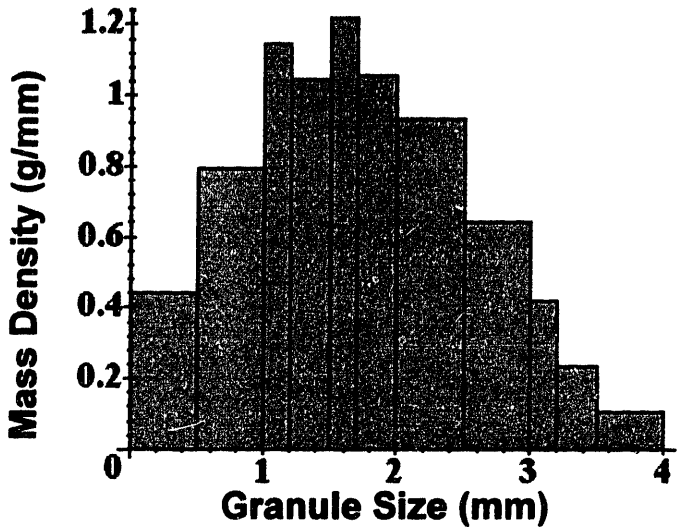

Figure 2-5: Density plot of sieve data.

tem which produces the sum of 50 independent "continuous die rolls," each of which yield a real number between 1 and 6 with uniform probability. The range of possible results of these sums is between 50 and 300. The results of 10,000 of these sums are plotted in Figure 2-6 as a bin distribution, where the integer values 50, 51, 52, ..., 299, 300 define the bin boundaries. Note how

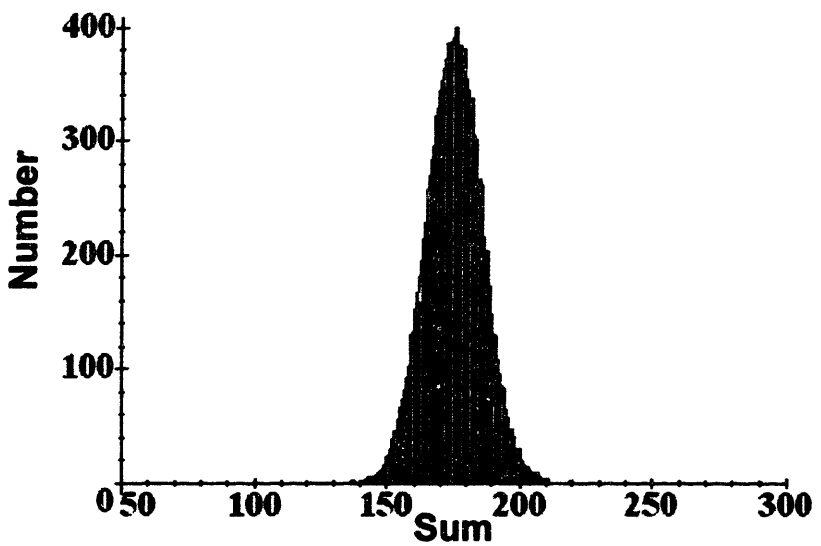

Figure 2-6: Bin representation of continuous die roll experiment data.

closely this distribution resembles the continuous distribution included for comparison purposes,

as evidenced by Table 2-8. These two distributions are in fact so close that Figure 2-7 is included

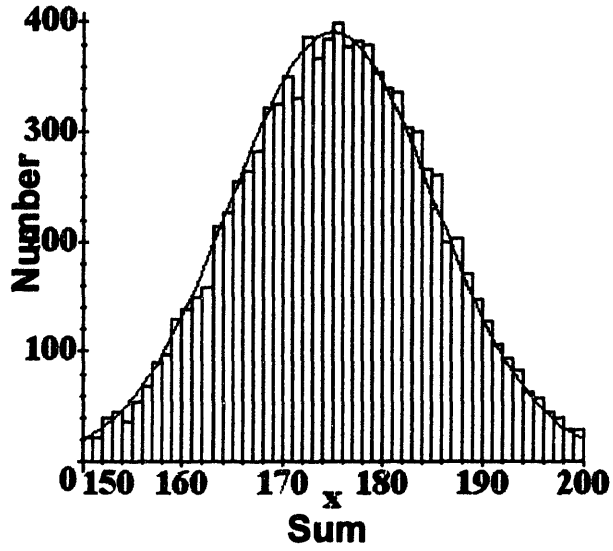

Figure 2-7: Close-up bin representation of "continuous dice" die roll experiment data.

to offer a close-up.

In general, as the bin width of any bin representation decreases, the representation approaches a continuous distribution; in this particular case, the representation approaches a Gaussian distribution.

Table 2-8: Comparison of sample and analytical representation statistics

Distribution	*Mean*	*Standard Deviation*
Data	174.986	10.206
Analytical	175.000	10.244

In the limit as bin width decreases in the discrete representation, $\Delta\phi \rightarrow 0$ and the expression for the number of particles in any given subdomain of the distribution is transformed from a summation into an integral:

$$N = \sum_{\phi_a < \phi_i \leq \phi_b} n_i(\phi_i - \phi_{i-1}) = \int_{\phi_a}^{\phi_b} n(\phi')d\phi' \tag{2.3}$$

The array of data points n_i becomes a continuous number distribution $n(\phi)$, defined as follows:

DEFINITION

The **number density** *function of particles is given by* $n(\phi, t)$ *such that* $n(\phi, t)d\phi$ *is the number particles in the size range* $[\phi, \phi + d\phi]$ *at time* t.

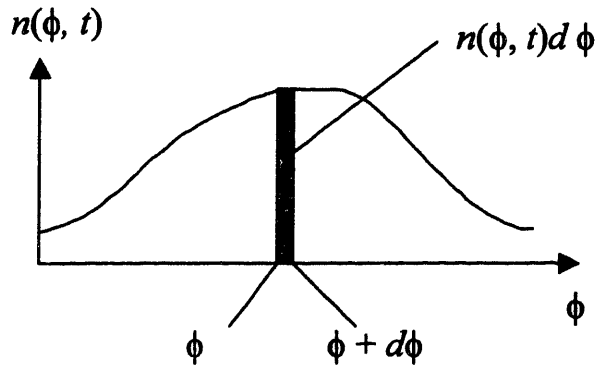

Figure 2-8: Number density representation with highlighted size range segment.

In many ways, the number density function is directly analogous to a probability density function, as shown in Table 2-9. For a more developed discussion of probability distributions, please refer to either Appendix D, Drake (1967), or Papoulis (1991).

Table 2-9: Probability density function and number density function comparison

Density function	*Notation*	*Distribution Slice*	*Interpretation*
Probability	$f_x(x)$	$f_x(x)dx$	probability of x taking on a value between x and $x + dx$
Number	$n(\phi)$	$n(\phi)d\phi$	number of particles between ϕ and $\phi + d\phi$

Figure 2-9.illustrates a sample probability density function. The probability that x lies between a and b can be calculated by integrating the probability density function from a to b:

$$Prob(a < x \leq b) = \int_a^b f_x(x)dx = \int_a^b f_x(\xi)d\xi \qquad (2.4)$$

Note the change of variables in the second integral to emphasize that distinction between x and the integration variable, ξ. Similarly, the number of particles between sizes ϕ_a and ϕ_b can be determined by evaluating the integral of $n(\phi)$ from ϕ_a to ϕ_b, as shown in Equation (2.5).

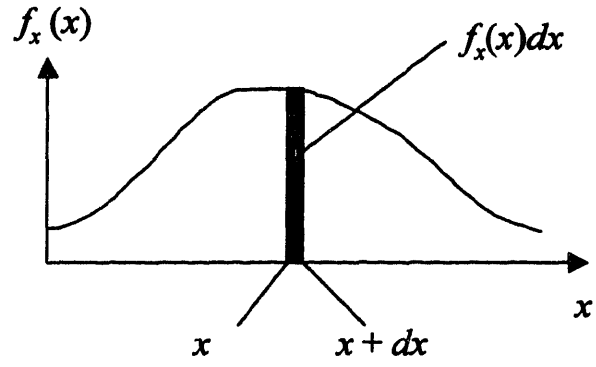

Figure 2-9: Probability density function representation with highlighted distribution segment.

$$N(\phi_a < \phi \leq \phi_b, t) = \int_{\phi_a}^{\phi_b} n(\psi)d\psi \tag{2.5}$$

Note again the change of integration variable, this time from ϕ to ψ. This emphasizes the fact that both variables denote mass, but the value of ψ is simply an integration variable where ϕ is the independent variable in the definition of $N(\phi)$.

The cumulative probability density function is defined as the total probability of x taking on a value less than or equal to x_0. This function is calculated by taking the integral of the probability density function for all possible values of x less than x_0.

$$p_{x\leq}(x_0) = Prob(x \leq x_0) = \int_{-\infty}^{x_0} f_x(\xi)d\xi \tag{2.6}$$

The cumulative number density function likewise represents the number of particles size ϕ or less and is defined as follows:

$$N(\phi) = \int_0^{\phi} n(\psi)d\psi \tag{2.7}$$

Clearly, if the upper limit of integration in Equation (2.7) were differentially increased from ϕ to $\phi + d\phi$, then $n(\phi)d\phi$ more particles would be added to the system and the new total number of particles would be $N(\phi) + n(\phi)d\phi$. For this reason, $n(\phi)$ is often written as $dN/d\phi$ to emphasize that it represents the incremental number of particles added to the system as ϕ is increased diffferentially.

$$N(\phi + d\phi) = N(\phi) + n(\phi)d\phi$$
$$N(\phi + d\phi) = N(\phi) + \frac{dN}{d\phi}(d\phi) \tag{2.8}$$

We can now construct an augmented version of Table to 2-1 which includes the this new number density notation.

Table 2-10: Common distribution functions $n(\phi)$

ϕ - *symbol*	ϕ - *meaning*	$n(\phi)$	$dN/d\phi$
D_p	particle diameter	$n(D_p)$	$\frac{dN}{dD_p}$
m	particle mass	$n(m)$	$\frac{dN}{dm}$
l	crystal length	$n(l)$	$\frac{dN}{dl}$
v	particle volume	$n(v)$	$\frac{dN}{dv}$

The total probability of all possible outcomes in a system is always equal to 1; here this result is presented as the integral of the probability density function from $-\infty$ to ∞ :

$$Prob(-\infty < x \leq \infty) = \int_{-\infty}^{\infty} f_x(\xi)d\xi = 1 \tag{2.9}$$

The number of particles in the distribution is computed by integrating over all possible values $(0, \infty)$:

$$N_{total} = N(0 < \phi \leq \infty) = \int_{0}^{\infty} n(\psi)d\psi \tag{2.10}$$

Table 2-11 summarizes the similarities between integrals over probability density and number

density functions.

Table 2-11: Probability Density and Number Density Function Comparison

Integrand	*Limits*	*Variable of integration*	*Value*	*Interpretation*
$f_x(x)$	(a, b)	dx	$Prob(a < x < b)$	Probability of $a < x < b$
$n(\phi)$	(ϕ_1, ϕ_2)	$d\phi$	$N(\phi_1)$	Number between ϕ_1, ϕ_2
$f_x(x)$	$(-\infty, b)$	dx	$Prob(x < b)$	Cumulative probability
$n(\phi)$	$(0, \phi_2)$	$d\phi$	$N(\phi_2)$	Cumulative number density
$f_x(x)$	$(-\infty, \infty)$	dx	1	Total probability of all outcomes
$n(\phi)$	$(0, \infty)$	$d\phi$	N	Total number in population

Note that if the units of $d\phi$ are *mass*, then the units of $n(\phi)$ must be $mass^{-1}$ in order for N_{total} to be dimensionless. However, when dealing with real systems, the number density must be expressed in terms of the size of the system where the population lives. For example, with railroad tracks, one might be interested in the population of the mass of defects per mile. In this case the number density of interest $n(\phi)$ would express the number of defects per mile of track and the units would be *defects/mile*.

2.5 Continuous Representation of Discrete system

As a final example, consider a process with a large number of discrete data points. Instead of the sum of 50 "continuous die rolls" we will use the sum of 50 regular die rolls. Plotting the distribution of 10,000 of these individual sum results in Figure 2-10, where the stems of the individual data points have been omitted for graphical clarity. Again, note how the close spacing of the data points results in a distribution which is closely approximated by a continuous distribution, again a normal distribution. Table 2-13 demonstrates how closely the population statistics match

the normal distribution.

Table 2-12: Comparison of die roll sums and Gaussian distribution statistics

Distribution	Mean	Standard Deviation
Data	174.980	12.076
Analytical	175.000	12.159

Figure 2-10 compares these distributions.

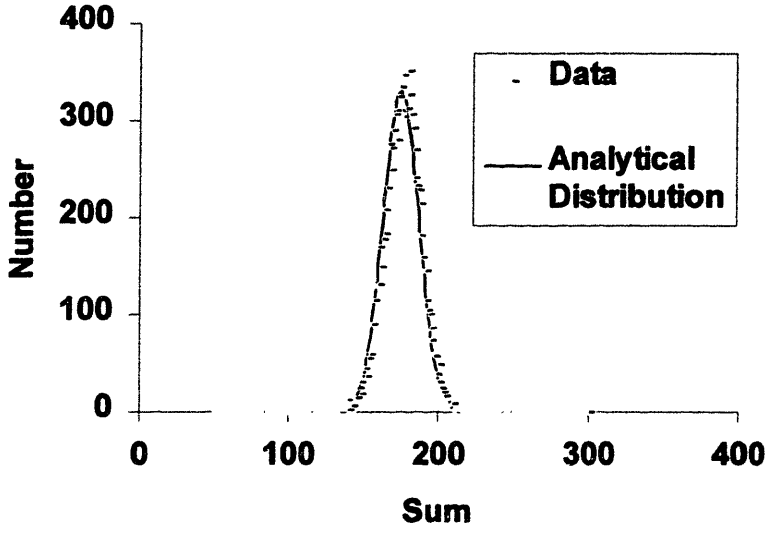

Figure 2-10: Comparison of "discrete dice" experiment and continuous distribution.

Although the process which generated this data is inherently discrete, the discrete data points are so close together that for all practical purposes this problem may be treated almost identically to the continuous process in Section 2.5 - both the continuous and discrete die roll systems produce the same mean and only a slightly different standard deviation.

In fact, many physical systems can ultimately be treated as *either* discrete or continuous systems. In the case of a distribution of aerosol particles, the number density function could be a function of either the number of molecules contained in a particle or the diameter of the particle. For larger aerosol particles, a number density function of the number of molecules would result in a discrete distribution with very close spacing, as in Figure 2-10; in this case it is more sensible to

use particle mass as the independent variable in the number density function. However, for very tiny nucleating particles that contain far fewer atoms, the discrete points in the number density function will be spaced much further apart to the point where a continuous distribution would be inappropriate. For further reference, Apostol (1969) presents an in-depth treatment of the relation between discrete and continuous distribution functions, drawing examples from probability theory.

2.6 Importance of Representations

The discussion of numerical solution techniques in Chapter 1 alludes to the importance of representations in the numerical solution of PDE systems. For population balance problems, the representation is the conceptual model which forms the framework upon which a system is built. The level of detail included in a representation defines the attributes of the population being studied and sets bounds on the level of detail and information in the model. To cite a well-known example, each United States census creates a representation of the population of the United States. The attributes - address, sex, age, income, race, etc. - included define the level of detail in the representation, which is a conceptual model of the true population. Of course, the census can-

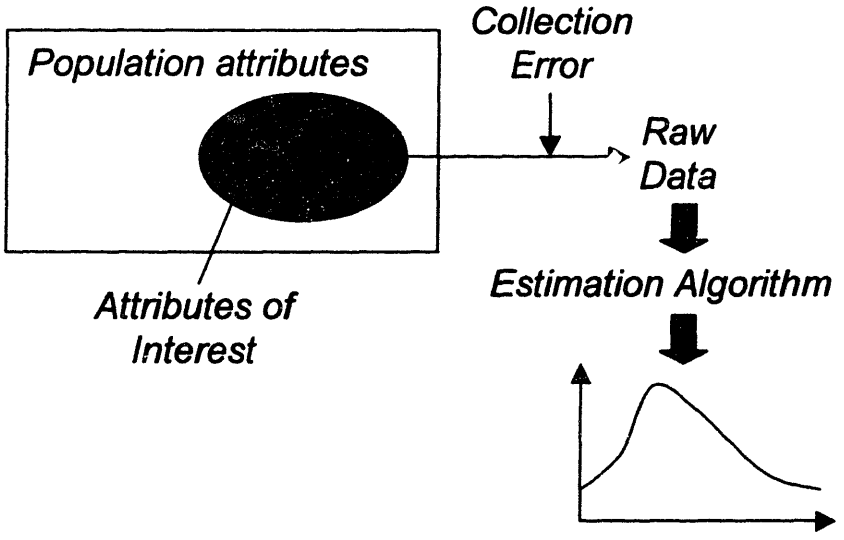

Figure 2-11: Diagram of conceptual and data representations of a population.

not collect *all* information about the population, so it is designed to collect what is deemed to be the most relevant information. Because the representation does not include data such as eye color or weight, this does not mean that the true population does not possess these attributes; it merely

means that the conceptual representation being used does not include these attributes. Choosing the attributes to be included in the representation is only the first step. Data collection procedures must be defined and statistical estimation techniques employed to ensure that the population data is of high quality - that the representation accurately matches the characteristics of the chosen attributes in the true population. In spite of all efforts taken to ensure high quality data collections, errors will always be present in the data as well as the collection methods. Estimation algorithms are used to compensate for these errors. For the United States census, this means that sophisticated statistical techniques are employed to ensure that the census accurately reflects the number of persons in the United States and their demographic information. As with many population processes, gathering, analyzing and interpreting data is no simple task - recent improvements in statistical techniques have been projected to save over $100 million in the 2000 census (Cohen, White and Rust, 1999). As we will see in the following chapters, many of the same challenges exist in most population balance systems. Furthermore, the dynamic population balance systems considered here place an additional requirement on the population representation: that it interfaces easily with the governing equations for the physical system. In summary, there are several key challenges in formulating an appropriate representation for a population balance process:

- correct choice of population attributes to accurately represent the true population
- collection of data and definition of statistical techniques to ensure that the representation accurately matches the attributes of the true population
- ability of the representation to accurately reproduce the physics of the system
- ease of implementation in a numerical solution

Often, this last challenge requires that some transformation of the initial representation is required to ensure that the data is properly *scaled* for use in a numerical model (see Chapter 6). Scaling transformations are necessary to transfer population representation data to and from formats which are used in experimental systems, computer models, and graphical or tabular presentation of the data.

Representations are also used to catalog data from experimental measurement systems. Rigorous understanding of these representations enables the translation of population balance system data from experimental measurement systems to computer models and vice versa. Representations are often motivated by the physics of the system in question, forming a common language

with which the processes in the system may communicate.

To simplify matters, the representation of populations with only one attribute of interest will be addressed first. In one-attribute population systems - also referred to as one-dimensional systems - there are two key questions:

1. which attribute is dominant?
2. what will be the metric for this attribute?
3. is the metric discrete or continuous?

For instance, take a system representing a population of polymer particles where size is the attribute of interest. If the polymer chains are very short and only contain a few monomers each, it makes sense to represent their size by a discrete set of "bins" which represent polymer chains containing a specific number of monomers, as illustrated in Figure 2-12.

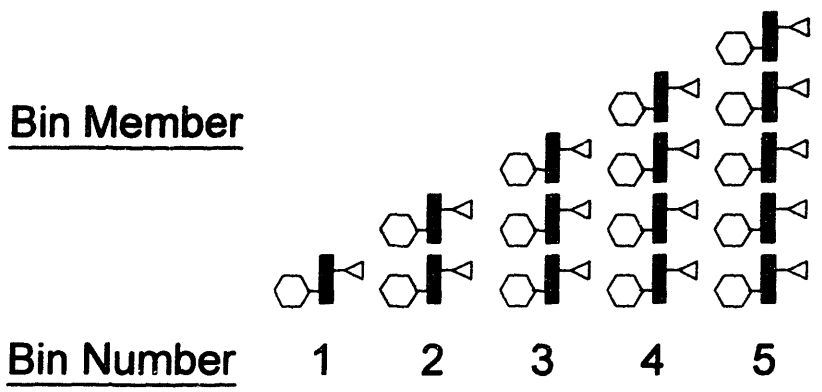

Figure 2-12: Polymer particle size bins corresponding to discrete numbers of monomers in each polymer.

This type of representation seems suitable so long as the maximum size polymer chain is small enough that a reasonable number of bins are necessary to represent the population. For example, if the largest polymer chains in this system contained less than 40 monomers, then 40 bins at most would be needed to represent the population. However, if the largest polymer chains contained upwards of 1,000,000 monomers, this representation would clearly be impractical. In such systems the differences between the masses of polymer chains are so miniscule that a continuous representation based on polymer chain mass might be a more manageable representation from a numerical standpoint. A more natural implementation of a continuous representation might apply

to a population of droplets in cloud formation where particle diameter could be used as a continuous attribute of the population. Other attributes can be used almost equally as well as discrete or continuous variables, such as age. One could easily see where the U.S. census might prefer to use a discrete representation for age where a nuclear physicist studying the half-life of an unstable nucleus would prefer to use nano- or micro-seconds as a continuous measure of decay time.

2.7 Discrete Population Representations Example

One way of cataloguing population data is to specify the number of members possessing certain properties. For a population of rabbits, one might list the number of rabbits associated with different age ranges, as shown in Table 2-13.

Table 2-13: Rabbit population data

Age Range (months)	Number
0-2	11
2-5	18
5-10	9
10-13	6
13-16	5
16-25	7
25-35	4
35-45	0
45-50	1

This data is readily convertible to a histogram, as shown in Figure 2-13. Note that this histogram represents the number of rabbits in each age range, plotted at a constant value over the entire age range, essentially dividing the age range into a series of bins which hold varying numbers of rabbits. If Figure 2-13 represented the steady state of a rabbit population, one would expect that the number of rabbits would decrease with age. If 11 rabbits are born each month, then how can there be 18 rabbits with an age 3 months? After rabbits are born, they can only be reduced in number due to death. Likewise, why does it appear that there are disproportionately more rabbits in the 16-25 month age range than in the 13-16 month age range.

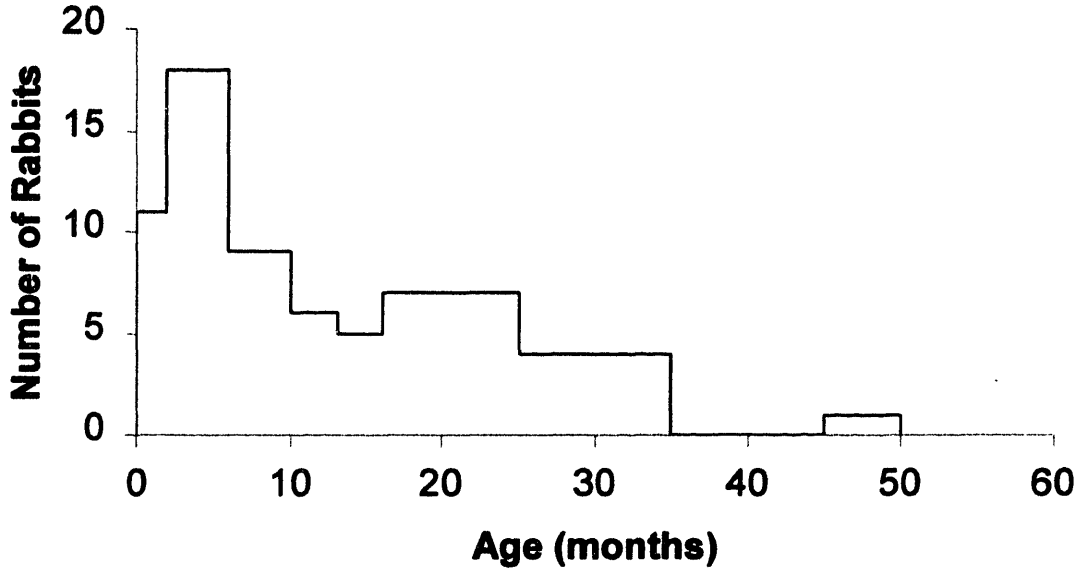

Figure 2-13: Discrete rabbit population example.

The key is to look at the number of rabbits *per month* in the distribution. There are actually 7/9, or 0.78 rabbits per month in the 16-25 month age range while there are 5/3, or 1.67 rabbits per year in the 13-16 month range - roughly twice as many!

In order to account for varying bin width, the concept of a number density function is introduced to normalize the data. If we think of the number of rabbits in the age range (N_i) as the product of the number distribution (n_i) and the width of the bin, then for age range i:

$$N_i = n_i \Delta age_i \tag{2.11}$$

and it follows that the number density can be calculated for each interval by dividing the total number in the interval by the length of the interval:

$$n_i = \frac{N_i}{\Delta \text{age}_i} \tag{2.12}$$

Note that N_i has units of rabbits and Δage has units of months; therefore the number density function has units of *rabbits/month.* Table 2-13 can now be augmented by adding in the number den-

sity function of rabbits.

Table 2-14: Rabbit population and number density data

Age Range (months)	*Number*	*Number Density*
0-2	11	5.50
2-5	18	4.5
5-10	9	2.25
10-13	6	2.00
13-16	5	1.67
16-25	7	0.78
25-35	4	0.40
35-45	0	0.0
45-50	1	0.20

While the discrete population plot of number of rabbits vs. age (Figure 2-13) indicates that the number of rabbits is an erratic function of age, the number distribution of rabbits shown in Figure 2-14 indicates that the number of rabbits declines monotonically with age through most of the distribution, a much more logical result.

Because the number distribution of rabbits is a function of the rabbit age, it is common to write the number distribution of rabbits as $n(age)$, which implies a number density function of age. In cases where particle sizes are concerned, this function becomes $n(size)$; often particle diameter, D_p, is used to represent particle size and $n(D_p)$ results. Likewise, if the symbol m is used to denote mass, the number density based on mass is $n(m)$. If the number distribution varies as a function of time, it is written $n(m, t)$.

2.8 Multiattribute & Multicomponent Distributions

2.8.1 Continuous representations

In many systems, just one single attribute ϕ is not sufficient to describe all of the population parameters of interest. In the general case, ϕ is a vector with n components $\phi_1, \phi_2, \ldots \phi_n$ each representing one attribute of the distribution. The basic definition of the number density distribution

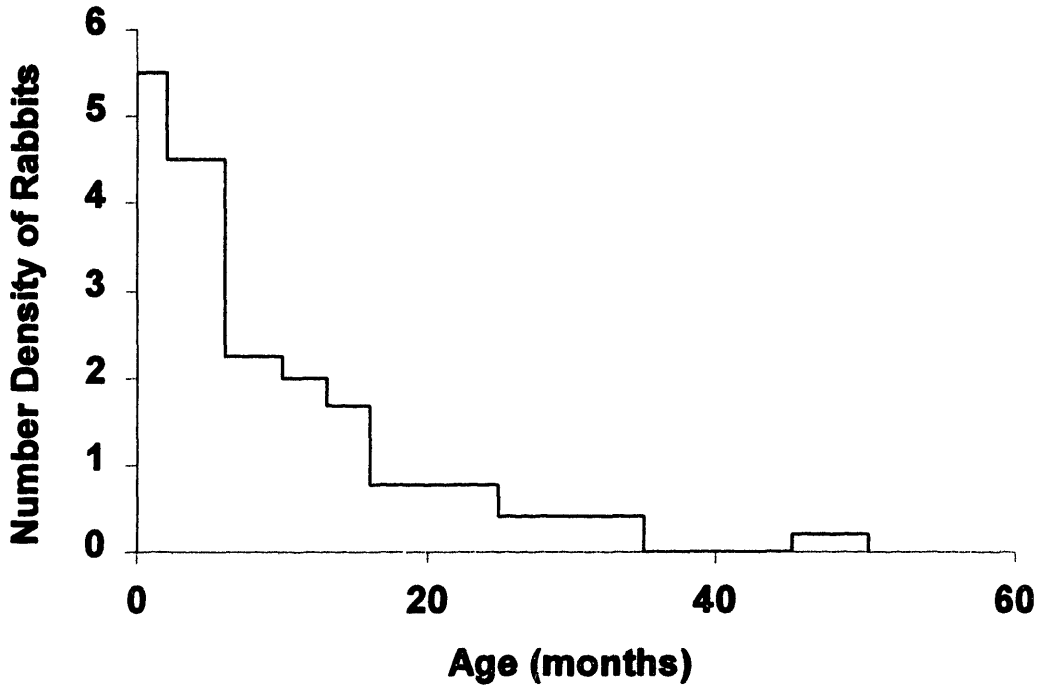

Figure 2-14: Density plot of rabbit population.

given in section 2.4 still applies, except that now the interval $[\phi, \phi + d\phi]$ exists in n dimensions. Accordingly, $n(\phi)d\phi$ now takes the form $n(\phi_1, \phi_2, ...,\phi_n)d\phi_1 d\phi_2 ... d\phi_n$ which now represents the number of particles in the multidimensional interval $[\phi_1, \phi_1 + d\phi_1, \phi_2, \phi_2 + d\phi_2, ..., \phi_n, \phi_n + d\phi_n]$. Tables 2-15 and 2-16 compare the list of attributes and their corresponding units for a pair of two-dimensional systems and the general case $n(\phi)$.

Table 2-15: Sample attributes for two-dimensional systems

System	*Attribute 1*	*Symbol 1*	*Units*	*Attribute 2*	*Symbol 2*	*Units*
General	-	f_1	-	-	ϕ_2	-
Crystals	Length	l	mm	# of Defects	k	-
Aerosol	Diameter	D_p	μm	Density	ρ	g/cm^3

Table 2-16: Summary of two-dimensional distributions and corresponding units.

System	*Distribution*	*Units*	*# of particles in "slice"*
General	$n(\phi_1, \phi_2)$	-	$n(\phi_1, \phi_2)\, d\phi_1 d\phi_2$
Crystals	$n(l, k)$	1/mm	$n(l, k)\, dl\, dk$
Aerosols	$n(D_p, \rho)$	$1/(\text{mm} \cdot \text{g/cm}^3)$	$n(D_p, \rho)\, dD_p\, d\rho$

Note that while the domain of the differential element $d\phi$ was previously a differential line segment, it is now a differential area element, as shown in Figure 2-15.

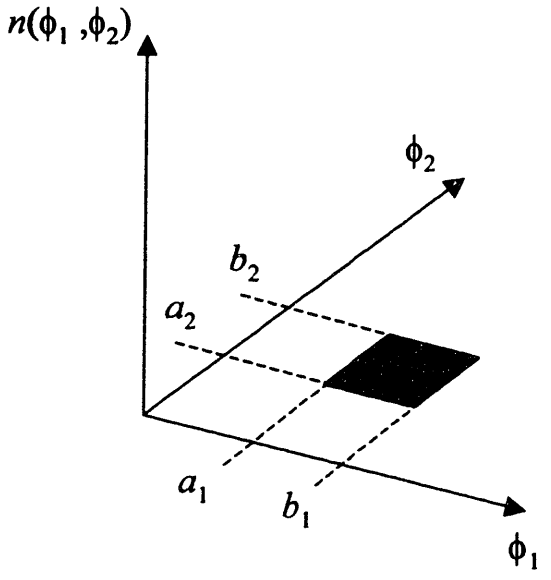

Figure 2-15: Illustration of a two-dimensional population domain.

Just as with the one-dimensional case, the same probability analogies apply to the two-dimensional population systems, and can be directly generalized from Table 2-10. For instance, to calculate the number of particles in the segment of the population ranging over the interval $\phi_1 = (a_1, b_1)$ and $\phi_2 = (a_2, b_2)$ the one-dimensional integral given in Equation (2.5) is expanded to a two-dimensional integral, as given in Equation (2.13).

$$N(a_1 < \phi_1 \leq b_1, a_2 < \phi_2 \leq b_2) = \int_{a_2}^{b_2} \int_{a_1}^{b_1} n(\psi_1, \psi_2) d\psi_1 d\psi_2 \tag{2.13}$$

If $n(\phi_1, \phi_2)$ were a two-dimensional normal distribution as given in Equation (2.14), then the integration given in Equation (2.13) would be measuring the *volume* shown in Figure 2-16.

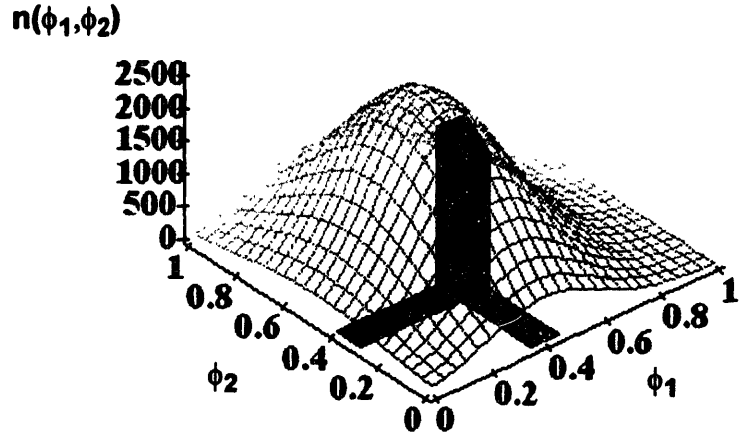

Figure 2-16: Population "slice" of a two-dimensional normal distribution.

$$n(\phi_1, \phi_2) = \frac{N_0}{2\pi\sigma_1\sigma_2}\exp\left(\frac{-(\phi_1-\mu_1)^2}{2\sigma_1{}^2}\right)\exp\left(\frac{-(\phi_2-\mu_2)^2}{2\sigma_2{}^2}\right) \qquad (2.14)$$

The distribution parameters and integration limits are summarized in Table 2-17.

Table 2-17: Summary of parameters used in Figure 2-16

Symbol	Parameter	Value
N_0	Total number in distribution	1000
μ_1	Mean of ϕ_1	0.4
μ_2	Mean of ϕ_2	0.5
σ_1	Standard deviation of ϕ_1	0.2
σ_2	Standard deviation of ϕ_2	0.3
a_1	Lower limit of ϕ_1	0.35
a_2	Lower limit of ϕ_2	0.3
b_1	Upper limit of ϕ_1	0.45
b_2	Upper limit of ϕ_2	0.4

2.8.2 Discrete multiattribute representations

Discrete multiattribute representations are very similar to single-attribute representations. In the example of a two-attribute system, the "stems" will be placed on the x - y plane of the graph and the number at that point will be shown in the z-direction.

2.8.3 Multiattribute bins representations

Just as with one-attribute properties, it is common that data for multi-attribute processes is gathered in bins. In the two-attribute case, these bins are two-dimensional. Take the example of a crystallization process with data on crystal length and the number of defects in a crystal given in Table 2-18. The first two columns and rows present data on crystal length and number of defect

bin sizes, while the remainder of the table reports the number of crystals in each of these bins.

Table 2-18: Two attribute crystal distribution bins data

Lower Range	# of Defects →	0	3	7	15	20	27
Crystal Length (mm) ↓	Upper Range	3	7	15	20	27	35
0	0.1	5	5	7	4	6	5
0.1	0.2	4	4	8	5	5	6
0.2	0.4	7	11	17	11	12	14
0.4	0.8	15	21	38	25	26	29
0.8	1.0	7	10	20	13	15	15
1.0	1.3	10	13	28	19	23	24
1.3	1.7	12	15	33	23	36	37
1.7	1.9	5	6	15	11	17	19
1.9	2.0	2	4	7	5	8	10

Plotting the heights of these two-dimensional bins as given by the raw data in Table 2-18 results in Figure 2-17. This representation suffers from the same normalization problem that affected the data in Table 2-6. However, now the bin data requires normalization along both of the attribute axes. Note that the data still needs to be normalized to produce a density function.

$$N_{i,j} = n_{i,j} \cdot \Delta\text{length}_i \cdot \Delta\text{defects}_j$$
$$n_{i,j} = \frac{N_{i,j}}{\Delta\text{length}_i \cdot \Delta\text{defects}_j} \tag{2.15}$$

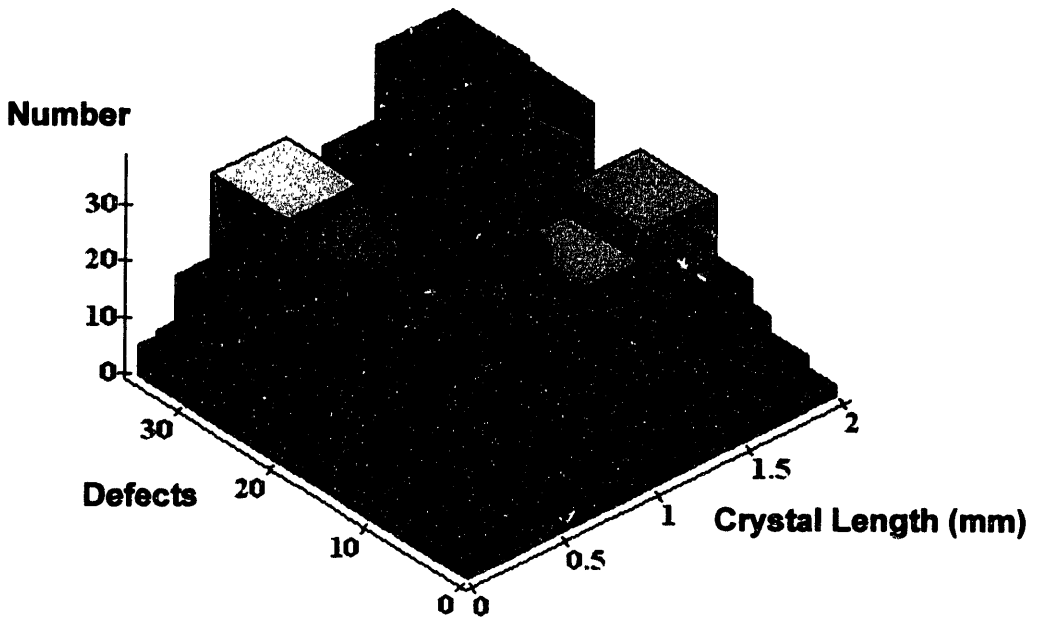

Figure 2-17: Two attribute crystal distribution as a function of size and defects.

The normalized data is presented in Table 2-19.

Table 2-19: Two attribute crystal distribution bins data

Lower Range	# of Defects →	0	3	7	15	20	27
Crystal Length (mm) ↓	Upper Range	3	7	15	20	27	35
0	0.1	16.67	12.50	8.75	8.00	8.57	6.25
0.1	0.2	13.33	10.00	10.00	10.00	7.14	7.50
0.2	0.4	11.67	13.75	10.63	11.00	8.57	8.75
0.4	0.8	12.5	13.13	11.88	12.50	9.29	9.06
0.8	1.0	11.67	12.50	12.50	13.00	10.71	9.38
1.3	1.3	11.11	10.83	11.67	12.67	10.95	10.00
1.3	1.7	10.00	9.38	10.31	11.50	12.86	11.56
1.7	1.9	8.33	7.50	9.38	11.00	12.14	11.88
1.9	2.0	6.67	10.00	8.75	10.00	11.43	12.50

Plotting this normalized data results in Figure 2-18. Clearly, where no trend was visible in

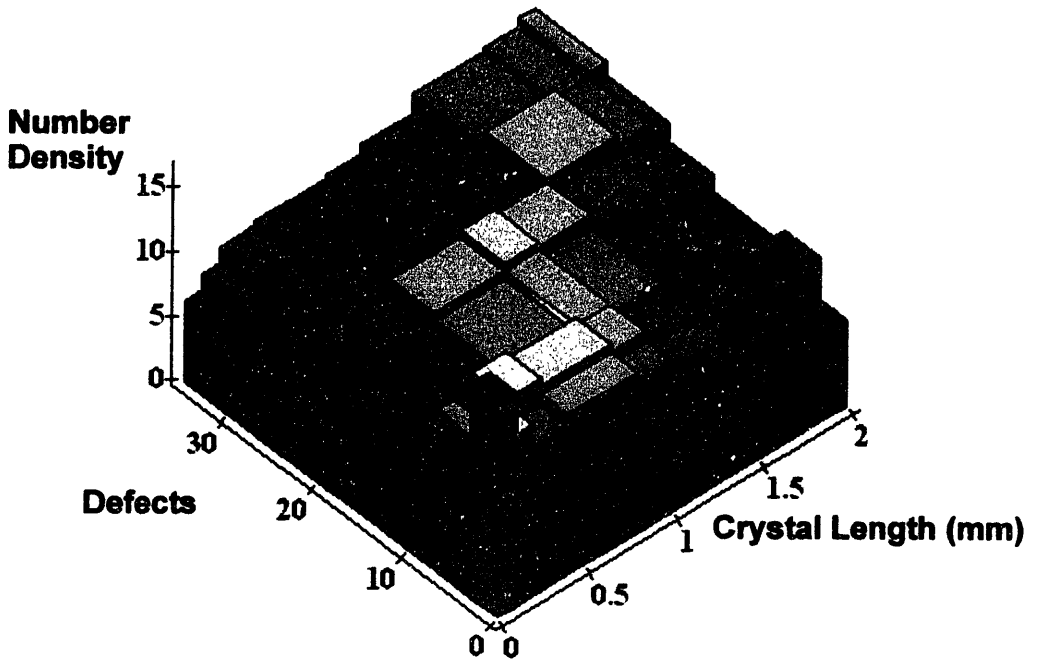

Figure 2-18: Two attribute crystal distribution as a function of size and defects.

Figure 2-17, this plot shows a distinct relation between crystal length and the number of defects. The units of this distribution are now 1/mm, as defects are unitless. Again, proper normalization correctly represents the data, greatly improving otherwise incoherent data.

References

[1] Apostol, Tom M. *Calculus,* 2nd Ed., John Wiley & Sons, 1969.

[2] Drake, Alvin W. *Fundamentals of Applied Probability Theory,* McGraw-Hill, Inc. 1967.

[3] Commission on Behavioral and Social Sciences and Education, *Counting People in the Information Age,* Duane L. Steffey and Norman M. Bradburn, Eds., National Academy Press, 1994.

[4] Commission on Behavioral and Social Sciences and Education, *Measuring a Changing Nation: Modern Methods for the 2000 Census,* Michael L. Cohen, Andrew A. White, and Keith F. Rust, Eds., National Academy Press, 1999.

[5] Papoulis, Athanasios *Probability, Random Variables, and Stochastic Processes,* 3rd Ed., McGraw-Hill, 1991.

[6] Pollock, Daniel P.; Kutzko, Joseph P.; Birck-Wilson, Eszter; Williams, Jennifer L.; Echelard, Yann; Meade, Harry M. *Transgenic Milk as a Method for the Production of Recombinant Antibodies,* Journal of Immunological Methods, **231**, 147-157, 1999.

[7] Press, William H.; Teukolsky, Saul A.; Vetterling, William T.; Flannery, Brian P. *Numerical Recipies in C: The Art of Scientific Computing,* 2nd Ed., Cambridge University Press, 1993.

[8] Seinfeld, John H.; Pandis, Spyros N. *Atmospheric Chemistry and Physics: From Air Pollution to Climate Change* John Wiley & Sons, 1998.

Chapter 3: Transformations of Population Representations

The ability to manipulate population representations is critical to their utility in a wide range of problems. In particular, two key operations are needed to efficiently work with population representations.

- transformations - the ability to change distributions between various forms, such as from a function of diameter $n(D_p)$ to a function of particle volume $n(v)$.
- scaling - the ability to manipulate the scale of the distribution to reflect wide range of particle sizes present in many systems.

As we will see in Chapter 6, the ability to transform number density distributions to a proper size scale is critical to the efficient numerical solution of particle growth problems in a wide variety of physical systems. The following sections detail the fundamentals of these transformations.

3.1 Common Transformations

Transformations are commonly used in the modeling of particle processes. Transformations change the independent variable over which the distribution is defined. One example of a transformation is used to change a distribution from $n(v)$ to $n(D_p)$:

$$n(D_p) = n(v)\frac{\pi D_p^2}{2} \tag{3.1}$$

Figure 3-1 shows the effects of transforming an exponential distribution from $n(v)$ to $n(D_p)$. Equation (3.2) presents the form of an exponential population distribution used to produce $n(v)$ in Figure 3-1, using the parameters summarized in Table 3-1.

$$n(v) = N_0 a \cdot e^{-av} \tag{3.2}$$

Note that the distribution parameter units are consistent with the fact that the units of $n(v)$ are 1/

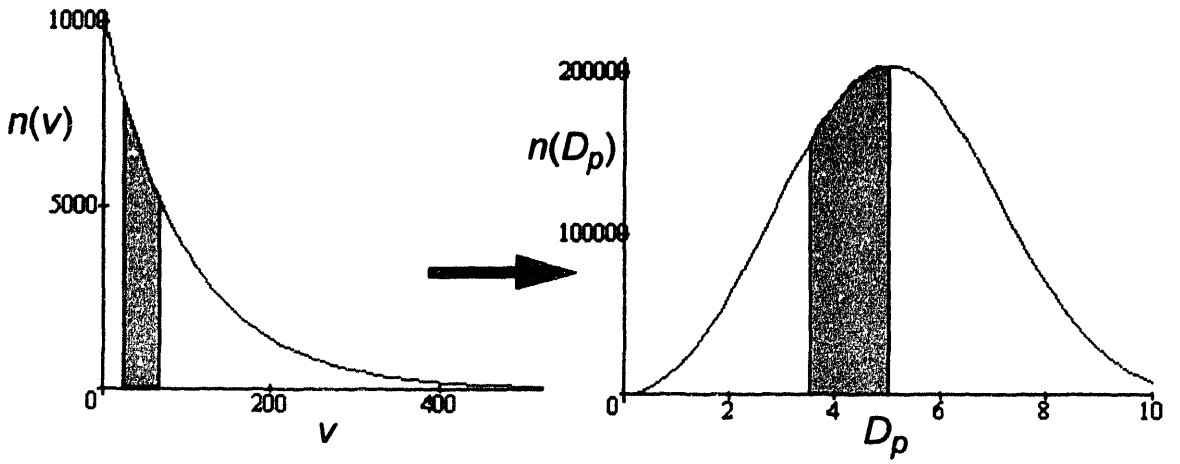

Figure 3-1: Example of transformation from $n(v)$ to $n(D_p)$.

cm^3 and the units for $n(D_p)$ are $1/\mu m$.

Table 3-1: Exponential population distribution parameters

Symbol	*Parameter*	*Value*	*Units*
a	exponential distribution parameter	1.0×10^{-2}	$1/cm^3$
N_0	total number of particles in distribution	1.0×10^{6}	-
V_{low}	lower range of V	5.24×10^{-7}	μm
V_{high}	upper range of V	5.24×10^{-2}	μm

3.2 Deriving Transformations

In order to derive these transformations we must first review the basic properties of number density functions which must be preserved under any valid transformation. Using these basic properties, an variety of useful number of transformations may be defined.

3.2.1 Basic properties

Consider the properties required to define a general transform from $n(\phi)$ to $n(\psi)$:

- the total number of particles, N_0, in both distribution forms should be the same:

$$\int_0^\infty n(\phi)d\phi = N_0 = \int_0^\infty n(\psi)d\psi \tag{3.3}$$

- the number of particles in corresponding "slices" of each distribution should be equal:

$$\int_{\phi_1}^{\phi_2} n(\phi)d\phi = \int_{\psi_1}^{\psi_2} n(\psi)d\psi \tag{3.4}$$

- some strictly monotonic one-to-one mapping must exist between ϕ and ψ to ensure that for each "slice" of the distribution $n(\phi)$ defined on (ϕ_1, ϕ_2) there exists a corresponding slice (ψ_1, ψ_2) of $n(\psi)$.

The condition given in Equation (3.4) must hold even on differentially small intervals (ϕ_1, ϕ_2) and (ψ_1, ψ_2). In addition, the strictly monotonic and one-to-one requirement requires that This leads to the final condition which is ultimately used to derive all one-component transformations:

$$n(\phi)d\phi = n(\psi)d\psi \tag{3.5}$$

3.2.2 Example transformation from $n(v)$ to $n(D_p)$

Recalling that each side of Equation (3.5) represents the number of particles in a differential slice of their respective distributions, this condition effectively requires that transformations conserve the number of particles throughout every segment of the respective distributions. For the example of $n(v)$ and $n(D_p)$, this means that:

$$\begin{aligned} n(D_p)dD_p &= n(v)dv \\ n(D_p) &= n(v)\frac{dv}{dD_p} \end{aligned} \tag{3.6}$$

Because v is a known one-to-one monotonic function of D_p, we can use this relation to calculate the derivative in Equation (3.6) and arrive at a transformation:

$$\begin{aligned} v &= \frac{4}{3}\pi r^3 = \frac{4}{3}\pi\left(\frac{D_p}{2}\right)^3 \\ \frac{dv}{dD_p} &= \frac{\pi D_p^2}{2} \\ n(D_p) &= n(v)\frac{\pi D_p^2}{2} \end{aligned} \tag{3.7}$$

Figure 3-1 illustrates the graphical results of this transformation, where the gray areas mark off corresponding segments of the two distributions. The first relation in Equation (3.7) gives the one-to-one continuous mapping between v and D_p, which can be used to calculate the limits of the highlighted area in $n(D_p)$ given the limits of the area in $n(v)$ and vice-versa.

Table 3-2: Limits of highlighted segments in respective distributions in Figure 3-1

Limit	*Symbol*	v	*Units*	*Symbol*	D_p	*Units*
Lower	v_1	23.4	μm^3	D_{p1}	3.55	μm
Upper	v_2	65.9	μm^3	D_{p2}	5.01	μm

The number of particles in each of these distributions segments can be calculated using the integral of the distribution function over the segment domain, as shown in Equation (3.8).

$$\begin{aligned}
\int_{v_1}^{v_2} n(v)dv &= \int_{v_1}^{v_2} N_0 a \cdot e^{-av} dv = -N_0 e^{-av}\Big|_{v_1}^{v_2} = 2.74\times10^5 \\
\int_{D_{p1}}^{D_{p2}} n(D_p)dD_p &= \int_{D_{p1}}^{D_{p2}} N_0 a \cdot \exp\left(-\frac{a\pi D_p^3}{6}\right)\frac{\pi D_p^2}{2} dD_p \\
&= -N_0 \exp\left(-\frac{a\pi D_p^3}{6}\right)\Big|_{D_{p1}}^{D_{p2}} = 2.74\times10^5
\end{aligned} \tag{3.8}$$

Note that both distribution segments contain the same number of particles, confirming that the transformation is correct. Recalling that the area of the segments is equal to the number of particles in that segment, we can write an expression equating these two areas over some equivalent width of the two distributions.

$$\begin{aligned}
n(\phi)\Delta\phi &= n(\psi)\Delta\psi \\
n(\phi) &= n(\psi)\frac{\Delta\psi}{\Delta\phi}
\end{aligned} \tag{3.9}$$

This relation is illustrated in Figure 3-2. Because these are corresponding intervals, we know that

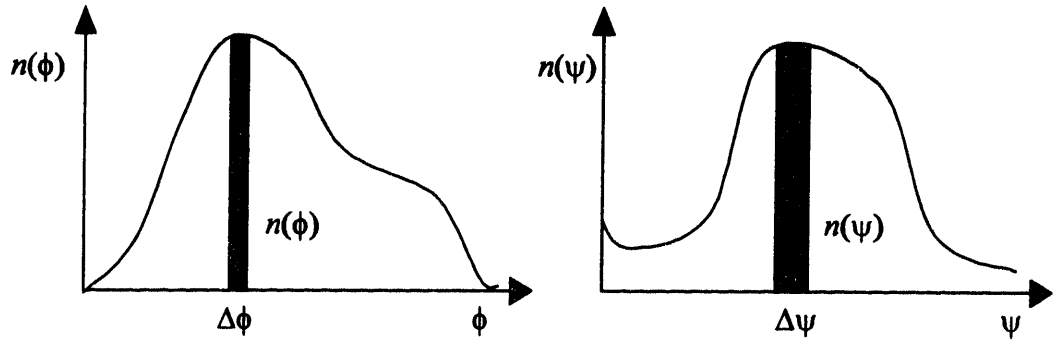

Figure 3-2: Corresponding segments in two distributions undergoing transformation between from $n(\phi)$ to $n(\psi)$.

$\Delta\psi$ is a function of $\Delta\phi$. We can therefore take the limit as the widths of the intervals $\Delta\phi$ and $\Delta\psi$ approach zero, and Equation (3.9) becomes:

$$\lim_{\Delta\phi \to 0} n(\phi) = n(\psi)\frac{\Delta\psi(\Delta\phi)}{\Delta\phi} = n(\psi)\frac{d\psi}{d\phi} \tag{3.10}$$

3.2.3 Proof of one-component transformation theorem

The result given Equation (3.10) can be stated more formally as a theorem.

THEOREM

For any two single-attribute distributions $n(\phi)$ and $n(\psi)$, if there exists a differentiable strictly monotonic mapping $\psi = f(\phi)$, then the transformation from $n(\psi)$ to $n(\phi)$ is given by

$$n(\phi) = n(\psi)\frac{d\psi}{d\phi} \tag{3.11}$$

PROOF

Start off with two corresponding distribution segments, as shown in Figure 3-2, then increment each of these intervals by a corresponding $\Delta\phi$ and $\Delta\psi$. Because we have $\psi = f(\phi)$, we can require that:

$$f(\phi + \Delta\phi) = \psi + \Delta\psi \tag{3.12}$$

This condition also stipulates that an equal number of particles have been added to these two distributions by incrementing by $\Delta\phi$ and $\Delta\psi$, respectively.

$$n(\phi)\Delta\phi = \Delta N = n(\psi)\Delta\psi \tag{3.13}$$

Figure 3-3 illustrates these increments added onto the initial distribution segments.

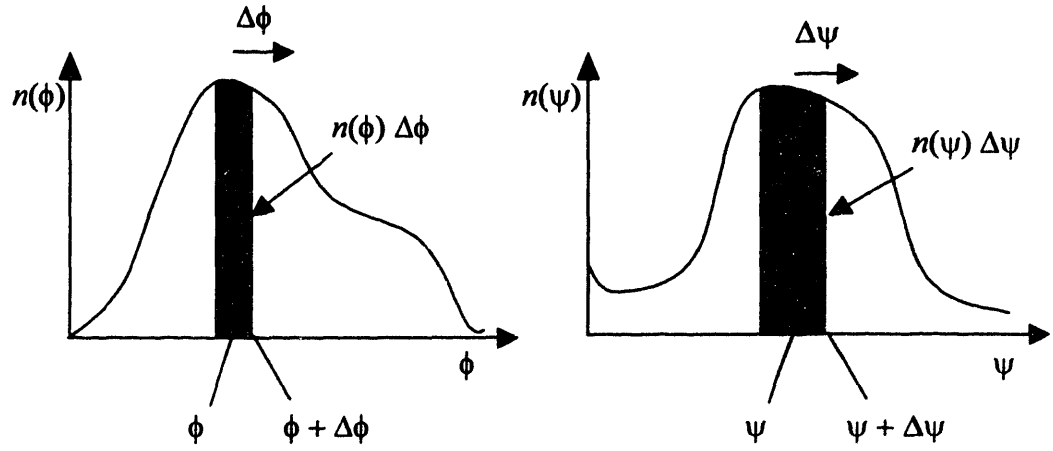

Figure 3-3: Equality of distribution transform from n(ϕ) to n(ψ) when interval is incremented.

However, we know that $\Delta\phi = (\phi + \Delta\phi) - \phi$ and $\Delta\psi = (\psi + \Delta\psi) - \psi$, so Equation (3.13) may be rewritten as:

$$\begin{aligned} n(\phi)[(\phi + \Delta\phi) - \phi] &= n(\psi)[(\psi + \Delta\psi) - \psi] \\ &= n(\psi)[f(\phi + \Delta\phi) - f(\phi)] \end{aligned} \tag{3.14}$$

Solving this expression for $n(\phi)$ yields:

$$\begin{aligned} n(\phi) &= n(\psi)\frac{[f(\phi + \Delta\phi) - f(\phi)]}{[(\phi + \Delta\phi) - \phi]} \\ &= n(\psi)\frac{f(\phi + \Delta\phi) - f(\phi)}{\Delta\phi} \end{aligned} \tag{3.15}$$

The limit of this expression as the length of the interval $\Delta\phi$ approaches zero is readily recognized as a derivative:

$$\begin{aligned} &\lim_{\Delta\phi \to 0}\left(n(\phi) = n(\psi)\frac{f(\phi + \Delta\phi) - f(\phi)}{\Delta\phi}\right) \\ &n(\phi) = n(\psi)\frac{df(\phi)}{d\phi} \\ &n(\phi) = n(\psi)\frac{d\psi}{d\phi} \end{aligned} \tag{3.16}$$

QED

Note that the mapping must obviously be strictly monotonic in order to ensure that each unique

interval in ϕ has a corresponding unique interval in ψ. Because f is differentiable, it is also continuous (Rudin, 1976). Also, because the mapping is 1-1 and continuous, there exists an inverse function $f^{-1}(\psi) = \phi$. Finally, if we assume that this inverse mapping is also differentiable, then the Inverse Function Theorem (Strichartz, 1995) states that:

$$\frac{df^{-1}(\psi)}{d\psi} = \frac{1}{\left(\frac{df(\phi)}{d\phi}\right)} = \frac{1}{\left(\frac{d\psi}{d\phi}\right)} \tag{3.17}$$

Note that this conveniently provides the inverse transformation:

$$n(\psi) = n(\phi)\frac{df^{-1}(\psi)}{d\psi} = \frac{n(\phi)}{\left(\frac{d\psi}{d\phi}\right)} \tag{3.18}$$

Using this general property, numerous different transformations can be performed, as summa-

rized in Table 3-3.

Table 3-3: Common transformations

From	*Units*	*To*	*Units*	*Relation*	*Transform*
$n(v)$	$1/cm^3$	$n(D_p)$	$1/cm^3$	$v = \frac{4}{3}\pi\left(\frac{D_p}{2}\right)^3$	$n(D_p) = n(v)\frac{\pi D_p^2}{2}$
$n(v)$	$1/cm^3$	$n(m)$	1/g	$v = \frac{m}{\rho}$	$n(m) = \frac{n(v)}{\rho}$
$n(v)$	$1/cm^3$	$n(y) = n(\ln(v))$	none	$y = \ln(v)$	$n(y) = \frac{n(v)}{v}$ $n(\ln(v)) = \frac{n(v)}{v}$
$n(v)$	$1/cm^3$	$n(w)$	none	$v = v_o e^{\gamma w}$	$n(w) = \frac{n(v)}{\gamma w}$
$n(v)$	$1/cm^3$	$n(s)$	$1/cm^2$	$v = \frac{4\pi}{3}\left(\frac{s}{4\pi}\right)^{3/2}$	$n(s) = \frac{n(v)}{2}\left(\frac{3v}{4\pi}\right)^{1/3}$
$n(v)$	$1/cm^3$	$n(y) = n(\log(v))$	none	$y = \log(v)$	$n(y) = \frac{n(v)}{2.303v}$ $n(\log(v)) = \frac{n(v)}{2.303v}$
$n(D_p)$	1/cm	$n(y) = n(\ln(D_p))$	none	$y = \ln(D_p)$	$(\log(D_p)) = \frac{n(D_p)}{2.303D_p}$

Figure 3-4 illustrates several of these transforms.

Often, distributions exist over many orders of magnitude, and are more clearly represented using logarithmic scales. Many different transformations between different scales can be constructed by simply conserving the number of particles in the transformation. For example, if we wish to use $\ln(m)$ as the independent variable instead of m, the new number density representation must contain the number of particles in the size range between $\ln(m)$ and $\ln(m + dm)$ as the $n(m)$ representation contained in the size range between m and $m + dm$.

3.2.4 One-component transformation example

Differentiating the cumulative number distribution Equation (2.7) with respect to particle

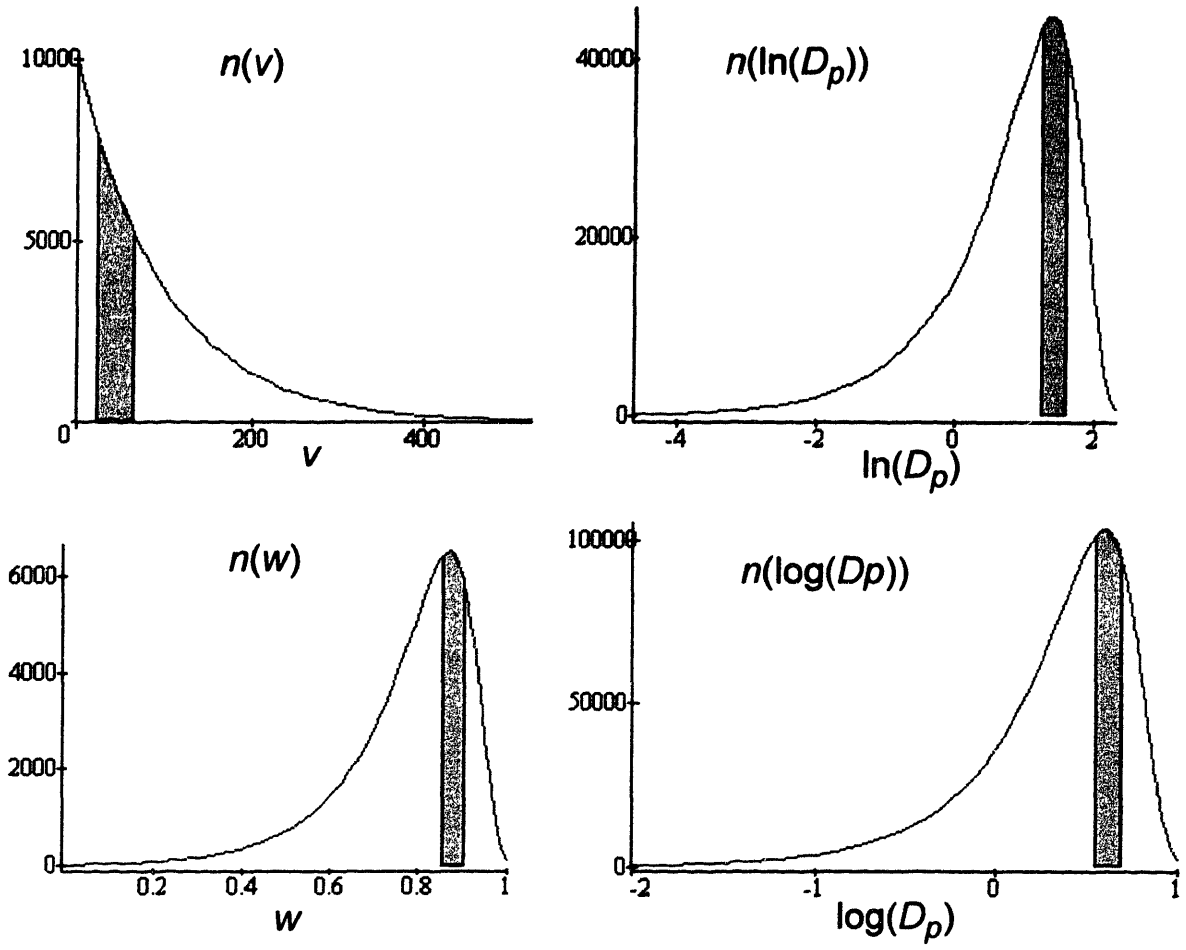

Figure 3-4: Summary of various transformations on *n(v)*.

mass gives the differential change in number of particles as a function of number distribution:

$$dN = n(m)dm \rightarrow n(m) = \frac{dN}{dm} \tag{3.19}$$

The key to performing a transformation is to ensure that the dN remains constant. Defining $n[\ln(m)]$ in the same spirit as $n(m)$:

$$N(m) = \int_0^m n[\ln(m')]d\ln(m') \rightarrow dN = n[\ln(m)]d\ln(m) = n[\ln(m)]\frac{1}{m}dm \tag{3.20}$$

which leads directly to the transformation:

$$n[\ln(m)]\frac{1}{m}dm = n(m)dm \rightarrow n(\ln(m)) = m \cdot n(m) \tag{3.21}$$

Because it is impossible to take the natural logarithm of a dimensioned quantity, $\ln(m)$ is actually implicitly understood to mean $\ln(m/1)$ where 1 has units of mass. Correspondingly, the quantity $n[\ln(m)]$ must also be dimensionless in order for $n(m)$ to be dimensionless as well. Some common logarithmic scaling transformations (Seinfeld and Pandis, 1998) are listed in Table 3-4.

Table 3-4: Common logarithmic scaling transformations

$n[\ln(m)] = m \cdot n(m) = \frac{dN}{d\ln(m)}$
$n[\log(m)] = \ln(10)m \cdot n(m) = \frac{dN}{d\log(m)}$

3.3 Multicomponent Transformations

In multicomponent systems, transformations still provide an important tool for manipulating distributions. Take the two-dimensional exponential distribution, for instance.

$$n(m_1, m_2) = N_0 \frac{e^{(-m_1/m_{10})}}{m_{10}} \frac{e^{(-m_2/m_{20})}}{m_{20}} \tag{3.22}$$

Just as in the one-component case, it is necessary that any transformation conserve number in a differential element of the distribution. For the general case where the transform is from $n(\phi_1, \phi_2)$ to $n(\psi_1, \psi_2)$, the conservation of number results in Equation (3.23).

$$n(\phi_1, \phi_2)d\phi_1 d\phi_2 = n(\psi_1, \psi_2)d\psi_1 d\psi_2 \tag{3.23}$$

3.3.1 Two-component transformation example: $n(m_1, m_2)$ to $n(\ln(m_1), \ln(m_2))$

For the case where the desired transform is from $n(m_1, m_2)$ to $n(\ln(m_1), \ln(m_2))$, it is easy to perform two successive one-dimensional transformations, as shown in Equation (3.24).

$$\begin{aligned} &(1) \qquad n(m_1, m_2) \rightarrow n(m_1, \ln(m_2)) \\ &(2) \qquad n(m_1, \ln(m_2)) \rightarrow n(\ln(m_1), \ln(m_2)) \end{aligned} \tag{3.24}$$

The first transformation is detailed in Equation (3.25).

$$\begin{aligned} n(m_1, \ln(m_2))dm_1 d\ln(m_2) &= n(m_1, m_2)dm_1 dm_2 \\ n(m_1, \ln(m_2))d\ln(m_2) &= n(m_1, m_2)dm_2 \\ n(m_1, \ln(m_2)) &= n(m_1, m_2)\frac{dm_2}{d\ln(m_2)} \\ n(m_1, \ln(m_2)) &= n(m_1, m_2)m_2 \end{aligned} \tag{3.25}$$

Note that the terms dm_1 on both sides of Equation (3.25) cancel in the second step. Equation (3.26) gives the form of $n(m_1, \ln(m_2))$ produced by this transformation.

$$\begin{aligned} n(m_1, \ln(m_2)) &= N_0 \frac{e^{(-m_1/m_{10})}}{m_{10}} \frac{e^{(-m_2/m_{20})}}{m_{20}} m_2 \\ &= N_0 \frac{e^{(-m_1/m_{10})}}{m_{10}} \frac{e^{(-e^{\ln m_2}/m_{20})}}{m_{20}} e^{\ln m_2} \end{aligned} \tag{3.26}$$

The transformation from $n(m_1, \ln(m_2))$ to $n(\ln(m_1), \ln(m_2))$ is very similar to the first transformation, as shown in Equation (3.27).

$$\begin{aligned} n(\ln(m_1), \ln(m_2))d\ln(m_1)d\ln(m_2) &= n(m_1, \ln(m_2))dm_1 d\ln(m_2) \\ n(\ln(m_1), \ln(m_2))d\ln(m_1) &= n(m_1, \ln(m_2))dm_1 \\ n(\ln(m_1), \ln(m_2)) &= n(m_1, \ln(m_2))\frac{dm_1}{d\ln(m_1)} \\ n(\ln(m_1), \ln(m_2)) &= n(m_1, \ln(m_2))m_1 \end{aligned} \tag{3.27}$$

Using both of these transformations in succession leads to the desired overall transformation, given in Equation (3.29).

$$\begin{aligned} n(\ln(m_1), \ln(m_2)) &= n(m_1, \ln(m_2))m_1 \\ &= [n(m_1, m_2)m_2]m_1 \end{aligned} \tag{3.28}$$

$$\boxed{n(\ln(m_1), \ln(m_2)) = n(m_1, m_2)m_1 m_2} \tag{3.29}$$

For the set of parameters given in Table 3-5, the resulting transformation from $n(m_1, m_2)$ to $n(m_1,$

$\ln(m_2)$) and then finally to $n(\ln(m_1), \ln(m_2))$ is illustrated in Figure 3-5.

Table 3-5: Two-dimensional exponential distribution parameters

Symbol	*Name*	*Value*	*Units*
N_0	Total number	1.0×10^{6}	-
m_{10}	First exponential parameter	1.0×10^{-13}	1/mass
m_{20}	Second exponential parameter	2.0×10^{-13}	1/mass

To check the accuracy of this transform, we can always integrate each distribution function over its corresponding range to determine the number of particles present in each segment. The respective integrals are given in Equation (3.30).

$$
\begin{aligned}
N &= \int_{b_1 a_1}^{b_2 a_2} \int n(m_1, m_2) dm_1 dm_2 \\
N &= \int_{b_1 a_1}^{b_2 a_2} \int n(m_1, \ln(m_2)) dm_1 d\ln(m_2) \\
N &= \int_{b_1 a_1}^{b_2 a_2} \int n(\ln(m_1), \ln(m_2)) d\ln(m_1) d\ln(m_2)
\end{aligned}
\tag{3.30}
$$

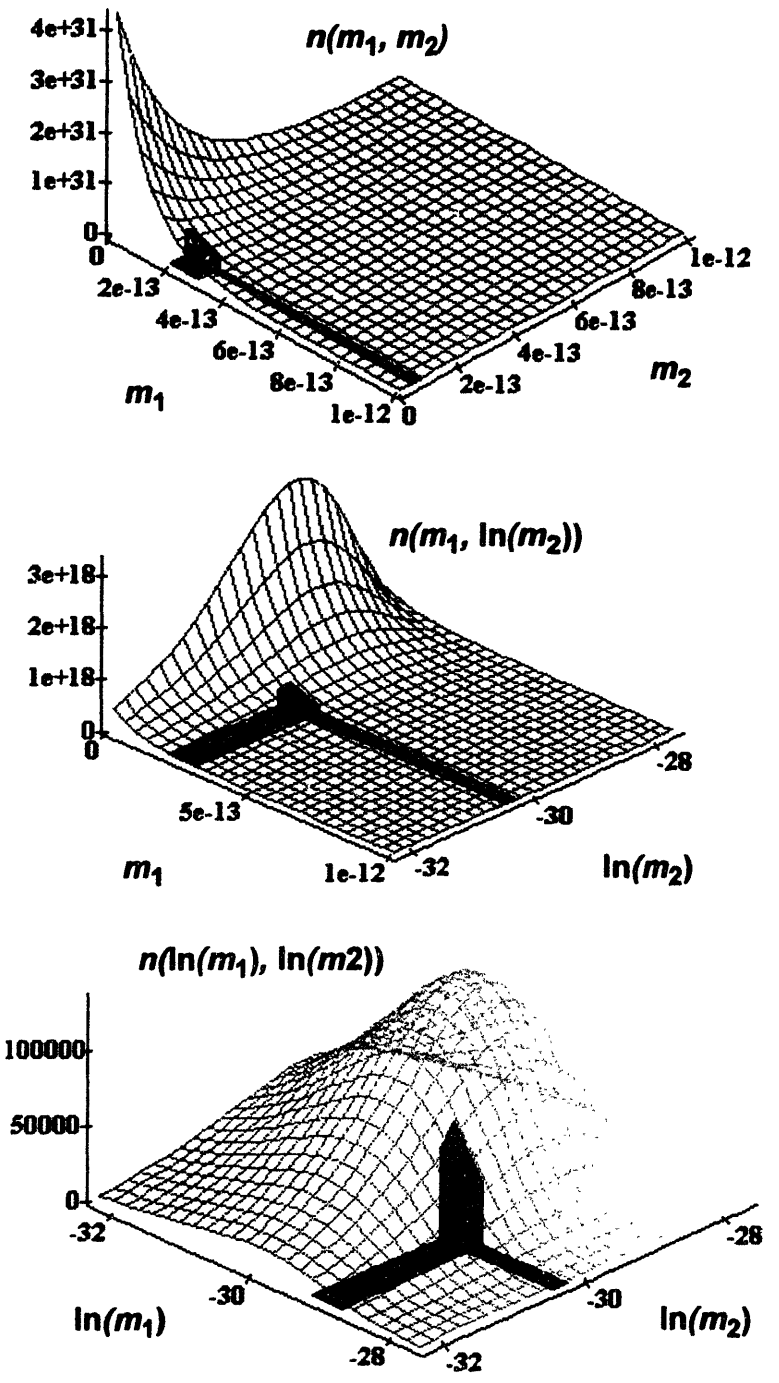

Figure 3-5: Two component transformation stepwise presentation from $n(m_1, m_2)$ to $n(\ln(m_1), \ln(m_2))$.

Table 3-6 gives the corresponding values of the integration limits for each set of integrals. Note

Table 3-6: Integration limits and N for $n(m_1, m_2)$ to $n(\ln(m_1), \ln(m_2))$ transformation

Distribution	a_1	a_2	b_1	b_2	N
$n(m_1, m_2)$	2.0×10^{-13}	3.0×10^{-13}	6.0×10^{-14}	8.0×10^{-14}	6031
$n(m_1, \ln(m_2))$	2.0×10^{-13}	3.0×10^{-13}	−30.4	−30.2	6031
$n(\ln(m_1), \ln(m_2))$	−29.2	−28.8	−30.4	−30.2	6031

the agreement in N, the total number of particles in each segment, validating the transformation.

3.3.2 Proof of two-component transformation theorem

This two-component transformation formula may be stated more generally for monotonic functions by the following theorem.

THEOREM

For any pair of two-component distributions $n(\phi_1, \phi_2)$ and $n(\psi_1, \psi_2)$, if there exists a differentiable monotonic mapping $\psi = f(\phi)$, then the transformation to $n(\phi_1, \phi_2)$ from $n(\psi_1, \psi_2)$ is given by

$$n(\phi_1, \phi_2) = n(\psi_1, \psi_2) \lim_{\Delta\phi_1, \Delta\phi_2 \to 0} \frac{[f_1(\phi + \Delta\phi)f_2(\phi + \Delta\phi) - f_1(\phi)f_2(\phi)]}{[\phi_1\Delta\phi_2 + \Delta\phi_1\Delta\phi_2 + \Delta\phi_1\phi_2]} \tag{3.31}$$

PROOF

Just as with the one-component case, we begin by analyzing the number of particles added to

the system as the boundaries of a population segment are increased.

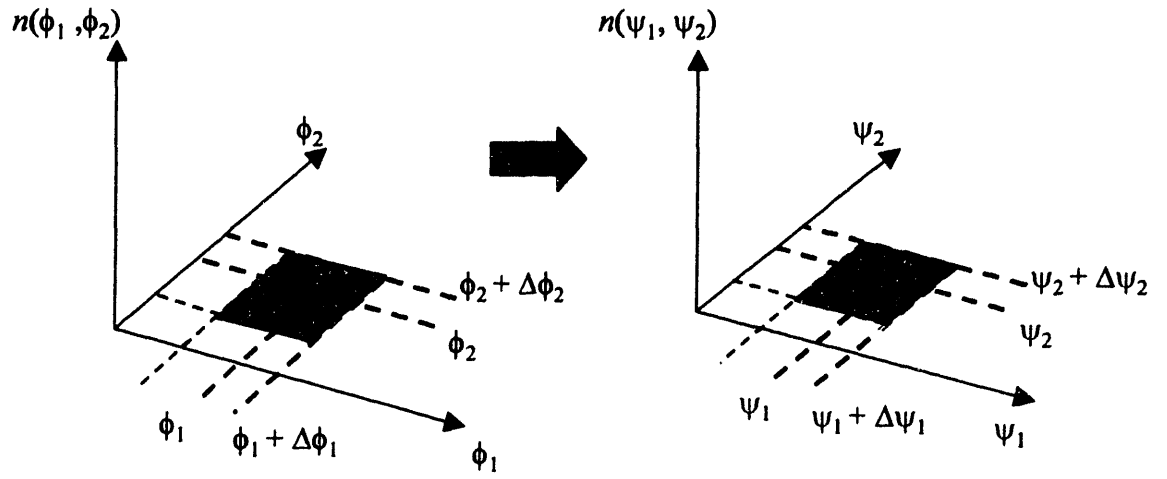

Figure 3-6: Area comparison of two-dimensional transformation.

For the corresponding two-dimensional distribution elements $(\phi_1 + \Delta\phi_1, \phi_2 + \Delta\phi_2)$ and $(\psi_1 + \Delta\psi_1, \psi_2 + \Delta\psi_2)$, shown in Figure 3-6, the relation equating the incremental increase in the number of particles in these element comes directly from the definition of a multicomponent distributions (see Section 2.8).

$$\begin{aligned} n(\phi_1, \phi_2) &= \frac{dN}{dA} = n(\psi_1, \psi_2) \\ n(\phi_1, \phi_2)dA_\phi &= dN = n(\psi_1, \psi_2)dA_\psi \end{aligned} \tag{3.32}$$

The increase in area with the increment in each dimension is calculated as the shaded areas of the corresponding parts of Figure 3-6.

$$\begin{aligned} dA_\phi &= (\phi_1 + \Delta\phi_1)(\phi_2 + \Delta\phi_2) - \phi_1\phi_2 \\ dA_\psi &= (\psi_1 + \Delta\psi_1)(\psi_2 + \psi_2) - \psi_1\psi_2 \end{aligned} \tag{3.33}$$

Substituting these expressions for the differential increase in area into Equation (3.32) results in Equation (3.34).

$$n(\phi_1, \phi_2)[(\phi_1 + \Delta\phi_1)(\phi_2 + \Delta\phi_2) - \phi_1\phi_2] = n(\psi_1, \psi_2)[(\psi_1 + \Delta\psi_1)(\psi_2 + \Delta\psi_2) - \psi_1\psi_2] \tag{3.34}$$

Recalling the condition that $\psi = f(\phi)$, Equation (3.34) can be rearranged as follows, where ϕ is used to denote the vector $\phi = [\phi_1, \phi_2]$:

$$n(\phi_1, \phi_2)[(\phi_1 + \Delta\phi_1)(\phi_2 + \Delta\phi_2) - \phi_1\phi_2]$$
$$= n(\psi_1, \psi_2)[f_1(\phi_1 + \Delta\phi_1, \phi_2 + \Delta\phi_2)f_2(\phi_1 + \Delta\phi_1, \phi_2 + \Delta\phi_2) - f_1(\phi_1, \phi_2)f_2(\phi_1, \phi_2)] \quad (3.35)$$
$$= n(\psi_1, \psi_2)[f_1(\phi + \Delta\phi)f_2(\phi + \Delta\phi) - f_1(\phi)f_2(\phi)]$$

Likewise, Equation (3.35) can be further rearranged to reflect a simplification in the ϕ_1 and ϕ_2 terms.

$$n(\phi_1, \phi_2)[(\phi_1 + \Delta\phi_1)(\phi_2 + \Delta\phi_2) - \phi_1\phi_2] = n(\phi_1, \phi_2)[\phi_1\Delta\phi_2 + \Delta\phi_1\Delta\phi_2 + \Delta\phi_1\phi_2] \quad (3.36)$$

Finally, solving for the desired expression $n(\phi_1, \phi_2)$ results in Equation (3.37).

$$n(\phi_1, \phi_2)[\phi_1\Delta\phi_2 + \Delta\phi_1\Delta\phi_2 + \Delta\phi_1\phi_2] = n(\psi_1, \psi_2)[f_1(\phi + \Delta\phi)f_2(\phi + \Delta\phi) - f_1(\phi)f_2(\phi)]$$
$$n(\phi_1, \phi_2) = n(\psi_1, \psi_2)\frac{[f_1(\phi + \Delta\phi)f_2(\phi + \Delta\phi) - f_1(\phi)f_2(\phi)]}{[\phi_1\Delta\phi_2 + \Delta\phi_1\Delta\phi_2 + \Delta\phi_1\phi_2]} \quad (3.37)$$

However, in order to obtain a final transformation from $n(\psi_1, \psi_2)$ to $n(\phi_1, \phi_2)$ we must take the limit of this expression as $\Delta\phi_1, \Delta\phi_2$ decrease to zero.

$$n(\phi_1, \phi_2) = n(\psi_1, \psi_2)\lim_{\Delta\phi_1, \Delta\phi_2 \to 0}\left(\frac{[f_1(\phi + \Delta\phi)f_2(\phi + \Delta\phi) - f_1(\phi)f_2(\phi)]}{[\phi_1\Delta\phi_2 + \Delta\phi_1\Delta\phi_2 + \Delta\phi_1\phi_2]}\right) \quad (3.38)$$

QED

3.4 Two-component Transformation Example: $n(m_1, m_2)$ to $n(m, x)$

3.4.1 Basis for the transformation

The transformation from $n(m_1, m_2)$ to $n(\ln(m_1), \ln(m_2))$ is a direct extension of single-component transformations. Using the result that both $\ln(m_1)$ and $\ln(m_2)$ are monotonic in both m_1 and m_2, we can apply Equation (3.38) to derive a transformation or we can perform successive one-dimensional transformations. However, consider a system that does not have a monotonic set of coordinate transformations.

$$\boxed{\begin{aligned} m &= m_1 + m_2 \\ x &= \frac{m_1}{m_1 + m_2} \end{aligned}} \Leftrightarrow \boxed{\begin{aligned} m_1 &= m \cdot x \\ m_2 &= m \cdot (1 - x) \end{aligned}} \quad (3.39)$$

$$\begin{aligned} m_1 &= f_1(m, x) = m \cdot x \\ m_2 &= f_2(m, x) = m \cdot (1 - x) \end{aligned} \quad (3.40)$$

The transformation from $n(m_1, m_2)$ to $n(m, x_1)$ is more complicated to derive; because it is not monotonic in both variables, a separate analysis comparing the differential areas of corresponding distribution segments must be undertaken.

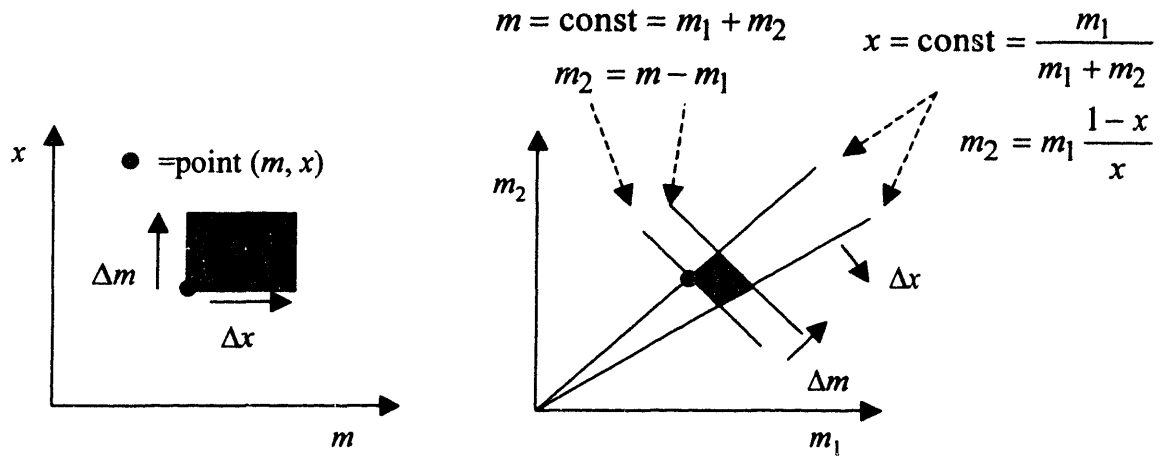

Figure 3-7: Corresponding segments for $n(m_1, m_2)$ and $n(m, x)$ distributions.

A quick glance at Figure 3-7 reveals that the simple area segment from the point (m, x) to $(m + \Delta m, x + \Delta x)$ is bounded by two lines in m - x space: two where x is constant and two more where m is constant. Translating these boundaries into m_1 - m_2 space results in the boundary lines illustrated in Figure 3-7, with the corresponding shaded segment. In order to define a transformation between these two coordinate systems, it in necessary to apply Equation (3.32) with the new set of variables.

$$\begin{aligned} n(\phi_1, \phi_2)dA_\phi &= n(\psi_1, \psi_2)dA_\psi \\ n(m, x)dA_1 &= n(m_1, m_2)dA_2 \\ n(m, x) &= n(m_1, m_2)\frac{dA_2}{dA_1} \end{aligned} \tag{3.41}$$

3.4.2 Derivation of the transformation

One method of calculating the ratios of these two areas is to start with a corresponding set of points (m, x) and (m_1, m_2) and then to create a differential area covering the range from m to $m + \Delta m$ and x to $x + \Delta x$ as shown on the left side of Figure 3-7. This differential area is trivial to calculate and familiar.

$$dA_1 = \Delta m \cdot \Delta x \tag{3.42}$$

However, the corresponding increase in the differential area dA_2 is a function of the increments in m and x, as related by Equation (3.39). Figure 3-8 illustrates the corresponding area dA_2 created by taking corresponding interval from the point (m_1, m_2), which is related to the original point (m, x) via Equation (3.39). The boundaries on this interval are determined by equations marking lines of constant m and x, respectively, in the m_1 - m_2 space.

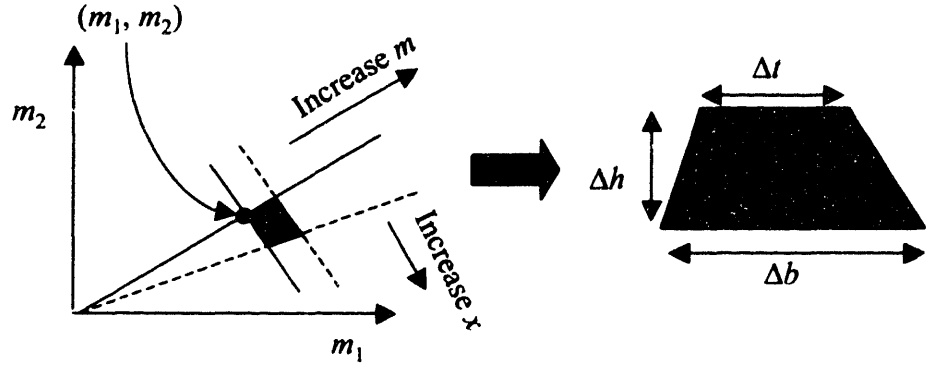

Figure 3-8: Area in the corresponding region of $n(m_1, m_2)$.

Noting that the lines of constant m all have slope -1 and are therefore paralliel, the area of dA_2 is given by Equation (3.43).

$$dA_2 = \frac{1}{2}(\Delta b + \Delta t)\Delta h \tag{3.43}$$

The key is now to related the quantities Δb, Δt, and Δh back to the original increments Δm and Δx and then take the limits the ratio dA_2/dA_1 with respect to these two variables to obtain the transform.

First, it should be noted that Δh will equal the amount that the constant m line moves as m is incremented. The distance this line moves can be measured using the aid of the line $x = 0.5$, which is perpendicular to the constant m lines, as shown in Figure 3-9. Recalling that the line $x = 0.5$ will intersect the constant m line at $(m/2, m/2)$, the distance Δh is easily calculated in Equation (3.44).

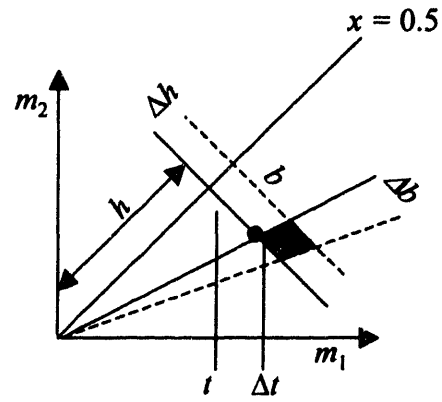

Figure 3-9: Distance of Δh as calculated using the perpendicular line $x = 0.5$.

$$h = \sqrt{m_1^2 + m_2^2} = \sqrt{\left(\frac{m}{2}\right)^2 + \left(\frac{m}{2}\right)^2} = \frac{m}{\sqrt{2}}$$

$$h + \Delta h = \sqrt{m_1^2 + m_2^2} = \sqrt{\left(\frac{m + \Delta m}{2}\right)^2 + \left(\frac{m + \Delta m}{2}\right)^2} = \frac{m + \Delta m}{\sqrt{2}} \tag{3.44}$$

$$\Delta h = \frac{\Delta m}{\sqrt{2}}$$

In order to solve for the values Δb and Δt, a similar approach is used to calculate the distance between points on the line m = constant and its intersection with the line $x = 0.5$. In Equation (3.45), the m^* values represent the coordinates at the intersection with the line $x = 0.5$.

$$\text{distance} = \sqrt{(m_1 - m_1^*)^2 + (m_2 - m_2^*)^2} \tag{3.45}$$

Recalling that $m_1 = m \cdot x$, $m_2 = m \cdot (1 - x)$ and that $m_1^* = m_2^* = \frac{m}{2}$ yields the correct distance formula.

$$\text{distance} = \sqrt{\left(mx - \frac{m}{2}\right)^2 + \left(m(1 - x) - \frac{m}{2}\right)^2}$$

$$= m\sqrt{\left(x - \frac{1}{2}\right)^2 + \left(\frac{1}{2} - x\right)^2} \tag{3.46}$$

$$\text{distance} = m\sqrt{2}\left(x - \frac{1}{2}\right)$$

Note that this is a general distance formula which allows us to calculate both Δb and Δt.

$$\begin{aligned} b &= (m+\Delta m)\sqrt{2}\left(x-\frac{1}{2}\right) \\ b+\Delta b &= (m+\Delta m)\sqrt{2}\left(x+\Delta x-\frac{1}{2}\right) \\ \Delta b &= (b+\Delta b)-b = (m+\Delta m)\sqrt{2}\Delta x \end{aligned} \tag{3.47}$$

Thus, Δb can be calculated entirely in terms of m, Δm, and Δx.

$$\boxed{\Delta b = (m+\Delta m)\sqrt{2}\Delta x} \tag{3.48}$$

Likewise, the distance formula can be used to calculate Δt.

$$\begin{aligned} t &= m\sqrt{2}\left(x-\frac{1}{2}\right) \\ t+\Delta t &= m\sqrt{2}\left(x+\Delta x-\frac{1}{2}\right) \\ \Delta t &= (t+\Delta t)-t = m\sqrt{2}\Delta x \end{aligned} \tag{3.49}$$

We can now state Δt entirely in terms of m and Δx.

$$\boxed{\Delta t = m\sqrt{2}\Delta x} \tag{3.50}$$

Substituting these expressions into Equation (3.43) yields the expression for a_2 and in turn the ratio of the areas.

$$\begin{aligned} dA_2 &= \frac{1}{2}(\Delta b+\Delta t)\Delta h \\ dA_2 &= \frac{1}{2}((m+\Delta m)\sqrt{2}\Delta x + m\sqrt{2}\Delta x)\frac{\Delta m}{\sqrt{2}} \\ \frac{dA_2}{dA_1} &= \frac{\frac{1}{2}[(m+\Delta m)\sqrt{2}\Delta x + m\sqrt{2}\Delta x]\frac{\Delta m}{\sqrt{2}}}{\Delta m \Delta x} \end{aligned} \tag{3.51}$$

Taking the limits of this ratio of areas with respect to Δm and Δx yields the desired transformation.

$$\boxed{n(m,x) = n(m_1,m_2)m = n(m_1,m_2)(m_1+m_2)} \tag{3.52}$$

3.4.3 Verification of the transformation

The validity of this transformation can again be checked by integrating over corresponding segments of two distributions. For convenience, the same limits in $n(m_1, m_2)$ are used as in previous sections with the usual exponential distribution. Note the transformed version of the distribution, given in Equation (3.50).

$$n(m,x) = N_0 \frac{e^{(-mx/m_{10})}}{m_{10}} \frac{e^{(-m(1-x)/m_{20})}}{m_{20}} m \tag{3.53}$$

In order to use the integration limits given in Table 3-6, we must first determine the translated integration limits in the m - x space. For the integration limit lines where m_1 is constant, we now have a hyperbola in the m - x space.

$$m_1 = \text{constant} = mx \rightarrow x = \frac{m_1}{m} \tag{3.54}$$

Likewise, the integration limits where m_2 is constant also translate into a hyperbola, as shown in Equation (3.55).

$$m_2 = \text{constant} = m(1-x) \rightarrow x = 1 - \frac{m_2}{m} \tag{3.55}$$

Translating both of the limits given in Table 3-6 to the new m - x coordinate system results in the new set of integration limits summarized in Table 3-7.

Table 3-7: Transformed integration limits in m - x coordinates

Old Limit	*Equation*	*New Limit*
Lower m_1	$m_{1,\text{low}} = 2.0\times10^{-13}$	$x = \frac{m_{1,\text{low}}}{m} = \frac{2.0\times10^{-13}}{m}$
Upper m_1	$m_{1,\text{high}} = 3.0\times10^{-13}$	$x = \frac{m_{1,\text{high}}}{m} = \frac{3.0\times10^{-13}}{m}$
Lower m_2	$m_{2,\text{low}} = 6.0\times10^{-14}$	$x = 1 - \frac{m_{2,\text{low}}}{m} = 1 - \frac{6.0\times10^{-14}}{m}$
Upper m_2	$m_{2,\text{high}} = 8.0\times10^{-14}$	$x = 1 - \frac{m_{2,\text{high}}}{m} = 1 - \frac{8.0\times10^{-14}}{m}$

Figure 3-10 graphs the transformed integration limits in the coordinate system m - x.

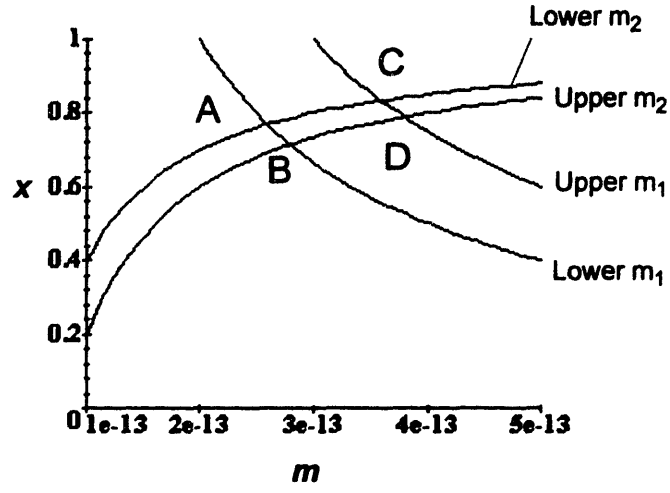

Figure 3-10: Transformed integration limits in m-x coordinates.

Note how the four vertices naturally split the m axis into three separate intervals for integration from points A to B, B to C, and C to D, respectively. The m coordinates of these points is calculated by taking the intersections of the corresponding limit lines as given in Table 3-7; the values of m at these vertices represent the various combinations of the upper and lower limits for m_1 and m_2, as summarized in Table 3-8.

Table 3-8: Transformed population limit vertices

Point	*symbolic m-value*	*numeric m-value*
A	$m_{1,\,low} + m_{1,\,high}$	2.6×10^{-13}
B	$m_{1,\,low} + m_{2,\,high}$	2.8×10^{-13}
C	$m_{1,\,high} + m_{2,\,low}$	3.6×10^{-13}
D	$m_{1,\,high} + m_{2,\,high}$	3.8×10^{-13}

Table 3-9 summarizes the resulting integration limits in both x and m coordinates.

Table 3-9: Summary of transformed integration limits

Integral	*Lower m*	*Upper m*	*Lower x*	*Upper x*	*Number*
$A \rightarrow B$	$m_{1,\,\mathrm{low}} + m_{1,\,\mathrm{high}}$	$m_{1,\,\mathrm{low}} + m_{2,\,\mathrm{high}}$	$\frac{m_{1,\,\mathrm{low}}}{m}$	$1 - \frac{m_{2,\,\mathrm{low}}}{m}$	908
$B \rightarrow C$	$m_{1,\,\mathrm{low}} + m_{2,\,\mathrm{high}}$	$m_{1,\,\mathrm{high}} + m_{2,\,\mathrm{low}}$	$1 - \frac{m_{2,\,\mathrm{high}}}{m}$	$1 - \frac{m_{2,\,\mathrm{low}}}{m}$	4754
$C \rightarrow D$	$m_{1,\,\mathrm{high}} + m_{2,\,\mathrm{low}}$	$m_{1,\,\mathrm{high}} + m_{2,\,\mathrm{high}}$	$1 - \frac{m_{2,\,\mathrm{high}}}{m}$	$\frac{m_{1,\,\mathrm{high}}}{m}$	369

Equations (3.56) through (3.58) write out these integrals in full and their respective values.

$$N_1 = \int_A^B \int_{\left(\frac{m_{1,\,\mathrm{low}}}{m}\right)}^{\left(1 - \frac{m_{2,\,\mathrm{low}}}{m}\right)} n(m,x)\,dx\,dm = 908 \tag{3.56}$$

$$N_2 = \int_B^C \int_{\left(1 - \frac{m_{2,\,\mathrm{high}}}{m}\right)}^{\left(1 - \frac{m_{2,\,\mathrm{low}}}{m}\right)} n(m,x)\,dx\,dm = 4754 \tag{3.57}$$

$$N_3 = \int_C^D \int_{\left(1 - \frac{m_{2,\,\mathrm{high}}}{m}\right)}^{\left(\frac{m_{1,\,\mathrm{high}}}{m}\right)} n(m,x)\,dx\,dm = 369 \tag{3.58}$$

Totaling the results from all three of these integrals yields 6031, the number of particles held in the corresponding segment of the $n(m_1, m_2)$ graph (see Table 3-6). The validity of this transformation has thus been demonstrated. Figure 3-11 shows the transformed distribution with the pop-

ulation segments highlighted.

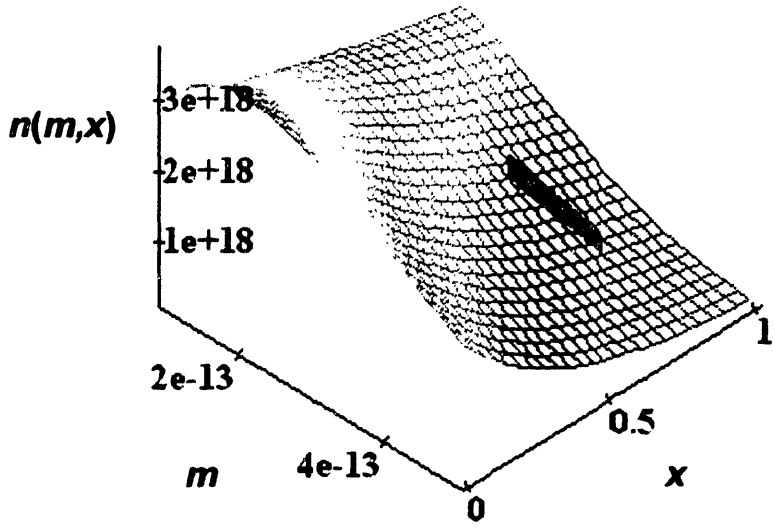

Figure 3-11: Example of transformation from $n(m_1, m_2)$ to $n(m, x)$.

3.4.4 General transformation formula

In general, multidimensional transformations use some function $\psi = f(\phi)$ to derive a transformation between coordinate systems. The heart of this transformation lies in the need to conserve the number of particles across each differential segment of these two distributions, expressed here in integral and differential form:

$$\begin{aligned} \int_T n(\phi)d\phi &= \int_{T'} n(\psi)d\psi \\ n(\phi)d\phi &= n(\psi)d\psi \end{aligned} \tag{3.59}$$

where T and T' represent respective integration regions. In fact, these transformations are directly analogous to transformations between probability density functions of random variables, and can be related by the following formula:

$$n(\psi) = n(\phi)|J| \tag{3.60}$$

where $|J|$ represents the determinant of the Jacobian J of the transformation function $f(\phi)$ with respect to the elements of ϕ. This formula is developed in Apostol (1969) and applied to examples of probability density functions for two-dimensional random variables.

References

[1] Apostol, Tom M. *Calculus,* 2nd Ed., John Wiley & Sons, 1969.

[2] Rudin, Walter *Principles of Mathematical Analysis,* McGraw-Hill, 1976.

[3] Seinfeld, John H.; Pandis, Spyros N. *Atmospheric Chemistry and Physics: From Air Pollution to Climate Change* John Wiley & Sons, Inc. 1998.

[4] Strichartz, Robert S. *The Way of Analysis,* Revised Edition, Jones & Bartlett, 2000.

Chapter 4: Dynamic Population Balance Equation

The dynamic population balance equation, also known as the general dynamic equation describes the dynamic evolution of a population. In its simplest form, it is used to model the number density of a population $n(\phi)$ as a function of time. As discussed in Chapter 2, ϕ can represent any of a large number of attributes including size, mass, volume, diameter, length, etc. More complex instances of the dynamic population balance occur when the number density of a population is modeled as a function of multiple characteristics, $n(\phi)$, where ϕ is a vector of characteristics. Models of this nature are referred to as multicomponent problems and will be addressed in Chapter 5. The dynamic population balance equation for a single component $n(\phi)$ is written as follows:

$$\frac{\partial n(\phi)}{\partial t} = \left.\frac{\partial n(\phi)}{\partial t}\right|_{Growth} + \left.\frac{\partial n(\phi)}{\partial t}\right|_{Coagulation} + \left.\frac{\partial n(\phi)}{\partial t}\right|_{Sources} + \left.\frac{\partial n(\phi)}{\partial t}\right|_{Fragmentation} + \text{etc.} \quad (4.1)$$

The following sections derive each of these terms individually. Note that the number of particles in these systems are not conserved; however, mass must be conserved, as always. For this reason, *mass is the natural variable to use to describe physical models because it is directly conserved.* For instance, because mass is conserved when particles coagulate it is easiest to express the mass of the resulting particle as a summation of the two coagulating particles. Contrast the ease of summing masses with the difficulty of determining the diameter of a particle created by the coagulation of two smaller particles.

$$\begin{aligned} m_1 + m_2 &= m \\ D_{p1} + D_{p2} &\neq D_p \end{aligned} \quad (4.2)$$

The dynamic population balance using mass as the basic representation variable is:

$$\frac{\partial n(m)}{\partial t} = \underbrace{\frac{1}{2}\int_0^m \beta(m-x,x)n(m-x)n(x)dx}_{\text{coagulation with smaller population members}} - \underbrace{n(m)\int_0^\infty \beta(m,x)n(x)dx}_{\text{coagulation with other population members}}$$
$$+ \underbrace{\int_m^\infty \gamma(x,m)n(x)dx}_{\text{fragmentation from larger members}} - \underbrace{n(m)\int_m^\infty \gamma(m,x)dx}_{\text{fragmentation to smaller members}}$$
$$- \underbrace{\nabla\cdot\mathbf{v}n(m)}_{\text{member convection}} + \underbrace{\nabla K\cdot\nabla n(m)}_{\text{member diffusion}} + \underbrace{f(m)}_{\text{special forcing effects}} \tag{4.3}$$

This equation describes the evolution of number density in a single-component system due to coagulation, fragmentation, and both convective and diffusive transport. The last term, "other functions" encompasses a wide variety of application-specific mechanisms, ranging from particle sources and sinks to growth, nucleation, etc. Before proceeding, the origin of each term in the dynamic population balance equation will be derived separately.

4.1 Coagulation

Coagulation refers to the process of two members of the population distribution colliding and combining to form one larger member of the population distribution. A classic example of coagulation occurs when you start to drive a wet car: some of the water droplets on the windshield begin to move and bump into other water droplets, forming larger water droplets. Each coagulation event involves two water droplets colliding to form one larger water droplet. If the resulting water droplet has mass c then the two colliding droplets must sum to this mass. Figure 4-1 illustrates the masses of coagulating particles.

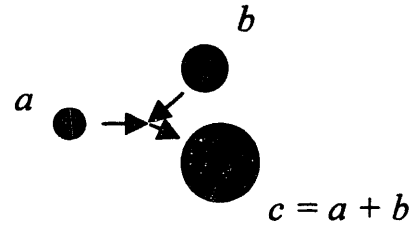

Figure 4-1: Binary coagulation of two smaller particles to form one larger particle.

Because typical population balance processes contain a large number of particles, a large number of coagulation events continuously occur. The coagulation kernel is defined as the rate expres-

sion describing the frequency of these coagulation events as a function of the coagulating particle sizes. Because coagulation is a binary process, we would expect that the overall coagulation rate follows a first-order rate law in the concentration of particles size a and b.

$$\text{rate} = k \cdot [a] \cdot [b] \tag{4.4}$$

However, instead of being a constant, k is a function of the particle sizes a and b. This function is formally defined as the coagulation kernel.

DEFINITION

The ***coagulation kernel*** $\beta(a, b)$ *is the rate function for the first-order process where particles of mass* $c = a + b$ *are formed due to the coagulation of two particles of masses a and b.*

$$\text{rate} = \beta(a, b) \cdot [a] \cdot [b] \tag{4.5}$$

Note that the coagulation kernel is a symmetrical function by definition as no distinction is made between the coagulating particles:

$$\beta(a, b) = \beta(b, a) \tag{4.6}$$

In any given system, coagulation can both create and usurp particles size m. These phenomena are referred to as *coagulation production* and *coagulation removal*, respectively. Coagulation production occurs when particles of mass m are created by the coagulation of smaller particles. Coagulation removal occurs when particles of mass m coagulate with other particles to form a larger particle, resulting in a net loss of particles of mass m. The following sections present contributions of these processes in the dynamic population balance equation.

4.1.1 Coagulation production

Coagulation production of particles with mass m occurs when two smaller particles coagulate. If one of these coagulating particles has mass x, then the other has mass $m - x$, as illustrated in Figure 4-2. Applying the definition of the coagulation kernel, $\beta(x, m - x)$ is the rate (units of *space* $\cdot$ *time*$^{-1}$ *particles*$^{-1}$) at which population members of mass m will be created by collisions between particles of mass x and $m - x$. The rate of increase of particles of mass m due to collisions between members of mass $m - x$ and x in a population $n(m)$ is the product of the coagulation kernel with the number of particles in each these respective mass ranges:

$$\frac{dn(m)\Delta m}{dt} = \beta(m-x, x)n(m-x)\Delta(m-x)n(x)\Delta x \tag{4.7}$$

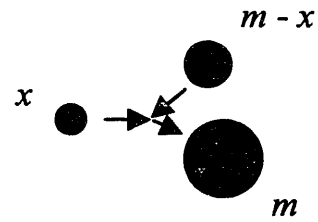

Figure 4-2: Coagulation production of particles with mass *m* due to the coagulation of two smaller particles of mass *x* and *m* - *x*.

Note the consistency of the units in this expression, as summarized in Equation (4.8) and Table 4-1.

Table 4-1: Coagulation production units

Symbol	*Units*
$n(m)$	$\frac{\text{particles}}{\text{cm}^3 \cdot \text{g}}$
Δm	g
dt	s
$\beta(m-x, x)$	$\frac{\text{cm}^3}{\text{particle} \cdot \text{s}}$
$n(m-x)$	$\frac{\text{particles}}{\text{cm}^3 \cdot \text{g}}$
$\Delta(m-x)$	g
$n(x)$	$\frac{\text{particles}}{\text{cm}^3 \cdot \text{g}}$
Δx	g

$$\frac{dn(m)\Delta m}{dt} = \beta(m-x, x)n(m-x)\Delta(m-x)n(x)\Delta x$$

$$\frac{\frac{\text{particles}}{\text{cm}^3 \cdot \text{g}} \cdot \text{g}}{\text{s}} = \frac{\text{cm}^3}{\text{particle} \cdot \text{s}} \cdot \frac{\text{particles}}{\text{cm}^3 \cdot \text{g}} \cdot \text{g} \cdot \frac{\text{particles}}{\text{cm}^3 \cdot \text{g}} \cdot \text{g} \tag{4.8}$$

In this formulation, the interval Δm must have the same width as both of the intervals $\Delta(m - x)$ and Δx added together, as shown in Figure 4-3.

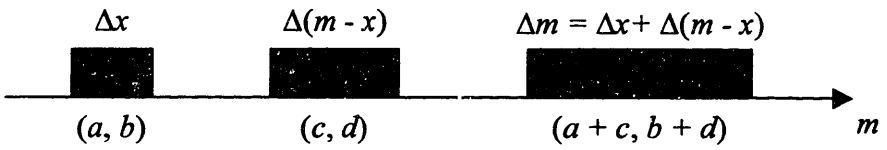

Figure 4-3: Binary coagulation intervals of two smaller particles to form one larger particle.

However, when the intervals Δm, $\Delta(m - x)$ and Δx become differentially small, these intervals shrink to differential widths and Equation (4.7) becomes a partial differential equation.

$$\frac{\partial n(m)dm}{\partial t} = \beta(m-x,x)n(m-x)d(m-x)n(x)dx \tag{4.9}$$

The terms $n(x)dx$ and $n(m - x)d(m - x)$ represent the *number* of population members in the differential slices in the size intervals $(x, x+ dx)$ and $(m - x, m - x + d(m - x))$, respectively, as shown in Table 4-2.

Table 4-2: Differential coagulation intervals

Variable	*Lower Limit*	*Upper Limit*	*Range*
x	x	$x + dx$	dx
$m-x$	$m-x$	$m-x+d(m-x)$	$d(m-x)$
m	m	$m + dm$	dm

Figure 4-4 shows an illustration of these differential coagulation intervals. Conveniently, the new

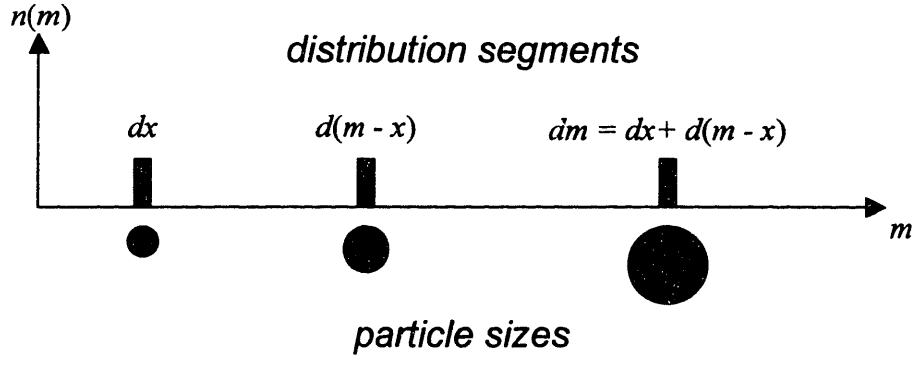

Figure 4-4: Differential coagulation intervals of two smaller particles to form one larger particle illustrated both as distribution segments and particle sizes.

definition of the combined particle interval *dm* is an identity enforced by the mass balance $m = x + (m - x)$. Note that we can divide Equation (4.9) through by *dm*, which results in:

$$\frac{\partial n(m)}{\partial t} = \beta(m-x, x)n(m-x)\frac{d(m-x)}{dm}n(x)dx \tag{4.10}$$

Recognizing that the derivative $d(m - x)/dm = 1$, the coagulation expression reaches its final form for two differential segments of a population containing particles sized x and $m - x$.

$$\frac{\partial n(m)}{\partial t} = \beta(m-x, x)n(m-x)n(x)dx \tag{4.11}$$

Note the consistency of units in this expression:

$$\underbrace{\frac{\partial n(m)dm}{\partial t}}_{\text{units}[=]\frac{1}{\text{time}\cdot\text{space}}} = \underbrace{\beta(m-x,x)}_{\text{units}[=]\frac{1}{\text{time}\cdot\text{space}}}\ \underbrace{n(m-x)d(m-x)}_{\text{units}[=]\frac{1}{\text{mass}}\cdot\text{mass}}\ \underbrace{n(x)dx}_{\text{units}[=]\frac{1}{\text{mass}}\cdot\text{mass}} \tag{4.12}$$

In general, "space" denotes normalization to the region where the population lives, be it in an area, volume, or linear space. For the windshield example, "space" would take on units of $length^2$. However, in most processes, space will take on some measure of volume - as given in Table 4-1. Note that this is a *binary* coagulation kernel because it only takes into account collisions of two population members at once to form a larger member. The effects of simultaneous collisions between more than two particles are neglected; in most cases this simplification is easily justified.

Finding the total contribution to members sized *m* from coagulation of all smaller population members requires that all combinations of particles size x and $m - x$ are taken into account (see Figure 4-5). As x takes on different values on the interval $(0, m)$, the value of $m - x$ also changes, as illustrated by the particles of different sizes and colors. In order to calculate the collective coagulation contribution from all of these smaller particle collisions over the continuous particle size range, one must integrate between 0 and *m*, as shown in Equation (4.13).

$$\boxed{\frac{\partial n(m)}{\partial t} = \frac{1}{2}\int_0^m \beta(x, m-x)n(x)n(m-x)dx} \tag{4.13}$$

As shown in Figure 4-5, each size particle is included twice when all of the combinations are

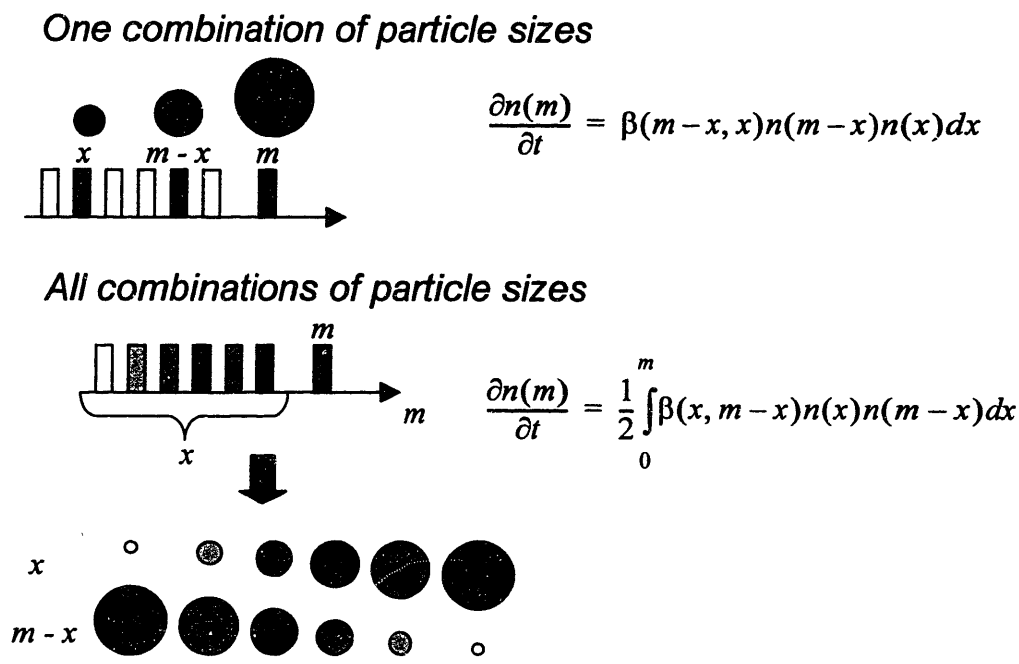

Figure 4-5: Integration of all combinations of *x* and *m-x* to form particles size *m*.

taken into account, once for the variable x and once for the variable $m - x$. To correct for this double-counting, the integral in Equation (4.13) is multiplied by a factor of ½. Note that we would arrive at this same result had we initially summed the coagulation contribution from a number of "bins" such as in Equation (4.7).

$$\frac{dn(m)\Delta m}{dt} = \frac{1}{2}\sum_i \beta(m-x,x_i)n(m-x)\Delta(m-x)n(x)_i\Delta x_i \tag{4.14}$$

As the Δx shrinks to a differential size interval, this expression is transformed into:

$$\frac{\partial n(m)dm}{\partial t} = \frac{1}{2}\int_0^m \beta(m-x,x)n(m-x)d(m-x)n(x)dx \tag{4.15}$$

where the fact that $d(m - x)/dm = 1$ reduces this expression to Equation (4.13).

4.1.2 Coagulation removal

By the same mechanism as in coagulation production, population members of size m can also be lost to coagulation, as shown in Figure 4-6. Using the same coagulation kernel as before, the loss of members size m due to coagulation with members size x is given in Equation (4.16).

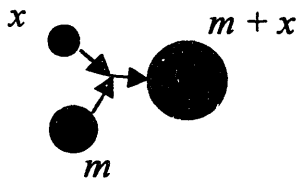

Figure 4-6: Loss of population members of mass *m* due to coagulation with other population members.

$$\frac{\partial n(m)dm}{\partial t} = -\beta(m,x)n(m)dm \cdot n(x)dx$$
$$\frac{\partial n(m)}{\partial t} = -\beta(m,x)n(m)n(x)dx \tag{4.16}$$

The coagulation kernel gives the rate at which particles of mass $m + x$ are created, however this is also the rate at which particles of mass m are usurped because one particle of mass $m + x$ is created for each particle of mass m which coagulated. Equation (4.16) gives the coagulation removal due to a particle of mass m coagulating with one other particle mass x. As shown in Figure 4-7, the total removal of particles mass m due to coagulation is due to coagulation with *all* other sized particles. Again, the aggregate coagulation rate is calculated with an integral summing the loss of

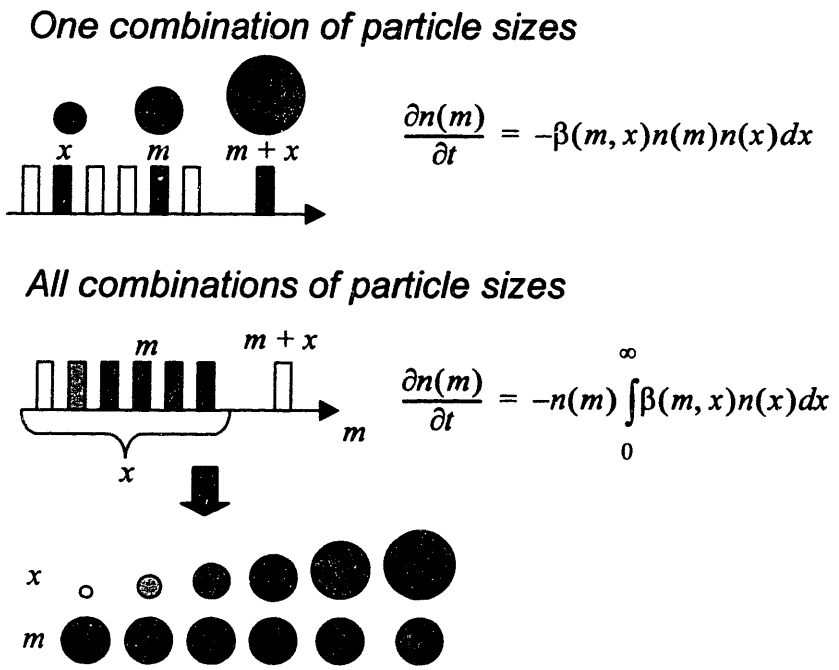

Figure 4-7: Coagulation removal due to coagulation of particles size *m* with particles of all other sizes *x*.

members size m due to coagulation with members of all possible sizes x, which range from zero to infinity:

$$\frac{\partial n(m)}{\partial t} = -n(m)\int_0^{\infty}\beta(m,x)n(x)dx \tag{4.17}$$

In this case, there is no double counting in the integration process so the factor ½ is not necessary. One may ask if infinity is the appropriate upper size limit, and if so, what is the physical meaning of an infinitely large particle? In fact an infinitely large particle signals a phase transition, also referred to as gelation (Gueron, 1998).

4.1.3 Reduction of the coagulation production integral

In many applications, the coagulation integral must be performed numerically over a wide range of particle sizes. In order to reduce the computational load of this integration, the integration limits of Equation (4.13) are reduced by utilizing the symmetry of the coagulation kernel. Because the coagulation kernel is symmetric, integrating over each half of the total integration range (0, m) yields the same value. Thus, instead of multiplying the integral by a factor of ½, computational load is decreased by simply integrating over half of the original integration range, (0, m/2). Figure 4-8 illustrates the symmetry of this integral and how it can be reduced.

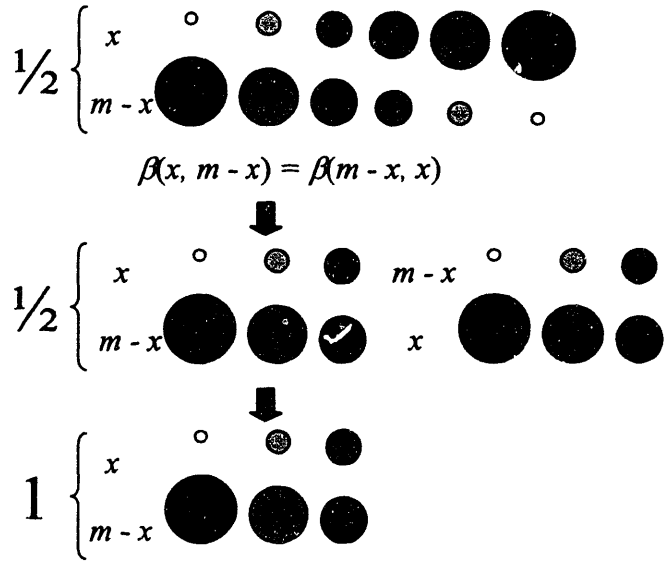

Figure 4-8: Reduction of the coagulation production integral by realization that the two halves of the original integration are equal and thus the factor ½ can be eliminated when only half the integration range is used.

In short, instead of counting each pair of colored segments twice - once when its value is x and again when its value is $m - x$ the integral is simply performed over half the interval. The following set of manipulations prove the validity of reducing the integration range. First, start off by dividing the integration range in half and changing the dummy variable of integration from x to z in the second integral:

$$\begin{aligned}\frac{\partial n(m)}{\partial t} &= \frac{1}{2}\int_0^m \beta(x, m-x)n(x)n(m-x)dx \\ &= \frac{1}{2}\left[\int_0^{\frac{m}{2}} \beta(x, m-x)n(x)n(m-x)dx + \int_{\frac{m}{2}}^m \beta(z, m-z)n(z)n(m-z)dz\right]\end{aligned} \tag{4.18}$$

Reversing the limits of the second integral and then applying the transformation $z = m - x$ yields the desired result:

$$\begin{aligned}\frac{\partial n(m)}{\partial t} &= \frac{1}{2}\left[\int_0^{\frac{m}{2}} \beta(x, m-x)n(x)n(m-x)dx + \int_{\frac{m}{2}}^m \beta(z, m-z)n(z)n(m-z)dz\right] \\ &= \frac{1}{2}\left[\int_0^{\frac{m}{2}} \beta(x, m-x)n(x)n(m-x)dx - \int_m^{\frac{m}{2}} \beta(z, m-z)n(z)n(m-z)dz\right] \\ &= \frac{1}{2}\left[\int_0^{\frac{m}{2}} \beta(x, m-x)n(x)n(m-x)dx - \int_0^{\frac{m}{2}} \beta(m-x, x)n(m-x)n(x)(-dx)\right] \\ &= \frac{1}{2}\left[\int_0^{\frac{m}{2}} \beta(x, m-x)n(x)n(m-x)dx + \int_0^{\frac{m}{2}} \beta(x, m-x)n(x)n(m-x)dx\right] \\ \frac{\partial n(m)}{\partial t} &= \frac{1}{2}\left[2\int_0^{\frac{m}{2}} \beta(x, m-x)n(x)n(m-x)dx\right]\end{aligned} \tag{4.19}$$

Thus the reduced scale coagulation production integral is:

$$\boxed{\frac{\partial n(m)}{\partial t} = \int_0^{\frac{m}{2}} \beta(x, m-x) n(x) n(m-x) dx} \tag{4.20}$$

4.1.4 Other coagulation kernel formulations

The preceding development applies to *binary* coagulation only. Note that in the case of a ternary coagulation kernel $\beta(a, b, c)$ where three the population members collide to produce one larger member, the coagulation integral would take the form:

$$\frac{\partial n(m)}{\partial t} = \frac{1}{2} \int_0^m \int_0^{m-y} \beta(x, y, m-x-y) n(x) n(y) n(m-x-y) dx dy \tag{4.21}$$

The factor of 1/2 is necessary because double counting occurs in the inner integral over x, as summarized in Table 4-3.

Table 4-3: Double counting in x integral

Variable	*Lower Limit*	*Upper Limit*
x	0	$(m - y)$
$n(x)$	$n(0)$	$n(m - y)$
$n(m - x - y)$	$n(m - y)$	$n(0)$

Now the inner integral:

$$\int_0^{m-y} \beta(x, y, m-y-x) n(x) n(y) n(m-y-x) dx \tag{4.22}$$

can be transformed into an equivalent form by substituting $k = m - y$.

$$n(y) \int_0^k \beta(x, y, k-x) n(x) n(k-x) dx \tag{4.23}$$

Note that this integral double counts the integrands exactly as in the binary coagulation case.

Describing the loss of particles due to coagulation is also similar to the previous case:

$$\frac{\partial n(m)}{\partial t} = -n(m)\int_0^\infty\int_0^\infty \beta(m,x,y)n(x)n(y)m\,dx\,dy \tag{4.24}$$

The units of the coagulation kernel remain unaltered in this case. Under normal circumstances, the frequency of ternary collisions is extremely low in comparison with binary collisions; as a result only binary coagulation kernels are considered in population balance models.

4.2 Fragmentation

Fragmentation, also called breakage, is the opposite of coagulation; instead of two members of a population combining to form a larger member of a population, fragmentation is the process of one member of a population splitting into two smaller members. Going back to the example of wet droplets, a fragmentation event occurs when a large water droplet moving across a windshield leaves a small droplet behind it. A slightly more dramatic fragmentation event might occur if a rock hit the windshield, shattering it into tiny pieces. In either case, one particle, droplet, or windshield would be fragmented into a number of smaller members, as illustrated in Figure 4-9.

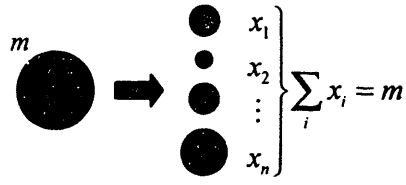

Figure 4-9: Fragmentation to form smaller population members.

Just as with coagulation, fragmentation can both create and remove particles in any given part of the number density distribution. The creation of particles of mass m due to the fragmentation of larger particles is referred to as *fragmentation production* while the removal due to the fragmentation of particles with mass m into smaller particles is referred to as *fragmentation removal*. The following sections outline the expressions for fragmentation production and removal as originally presented by Valentas, Bilous, and Amundson (Valentas, Bilous, and Amundson, 1966; Valentas and Amundson, 1966).

4.2.1 Fragmentation removal

Fragmentation removal describes the rate at which population members of mass m within a given space will fragment into smaller members of mass x. This is a unary process because it only

requires one population member for a fragmentation event to occur. For this reason, it is natural to describe the fragmentation removal as first order process with respect to the number of particles with mass m:

$$\begin{aligned} \frac{dn(m)\Delta m}{dt} &= -g(m)n(m)\Delta m \\ \int_{m_1}^{m_2} \frac{\partial n(m)}{\partial t} dm &= -\int_{m_1}^{m_2} g(m)n(m)dm \\ \frac{\partial n(m)}{\partial t} &= -g(m)n(m) \end{aligned} \tag{4.25}$$

where $g(m)$ is the removal rate expression with units 1/s. The first expression in Equation (4.25) gives the balance on a population "bin" while the second expression gives the balance over a continuous population segment (m_1, m_2) and the final expression gives the dynamic population balance form. Table 4-4 summarizes the units used in these expressions.

Table 4-4: Units of fragmentation loss expression

Symbol	*Definition*	*Units*
$n(m)$	number density	$\frac{\#\ \text{particles}}{\text{g} \cdot \text{cm}^3}$
dm, Δm	(differential) mass range	g
dt	(differential) time range	s
$g(m)$	fragmentation rate	1/s

4.2.2 Fragmentation production

Unlike the coagulation kernel, fragmentation is *not* assumed to be a binary process - a large particle fragments into a number of smaller particles. Thus, for each large particle which fragments, an entire distribution of smaller particles are created, as illustrated in Figure 4-10. In order to create an expression for the gain of particles to any given population segment dm from the fragmentation of larger particles, several quantities must be known:

- the number of larger particles which are fragmented
- how many smaller particles are created from each larger particle

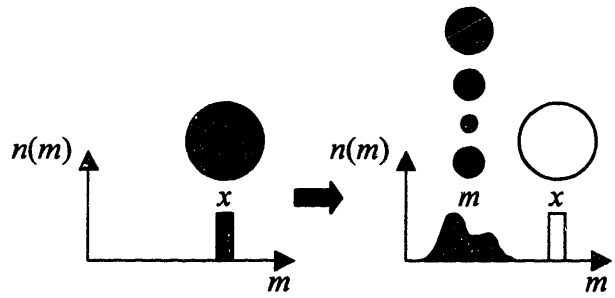

Figure 4-10: Distribution of smaller particles created by the fragmentation of one large particle.

- how these smaller particles are distributed with respect to size

The first piece of information is actually given by the fragmentation removal term. The second quantity is described by $v(m)$, the number of smaller particles created by the fragmentation of a particle of mass m. The third quantity is given by the *fragmentation kernel*, $\gamma(x, m)$, which describes how the fragments from a particle size x are distributed with respect to mass after fragmentation. This kernel essentially describes the *shape* of the fragmented particle distribution, as illustrated in Figure 4-10, and is defined as follows:

DEFINITION

The fragmentation kernel $\gamma(x, m)dm$ describes the fraction of total particles distributed into the mass range $(m, m + dm)$ from the fragmentation of a particle of mass x.

Just as before, we can derive the form of the population balance for fragmentation production directly from the fragmentation kernel, $v(m)$, and the rate expression for the loss of large particles.

$$\frac{dn(m)\Delta m}{dt} = \frac{-dn(x)\Delta x}{dt} v(x)\gamma(x, m)\Delta m \tag{4.26}$$

The first term on the right hand side is the fragmentation loss expression for large particles, which can be substituted from Equation (4.25).

$$\frac{dn(m)\Delta m}{dt} = g(x)n(x)\Delta x \cdot v(x)\gamma(x, m)\Delta m \tag{4.27}$$

In order to confirm the validity of Equation (4.27), we perform a quick unit check, as summarized

in Table 4-5 and Equation (4.28).

Table 4-5: Units of fragmentation production parameters

Symbol	*Definition*	*Units*
$n(m)$	number density of produced fragments	$\frac{\#\ \text{particles}}{\text{g} \cdot \text{cm}^3}$
dm, Δm	(differential) mass range	g
dt	(differential) time range	s
$g(x)$	fragmentation rate	1/s
$n(x)$	number density of fragmenting particles	$\frac{\#\ \text{particles}}{\text{g} \cdot \text{cm}^3}$
$v(x)$	fragments produced per fragmented particle	-
$\gamma(x, m)$	fragmentation kernel	1/g

$$\frac{dn(m)\Delta m}{dt} = g(x)n(x)\Delta x \cdot v(x)\gamma(x, m)\Delta m$$

$$\frac{\frac{\text{particles}}{\text{g} \cdot \text{cm}^3} \cdot \text{g}}{\text{s}} = \frac{1}{\text{s}} \cdot \frac{\text{particles}}{\text{g} \cdot \text{cm}^3} \cdot \text{g} \cdot \frac{1}{\text{g}} \cdot \text{g} \qquad (4.28)$$

Note that the last term $\gamma(x, m)\Delta m$ is unitless but because Δm has units of g; $\gamma(x, m)$ must therefore have units of 1/g.

Of course, Equation (4.27) only describes the contribution to the mass range Δm by fragmentation of particles in *one* mass range covered by Δx. In order to find the aggregate fragmentation to production, it is necessary to consider the contribution to particles of mass m from the fragmentation of all larger particles x. Figure 4-11 compares the fragmentation production of particles

from just one mass range of x and all mass ranges of x.

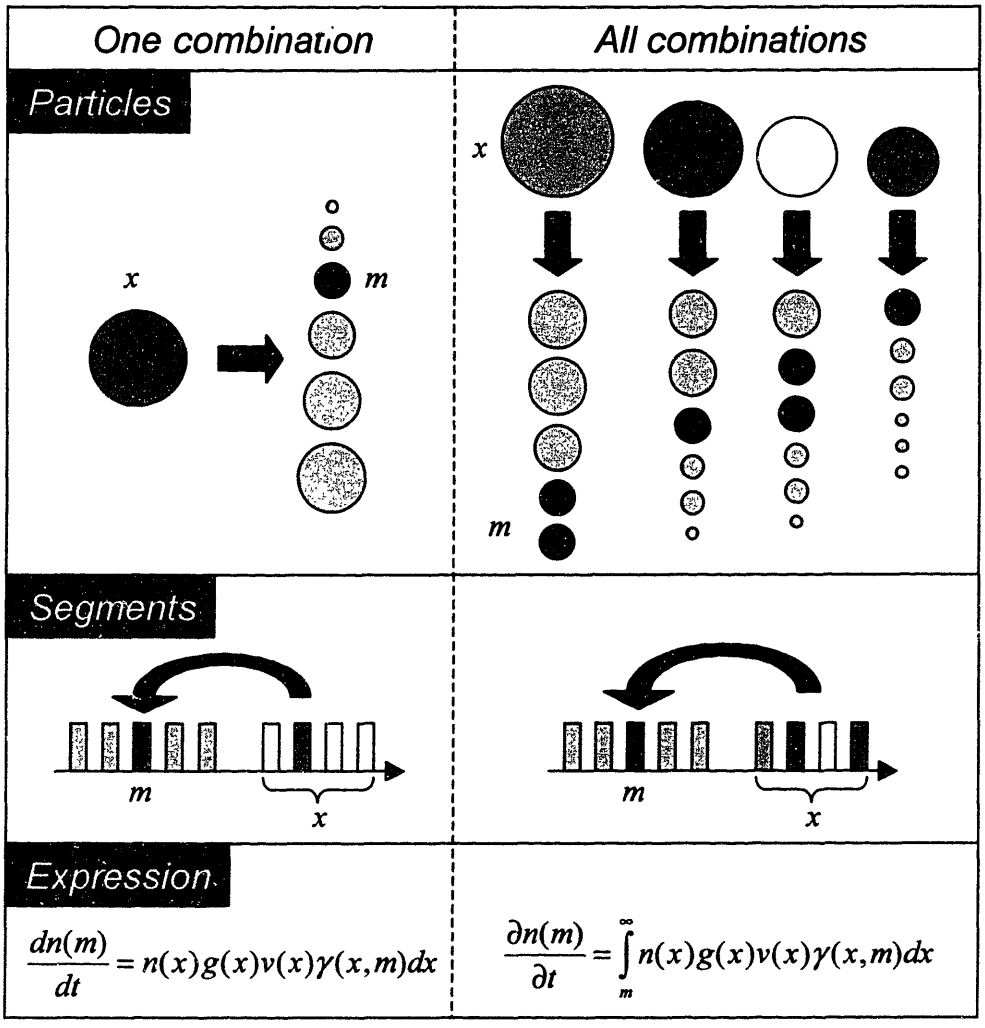

Figure 4-11: Fragmentation production of particles size *m* by fragmentation from mass range.

For all combinations of particles, the fragments of mass m produced are all colored solid, demonstrating how different sized large particles do not produce the same distribution of fragments. In order to include the contribution from *all* ranges of fragmenting particles, we must sum over all possible mass ranges Δx_i:

$$\frac{dn(m)\Delta m}{dt} = \sum_i (g(x)n(x)\Delta x_i \cdot v(x)\gamma(x, m)\Delta m) \tag{4.29}$$

Of course, we can cancel Δm from both sides of the equation and then shrink the segments Δx until the summation becomes an integral:

$$\boxed{\frac{\partial n(m)}{\partial t} = \int_{m}^{\infty} g(x)n(x)v(x)\gamma(x, m)dx} \tag{4.30}$$

which is the dynamic population balance equation expression for fragmentation production. Note that the integral for x ranges from m to infinity because particles of mass m can only be produced by particles of a greater mass. While the origin of Equation (4.30) is well-defined, some work still needs to be done to thoroughly define $v(x)$ and $\gamma(x, m)$.

Particles produced by fragmentation of a particle of mass x can only take on smaller $m < x$. For this reason, $\gamma(x, m)$ is only defined on the interval $(0, x)$. Because $\gamma(x, m)dm$ represents the *fraction* of fragments in the interval from m to $m + dm$ (see Figure 4-10), we would expect the sum over all intervals to equal one, which of course is an integral when differential segments dm are considered:

$$\int_{0}^{m} \gamma(m, x)dx = 1 \tag{4.31}$$

Note the consistency with the units given in Table 4-5.

Just as with coagulation, fragmentation processes must conserve mass. The mass balance is expressed by equating the mass lost in a differential segment of the number density distribution with the corresponding mass gained in other population segments due to this same fragmentation:

$$-\frac{\partial n(m)}{\partial t}m = n(m)g(m)v(m)\int_{0}^{m} \gamma(m, x)x dx \tag{4.32}$$

The left hand side expresses the mass lost in the interval located at mass m, while the right hand side expresses the mass gained in other intervals by this fragmentation. Specifically, $n(m)g(m)$ gives the rate of fragmentation of particles size m, multiplying this by $v(m)$ results in the total number of smaller fragments, and finally the integral on the right hand side calculates the total mass per fragment particle produced. Manipulating this expression yields:

$$\frac{\partial n(m)}{\partial t} = -n(m)g(m)\frac{v(m)}{m}\int_{0}^{m} \gamma(m, x)x dx \tag{4.33}$$

Comparing this expression to Equation (4.25) yields the relation:

$$\frac{v(m)}{m}\int_0^m \gamma(m,x)x\,dx = 1$$

$$v(m) = \frac{m}{\int_0^m \gamma(m,x)x\,dx} \tag{4.34}$$

This condition on $v(m)$ ensures that the mass balance is satisfied. For an example of an application of the fragmentation kernel, please refer to Section 4.5.4.

4.3 Growth

The previous section discussed the effects of coagulation and fragmentation processes on populations. Both of these mechanisms have the ability to both create and usurp particles from any given range of the number density distribution. Another classical process contributing to the formation of particles is the growth process. Unlike coagulation and fragmentation, growth does not change the number of particles in the system, rather it moves the particles which are already in the system from one part of the mass range to another. For this reason, the growth mechanism is said to conserve number but not mass. In contrast, the coagulation and fragmentation processes conserve mass but not number.

4.3.1 Analogy between growth and convection processes

As an example of growth occurring within the members of a population, consider a population of rabbits growing at a uniform rate I -that is, each rabbit grows at the rate of I units of mass per unit time. One would expect that the mass distribution of rabbits would shift to the right in Figure

4-12 as a function of time:

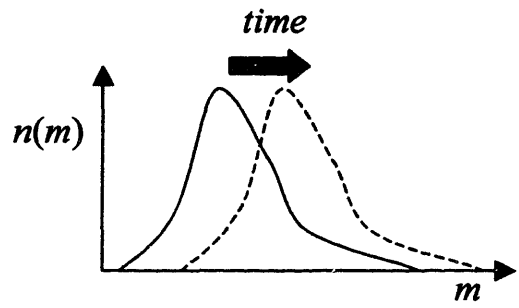

Figure 4-12: Effects of uniform growth on a number density distribution over time.

This phenomenon is analogous to convection within a fluid in a one dimensional regime with spatial coordinate z:

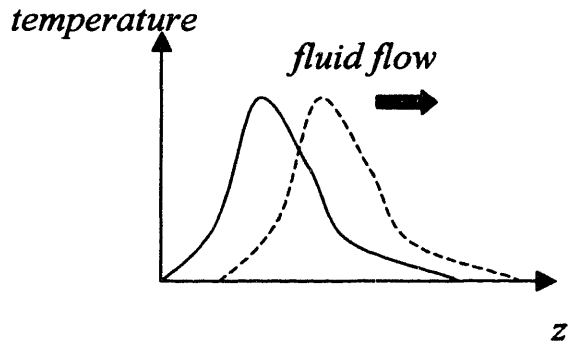

Figure 4-13: Effect of one-dimensional convection on a temperature distribution over time.

Using the mathematical form of the convection equation cast in the nomenclature of population distributions elicits the following expression:

$$\frac{\partial n(m)}{\partial t} = -\frac{\partial (G(m)n(m))}{\partial m} \tag{4.35}$$

where the growth rate may be a function of member size m.

4.3.2 Derivation of the growth expression

The validity of the growth expression given in Equation (4.35) can be proved by investigating the case of growth in a discrete population balance for two segments of the population, denoted by

the subscripts i - 1 and i, as illustrated in Figure 4-14.

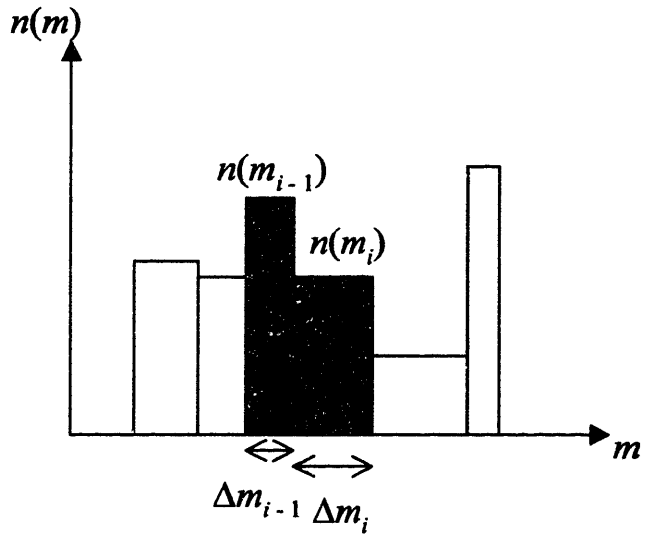

Figure 4-14: Growth model over two segments in a bin-based number density distribution.

Growth within the population shown will affect the number of population members in segment i in two ways. First, population members in segment i will grow larger and move into the next larger population segment, causing a decrease in the number of members in the interval spanned by Δm_i. Second, the number of population members in the interval spanned by Δm_i will increase due to growth of population members in the interval spanned by Δm_{i-1}. If a probabilistic framework is used to describe the population growth and $P_{G,i}(\omega)$ is defined as the probability that a population member of segment i will grow to the next larger population segment within some time interval, then the growth expression is:

$$\underbrace{n(m_i)\Delta m_i\big|_{new} - n(m_i)\Delta m_i\big|_{old}}_{\text{change in number of members in segment}} = \left[\underbrace{P_{G,i-1}(\omega)n(m_{i-1})\Delta m_{i-1}}_{\substack{\text{rate of members from segment} \\ i\text{-1 growing into segment } i}} - \underbrace{P_{G,i}(\omega)n(m_i)\Delta m_i}_{\substack{\text{rate of members from segment} \\ i \text{ growing into segment } i+1}}\right]\underbrace{\Delta t}_{\text{time step}} \tag{4.36}$$

Note that $P_{G,i}(\omega)$ has units of $1/time$ and therefore can be expressed at the reciprocal of some time constant:

$$n(m_i)\Delta m_i\big|_{new} - n(m_i)\Delta m_i\big|_{old} = \left[\frac{1}{\Delta t_{i-1}}n(m_{i-1})\Delta m_{i-1} - \frac{1}{\Delta t_i}n(m_i)\Delta m_i\right]\Delta t \tag{4.37}$$

Rearranging and taking the limit as $\Delta t \to 0$ converts the expression to a differential equation with

respect to time:

$$\frac{dn(m_i)\Delta m_i}{dt} = \frac{1}{\Delta t_{i-1}} n(m_{i-1})\Delta m_{i-1} - \frac{1}{\Delta t_i} n(m_i)\Delta m_i \tag{4.38}$$

Rearranging still further creates groupings of the form $\Delta m_i/\Delta t_i$. These groupings become the definition of continuous growth rate, dm/dt in the limit as the intervals Δm and Δt go to zero. In the population balance equation, growth rate is denoted by G_i:

$$\begin{aligned} \frac{dn(m_i)\Delta m_i}{dt} &= \frac{\Delta m_{i-1}}{\Delta t_{i-1}} n(m_{i-1}) - \frac{\Delta m_i}{\Delta t_i} n(m_i) \\ \frac{dn(m_i)\Delta m_i}{dt} &= G_{i-1} n(m_{i-1}) - G_i n(m_i) \end{aligned} \tag{4.39}$$

Dividing this expression through by Δm_i and taking the limit as $\Delta m_i \to 0$ yields the continuous expression for growth rate:

$$\begin{aligned} \lim_{\Delta m_i \to 0} \frac{\partial n(m_i)}{\partial t} &= \frac{G_{i-1} n(m_{i-1}) - G_i n(m_i)}{\Delta m_i} \\ \frac{\partial n(m)}{\partial t} &= -\frac{\partial (G(m) n(m))}{\partial m} \end{aligned} \tag{4.40}$$

where the dependence of G on particle size is no longer expressed through the subscript i; growth rate is instead a function of size $G(m)$.

4.3.3 Special case of constant growth

Growth within a mass-based population distribution is analogous to aging within an age-based distribution - all members of the population age at the same rate. This creates a system where every part of the distribution is translated an equal amount along the horizontal axis, as shown in Figure 4-15. Of course, because aging occurs at a uniform, linear rate, this is a special case of Equation (4.35) where $G(m) = 1$.

4.4 Sources and Sinks

A number of other effects also act on populations, including sources and sinks of population members and other mechanisms that change the properties of a population member. Sources and sinks include processes such as birth of rabbits or nucleation of aerosol particles. Other types of sources and sinks include consumption or production of species due to reaction.

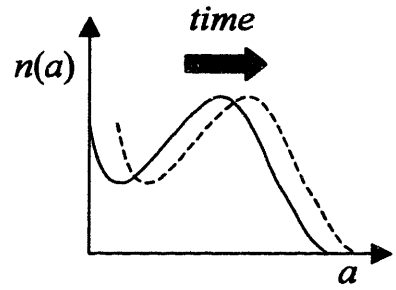

Figure 4-15: Effects of aging on a population density distribution with age as the independent variable.

4.4.1 Sources within the domain of the number density distribution

Sources and sinks are processes that either add or take away population members. These may include changes due to movement of the members across a system boundary or creation/destruction of members within the system boundary. The magnitude of the source or sink may vary as a function of population member size or some other property:

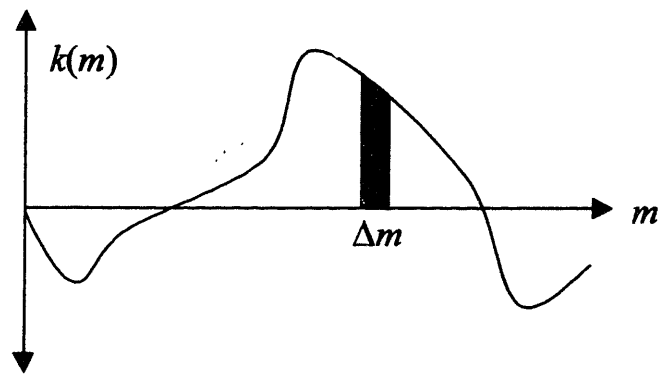

Figure 4-16: Source/sink function as a function of particle mass.

If $k(m)\Delta m$ is interpreted as the number rate of population members being added to the size range between m and $m + \Delta m$, then the following expressions are all valid:

$$\frac{dn(m)\Delta m}{dt} = k(m)\Delta m$$
$$\frac{dn(m)dm}{dt} = k(m)dm \qquad (4.41)$$
$$\frac{\partial n(m)}{\partial t} = k(m)$$

The first and second expressions in Equation (4.41) express the source/sink contribution to the

number of members in a given slice of the population distribution, for both finite and differentially small distribution intervals. The last expression gives the source/sink term $k(m)$ in the form of a term in the continuous general dynamic equation, with expected units of $1/g \cdot cm^3 \cdot s$, which are consistent with $\partial n(m)/\partial t$. In this sense, $k(m)$ represents the number contribution from the source per unit of the distribution independent variable. Note that the net number contribution of population members within any interval of the population distribution is given by:

$$\begin{aligned} \frac{\partial n(m)}{\partial t} &= k(m) \\ \frac{dN(m_1 < m < m_2)}{dt} &= \int_{m_1}^{m_2} k(m)dm \end{aligned} \tag{4.42}$$

Note that in the special case of a point source, the source adds population members of uniform size m_0 at a specified rate K_0 we have (note $m_1 < m_0 < m_2$):

$$\begin{aligned} k(m) &= K_0\delta(m_0) \rightarrow \frac{dn(m)}{dt} = K_0\delta(m_0) \\ \frac{dN(m_1 < m < m_2)}{dt} &= \int_{m_1}^{m_2} k(m)dm = \int_{m_1}^{m_2} K_0\delta(m_0)dm \\ \frac{dN(m_1 < m < m_2)}{dt} &= K_0 \end{aligned} \tag{4.43}$$

While K_0 has units of $1/(s \cdot cm^3)$ and represents the total rate of particle contribution from the source, the expression $K_0\delta(m_0)$ actually has units of $1/(g \cdot s \cdot cm^3)$. This is easily confirmed by taking the partial derivative of the middle expression in Equation (4.43) with respect to mass:

$$\begin{aligned} \frac{\partial}{\partial m}\left(\frac{dN(m_1 < m < m_2)}{dt}\right) &= \frac{\partial}{\partial m}\int_{m_1}^{m_2}\frac{d}{dt}n(m)dm = \frac{\partial}{\partial m}\int_{m_1}^{m_2} K_0\delta(m_0)dm \\ \frac{\partial n(m)}{\partial t} &= K_0\delta(m_0) \end{aligned} \tag{4.44}$$

which is exactly the form for a point source in continuous population balances.

4.4.2 Boundary sources

Another type of source are point sources placed at the system boundary. Most commonly, this is a boundary condition representing nucleation of particles entering the system at the smallest

size (see Figure 4-17).

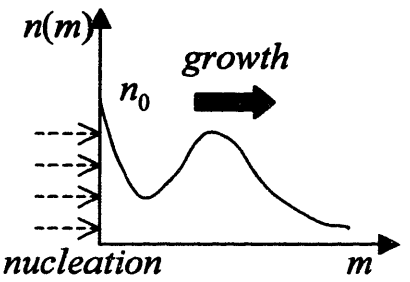

Figure 4-17: Addition of particles from nucleation into a growing number density distribution.

Generally, in such systems both the nucleation rate and growth rates are known. In order to calculate the correct boundary value n_0, we start off with a population balance on a population segment which borders on the left boundary, as shown in Figure 4-18.

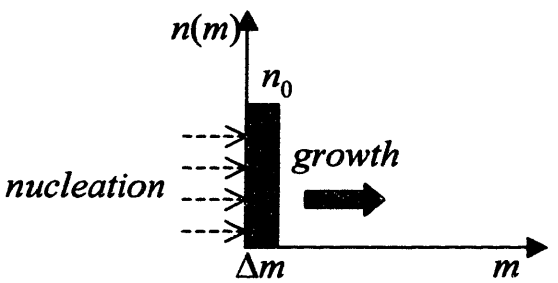

Figure 4-18: Population balance around segment of distribution adjacent to the left boundary.

Equation (4.45) presents the population balance on this element:

$$\underbrace{\frac{dn(m)\Delta m}{dt}}_{\substack{\text{number of members}\\ \text{between 0 and } \Delta m}} = \underbrace{N_0}_{\substack{\text{nucleation rate}\\ \text{units: \#/time}}} + \underbrace{G_{-1}n(m_{-1})}_{\substack{\text{increase from number}\\ \text{of growing members}}} - \underbrace{G_0 n(m_0)}_{\substack{\text{decrease from number}\\ \text{of growing members}}} \tag{4.45}$$

Note that the second term is zero because $n(m_{-1}) = 0$; that is, there are no particles at a smaller than *mass* = 0. Shrinking Δm to a differential size and assuming the element stays at steady state is equivalent to requiring that the rate of particles entering the system at the boundary is equal to the nucleation rate. This assumption also sets the left hand side of Equation (4.45) to zero:

$$0 = N_0 - G_0 n(m_0) \tag{4.46}$$

Noting that G_0 is equivalent to the growth rate at the left boundary, $G(m_0)$, this expression is

readily solved to yield the boundary value $n(m_0)$:

$$\boxed{n(m_0) = \frac{N_0}{G(m_0)}} \tag{4.47}$$

Note that the units of this expression are consistent, as summarized in Table 4-6.

Table 4-6: Boundary condition variable units

Symbol	*Description*	*Units*
$n(m_0)$	left boundary number density	$\frac{\#\text{ particles}}{g \cdot cm^3}$
N_0	nucleation rate	$\frac{\#\text{ particles}}{s \cdot cm^3}$
G_0	growth rate	g/s

This is the appropriate boundary condition for all systems where particles are entering the boundary and then growing to larger sizes.

4.5 Examples

The following sections outline the development of the dynamic population for several example systems including nucleation, growth, and fragmentation mechanisms.

4.5.1 Crystallization

One example is crystallization in a continuously mixed crystallizer, as shown in Figure 4-19. Here, crystals are formed in a vessel which is continuously fed with concentrated solution. Crystals form due to nucleation and grow to larger sizes, which is measured in terms of crystal length. The outlet pipe from the vessel acts as a continuous sink.

If the crystallizer is fed with aqueous potassium sulfate solution, then the growth rate expression for the resulting potassium sulfate crystals in aqueous solution in the form used by Equation (4.30) is (Chianese et al., 1987):

$$G(L) = 892\sigma^2(1 + 5.87L) \tag{4.48}$$

where σ is the degree of supersaturation in the liquid medium and L is the crystal length. In order to prevent negative values of supersaturation, we use the expression:

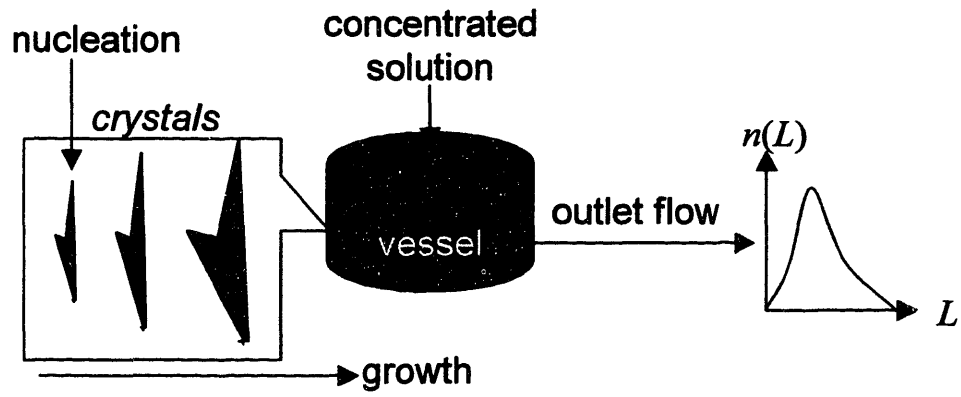

Figure 4-19: Crystallization of particles in a continuously mixed crystallizer.

$$\sigma = \max(c - c_{eq}, 0) \tag{4.49}$$

Figure 4-20 plots the growth rate as a function of crystal length for $\sigma = 0.0346$.

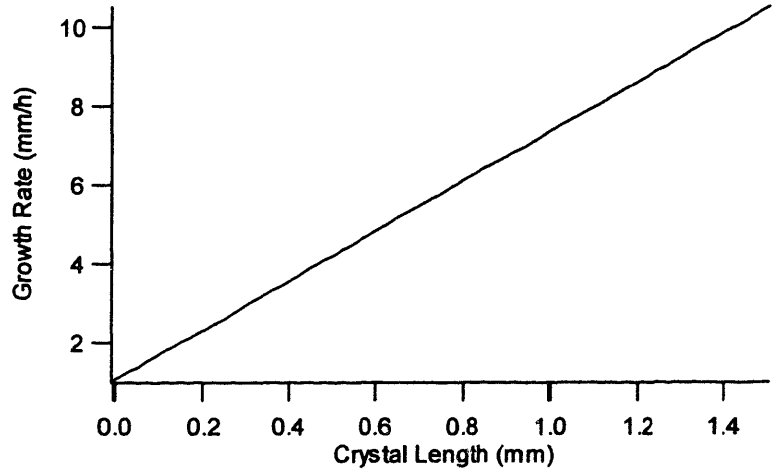

Figure 4-20: Crystal growth rate as a function of crystal length.

The saturation concentration is (Perry, Green, and Mahoney, 1984):

$$c_{eq} = 0.0735 + 1.375\times10^{-3}T \tag{4.50}$$

A separate growth rate specific to crystal nuclei is also reported (Chianese et al., 1987):

$$G_0 = 847\sigma^2 \tag{4.51}$$

The nucleation expression gives the birth rate of crystals:

$$N_0 = 4.12\times10^{14} M_t \sigma^{3.4} \tag{4.52}$$

where M_t is the magma density, defined as:

$$M_t = \rho_s \int_0^\infty K_v(L) L^3 n(L, t) dt \tag{4.53}$$

which calculates the total kg of solvent present in the crystals per m^3 of fluid. The symbol ρ_s is the solid density and K_v is the crystal shape factor, defined as:

$$\begin{aligned} K_v(L) &= 0.898 \exp[0.168\sqrt{1000L} - 8.234L] && L \le 0.1 \text{ mm} \\ K_v(L) &= 4.460 \exp[-0.0797\sqrt{1000L} + 0.676L] && L > 0.1 \text{ mm} \end{aligned} \tag{4.54}$$

Figure 4-21 graphs the crystal shape factor as a function of crystal length.

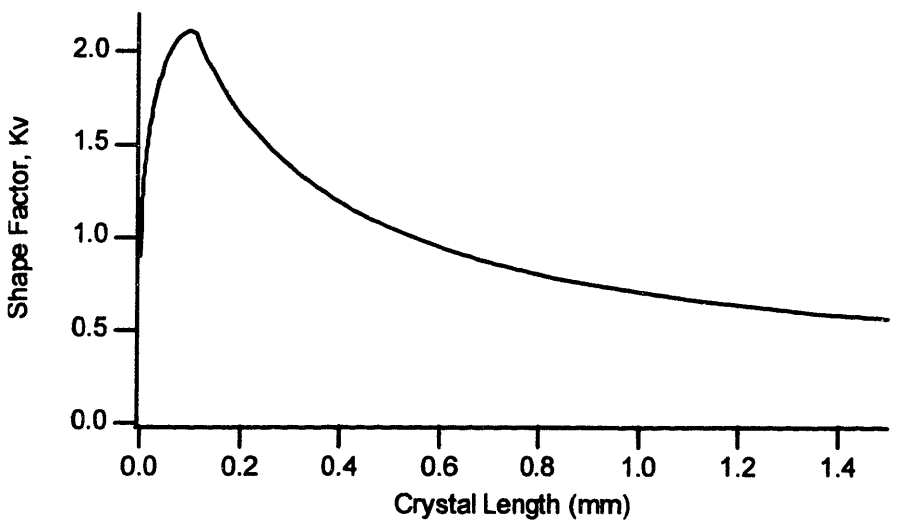

Figure 4-21: Crystal shape factor as a function of crystal length.

The dynamic population balance for this system must naturally include the effects of nucleation, growth and loss due to flow out of the crystallizer. Because the vessel is well-mixed and has volume V with a volumetric flowrate of v, the expression for loss of number density with respect to unit time is:

$$V\frac{\partial n(L)}{\partial t} = -v \cdot n(L)$$
$$\frac{\partial n(L)}{\partial t} = -\frac{v}{V} \cdot n(L) \tag{4.55}$$
$$\frac{\partial n(L)}{\partial t} = -\frac{1}{\tau} \cdot n(L)$$

where τ is the residence time of the crystallizer. Note that this acts as a uniform sink on the population and is referred to as the removal term. Adding this term to the growth term produces the dynamic population balance equation for this application:

$$\frac{\partial n(L)}{\partial t} = -\frac{\partial (n(L)G(L))}{\partial L} - \frac{1}{\tau} \cdot n(L) \tag{4.56}$$

The boundary condition for this system is determined by the nucleation rates and growth rates, as described in Section 4.4.2. As outlined in the previous section, nucleation is an example of a point source because it acts as a source of particles which are uniformly at some minimum size. If the growth rate in the system is known as a function of crystal length, then the boundary condition is:

$$n(0) = \frac{N_0}{G_0} \tag{4.57}$$

Note in this case that the minimum particle size is assumed to be zero because more accurate data on minimum crystal size is not readily available.

Finally, for the mixed crystallizer system, some balance is needed on the liquid phase to account for changes in liquid phase solute concentration due to uptake as the crystals grow. This equation takes the normal form for liquid phase concentration in a continuously mixed reactor with the exception that the loss term also includes the magma density.

$$\tilde{c} = c + \frac{M_T}{\rho}$$
$$\frac{d\tilde{c}}{dt} = \frac{1}{\tau}(c_{in} - \tilde{c}) \tag{4.58}$$

In this way, the variable $\tilde{c}$ is used to perform the total mass balance on the crystallizer, while the uptake inherently calculated by the first equation, which is essentially a mass balance of solute between the two phases. It is easy to see how uptake of solute creates longer crystals which in

turn results in a higher value of an M_T and a lower value of c.

4.5.2 Numerical solution of crystallization example

In order to solve this model, a numerical solution is implemented for the two governing equations given Equations (4.56) and (4.58). Because Equation (4.58) is an ordinary differential equation (ODE), it is ready for numerical integration. However, Equation (4.56) is a partial differential equation (PDE), and therefore must first be converted into a set of ODE's.

In general, there are three steps in generating a set of ODE's for numerical integration from a PDE:

1. Propose an approximate solution
2. Formulate an error expression
3. Minimize the error expression

For this particular problem, the method of finite elements will be used.

Step 1: Propose an approximate solution

The first step in solving the governing equations is to propose an approximate solution. The first expression is a partial differential equation, so the continuous solution $n(L)$ will be approximated by a linear piecewise representation $n^*(L)$, as shown in Figure 4-22:

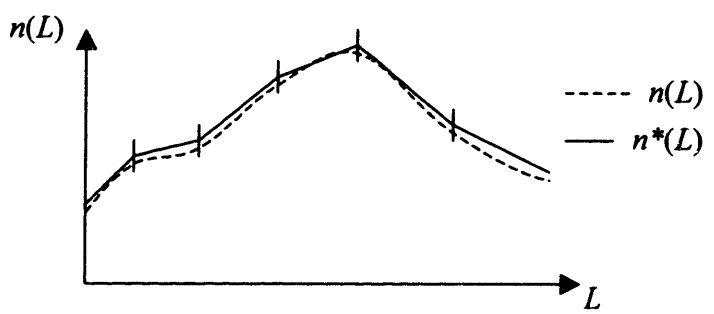

Figure 4-22: True solution *n(L)* and approximate numerical representation *n*(L)*.

This representation can be written as a linear combination of node points and "hat" functions:

$$n^*(L) = \sum_i n_i(L)\phi_i(L) \tag{4.59}$$

where $n_i(L)$ are the values at the node points where the line segments meet in the piecewise representation. The functions ϕ_i are "hat functions" which have value 1 at the node point i, and linearly

decrease to zero at the node points $i + 1$ and $i - 1$, as shown in Figure 4-23. In essence, this repre-

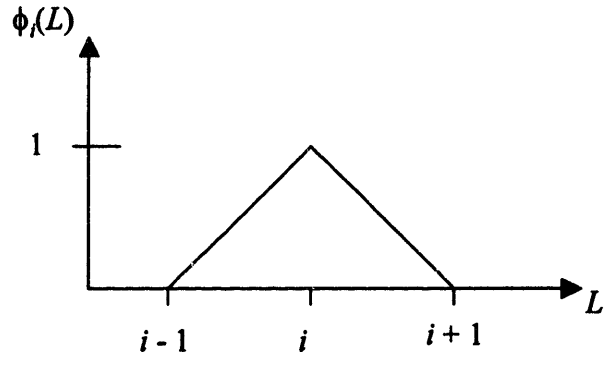

Figure 4-23: Hat function used in approximate solution.

sentation can be viewed much like a Fourier series or any other orthogonal expansion where the $n_i(L)$ represent the coefficients and the ϕ_i are the basis functions.

Step 2: Formulate an error expression

The error in our solution can be expressed as the difference between the right and left sides of Equation (4.56) after substituting in the representation $n^*(L)$ for $n(L)$:

$$R(L) = \frac{\partial n^*(L)}{\partial t} + \frac{\partial (n^*(L)G(L))}{\partial L}\frac{1}{\tau} \cdot n^*(L) \tag{4.60}$$

where $R(L)$ is the residual function representing the error. When this residual function is forced to zero, then Equation (4.60) is identical to Equation (4.56) and $n^*(L) = n(L)$.

Step 3: Minimize the error expression

In order to minimize the error expression, we take the inner product of the residual function and the basis set, and set this quantity to zero.

$$\langle R(L), \phi_i(L) \rangle = 0 \qquad \forall i \tag{4.61}$$

In practice, this inner product is performed over the domain of the solution $(0, L)$ and produces a set of i ordinary differential equations which define the evolution of the node point values $n_i(L)$. These equations are often written in matrix form:

$$\mathbf{A}\frac{d\mathbf{n}}{dt} = \mathbf{B} \cdot \mathbf{n} + \mathbf{f}(\mathbf{n}) + \ldots \tag{4.62}$$

where the $\mathbf{f}(\mathbf{n})$ is a nonlinear vector function. These equations are then solved by numerical inte-

gration (see Appendix B).

In theory, the inner product actually forces the error to be orthogonal to the representation, which is equivalent to taking the projection of the true solution onto the approximate solution. In vector space, this is the same as taking the projection of an n-dimensional vector onto an l-dimensional vector, where $l < n$. Take the projection of a two-dimensional vector onto the unit x vector, as illustrated in Figure 4-24. In this case, however, the projections are not performed on vectors,

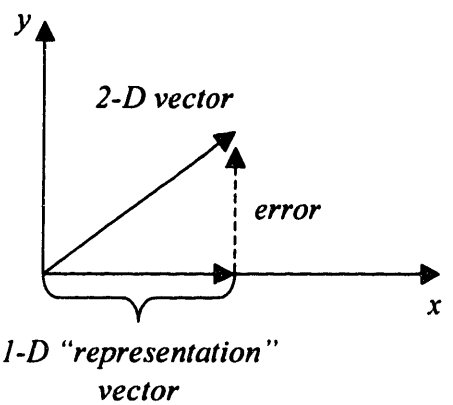

Figure 4-24: Projection of a two-dimensional vector onto a one-dimensional "representation" vector results in an error vector which is orthogonal to the representation vector.

but rather on functions. Nevertheless, the true solution is an arbitrary function, which can only be perfectly represented by an expansion of the form given in Equation (4.59) if it has infinitely many terms. However, it is only practical to represent our solution with a finite number N of node points. In this sense, we are really using an N-dimensional function expansion to approximate the infinite-dimensional true expansion. To find the closest approximation, we simply take the projection of the true expansion onto our approximation, which forces the error to be orthogonal to our basis function representation, as expressed in Equation (4.61). For more information on the theory of orthogonal approximation of functions, good starting points include Papoulis's (1991) treatment of Karhunen-Loeve expansions and the section on approximation of polynomial functions in *Numerical Recipes in C* (Press et al., 1993).

Numerical solution and results

In order to calculate the solution the necessary parameters in the governing equations are

specified in Table 4-7. Using these parameters, the solution was generated over the domain (0,

Table 4-7: Crystallization simulation parameters

Parameter	*Value*	*Units*
c @ $t = 0$	0	kg solid/kg solvent
τ	0.5	hr
T	25	°C
ρ	1000	kg/m^3
ρ_s	2660	kg/m^3
L_{max}	1.5	mm

L_{max}) over the time period from $t = 0$ to 6 hours. Number density results are plotted as a function of time in Figure 4-25, and compare closely to other results generated in the literature (Pantelides and Oh, 1996). Note that at time = 0, the number density distribution is uniformly zero, indicating

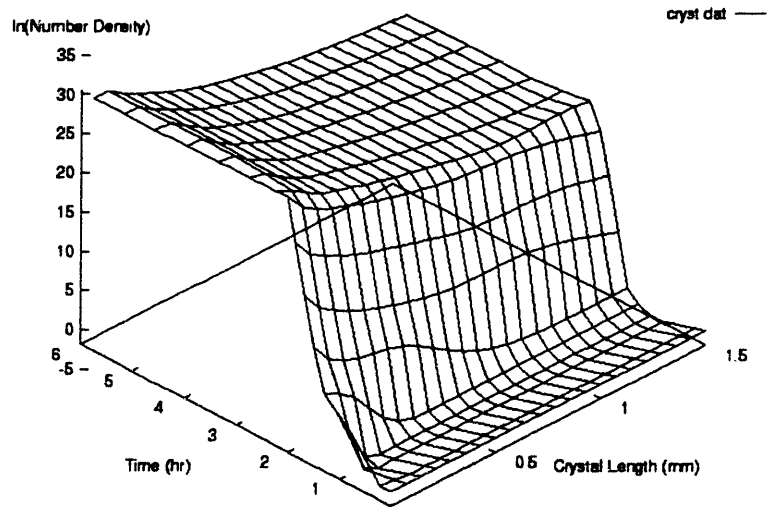

Figure 4-25: Evolution of the crystal length distribution as a function of time.

the lack of any particles in the system. As time increases, however, the number density at the size $L = 0$ begins to increase and then propagate in the L direction as new particles nucleate and grow. Note that the number density in the upper crystal size range maintains a high value in this system.

This indicates that a large fraction of the total particles nucleated are actually growing *out* of the upper size limit of the numerical solution. Because these particles are no longer in the system, they no longer grow or contribute to the magma density, and therefore the uptake of mass by these larger particles is unaccounted for by the model. Consequently, the magma density is underestimated and the nucleation rate is overestimated. In order to remedy this, the upper size limit needs to be increased until the number density at the upper size limit is roughly zero. In many population balance processes, the particles actually grow very fast and have the potential to become many orders of magnitude greater in size than the nuclei. In order to properly solve these systems, the solution domain must also cover many orders of magnitude, however significant numerical challenges exist in solving over such a large range of particle sizes, as will be discussed in the following chapters.

4.5.3 Rabbit population

For a population of rabbits, it is easy to imagine that three processes determine the number density of rabbits as a function of age: birth, death, and aging. If a is the variable for age and $n(a)$ is the age distribution of rabbits, we can express birth and death as source and sink processes, respectively. Thus we would expect the population balance equation to take the form:

$$\frac{\partial n(a)}{\partial t} = \left.\frac{\partial n(a)}{\partial t}\right|_{Birth} + \left.\frac{\partial n(a)}{\partial t}\right|_{Death} + \left.\frac{\partial n(a)}{\partial t}\right|_{Growth} \tag{4.63}$$

Aging acts much like a growth process, which adds age to the population member instead of mass.

$$\begin{aligned} &\text{Aging term:} \left.\frac{\partial n(a)}{\partial t}\right|_{Growth} = -\frac{\partial (n(a)G(a))}{\partial a} \\ &\text{Aging rate expression:} G(a) = \frac{da}{dt} = 1 \end{aligned} \tag{4.64}$$

A typical birth function might be defined as follows:

$$\left.\frac{\partial n(a)}{\partial t}\right|_{Birth} = b(a) = \delta(0) k_b \int_{a_{min}}^{a_{max}} n(a)da \tag{4.65}$$

The birthrate at age zero is equal to the product of the number of population members in the fertile age interval (a_{min}, a_{max}) and some birthrate factor k_b. In the birth expression, $\delta(0)$ indicates that

the birth function is zero for all values except for $a = 0$, which is means that birth will only add members to the population at *age* = 0. Thus, the birth process will act much like nucleation by adding population members at the left boundary of the population distribution.

$$n(0) = \frac{b(0)}{G(a)|_{a=0}} \tag{4.66}$$

This boundary condition is derived from the assumption that the number of rabbits at age zero is at steady state and that the affects of death at birth are accounted for in the birth rate factor k_b:

$$\begin{aligned} \frac{\partial n(a)}{\partial t} &= b(a) - \frac{\partial (n(a)G(a))}{\partial a} \qquad a = 0 \\ \frac{\partial n(a)}{\partial t} &= b(a) - G(a)\frac{\partial n(a)}{\partial a} - n(a)\frac{\partial G(a)}{\partial a} \end{aligned} \tag{4.67}$$

Because the growth rate is constant $G(a) = 1$, the last term in Equation (4.67) drops. The steady state assumption allows elimination of the first term, leaving:

$$\begin{aligned} b(a) - G(a)\frac{\partial n(a)}{\partial a} &= 0 \\ \frac{\partial n(a)}{\partial a} &= \frac{b(a)}{G(a)} \end{aligned} \tag{4.68}$$

A typical death expression would indicate that the death rate is proportional to both the age of the population members and the number of members at that age.

$$\left.\frac{\partial n(a)}{\partial t}\right|_{Death} = -k_d a \cdot n(a) \tag{4.69}$$

Note that in the birth expression, the units of k_b must be in $time^{-2}\ space^{-1}$ order for the units to be consistent (age is expressed in units of time); coincidentally k_d in the second expression is also expressed in units of $time^{-2}\ space^{-1}$. Substituting the appropriate terms into Equation (4.63) yields the final form of the population balance equation:

$$\frac{\partial n(a)}{\partial t} = -\frac{\partial (n(a)G(a))}{\partial a} - k_d a \cdot n(a) \tag{4.70}$$

where the birth term is conspicuously absent because it takes the form of a boundary condition and does not affect the number density on the interval $a = (0, \infty)$.

4.5.4 Fragmentation example

Most antibiotics are produced by culturing filamentous fungi in large well-mixed fermentation vessels. The well-mixed character of the vessel is maintained by a mixing impeller. The fungi grow in long filaments, called hyphae, which are entangled together to form large clumps of fungi. The impeller sometimes collides with the fungi, fragmenting off a tiny group of the filamentous hyphae through, as shown in Figure 4-26:

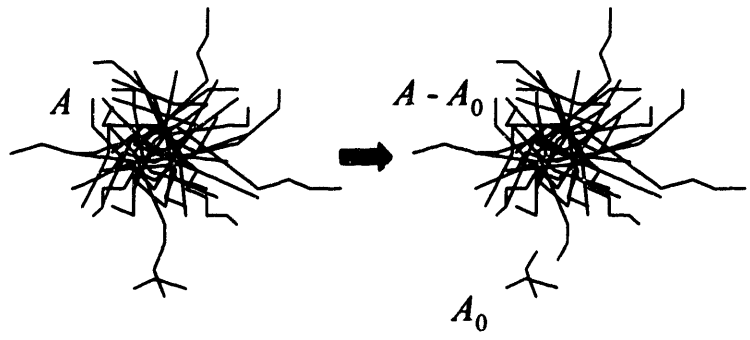

Figure 4-26: Fragmentation in filamentous fungi.

Jüsten et al. (1997) reports that below a certain minimum fungal area A_0 fragmentation no longer occurs, and thus develops a model where fragmentation is manifested as a gradual reduction in area of large hyphal clumps through the loss of a small hyphal clumps of area A_0. Jüsten et al. report the dynamic population balance for this process:

$$\frac{\partial n(A)}{\partial t} = -\frac{\partial(n(A)\cdot f(A))}{\partial A} \tag{4.71}$$

and define the "fragmentation rate function" f as:

$$f(A) = -K(A - A_0)^G \tag{4.72}$$

where $G = 1$. If we examine Equation (4.71) is examined over a size interval ΔA which is the same size as a hyphal fragment then we have:

$$\begin{aligned} \frac{\partial n(A)}{\partial t} &= -\frac{\partial(n(A)\cdot f(A))}{\partial A} \qquad A > A_0 \\ \frac{dn(A)}{dt} &= -\frac{n(A+\Delta A)\cdot f(A+\Delta A) - n(A)\cdot f(A)}{\Delta A} \end{aligned} \tag{4.73}$$

where $\Delta A = A_0$. Then substituting the fragmentation rate function f yields:

$$\begin{aligned}
\frac{dn(A)}{dt} &= -\frac{n(A+\Delta A)\cdot(-K(A+\Delta A-A_0))-n(A)\cdot(-K(A-A_0))}{\Delta A} \\
\frac{dn(A)}{dt} &= \frac{n(A+\Delta A)\cdot K\cdot A-n(A)\cdot K\cdot(A-A_0)}{\Delta A} \\
\frac{dn(A)}{dt} &= \frac{n(A+\Delta A)\cdot K\cdot A-n(A)\cdot K\cdot(A-A_0)}{A_0} \\
\frac{dn(A)}{dt} &= \frac{n(A+\Delta A)\cdot K\cdot A}{A_0}-\frac{n(A)\cdot K\cdot(A-A_0)}{A_0}
\end{aligned} \tag{4.74}$$

The units of A are given in mm^2 while K is a rate constant with units 1/s.

Close inspection of Figure 4-26 and the fragmentation rate function given in Equation (4.72) reveals that the fragmentation kernel can also be used to describe this process. Because an hypha of size A fragments into two pieces of area A - A_0 and A_0, we can propose the fragmentation kernel:

$$\gamma(A,x) = \frac{1}{2}\delta(x-A_0)+\frac{1}{2}\delta(x-(A-A_0)) \tag{4.75}$$

This fragmentation kernel gives the distribution of fragment sizes x created by the fragment of one particle size a. Because $\delta(x) = 1$ only when $x = 0$, the first term takes on a value of ½ when $x = A_0$, which means that ½ of the total fragments are of size A_0. Likewise, the second term in Equation (4.75) expresses the fact that the other ½ of the fragments are of size A - A_0.

Applying Equation (4.34) reveals that $\nu(A) = 2$, as expected because two particles are created for every fragmentation event.

$$\begin{aligned}
\nu(A) &= \frac{A}{\int_0^A \gamma(A,x)x\,dx} \\
\nu(A) &= \frac{A}{\int_0^A \left(\frac{1}{2}\delta(x-A_0)+\frac{1}{2}\delta(x-(A-A_0))\right)x\,dx} \\
\nu(A) &= \frac{A}{\frac{A_0}{2}+\frac{(A-A_0)}{2}} = \frac{A}{\left(\frac{A}{2}\right)} \\
\nu(A) &= 2
\end{aligned} \tag{4.76}$$

The last expression needed to fully describe the fragmentation kernel is $g(A)$, which describes the fragmentation removal rate for hyphae of area A in the same the form given in Equation (4.25):

$$\frac{\partial n(A)}{\partial t} = -n(A)g(A) \tag{4.77}$$

As shown in Figure 4-27, the fragmentation rate can be interpreted as a negative growth rate. It

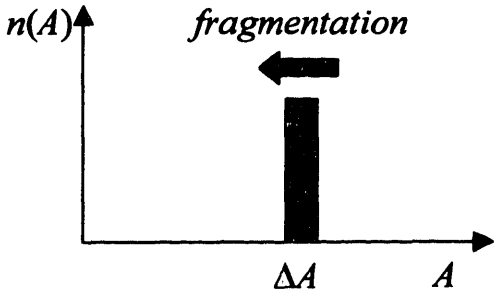

Figure 4-27: Interpretation of the fragmentation rate as a negative growth rate.

follows that the fragmentation rate constant would be defined by the characteristic time required for a particle of area A to erode in area by ΔA at the rate prescribed by the function $f(A)$.

$$\begin{aligned} \Delta A &= \Delta t \cdot f(A) \\ \Delta A &= \Delta t \cdot K(A - A_0) \\ \Delta t &= \frac{\Delta A}{K \cdot (A - A_0)} \end{aligned} \tag{4.78}$$

The inverse of this characteristic time can be interpreted as the frequency of fragmentation and is analogous to $g(A)$, recalling that $\Delta A = A_0$:

$$\begin{aligned} g(A) &= \frac{K \cdot (A - A_0)}{\Delta A} \\ g(A) &= \frac{K \cdot (A - A_0)}{A_0} \end{aligned} \tag{4.79}$$

Now that all of the necessary functions have been defined for the fragmentation process, we can write the form of the dynamic population balance, following the form given in Equations (4.25) and (4.30):

$$
\begin{aligned}
\frac{\partial n(A)}{\partial t} &= \int_A^\infty g(x)n(x)v(x)\gamma(x,A)dx - n(A)g(A) \\
\frac{\partial n(A)}{\partial t} &= \int_A^\infty \frac{K\cdot(x-A_0)}{A_0} n(x) 2\left[\frac{1}{2}\delta(A-A_0)+\frac{1}{2}\delta(A-(x-A_0))\right]dx - n(A)\frac{K\cdot(A-A_0)}{A_0} \\
\frac{\partial n(A)}{\partial t} &= \int_A^\infty \frac{K\cdot(x-A_0)}{A_0} n(x)[\delta(A-A_0)+\delta((A+A_0)-x)]dx - n(A)\frac{K\cdot(A-A_0)}{A_0} \\
\frac{\partial n(A)}{\partial t} &= \int_A^\infty \frac{K\cdot(x-A_0)}{A_0} n(x)[\delta(A-A_0)+\delta((A+A_0)-x)]dx - n(A)\frac{K\cdot(A-A_0)}{A_0} \\
\frac{\partial n(A)}{\partial t} &= \frac{K\cdot((A+A_0)-A_0)}{A_0} n(A+A_0) - n(A)\frac{K\cdot(A-A_0)}{A_0} \\
\frac{\partial n(A)}{\partial t} &= \frac{K\cdot A}{A_0} n(A+A_0) - n(A)\frac{K\cdot(A-A_0)}{A_0}
\end{aligned}
\tag{4.80}
$$

Comparison with Equation (4.74) reveals that these two forms of the dynamic population balance are identical! This means that the an erosion process where clumps of size A_0 are breaking off from a large particle is equivalent to the corresponding fragmentation process where two fragments size A and A - A_0 are created.

4.5.5 Relation between fragmentation, growth, and coagulation processes

The interesting observation to be made here is that in the limit as the size of the fragment breaking off from a large population member goes to zero, the population balance term describing fragmentation distributions goes to a growth term with a negative growth rate. Thus, growth/erosion processes and fragmentation together cover the entire range of mechanisms where a large particle loses mass, ranging from the continuous loss of molecules in the evaporation process to the discrete loss of large fragments observed in a fragmentation mechanism.

This also has implications on the type of representation used for a process (see Chapter 2). For example, if the smallest amount of mass that can be lost from a particle of any size is Δm, then it is possible to use a discrete representation with spacing Δm to properly represent the system. However, if the particles can lose very small amounts of mass through a "continuous" loss process such as evaporation, then a continuous representation must be used. Note that no truly "continu-

ous" loss process can exist, and Δm never actually reaches zero. In fact, the smallest amount of matter Δm that can be lost by a particle will always be a finite quantity at least equal to the mass of the smallest atom or molecule in the particle. The representations used in these models are referred to as "monomer size distributions" because they rely on a description based on the smallest possible particle element in the system (Jacobson, 1999). A "continuous" process actually refers to the process where Δm is so small compared to the magnitude of m that the process is most effectively treated as a continuous process. For instance, take a model of a population of swimming pools in a suburban area. The mass of water in the swimming pools could form a population which could be described by growth/evaporation mechanisms, but the mass of water in each swimming pool is very large compared to the mass of a water molecule. For this reason, a continuous model describing kg of water in each swimming pool would be appropriate. A discrete model describing the population density function with the number of molecules in each swimming pool as the independent variable would not only be ludicrous, but would require so many bins to describe the population that a solution would not be tractable.

Using a similar method to the derivation given in Section 4.5.4, it is possible to derive the coagulation kernel for a deposition process where particles of size A gradually accumulate on particles of constant size A_0 to produce particles of size $A + A_0$.

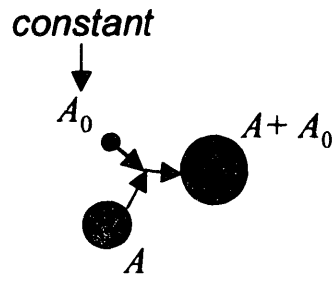

Figure 4-28: Coagulation process where particles of varying size *A* coagulate with tiny particles of constant size A_0.

This derivation is very similar to the one already given and can be broken into the following steps:

1. Derive the population balance for coagulation from the coagulation loss and production expressions for constant coagulation kernel with $\beta(x, y) = K$, where the units of K are s^{-1} cm^{-3}.

2. Derive an equivalent population balance for growth based on this coagulation mechanism.

The following two assumptions facilitate this derivation:

1. Assume that the equilibrium concentration (c_{eq}) for the growth kernel is zero (see the growth process example in section 4.5.1)

2. Assume that the number density of smaller particles A_0 in the coagulation production expression is analogous to the bulk phase gas concentration (c).

4.5.6 Critical population size for coagulation and fragmentation kernels

Note that the use of an integral expression for coagulation and fragmentation processes applies only in the limit as a large number of population members are present. Only when the number of population members is large will the "law of large numbers" from probability theory (Drake, 1967) apply and allow the use of deterministic fragmentation and coagulation kernels. For small populations, the characteristics of the population is not as evenly averaged and the stochastic nature of the behavior of individual population members becomes the driving force behind population dynamics. Please refer to Gueron (1998) for more discussion of the validity conditions for deterministic integral equations in population balances. Ramkrishna and Frederickson (2000) present extensive material on stochastic population balances.

4.6 Summary

A population balance process may include a number of the mechanisms listed above as well as other mechanisms. For more examples of crystal growth rate expressions, please refer to have been studied in a number of systems and are reported in literature Chianese et al. (1995), Karel et al. (1994), and Söhnel et al. (1996). Studies of fragmentation (Chianese, Sangl, and Mersmann, 1996) and nucleation (Chianese, Contaldi and Mazzarotta, 1986; Chianese, Karel, and Mazzarotta,1995) are also available.

References

[1] Albrecht, B., A. *Aerosols, cloud microphysics, and gractional cloudiness,* Science, **254** 1227-1230, 1989.

[2] Chianese, A.; Contaldi, A.; Mazzarotta, B. *Primary Nucleation of Sodium Perborate in Aqueous Solutions,* Journal of Crystal Growth, **78**(2) 279-290, 1986.

[3] Chianese, A.; Dicave, S.; Mazzarotta, B. *Crystallization Kinetics of Potassium-Sulfate in an MSMPR Cooling Crystallizer,* Chimica et l'Industria, **69**(6), 8-13, 1987.

[4] Chianese, A.; Karel, M.; Mazzarotta, B. *Nucleation Kinetics of Pentaerythritol,* The Chemical Engineering Journal and the Biochemical Engineering Journal, **58**(3), 209-214, 1995.

[5] Chianese, A.; Karel, M.; Mazzarotta, B. *Crystal Growth Kinetics of Pentaerythritol,* The Chemical Engineering Journal and the Biochemical Engineering Journal, **58**(3), 215-221, 1995.

[6] Chianese, Angelo; Sangl, Reinhard; Mersmann, Alfons *On the Size Distribution of Fragments Generated by Crystal Collisions,* Chemical Engineering Communications, **146** 1-12, 1996.

[7] Drake, Alvin.W. *Fundamentals of Applied Probability Theory,* McGraw-Hill, Inc. 1967.

[8] Gueron, Shay. *The Steady-State Distributions of Coagulation-Fragmentation Processes,* Journal of Mathematical Biology, **37**, 1-27, 1998.

[9] Jacobson, Mark Z. *Fundamentals of Atmospheric Modeling,* Cambridge University Press, 1999.

[10] Jüsten, P.; Paul, C. G.; Nienow, A. W.; and Thomas. C. R. *A Population Balance Model for Fragmentation of Filamentous Micro-Organisms,* 4th International Conference on Bioreactor & Bioprocess Fluid Dynamics, ed. A. W. Nienow, Mechanical Engineering Publications Limited, 1997.

[11] Karel, Miloslav; Nyvylt, Jaroslav; Chianese, Angelo *Crystallization of Pentaerythritol I. Solubility, Density and Metastable Zone Width,* Collection of Czechoslovak Chemical Communications, **59**(6), 1270-1288, 1994.

[12] Pantelides, Constantinos C.; Oh, Min *Process Modelling Tools and Their Application to Particulate Processes,* Powder Technology **87**, 13-20, 1996.

[13] Papoulis, Athanasios *Probability, Random Variables, and Stochastic Processes,* 3rd Ed., McGraw-Hill, 1991.

[14] Perry, Robert H.; Green, Don W.; Maloney, James O. *Perry's Chemical Engineers' Handbook,* 5th Ed., McGraw-Hill, 1984.

[15] Press, William H.; Teukolsky, Saul A. Vetterling, William T.; and Flannery, Brian P. *Numerical Recipies in C: The Art of Scientific Computing,* 2nd Ed., Cambridge University Press, 1993.

[16] Ramkrishna, Doraiswami; Fredrickson, Arnold G. *Population Balances: Theory and Applications to Particulate Systems in Engineering,* Academic Press, 2000.

[17] Söhnel, O.; Bravi, M.; Chianese, A.; Mazzarotta, B. *Growth Kinetics of Sodium Perborate from Batch Crystallization,* Journal of Crystal Growth **160**(3-4), 355-360, 1996.

[18] Valentas, Kenneth J.; Amundson, Neal R. *Breakage and Coalescence in Dispersed Phase Systems,* Industrial and Engineering Chemistry Fundamentals, **5,** 533-542, 1966.

[19] Valentas, Kenneth J.; Bilous, Olegh; Amundson, Neal R. *Analysis of Breakage in Dispersed Phase Systems,* Industrial and Engineering Chemistry Fundamentals, **5**, 271-279, 1966.

Chapter 5: Multicomponent Dynamic Population Balance Equation

The previous chapter rigorously derived the expressions for growth, nucleation, coagulation, and fragmentation directly from principles of physics. However, many particulate systems contain more than one component of primary interest. Some examples of these systems include crystallization, where often crystals are formed in an effort to purify a liquid phase component, and atmospheric aerosols, where composition has a strong effect on the condensation growth rate of the particles. These systems require a multicomponent population balance equation to describe the evolution of the particles in the system. These multicomponent systems are described by multicomponent number density functions, as introduced in Chapter 2.

5.1 Multicomponent number distribution

With more independent variables, the definition for number distribution must be expanded to include multiple components:

DEFINITION

The **number density** *function of population members with s attributes is completely specified by the vector* $\mathbf{m}=\{m_1, m_2, m_3, ..., m_s\}$ *is given by* $n(\mathbf{m})$ *such that* $n(\mathbf{m})d\mathbf{m}$ *is the number of population members in the attribute range* $[m_1, m_1+dm_1][m_2, m_2+dm_2][m_3, m_3+dm_3]...[m_s, m_s+dm_s]$.

It follows from the definition that the units of $n(\mathbf{m})$ is $1/(cm^3\ g^s)$ where s is the number of species in the system. Alternatively, the number density distribution may be represented as a function of particle size and the composition of s - 1 species. Chapter 2 illustrates such an example in a two-component system.

In general, if the individual species masses in each population member are specified, then the attributes $m_1...m_s$ are all defined as individual species masses. If instead, the total mass of the particle and mass fractions for the first s - 1 species were used to specify the number distribution of population members, then the first attribute would be mass and the remaining s - 1 species would be mass fraction. If m were used to denote total particle mass and x_i defined as the mass fraction of component i, the number density would be written as $n(m, x_1, x_2,..., x_{s-1})$, or $n(m, \mathbf{x})$ where $\mathbf{x}$ =

$\{x_1, x_2, \ldots, x_{s-1}\}$. Using the $n(m)$ representation, the following sections derive the multicomponent dynamic population balance equation.

5.2 Coagulation

When two multicomponent population members with mass composition vectors **x** and **y** coagulate, they form a new population member with mass $\mathbf{m} = \mathbf{x} + \mathbf{y}$.

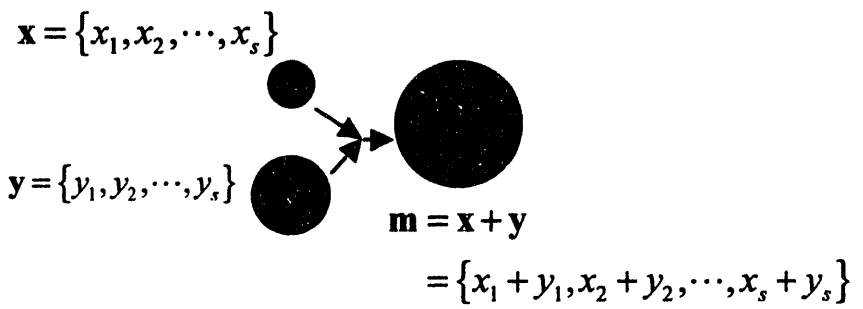

Figure 5-1: Multicomponent coagulation.

Note that the composition of the particles is now described by a vector of the individual component masses. The previous definition of the coagulation kernel $\beta(x, y)$ from Chapter 4 must be augmented to account for this.

DEFINITION

The **multicomponent coagulation kernel** $\beta(\mathbf{x}, \mathbf{y})$ *is the rate function (with units of* space $\cdot$ time^{-1}*) for the first-order process where particles of composition* **x** *and* **y** *in a given space will collide and coagulate into one larger member with composition* $\mathbf{m} = \mathbf{x} + \mathbf{y}$.

As in the single-component case, coagulation may both produce and remove particles of any given size **m**. These two processes are referred to as coagulation production and coagulation removal and are addressed separately in the following sections.

5.2.1 Coagulation production

As in the one-component case, coagulation production results from the agglomeration of smaller particles to form a larger particle. In the one-component case, this meant that particles of size m could be produced by the agglomeration of particles of size x and $m - x$. In the vector case, this means that the mass of *each component* in the new particle is the sum of the masses of that component in the two smaller particles:

$$\begin{aligned} m_1 &= x_1 + (m_1 - x_1) \\ m_2 &= x_2 + (m_2 - x_2) \\ &\vdots \\ m_s &= x_s + (m_s - x_s) \end{aligned} \tag{5.1}$$

This set of relations is often expressed in the equivalent vector form: $\mathbf{m} = \mathbf{x} + (\mathbf{m} - \mathbf{x})$. The corresponding expression for coagulation production in the population segment between $\mathbf{m}$ and $\mathbf{m} + d\mathbf{m}$ is:

$$\begin{aligned} \frac{dn(\mathbf{m})\Delta\mathbf{m}}{dt} &= \beta(\mathbf{m}-\mathbf{x},\mathbf{x})n(\mathbf{m}-\mathbf{x})\Delta(\mathbf{m}-\mathbf{x})n(\mathbf{x})\Delta\mathbf{x} \\ \frac{dn(\mathbf{m})\Delta m_1 \Delta m_2 \ldots \Delta m_s}{dt} &= \beta(\mathbf{m}-\mathbf{x},\mathbf{x})n(\mathbf{m}-\mathbf{x})\Delta(m_1-x_1)\ldots\Delta(m_s-x_s)n(\mathbf{x})\Delta x_1 \ldots \Delta x_s \end{aligned} \tag{5.2}$$

When the intervals for Δm_i, $\Delta(m_i - x_i)$, and Δx_i become differentially small, Equation (5.2) becomes:

$$\frac{\partial n(\mathbf{m}) dm_1 dm_2 \ldots dm_s}{\partial t} = \beta(\mathbf{m}-\mathbf{x},\mathbf{x})n(\mathbf{m}-\mathbf{x})d(m_1-x_1)\ldots d(m_s-x_s)n(\mathbf{x})dx_1\ldots dx_s \tag{5.3}$$

The units of this expression are:

$$\underbrace{\frac{\partial n(\mathbf{m}) dm_1 dm_2 \ldots dm_s}{\partial t}}_{\text{units}[=]\frac{1}{\text{time}\cdot\text{space}}\cdot\frac{1}{\text{mass}^s}\cdot\text{mass}^s} = \underbrace{\beta(\mathbf{m}-\mathbf{x},\mathbf{x})}_{\text{units}[=]\frac{1}{\text{time}\cdot\text{space}}} \underbrace{n(\mathbf{m}-\mathbf{x})d(m_1-x_1)\ldots d(m_s-x_s)}_{\text{units}[=]\frac{1}{\text{mass}^s}\cdot\text{mass}^s} \underbrace{n(\mathbf{x})dx_1\ldots dx_s}_{\text{units}[=]\frac{1}{\text{mass}^s}\cdot\text{mass}^s} \tag{5.4}$$

Using the fact that:

$$\frac{d(m_i - x_i)}{dm_i} = 1 \qquad \forall i \tag{5.5}$$

enables further simplification of Equation (5.3):

$$\begin{aligned} \frac{\partial n(\mathbf{m}) dm_1 dm_2 \ldots dm_s}{\partial t} &= \beta(\mathbf{m}-\mathbf{x},\mathbf{x})n(\mathbf{m}-\mathbf{x})d(m_1-x_1)\ldots d(m_s-s)n(\mathbf{x})dx_1\ldots dx_s \\ \frac{\partial n(\mathbf{m})}{\partial t} &= \beta(\mathbf{m}-\mathbf{x},\mathbf{x})n(\mathbf{m}-\mathbf{x})\frac{d(m_1-x_1)}{dm_1}\frac{d(m_2-x_2)}{dm_2}\ldots\frac{d(m_s-x_s)}{dm_s}n(\mathbf{x})dx_1\ldots dx_s \\ \frac{\partial n(\mathbf{m})}{\partial t} &= \beta(\mathbf{m}-\mathbf{x},\mathbf{x})n(\mathbf{m}-\mathbf{x})n(\mathbf{x})dx_1\ldots dx_s \end{aligned} \tag{5.6}$$

Summing over all possible combinations of coagulating population member attributes requires integration with respect to each attribute variable:

$$\frac{\partial n(\mathbf{m})}{\partial t} = \frac{1}{2}\int_0^{m_s}\cdots\int_0^{m_2}\int_0^{m_1}\beta(\mathbf{m}-\mathbf{x},\mathbf{x})n(\mathbf{m}-\mathbf{x})n(\mathbf{x})dx_1dx_2\ldots dx_s \tag{5.7}$$

The factor ½ corrects for double counting caused by integration. In the one-component case the factor of ½ corrected double counting in one dimension. In this case, the multiple integration still produces double counting, which is remedied by the factor ½. Equation (5.7) is equivalent to determining the coagulation contribution from Equation (5.2) by summing over all possible combinations of coagulating compositions:

$$\frac{dn(\mathbf{m})}{dt} = \frac{1}{2}\sum_{x_s}^{x_s<m_s}\cdots\sum_{x_2}^{(x_2<m_2)}\sum_{x_1}^{x_1<m_1}\beta(\mathbf{m}-\mathbf{x},\mathbf{x})n(\mathbf{m}-\mathbf{x})n(\mathbf{x})\Delta x_1\ldots\Delta x_s \tag{5.8}$$

and taking the limit as the intervals go to zero results in the expression and produces a partial differential equation:

$$\frac{\partial n(\mathbf{m})}{\partial t} = \frac{1}{2}\int_0^{m_s}\cdots\int_0^{m_2}\int_0^{m_1}\beta(\mathbf{m}-\mathbf{x},\mathbf{x})n(\mathbf{m}-\mathbf{x})n(\mathbf{x})dx_1dx_2\ldots dx_s \tag{5.9}$$

5.2.2 Reduction of coagulation production integrals

As with the one-component case, double counting may be eliminated by reducing the integration range of the outermost integration limit:

$$\frac{\partial n(\mathbf{m})}{\partial t} = \int_0^{\frac{m_s}{2}}\cdots\int_0^{m_2}\int_0^{m_1}\beta(\mathbf{m}-\mathbf{x},\mathbf{x})n(\mathbf{m}-\mathbf{x})n(\mathbf{x})dx_1dx_2\ldots dx_s \tag{5.10}$$

The outer integration limit is effectively a one-dimensional integral because all of the other variables have already been integrated out; therefore the same reduction of integration range as in the one-component case can implemented. Note that this still represents a large reduction in the total integration range, effectively cutting it in half.

5.2.3 Coagulation loss

The coagulation loss term is also derived from a balance on a multidimensional population segment:

$$\frac{dn(\mathbf{m})\Delta m_1 \Delta m_2 \ldots \Delta m_s}{dt} = -\beta(\mathbf{m}, \mathbf{x}) n(\mathbf{m}) \Delta m_1 \Delta m_2 \ldots \Delta m_s n(\mathbf{x}) \Delta x_1 \Delta x_2 \ldots \Delta x_s \tag{5.11}$$

Dividing through by all the Δm_i's, this expression trivially reduces to:

$$\frac{\partial n(\mathbf{m})}{\partial t} = -\beta(\mathbf{m}, \mathbf{x}) n(\mathbf{m}) n(\mathbf{x}) \Delta x_1 \Delta x_2 \ldots \Delta x_s \tag{5.12}$$

which describes the rate at which particles of size **m** are lost due to coagulation with particles size **x**. In order to determine the total loss or particles size **m** due to coagulation with all other particle sizes, it is necessary to sum over all possible intervals Δx_i.

$$\frac{\partial n(\mathbf{m})}{\partial t} = \sum_{\Delta x_s} \ldots \sum_{\Delta x_2} \sum_{\Delta x_1} -\beta(\mathbf{m}, \mathbf{x}) n(\mathbf{m}) n(\mathbf{x}) \Delta x_1 \Delta x_2 \ldots \Delta x_s \tag{5.13}$$

As usual, this expression reduces to an integral when the intervals Δx_i are reduced to zero:

$$\frac{\partial n(\mathbf{m})}{\partial t} = \int_0^\infty \ldots \int_0^\infty \int_0^\infty -\beta(\mathbf{m}, \mathbf{x}) n(\mathbf{m}) n(\mathbf{x}) dx_1 dx_2 \ldots dx_s \tag{5.14}$$

which also converts the expression to a partial differential equation. Realizing that **m** is constant within these multidimensional integrals results in the final form of the coagulation removal expression:

$$\boxed{\frac{\partial n(\mathbf{m})}{\partial t} = -n(\mathbf{m}) \int_0^\infty \ldots \int_0^\infty \int_0^\infty \beta(\mathbf{m}, \mathbf{x}) n(\mathbf{x}) dx_1 dx_2 \ldots dx_s} \tag{5.15}$$

Note that the units for the coagulation kernel are cm^3/s and remain unchanged from the single component case.

5.3 Fragmentation

As with the single component case, fragmentation can both produce and usurp particles in any given size range $n(\mathbf{m})$ of a number density distribution. Particles of size **m** may be produced by the fragmentation of larger particles, a process referred to as fragmentation production, while

fragmentation removal refers to the process by which particles of size **m** are lost due to fragmentation into smaller particles. The following two sections detail the derivation of these two fragmentation contributions in the dynamic population balance equation.

5.3.1 Fragmentation removal

The removal of particles due to fragmentation, as in the one-component case, is a first order process. Performing a balance over one multidimensional population segment yields:

$$\frac{dn(\mathbf{m})\Delta m_1 \Delta m_2 \ldots \Delta m_s}{dt} = -g(\mathbf{m})n(\mathbf{m})\Delta m_1 \Delta m_2 \ldots \Delta m_s \tag{5.16}$$

The continuum form of this equation is a partial differential equation is given in Equation (5.17):

$$\frac{\partial n(\mathbf{m})}{\partial t} = -g(\mathbf{m})n(\mathbf{m}) \tag{5.17}$$

5.3.2 Fragmentation production

In order to describe the production of particles due to fragmentation, we define the multicomponent coagulation kernel to describe the resulting distribution of fragments when a large particle undergoes fragmentation.

DEFINITION

The multicomponent fragmentation kernel $\gamma(\mathbf{x}, \mathbf{m})dm_1 dm_2 \ldots dm_s$ *describes the fraction of total particles distributed into the mass range* $[m_1, m_1+dm_1][m_2, m_2+dm_2][m_3, m_3+dm_3]\ldots [m_s, m_s+dm_s]$ *from the fragmentation of a particle of composition* **x**.

As in the one component case, because $\gamma(\mathbf{x}, \mathbf{m})$ is a fraction, the integral over the domain of all possible smaller particle sizes must sum to one. Because the particle fragments may have any composition so long as $m_i < x_i$ for all i, resulting in the following s-dimensional integral:

$$\int_0^{m_s} \ldots \int_0^{m_2} \int_0^{m_1} \gamma(\mathbf{m}, \mathbf{x}) dx_1 dx_2 \ldots dx_s = 1 \tag{5.18}$$

Much like the one-component case, the total production of particles in a given bin range is the product of the rate at which the larger prattles fragment multiplied by the number of smaller particles created by each fragmentation $\nu(\mathbf{x})$ and the fraction of these smaller fragments which have size **m**, $\gamma(\mathbf{x}, \mathbf{m})$.

$$\frac{n(\mathbf{m})\Delta m_1 \Delta m_2 \ldots \Delta m_s}{dt} = \frac{-dn(\mathbf{x})\Delta x_1 \Delta x_2 \ldots \Delta x_s}{dt} v(\mathbf{x})\gamma(\mathbf{x}, \mathbf{m})\Delta m_1 \Delta m_2 \ldots \Delta m_s \tag{5.19}$$

The Δm_i terms on both sides of this expression can be canceled:

$$\frac{\partial n(\mathbf{m})}{\partial t} = \frac{-dn(\mathbf{x})\Delta x_1 \Delta x_2 \ldots \Delta x_s}{dt} v(\mathbf{x})\gamma(\mathbf{x}, \mathbf{m}) \tag{5.20}$$

In order to account for the contribution from all possible population segments, it is necessary to sum over all of the larger particle sizes that could fragment to produce a particle size **m**:

$$\begin{aligned} \frac{\partial n(\mathbf{m})}{\partial t} &= \frac{-dn(\mathbf{x})}{dt} v(\mathbf{x})\gamma(\mathbf{x}, \mathbf{m})\Delta x_1 \Delta x_2 \ldots \Delta x_s \\ \frac{\partial n(\mathbf{m})}{\partial t} &= \sum_{\Delta x_s} \cdots \sum_{\Delta x_2 \Delta x_1} \sum \left(-\frac{dn(\mathbf{x})}{dt}\right) v(\mathbf{x})\gamma(\mathbf{x}, \mathbf{m})\Delta x_1 \Delta x_2 \ldots \Delta x_s \end{aligned} \tag{5.21}$$

In the case where the intervals Δx_i are reduced in size, this expression becomes a multidimensional integral:

$$\frac{\partial n(\mathbf{m})}{\partial t} = \int_{x_s}^{\infty} \cdots \int_{x_2 x_1}^{\infty \infty} \left(-\frac{dn(\mathbf{x})}{dt}\right) v(\mathbf{x})\gamma(\mathbf{x}, \mathbf{m}) dx_1 dx_2 \ldots dx_s \tag{5.22}$$

Finally, substituting the expression for the rate of larger particle fragmentation from Equation (5.17) yields the final expression for fragmentation production:

$$\boxed{\frac{\partial n(\mathbf{m})}{\partial t} = \int_{x_s}^{\infty} \cdots \int_{x_2 x_1}^{\infty \infty} g(\mathbf{x}) v(\mathbf{x}) \gamma(\mathbf{x}, \mathbf{m}) dx_1 dx_2 \ldots dx_s} \tag{5.23}$$

As with the one component case, a mass balance can be written which matches the amount of a given species lost due to fragmentation removal in a given population segment **m** to the amount of that species gained by the fragments of these particles.

$$\begin{aligned} \frac{\partial n(\mathbf{m}) m_i}{\partial t} &= -g(\mathbf{m}) n(\mathbf{m}) v(\mathbf{m}) \int_0^{m_s} \cdots \int_{0\ 0}^{m_2 m_1} \gamma(\mathbf{m}, \mathbf{x}) x_i dx_1 dx_2 \ldots dx_s \\ \frac{\partial n(\mathbf{m}) m_i}{\partial t} &= -g(\mathbf{m}) n(\mathbf{m}) m_i \end{aligned} \tag{5.24}$$

The first expression equates the amount of mass lost from the population segment at **m** to the

mass gained by the smaller particles; the second equation gives the expression for the loss of these particles size **m**. Combining these two expressions yields the mass balance relation:

$$g(\mathbf{m})n(\mathbf{m})m_i = g(\mathbf{m})n(\mathbf{m})v(\mathbf{m})\int_0^{m_s}\cdots\int_0^{m_2}\int_0^{m_1}\gamma(\mathbf{m},\mathbf{x})x_i dx_1 dx_2\ldots dx_s$$

$$m_i = v(\mathbf{m})\int_0^{m_s}\cdots\int_0^{m_2}\int_0^{m_1}\gamma(\mathbf{m},\mathbf{x})x_i dx_1 dx_2\ldots dx_s \tag{5.25}$$

$$m = v(\mathbf{m})\int_0^{m_s}\cdots\int_0^{m_2}\int_0^{m_1}\gamma(\mathbf{m},\mathbf{x})\left(\sum_i x_i\right)dx_1 dx_2\ldots dx_s$$

Where the last statement is obtained by summing the second expression over all species. Knowing $\gamma(\mathbf{m}, \mathbf{x})$ and m, this expression makes it easy to directly calculate $v(\mathbf{m})$.

$$v(\mathbf{m}) = \frac{m}{\int_0^{m_s}\cdots\int_0^{m_2}\int_0^{m_1}\gamma(\mathbf{m},\mathbf{x})\left(\sum_i x_i\right)dx_1 dx_2\ldots dx_s} \tag{5.26}$$

5.4 Growth

For a multicomponent model, growth may occur due to the accumulation of any given component. An expression for growth due to accumulation of any single species *i* is identical to the single component expression for growth of a single component:

$$\frac{\partial n(\mathbf{m})}{\partial t} = -\frac{\partial n((\mathbf{m})G_i(\mathbf{m}))}{\partial m_i} \tag{5.27}$$

where $G_i(\mathbf{m}) = dm_i/dt$, the rate of accumulation of species i in a particles of size **m**.

This expression can be derived directly from a balance on a differential population segment. For the two-component case, the differential population segments are illustrated in Figure 5-2. Analyzing the rate at which particles move along the axis of species 1 results in the two-component population segment balance given in Equation (5.28).

$$\frac{dn(m_1,m_2)\Delta m_1\Delta m_2}{dt} = \frac{1}{\Delta t_{i-1}}n(m_1-\Delta m_1,m_2)\Delta m_1\Delta m_2 - \frac{1}{\Delta t_i}n(m_1,m_2)\Delta m_1\Delta m_2 \tag{5.28}$$

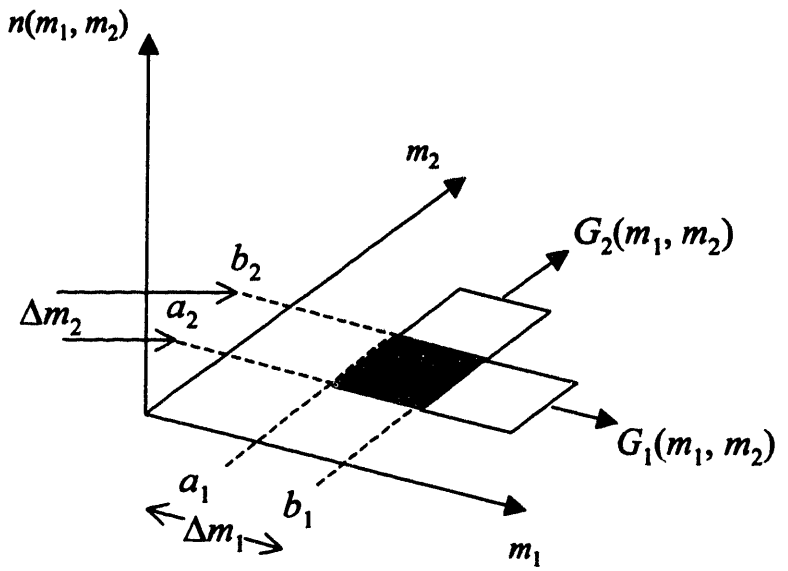

Figure 5-2: Growth rates of different components and the direction of growth in the two-component number density scenario.

which is the direct two-component interpretation of Equation (4.38). This expression is a balance which tracks the rate at which particles move along the m_1 axis; physically this is equivalent to the rate at which particles grow due to accumulation of species 1. For the general case of an s-component system where the balance is written around species i:

$$\frac{dn(m_1, \ldots m_i, \ldots m_s)\Delta m_1 \ldots \Delta m_i \ldots \Delta m_s}{dt} = \frac{1}{\Delta t_{i-1}} n(m_1, \ldots m_i - \Delta m_i, \ldots m_s)\Delta m_1 \ldots \Delta m_i \ldots \Delta m_s - \frac{1}{\Delta t_i} n(m_1, \ldots m_i, \ldots m_s)\Delta m_1 \ldots \Delta m_i \ldots \Delta m_s \tag{5.29}$$

Canceling out all of the Δm's except for Δm_i:

$$\frac{dn(m_1, \ldots m_i, \ldots m_s)\Delta m_i}{dt} = \frac{1}{\Delta t_{i-1}} n(m_1, \ldots m_i - \Delta m_i, \ldots m_s)\Delta m_i - \frac{1}{\Delta t_i} n(m_1, \ldots m_i, \ldots m_s)\Delta m_i \tag{5.30}$$

Rearranging this expression:

$$\frac{dn(m_1, \ldots m_i, \ldots m_s)\Delta m_i}{dt} = \frac{\Delta m_i}{\Delta t_{i-1}} n(m_1, \ldots m_i - \Delta m_i, \ldots m_s) - \frac{\Delta m_i}{\Delta t_i} n(m_1, \ldots m_i, \ldots m_s) \tag{5.31}$$

we can now reinterpret the $\Delta m_i/\Delta t$ terms as growth rates representing the mass of component i which the particles accumulate per unit time. Taking the limit of these expressions as Δt approaches zero allows the substitution of the continuous growth rate expression $G_i(\mathbf{m})$:

$$\frac{dn(m_1, \ldots m_i, \ldots m_s)\Delta m_i}{dt} = G_i(m_1, \ldots m_i - \Delta m_i, \ldots m_s) n(m_1, \ldots m_i - \Delta m_i, \ldots m_s) - G_i(m_1, \ldots m_i, \ldots m_s) n(m_1, \ldots m_i, \ldots m_s) \tag{5.32}$$

Dividing this expression through by Δm_i yields:

$$\frac{dn(m_1, \ldots m_i, \ldots m_s)}{dt} = \frac{G_i(m_1, \ldots m_i - \Delta m_i, \ldots m_s) n(m_1, \ldots m_i - \Delta m_i, \ldots m_s) - G_i(m_1, \ldots m_i, \ldots m_s) n(m_1, \ldots m_i, \ldots m_s)}{\Delta m_i} \tag{5.33}$$

Taking the limit as Δm_i goes to zero results in the growth expression for species i:

$$\boxed{\frac{\partial n(\mathbf{m})}{\partial t} = -\frac{\partial (n(\mathbf{m}) G_i(\mathbf{m}))}{\partial m_i}} \tag{5.34}$$

In order to account for the growth of all species in the system, it is necessary to sum the growth expressions for all species i:

$$\frac{\partial n(\mathbf{m})}{\partial t} = -\sum_i \frac{\partial n((\mathbf{m}) G_i(\mathbf{m}))}{\partial m_i} \tag{5.35}$$

5.5 Sources and Sinks

Just as with the one-component case, sources and sinks may either be manifested as boundary conditions or sources within the domain of the number density distribution.

5.5.1 Sources within the number density distribution domain

Sources within the domain of the number density distribution add particles at a given rate over some range of the number density distribution. If $k(\mathbf{m})\Delta\mathbf{m}$ is the rate at which these particles are added, then the population balance over a differential population segment is:

$$\frac{dn(m_1, m_2, \ldots m_s)\Delta m_1 \Delta m_2 \ldots \Delta m_s}{dt} = k(m_1, m_2, \ldots m_s)\Delta m_1 \Delta m_2 \ldots \Delta m_s \tag{5.36}$$

Note that the units of $k(\mathbf{m})$ are $1/(\text{cm}^3 \cdot \text{s} \cdot \text{g}^s)$ where s is the number of species and "s" is seconds. Taking the limit as the population intervals Δm_i are reduced in size transforms this expression into a partial differential equation:

$$\begin{aligned} \frac{\partial n(m_1, m_2, \ldots m_s) dm_1 dm_2 \ldots dm_s}{\partial t} &= k(m_1, m_2, \ldots m_s) dm_1 dm_2 \ldots dm_s \\ \frac{\partial n(\mathbf{m}) dm_1 dm_2 \ldots dm_s}{\partial t} &= k(\mathbf{m}) dm_1 dm_2 \ldots dm_s \end{aligned} \tag{5.37}$$

Finally, dividing through by all of the dm_i terms results in the final form of the population balance expression for sources and sinks in the number density distribution domain:

$$\frac{\partial n(\mathbf{m})}{\partial t} = k(\mathbf{m}) \tag{5.38}$$

5.5.2 Boundary nucleation sources

In one-component systems where the smallest particles present are newly formed nuclei, the nucleation and growth rates specify a natural boundary condition, as shown in Chapter 4. However, this does not hold in multicomponent systems. Consider a two-component system with species a and b. Depending on the particular system, several cases may arise:

- nucleation is due primarily due to formation of particles of pure a
- nucleating particles contain a mix of species a and b
- nucleating particles contain primarily pure a or pure b

The first case will produce particles of mass $(a_{min}, 0)$ where a_{min} denotes the mass of a critical nucleus of pure component a. This acts as a point source in the form of Equation (5.38):

$$k(a, b) = N_0 \delta(a - a_{min})\delta(b) \tag{5.39}$$

where N_0 is the nucleation rate in terms of particles/$(\text{cm}^3 \cdot \text{s})$. The second case will produce a nucleation function in the form of Equation (5.38) which covers some finite domain of the num-

ber density distribution, as shown in Figure 5-3.

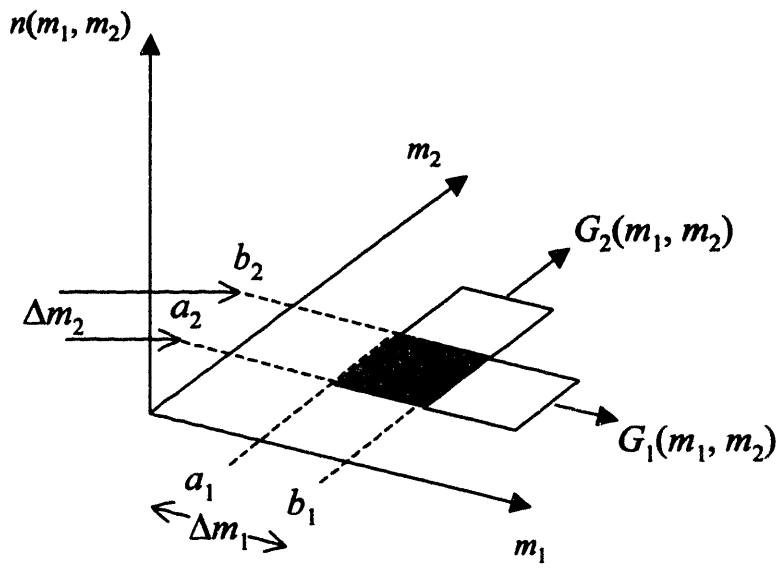

Figure 5-3: Growth rates of different components and the direction of growth in the two-component number density scenario.

Finally, the third case is merely an extension of the first case, where $k(a, b)$ is represented by two point sources:

$$k(a,b) = N_a\delta(a-a_{min})\delta(b) + N_b\delta(a)\delta(b-b_{min}) \tag{5.40}$$

where N_a is the nucleation rate for particles of pure a and N_b is the nucleation rate for particles of pure b.

References

[1] Danckwerts, P. V. *Gas-Liquid,* McGraw-Hill, 1970.

[2] Doraiswamy, L. K.; Sharma, M. M. *Heterogeneous Reactions*, John Wiley & Sons, 1984.

[3] Froment, G. F.; Bischoff, K. B. *Chemical Reactor Analysis and Design*, 2nd Ed. John Wiley & Sons, 1990.

[4] Rodriguez, A.; Callo, J. M.; Sweed, N.; Ed. *Multiphase Chemical Reactors*, Sijthoff and Noordhoff, 1981.

Chapter 6: Scale Analysis of Growth Mechanisms

Growth is one of the most important processes in the formation of particles. Depending upon specific conditions and chemistry, particle growth can be driven by a number of processes. The process of incorporating a gaseous vapor into a particle may include a number of distinct steps and mechanisms. For example, diffusion typically transports gas phase species to particle surfaces, while the process of incorporating these species into the particle may be limited by either surface reactions or reactions within the entire particle volume. Examples include:

- deposition processes where the particle grows by chemically reacting with gas phase species on its surface. When this reaction is the limiting step, a surface reaction-limited growth law is used.
- often some gas phase species are consumed by reaction within a particle or droplet. As the species is depleted in the droplet, it is replenished by absorption from the gas phase. When the rate-limiting step is reaction within the droplet, a volume reaction-limited growth law is used

Figure 6-1 depicts the relationship between the various growth processes that occur in particles.

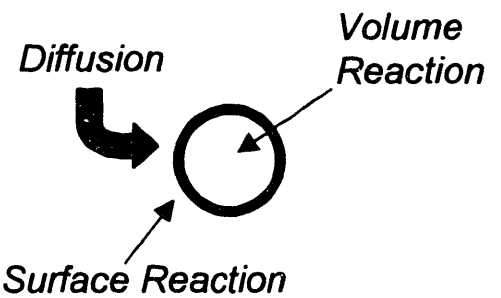

Figure 6-1: Particle growth mechanisms.

Depending on which step of the growth process is limiting, vastly different growth laws result. Different growth laws produce marked differences in the dynamics of the respective population balance equation for that system, motivating the use of different solution methods. The following sections investigate these varying growth processes and summarize the resulting differences in solution methods.

6.1 Diffusion-Limited Particle Growth

Often in physical processes, growth of particles is constrained by the rate at which molecules from the gas phase diffuse to the surface of the particle. In the case where the particles are greater than the mean free path of the gas molecules, the growth law for these particles is given by:

$$\frac{dm}{dt} = 2\pi D_p D(c_\infty - c_s)W$$
$$G(D_p) = 2\pi D_p D(c_\infty - c_s)W \tag{6.1}$$

This growth rate represents the rate at which mass of component *i* is added to particles of size D_p (Friedlander, 2000). Table 6-1 summarizes the symbols in this expression and their units.

Table 6-1: Summary of symbols for continuum condensational growth expression

Symbol	*Name*	*Units*
m	Mass of the condensing species in the particle	g
D_p	Particle diameter	cm
D	Diffusivity of condensing species in bulk gas	cm^2/s
C_∞	Concentration of the condensing species in the bulk gas	mol/cm^3
C_s	Equilibrium concentration in the gas phase at the particle surface	mol/cm^3
W	Molecular weight of the condensing species	g/mol

6.2 Implementation in Numerical Solution

The dynamic population balance equation for a one-component system undergoing growth is:

$$\frac{\partial n(m)}{\partial t} = -\frac{\partial(n(m)\cdot G(m))}{\partial m} \tag{6.2}$$

Please refer to section 4.3 for a full derivation of the growth expression. Note that in this form, $G(m)$ is expressed in the form dm_i/dt - which is consistent with the units required for this form of the population balance. However, $G(D_p)$ from Equation (6.1) must first be converted to $G(m)$. Assuming spherical-shaped particles/droplets, the formula for volume of a sphere can be used to develop a relationship between D_p and m.

$$v = \frac{4}{3}\pi r^3 = \frac{\pi}{6}D_p^3$$

$$m = \rho v = \frac{\rho\pi}{6}D_p^3 \tag{6.3}$$

$$D_p = \left(\frac{6m}{\rho\pi}\right)^{1/3}$$

Substituting this result into $G(D_p)$ yields the desired growth rate $G(m)$.

$$G(m) = 2\pi\left(\frac{6m}{\rho\pi}\right)^{1/3} D(c_\infty - c_s)W \tag{6.4}$$

The lumping all the parameters except m into the parameter K results in the simplified form of the growth law.

$$K = 2\pi D(c_\infty - c_s)W\left(\frac{6}{\rho\pi}\right)^{1/3}$$

$$G(m) = Km^{1/3} \tag{6.5}$$

Substituting this form of the growth law $G(m)$ into Equation (6.2) produces the population balance equation for a system undergoing diffusion-limited particle growth.

$$m = \frac{\rho\pi}{6}D_p^3 \rightarrow D_p = \left(\frac{6m}{\rho\pi}\right)^{1/3}$$

$$\frac{\partial n(m)}{\partial t} = -2\pi D(c_\infty - c_s)W\frac{\partial(n(m)\cdot D_p)}{\partial m} \Rightarrow \tag{6.6}$$

$$\frac{\partial n(m)}{\partial t} = -\frac{\partial(n(m)\cdot(Km^{1/3}))}{\partial m}$$

By using the method of characteristics, this expression can be solved to describe the evolution of $n(m)$ as a function of t.

6.3 Characteristic Curves

The method of characteristics (Zauderer, 1989; Zwillinger, 1992) provides a method of drawing the "characteristic curves" which describe the dynamics of hyperbolic partial differential quietens. For partial differential equations of the general form:

$$a(x,t)\frac{\partial y}{\partial x} + b(x,t)\frac{\partial y}{\partial t} = c(x,t)y + d(x,t) \tag{6.7}$$

the method of characteristics provides the following set of ordinary differential equations regarding the dynamic evolution of x, y, and t.

$$\begin{aligned} \frac{dt}{ds} &= b(x,t) \\ \frac{dx}{ds} &= a(x,t) \end{aligned} \tag{6.8}$$

Solving these two differential equations yields two curves, $x(s)$ and $t(s)$ which parametrically describe the evolution of x and t in the system. Along each of these curves, the evolution of y is specified by:

$$\frac{dy}{ds} = c(x,t)y + d(x,t) \tag{6.9}$$

Note that Equations (6.8) and (6.9) can quickly be validated by comparing Equation (6.7) with the identity:

$$\begin{aligned} \frac{dy}{ds} &= \frac{\partial y}{\partial x}\frac{dx}{ds} + \frac{\partial y}{\partial t}\frac{dt}{ds} \\ \frac{dy}{ds} &= \frac{\partial y}{\partial x}a(x,t) + \frac{\partial y}{\partial t}b(x,t) \\ \frac{dy}{ds} &= c(x,t)y + d(x,t) \end{aligned} \tag{6.10}$$

The most common application of the method of characteristics is to analyze the dynamics of convective systems.

6.3.1 Convective system constant velocity: characteristics example

Flow of a chemical component A in a one-dimensional system is given by the familiar relation:

$$\frac{\partial C_A}{\partial t} = -\frac{\partial (C_A \cdot v)}{\partial z} \tag{6.11}$$

where the flow is in the z-direction at velocity v. In the case where v is constant, this expression reduces to:

$$\frac{\partial C_A}{\partial t} = -v\frac{\partial C_A}{\partial z} \tag{6.12}$$

In order to apply the method of characteristics, it is first necessary to identify corresponding components in Equations (6.7) and (6.12).

Table 6-2: Variable correspondence between Equations (6.7) *and* (6.12)

Equation (6.7) component	*Equation (6.12) component*	*Variable Definition*
x	z	distance
y	C_A	concentration
t	t	time
$a(x, t)$	v	velocity
$b(x, t)$	1	n/a
$c(x, t)$	0	n/a
$d(x, t)$	0	n/a

The corresponding set of differential equations for this system follow directly from using the relations given in Table 6-2.

$$\begin{aligned} \frac{dt}{ds} &= 1 \\ \frac{dz}{ds} &= v \end{aligned} \tag{6.13}$$

If the initial set of conditions for this system are $t = t_0$ and $z = z_0$, and $s = 0$, then integrating with respect to s yields the following set of curves.

$$\begin{aligned} t(s) &= t_0 + s \\ z(s) &= z_0 + v \cdot s \end{aligned} \tag{6.14}$$

For this particular system, it is possible to eliminate s from Equation (6.14) and solve directly for z as a function of t and vice-versa.

$$\begin{aligned} z(t) &= z_0 + v(t - t_0) \\ t(z) &= \frac{z - z_0}{v} + t_0 \end{aligned} \tag{6.15}$$

Using this relation, it is possible to construct a set of "characteristic curves" describing the position of individual "packets" of concentration starting at various points z_0.

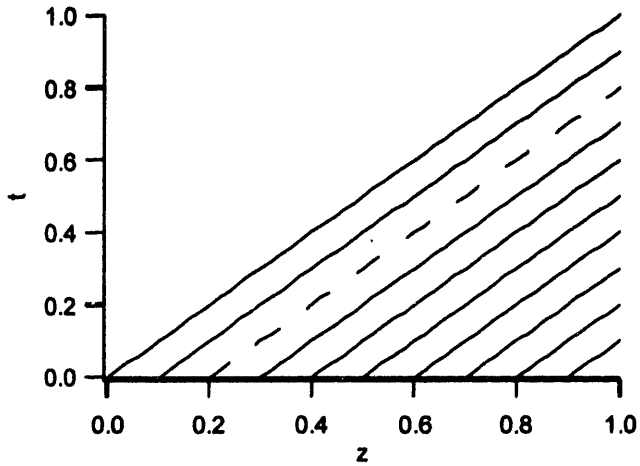

Figure 6-2: Convective system characteristic curves for constant velocity.

Figure 6-2 illustrates a set characteristic curves for the case where $t_0 = 0$, $v = 1$ and the points z_0 are evenly spaced between zero and one. Examining the line starting at $z = 0.3$, shown as a dashed line in the figure, this line proceeds at a constant rate to higher values of z as t increases. The derivative of the line at any given point is the inverse of the velocity, which is constant at 1. Thus, a "packet" of concentration originally located at the point $z_0 = 0.2$ travels at constant velocity to the right, creating the characteristic curve trajectory in t - z space. Note also that:

$$\frac{dC_A}{ds} = 0 \tag{6.16}$$

so the value of C_A is constant along each characteristic curve.

6.3.2 Convective system, varying velocity

In the case where the velocity v is a function of position, the results are more complicated. Take the system where $v(z) = 1 + z$. In this case, the derivative in Equation (6.11) is expanded:

$$\begin{aligned} \frac{\partial C_A}{\partial t} &= -\frac{\partial (C_A \cdot v(z))}{\partial z} = -v(z)\frac{\partial C_A}{\partial z} - C_A \frac{\partial v(z)}{\partial z} \\ \frac{\partial C_A}{\partial t} &= -(1+z)\frac{\partial C_A}{\partial z} - C_A \end{aligned} \tag{6.17}$$

Table 6-3 lists the correspondence between terms in Equations (6.7) and (6.17).

Table 6-3: Variable correspondence between Equations (6.7) *and* (6.17)

Equation (6.7) component	*Equation (6.17) component*	*Variable Definition*
x	z	distance
y	C_A	concentration
t	t	time
$a(x, t)$	$1 + z$	velocity (v)
$b(x, t)$	1	dv/dz
$c(x, t)$	0	n/a
$d(x, t)$	0	n/a

The corresponding set of differential equations for this system is now:

$$\begin{aligned} \frac{dt}{ds} &= 1 \\ \frac{dz}{ds} &= (1 + z) \end{aligned} \tag{6.18}$$

Note that in any process where $dt/ds = 1$, if initial conditions are such that $t_0 = s_0 = 1$, then $t = s$. As a result, the second differential equation can be restated in terms of z and t and integrated directly to yield the characteristic curve.

$$\frac{dz}{dt} = (1 + z) \tag{6.19}$$

This yields the characteristic curve:

$$t = \ln\left(\frac{1 + z}{1 + z_0}\right) \tag{6.20}$$

Plotting the set of characteristic curves evenly spaced between $z = 0$ and $z = 1$ yields Figure 6-3. Note that now the characteristic lines are curved, indicating that individual "packets" of concentration actually gain velocity as they move to higher values of z, a fact that is consistent with the velocity $v = 1 + z$. In addition, C_A now evolves according to the expression:

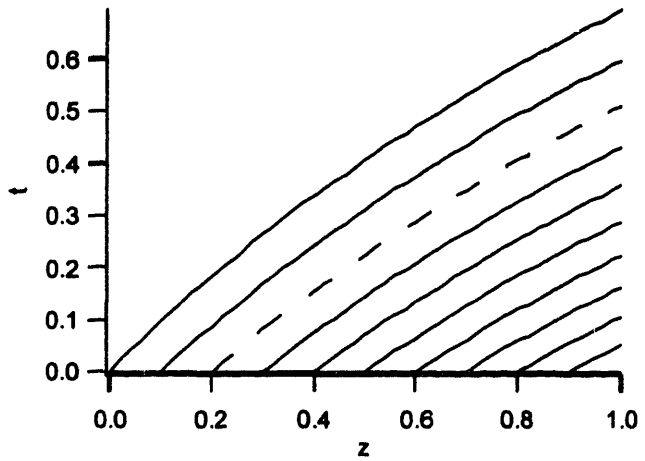

Figure 6-3: Characteristic curves for convective system with varying velocity.

$$\frac{dC_A}{ds} = -C_A \tag{6.21}$$

which can be solved by integration with respect to the characteristic curve parameter s.

6.4 Diffusion-Limited Growth Characteristics

Using the method of characteristics, it is also possible to calculate the characteristic curves of population balance problems involving growth. For a system undergoing growth, the governing equation is:

$$\begin{aligned} \frac{\partial n(m)}{\partial t} &= -\frac{\partial (n(m) \cdot G(m))}{\partial m} \\ \frac{\partial n(m)}{\partial t} &= -n(m)\frac{\partial G(m)}{\partial m} - G(m)\frac{\partial n(m)}{\partial m} \end{aligned} \tag{6.22}$$

Applying the method of characteristics as prescribed by Equation (6.7):

$$\begin{aligned} \frac{dt}{ds} &= 1 \\ \frac{dm}{ds} &= G(m) \end{aligned} \tag{6.23}$$

Again, because $t_0 = 0$ and $s_0 = 0$, we have $s = t$ and therefore:

$$\boxed{\frac{dm}{dt} = G(m)} \tag{6.24}$$

This result applies to all systems of the form given in Equation (6.22). Substituting the appropriate growth law from Equation (6.5) and integrating this expression yields the characteristic curve.

$$\frac{dm}{dt} = Km^{1/3}$$

$$\int_{t_0}^{t} dt = \int_{m_0}^{m} \frac{1}{Km^{1/3}} dm \tag{6.25}$$

$$t - t_0 = \frac{3}{2K}(m^{2/3} - m_0^{2/3})$$

Figure 6-4 shows a plot of these characteristic lines spaced evenly in m with $K = 1.15\times10^{-4}$ and $t_0 = 0$.

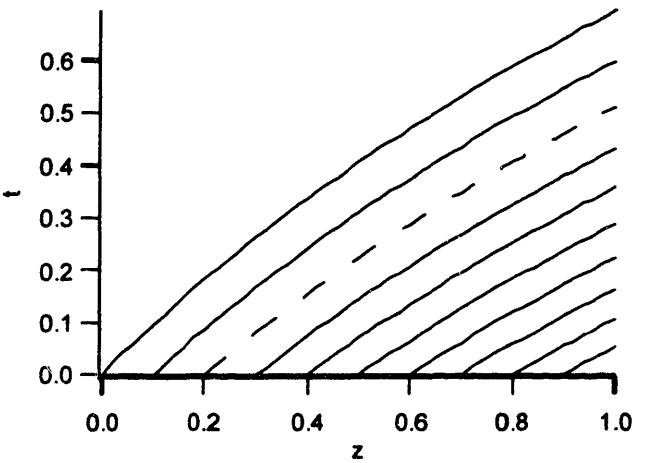

Figure 6-4: Characteristic curves spaced evenly in *m* for diffusion-limited growth law.

Note the even spacing of the characteristic lines, with the smallest particles growing slightly slower at first and then leveling off as they increase in size. The almost-uniform growth rate for this system is well-scaled and readily adaptable to numerical solution. Plotting the same characteristic curves on a log scale with the m points evenly spaced along this scale reveals a very differ-

ent result, as shown in Figure 6-5. Comparison with the characteristic curves in Figure 6-4 show

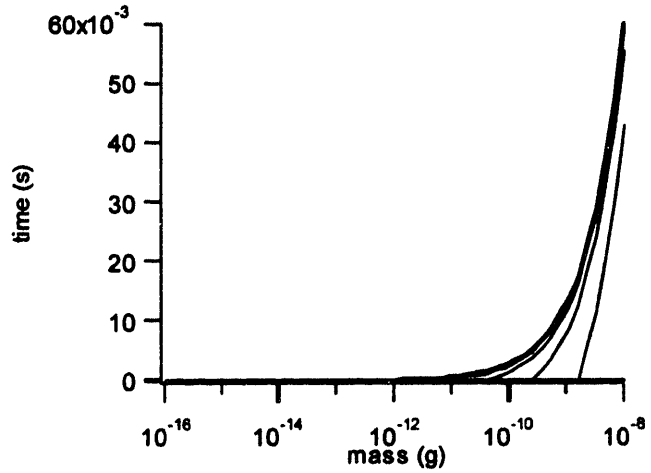

Figure 6-5: Logarithmically spaced characteristic curves as a function of *m* for diffusion-limited growth law.

that the characteristic curves have a markedly different appearance despite the fact that this graph still represents the same physical growth model.

In fact, the characteristic curves shown in Figure 6-4 are actually the characteristic curves of the logarithmic-scaled system of governing equations. These governing equations can be derived from the original system of governing equations by introducing a logarithmic scaling transformation:

$$m = m_0 e^{\gamma w} \tag{6.26}$$

where the new system of governing equations will describe the evolution of a distribution with w as the independent variable, $n(w)$. The following section derives this logarithmic-scaled growth expression from the original governing equation for growth derived in section 4.3.

6.4.1 Rescaled diffusion-based growth expression

Just as number density distributions can be rescaled (see Chapter 3), the governing equations can also be rescaled to describe the evolution of a particle system. Using the transformation given in Equation (6.26), the number density distributions are transformed as follows:

$$\begin{aligned} m &= m_0 e^{\gamma w} \\ n(w)dw &= n(m)dm \\ n(w) &= n(m)\frac{dm}{dw} = n(m)m\gamma \\ n(m) &= n(w)\frac{dw}{dm} = \frac{n(w)}{m\gamma} \end{aligned} \tag{6.27}$$

In order to perform a similar transformation on the governing equations, we seek a transformation of the form:

$$\frac{\partial n(m)}{\partial t} = -\frac{\partial(n(m)G(m))}{\partial m} \rightarrow \frac{\partial n(w)}{\partial t} = ? \tag{6.28}$$

which can be reached by directly substituting the expression for $n(m)$ from the last line of Equation (6.26) into the population balance equation for growth:

$$\begin{aligned} \frac{\partial n(m)}{\partial t} &= -\frac{\partial(n(m)G(m))}{\partial m} \\ \frac{\partial\left(n(w)\frac{dw}{dm}\right)}{\partial t} &= -\frac{\partial\left(n(w)\frac{dw}{dm}G(m)\right)}{\partial m} \end{aligned} \tag{6.29}$$

The growth rate expression must accordingly be converted from $G(m)$ to $G(w)$, or from dm/dt to dw/dt.

$$\begin{aligned} m &= m_{\min} e^{\gamma w} \rightarrow \frac{dw}{dm} = \frac{1}{\gamma m} \\ G(m) &= \frac{dm}{dt} \rightarrow G(w) = \frac{dw}{dt} = \frac{dm}{dt}\cdot\frac{dw}{dm} = G(m)\cdot\frac{dw}{dm} \\ G(w) &= G(m)\cdot\frac{dw}{dm} \end{aligned} \tag{6.30}$$

Finally, incorporating the results of Equation (6.30) and the chain rule reveals the final form of the population balance equation as given by Equation (6.31).

$$\frac{\partial\left(n(w)\frac{dw}{dm}\right)}{\partial t} = -\frac{\partial\left(n(w)\frac{dw}{dm}G(m)\right)}{\partial m} \rightarrow \frac{\partial n(w)}{\partial t}\frac{dw}{dm} = -\frac{dw}{dm}\frac{\partial\left(n(w)\frac{dw}{dm}G(m)\right)}{\partial w}$$

$$\frac{\partial n(w)}{\partial t} = -\frac{\partial\left(n(w)\frac{dw}{dm}G(m)\right)}{\partial w} = -\frac{\partial\left(n(w)\frac{dw}{dm}G(w)\frac{dm}{dw}\right)}{\partial w} \tag{6.31}$$

$$\frac{\partial n(w)}{\partial t} = -\frac{\partial(n(w)G(w))}{\partial w}$$

Using this result, the growth characteristics for this system may be calculated as a function of w.

6.4.2 Log-scaled growth characteristics

Using the log-rescaled growth expression for diffusion-limited growth, $G(w)$ is evaluated as in Equation (6.32):

$$G(w) = G(m)\cdot\frac{dw}{dm} = \frac{Km^{1/3}}{\gamma m} = \frac{K}{\gamma}m^{-2/3} \tag{6.32}$$

Recalling that $m = m_{\min}e^{\gamma w}$ results in the final rescaled population balance given in Equation (6.33), the final rescaled growth rate expression is:

$$G(w) = \frac{K}{\gamma}(m_{\min}e^{\gamma w})^{-2/3} \tag{6.33}$$

Together with the rescaled population balance equation for growth:

$$\frac{\partial n(w)}{\partial t} = -\frac{\partial(n(w)G(w))}{\partial w} \tag{6.34}$$

it is possible to derive the characteristic curves for the logarithmically scaled growth expression given in Equations (6.31).

It is evident that the form of the population balance equation for this system is identical to that in Equation (6.22) with the exception that w is substituted for m. It follows that the method of characteristics for this system results in the differential equation:

$$\frac{dw}{dt} = G(w) \tag{6.35}$$

Substituting the proper growth expression and integrating from $t = 0$ to t and w_0 to w yields the characteristic curve:

$$\frac{dw}{dt} = \frac{K}{\gamma}(m_{\min}e^{\gamma w})^{-2/3}$$

$$\int_0^t dt = \int_{w_0}^{w} \frac{\gamma}{K}(m_{\min}e^{\gamma w})^{2/3}dw \tag{6.36}$$

$$t = \frac{3}{2K}m_{\min}^{2/3}\left(e^{\frac{2\gamma w}{3}} - e^{\frac{2\gamma w_0}{3}}\right)$$

Coincidentally, the same result would have been reached had the expressions $m = m_{\min}e^{\gamma w}$ and $m_0 = m_{\min}e^{\gamma w_0}$ been substituted directly into Equation (6.25),

$$t = \frac{3}{2K}[(m_{\min}e^{\gamma w})^{2/3} - (m_{\min}e^{\gamma w_0})^{2/3}]$$

$$t = \frac{3}{2K}m_{\min}^{2/3}\left(e^{\frac{2\gamma w}{3}} - e^{\frac{2\gamma w_0}{3}}\right) \tag{6.37}$$

which emphasizes the fact that Equations (6.25) and (6.37) represent the same physical process with a different scaling system.

In order to plot these characteristic curves for the purposes of comparison with Figure 6-4, it is necessary to first establish the values of the variables in these two characteristic plots. Table 6-4

lists typical parameter values for a system of condensing water droplets.

Table 6-4: Diffusion-limited growth characteristic curve parameters

Symbol	*Definition*	*Value*	*Units*
c_∞	bulk gas H_2O concentration	4.57×10^{-5}	mol/cm^3
c_s	H_2O concentration at particle surface	4.15×10^{-5}	mol/cm^3
W	molecular weight	18.0	g/mol
r	density	1.0	g/cm^3
D	diffusivity	0.0242	cm^2/s
m_{min}	minimum particle mass	1.0×10^{-16}	g
m_{max}	maximum particle mass	1.0×10^{-8}	g
γ	logarithmic scaling factor	18.42	n/a
K	growth constant	1.15×10^{-4}	$g^{2/3}/s$

The note that the minimum particle mass corresponds roughly to aqueous particles 70 nm in diameter, or the mean free path of air. Figure 6-6 plots the characteristic curves as a function of w.

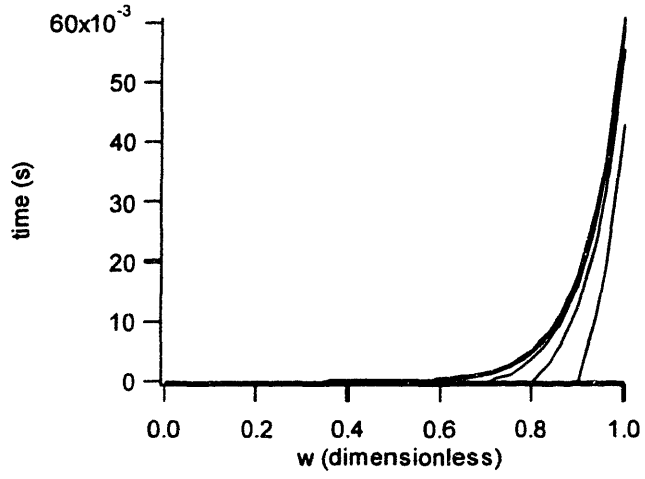

Figure 6-6: Logarithmic scaled characteristic curves for diffusion-limited growth law.

6.4.3 Comparison of diffusion-limited characteristic curves

Observing the characteristic curves in Figures 6-4 and 6-6 reveals that the growth rate $G(m)$ or $G(w)$ is essentially the inverse slope of the characteristic line at any (t, m) or (t, w) point, respectively. Whereas the growth rate based on w varies wildly based on position in the system, the growth rate based on m is a much more uniform function, and therefore more amenable to solution by numerical methods. The impact of scaling on the ease of numerical simulation will be further analyzed in section 6.6.

6.5 Surface Reaction-Limited Growth Characteristics

In many systems, particle growth is limited by a surface reaction. For example, deposition processes often involve a chemical reaction at the particle surface. Friedlander (2000) presents the surface-reaction limited growth expression.

$$G(m) = \frac{\alpha(\rho\pi)^{1/3} v_m 6^{2/3}}{\sqrt{2\pi M_w kT}} m^{2/3} = Km^{2/3} \tag{6.38}$$

Table 6-5 summarizes the definition and units of the symbols in Equation (6.38).

Table 6-5: Symbols definitions for surface reaction-limited growth kernel

Symbol	Definition	Units
a	accommodation coeffi-cient	-
r	density	g/cm^3
v_m	molecular volume	cm^3
M_w	molecular mass	g/mol
k	Boltzmann constant	J/K
T	temperature	Kelvin
m	particle mass	g
K	$\frac{\alpha(\rho\pi)^{1/3} v_m 6^{2/3}}{\sqrt{2\pi M_w kT}}$	$g^{1/3}/s$

Applying the method of characteristics to this growth expression yields the following differential

equation.

$$\boxed{\frac{dm}{dt} = Km^{2/3}} \tag{6.39}$$

Integrating this expression results in the characteristic curve for this system.

$$\begin{aligned} \int_{t_0}^{t} dt &= \int_{m_0}^{m} \frac{1}{Km^{2/3}} dm \\ t - t_0 &= \frac{3}{K}(m^{1/3} - m_0^{1/3}) \end{aligned} \tag{6.40}$$

In the special case where $t_0 = 0$, the characteristic curve reduces to the form given in Equation (8.33).

$$t = \frac{3}{K}(m^{1/3} - m_0^{1/3}) \tag{6.41}$$

Figure 6-7 plots these characteristic curves assuming that $K = 1.15\times10^{-4}$, the same value as the growth constant in the diffusion-controlled growth case.

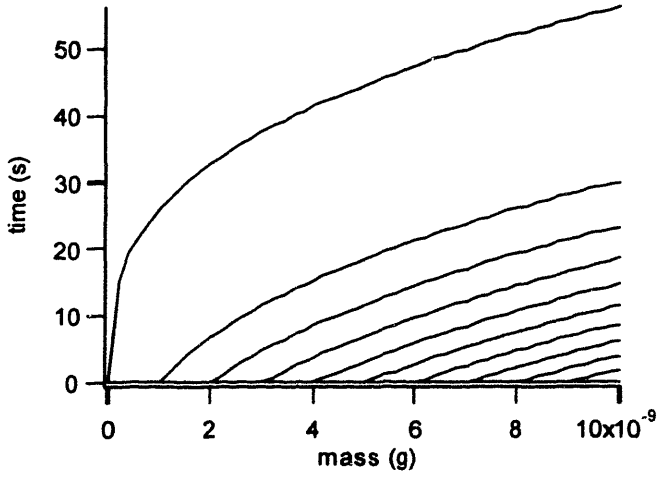

Figure 6-7: Surface reaction-limited characteristic curves as a function of *m*.

As with the diffusion-limited case, the logarithmic-scale characteristic curves are obtained by substituting $m = m_{\min}e^{\gamma w}$ and $m_0 = m_{\min}e^{\gamma w_0}$ into Equation (8.32).

$$t = \frac{3}{K}[(m_{\min}e^{\gamma w})^{1/3} - (m_{\min}e^{\gamma w_0})^{1/3}]$$
$$t = \frac{3m_{\min}^{1/3}}{K}\left(e^{\frac{\gamma w}{3}} - e^{\frac{\gamma w_0}{3}}\right) \tag{6.42}$$

Figure 6-8 graphs these logarithmically scaled characteristic curves. As in the diffusion-limited

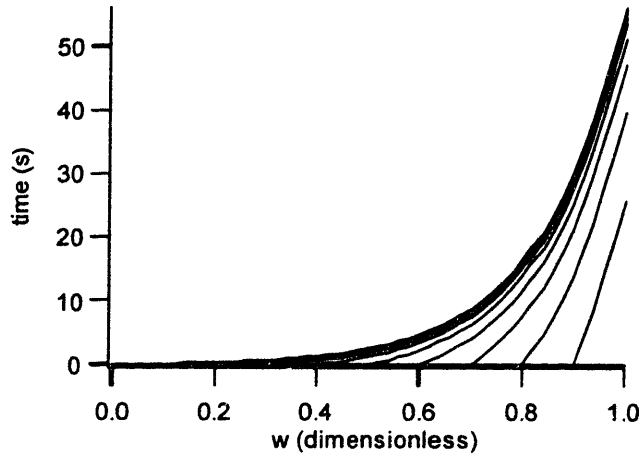

Figure 6-8: Logarithmic scale surface reaction-limited characteristic curves.

case, the logarithmic-scaled characteristics indicate a very fast growth rate for the smallest particles in the system and a much smaller growth rate for the largest particles. Conversely, when viewing the characteristics from a mass-based scale, the smallest particles appear to grow the slowest, while most of the particles in the system are at a much faster growth rate.

6.5.1 Volume reaction-limited growth characteristics

Many systems undergo reactions within particles that drive the transport of the reacting species to the particle surface. Friedlander (2000) cites examples of these mechanisms.

$$G(m) = \frac{\left(\sum_i M_i v_i\right) r}{\rho_p} \cdot m$$
$$G(m) = K \cdot m \tag{6.43}$$

The parameters used in Equation (6.43) are summarized in Table 6-6.

Table 6-6: Volume reaction-limited growth law parameters

Symbol	Definition	Units
M_i	molecular weight	g/mol
v_i	stoichiometric coefficient	mol/mol
r	rate of reaction per unit volume	mol/(s·cm^3)
ρ_p	particle density	g/cm^3
m	paricle mass	g
K	$\dfrac{\left(\sum_i M_i v_i\right) r}{\rho_p}$	1/s

Applying the method of characteristics to this system yields the differential equation:

$$\boxed{\frac{dm}{dt} = Km} \tag{6.44}$$

Integrating this expression as usual yields the characteristic curves.

$$\begin{aligned} \int_0^t dt &= \int_{m_0}^{m} \frac{1}{Km} dm \\ t &= \frac{1}{K} \ln\left(\frac{m}{m_0}\right) \end{aligned} \tag{6.45}$$

Figure 6-9 plots the characteristic curves given $K = 1.15 \times 10^{-4}$, as in both the previous exam-

ples. Rescaling by substituting $m = m_{min}e^{\gamma w}$ and $m_0 = m_{min}e^{\gamma w_0}$ results in the characteristic

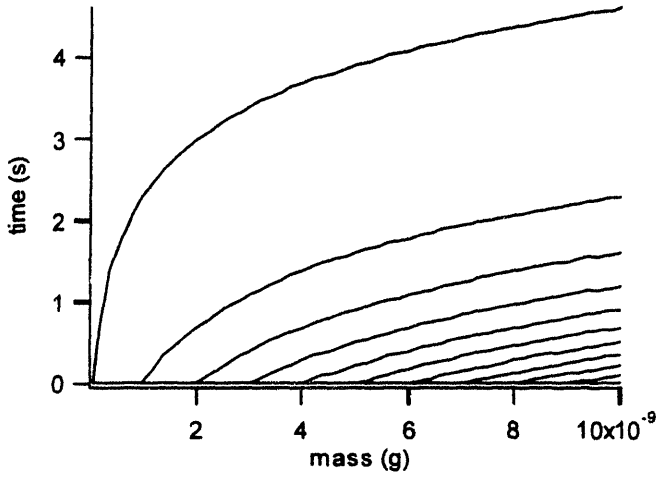

Figure 6-9: Volume reaction-limited characteristic curves as a function of *m*.

curves expressed as a function of w:

$$t = \frac{\gamma}{K}(w - w_0) \tag{6.46}$$

which are plotted in Figure 6-10.

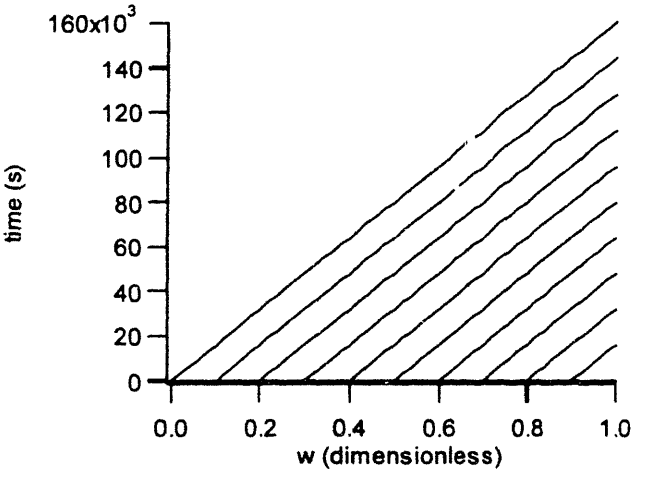

Figure 6-10: Volume reaction-limited characteristic curves as a function of *w*.

For this system, the logarithmic scale results in a constant growth rate, while the mass scale results in a large discrepancy in growth rates between large and small particles, indicating that the logarithmic scale system is much easier to solve from a numerical perspective.

6.6 Comparison and Analysis of Growth Rate Scaling

As shown in the previous sections, the growth rate expression $G(m)$ or $G(w)$ used in the population balance problem varies depending on physics and chemistry of the system. Specifically, growth rates may be limited by diffusion to the particle surface, by reaction at the particle surface, or by reaction within the entire particle or droplet volume.

6.6.1 Solution time constraints: Courant condition

Typically, a numerical implementation will divide the domain of solution up into a number of equally spaced elements (see Appendix B). Each solution method chooses some representation to approximate the number of particles in that element. In many ways this is similar to dividing the population distribution up into small "bins" in which the particles are placed (see Chapter 2). Depending on the solution method used and the form of the population balance equation, various restraints exist to ensure the stability of the numerical solution (Morton, 1996). One particular constraint is imposed based on the Courant number (Strang, 1986) and is known as the Courant condition. This condition is valid for systems governed by the differential equation:

$$\frac{dC_A}{dt} = -v\frac{\partial C_A}{\partial z} \tag{6.47}$$

Figure 6-11 depicts a sample distribution of C_A and the element or bin spacing for three adjacent nodes in a sample system.

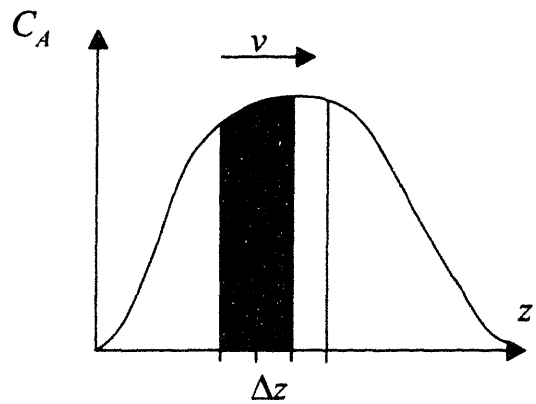

Figure 6-11: Elements in a concentration distribution undergoing one-dimensional convection.

For this system, the Courant condition places a restriction on the maximum time step Δt which a numerical integration algorithm can take while maintaining stability:

$$\Delta t \leq \frac{\Delta z}{v} \tag{6.48}$$

When the Courant condition is violated, a numerical artifact known as *aliasing* can occur, which allows the convected species to skip over adjacent elements, causing an instability. For a more complete explanation of the basis for this condition, please refer to Strang (1986).

If we approximate the growth rates $G(m)$ and $G(w)$ in Equations (6.2) and (6.31) as constant over a given element in the solution domain, then the Courant condition can be applied to estimate the minimum number of time steps required to generate a solution. In this case, the respective growth rate $G(m)$ or $G(w)$ is equivalent to velocity, v, and the element width is given as either Δm or Δw. Thus, the Courant condition requires that:

$$\begin{aligned} \Delta t &\leq \frac{\Delta m}{G(m)} \\ \Delta t &\leq \frac{\Delta w}{G(w)} \end{aligned} \tag{6.49}$$

As demonstrated in the previous sections, the growth rates $G(m)$ and $G(w)$ vary widely based on both the growth law and particle size. However, the minimum time step for the entire system will be based on the smallest minimum time step for all of the elements. Armed with this knowledge, we can apply the Courant condition on the first and last elements to determine whether normal or logarithmic scaling result in a lower minimum number of time steps.

6.6.2 Scaling effects on solution time

Using values of K which result in 10^3 time steps over a solution time of 1 second for the m-scaled growth laws, Figure 6-12 compares the solution times for the m and w scales with each

growth law.

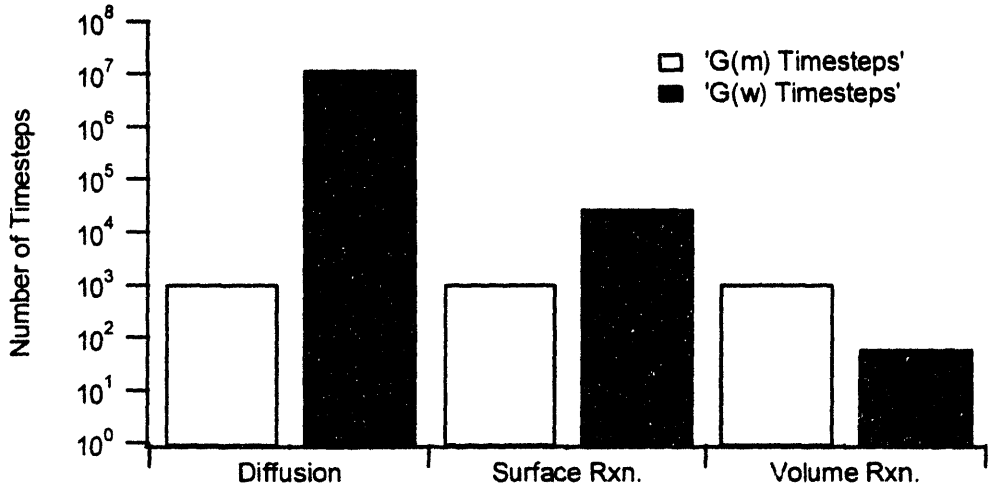

Figure 6-12: Comparison of minimum number of time steps under varying growth law.

Table 6-7 summarizes the growth rate and time step information for the system depicted in Figure

Table 6-7: Minimum number of time steps under different growth laws

	Diffusion-Limited Growth	*Surface Reaction-Limited Growth*	*Volume Reaction-Limited Growth*
K	0.0004808	0.2311	111.1
$G(m_{\min})$	2.23×10^{-9}	4.98×10^{-12}	1.11×10^{-14}
$G\left(m_{\min}+\frac{m_{\max}-m_{\min}}{10}\right)$	1.00×10^{-6}	1.00×10^{-6}	1.00×10^{-6}
m Timesteps	1.00×10^{3}	1.00×10^{3}	1.00×10^{3}
$G(w_{\min})$	1.21×10^{6}	2.70×10^{3}	6.03
$G(0.9w_{\max})$	1.92×10^{1}	1.08×10^{1}	6.03
w Timesteps	1.21×10^{7}	2.70×10^{4}	6.03×10^{1}
Optimal scaling	m	m	w

6-12. Because the number of timesteps is roughly proportional to the total solution time, the *m*-scaled system would be expected to yield a solution 10,000 times faster than the *w*-scaled system for a diffusion-limited growth law. Similarly, the surface-reaction based solution would be expected to reach a solution 100 times faster with a *m*-scaled than *w*-scaled system. For the system with *w*-scaled growth law, however, the volume reaction-limited growth law is roughly an order of magnitude faster to solve. Recall, however, that the characteristic curve expressions are not only a function of K, but also often include some expression such as γ, m_{min} or m_{max} related to the total range of particle sizes. The next section explores these effects on solution times.

6.6.3 Effect of varying particle size range on solution time

Table 6-8 summarizes the various systems and their corresponding growth laws.

Table 6-8: Summary of growth laws

System	$G(m)$	$G(w)$	K
Diffusion-limited	$Km^{1/3}$	$\frac{K}{\gamma}(m_{\min}e^{\gamma w})^{-2/3}$	$2\pi D(c_\infty - c_s)W\left(\frac{6}{\rho\pi}\right)^{1/3}$
Surface reaction-limited	$Km^{2/3}$	$\frac{K}{\gamma}(m_{\min}e^{\gamma w})^{-1/3}$	$\frac{\alpha(\rho\pi)^{1/3}v_m 6^{2/3}}{\sqrt{2\pi M_w kT}}$
Volume reaction-limited	Km	$\frac{K}{\gamma}$	$\left\{\frac{\left(\sum_i M_i v_i\right)r}{\rho_p}\right\}$

Figure 6-13 compares the number of timesteps required by *w* scaling with *m* scaling as a function of increasing range of particle sizes. Similar to the previous section, the parameter K was varied for each growth law as a function of size to keep the number of *m* timesteps constant at 1,000 as an even basis of comparison with *w* timesteps. Note that the example in the previous section corresponds to a value of M_{max}/M_{min} of 10^8 in this graph. The graph clearly shows that the differences in the number of timesteps grow larger as the particle size range increases. In fact, with a size range covering 15 orders of magnitude, *w*-based scaling in a diffusion-limited system would take at least 10^{11} timesteps compared with 10^3 timesteps with *m* scaling, increasing the estimated

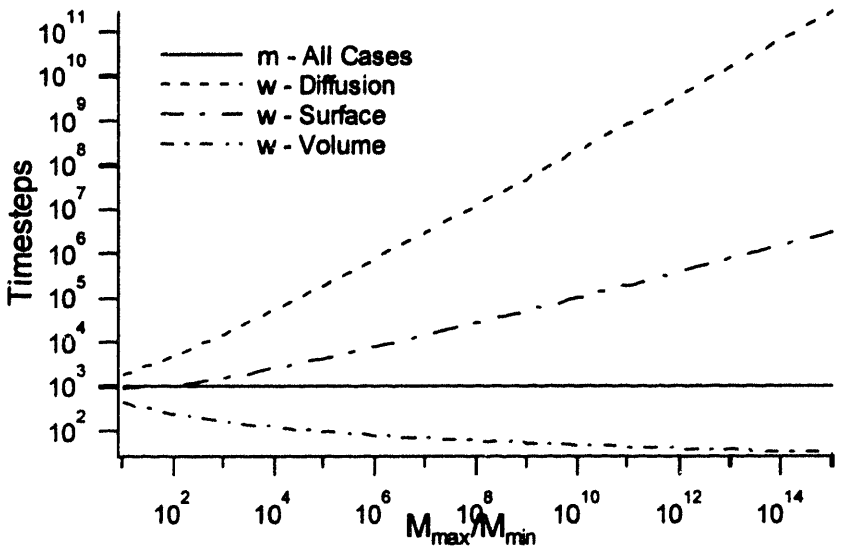

Figure 6-13: Comparison of minimum number of time steps with *m* and *w* scaling as required by the Courant condition under varying growth laws.

solution time by a factor of 10^8! Also note that the optimal scaling method holds over all particle size ranges, proving the universal applicability and utility of this analysis.

6.6.4 Note for multi-component systems

When more than one component is present, then one or more components may be actively contributing to particle growth. It is also possible that each species is incorporated into the particles by a different growth mechanism. For systems where the growth laws of the species are independent and follow one of the growth mechanisms presented in this chapter, the optimal scaling with respect to each component will be determined by Table 6-7. For example, in a system with two species where the growth from the first species is limited by diffusion and the growth from the second species is limited by volume reaction, then the optimal scaling for this system would be $n(m_1, w_2)$ where

$$\begin{aligned} m_2 &= m_0 e^{\gamma_2 w} \\ w_2 &= \frac{1}{\gamma_2}\ln\left(\frac{m_2}{m_0}\right) \end{aligned} \tag{6.50}$$

In systems where the growth rates due to the individual species are highly correlated, then a characteristics analysis of the growth rates must be carried out over the domain of particle sizes in the system to determine the optimal scaling.

6.7 Summary

The process of growth is critical to the formation of new particles in a wide range of particulate processes; yet the growth mechanisms in various systems can vary considerably. Depending on whether particle growth is limited by diffusion to the particle surface, reaction on the particle surface, or reaction within the particle volume, growth laws take on very different mathematical forms which require particular treatment for efficient numerical solution. In particular, diffusion-limited and surface reaction-limited growth systems should be solved using number density domains scaled as particle mass, while volume reaction-limited systems are more amenable to solution when the number density domain is scaled as the logarithm of particle mass. As the range of particle sizes covered by the number density distribution increases, the benefits of using correct scaling becomes more pronounced. Finally, the characteristics analysis can be readily applicable to multicomponent systems, where the insights of characteristic analysis provide a framework for choosing the scaling of the multicomponent number density distribution.

References

[1] Friedlander, Sheldon K. *Smoke Dust, and Haze: Fundamentals of Aerosol Dynamics,* 2nd Ed., Oxford University Press, 2000.

[2] Morton, K. W. *Numerical Solution of Convection-Diffusion Problems,* Chapman & Hall, 1996.

[3] Strang, Gilbert *Introduction to Applied Mathematics,* Wellesley-Cambridge Press, 1986.

[4] Zauderer, Erich *Partial Differential Equations of Applied Mathematics,* 2nd Ed., John Wiley & Sons, 1989.

[5] Zwillinger, Daniel *Handbook of Differential Equations,* 2nd Ed., Academic Press, 1992.

Chapter 7: Solution Methods for Multicomponent Dynamic Population Balances

7.1 Introduction

One particularly challenging class of population balance problems is multicomponent particulate systems. Typical phenomena which occur in these systems include coagulation, fragmentation, growth; condensation, nucleation, and many others. These phenomena describe processes in virtually every class of chemical process, including emulsions, aerosols, micelles, crystallization, combustion, and polymer condensation. Industrial applications range from nanotechnology to air pollution, pharmaceuticals and mining. In spite of the ubiquitous nature of particulate systems, accurate and computationally tractable models of multicomponent particulate systems have not been developed due to the difficulty involved in framing the solution with a compact representation, especially for coagulation processes. This chapter introduces a new representation for multicomponent particulate systems which is both accurate and computationally much faster than other methods and applies this representation to a two-component aerosol coagulation model.

7.2 Representation of Population Distribution

Because population balances can describe such a wide array of physical systems and processes, a general representation is needed to define a population distribution. In order to meet this need, a population distribution is defined by a number density function $n(\phi)$ such that $n(\phi)d\phi$ represents the concentration of particles in the population with characteristics between ϕ and $\phi + d\phi$. Depending on the system of interest, ϕ can take on a number of different forms. Examples are given in Table 7-1, assuming that the all particle concentrations are given in terms of number of particles per cubic meter. In a system such as the second row in Table 7-1, where the only population characteristic of interest is particle mass, ϕ would be defined as particle mass, and the population distribution function might be represented as in Figure 1. Because the cumulative number of particles per unit volume smaller than size m^* is given by:

$$N(\leq m^*) = \int_0^{m^*} n(m)dm \tag{7.1}$$

the number density function $n(m)$ is often given the name dN/dm because it represents the incremental increase in the cumulative number of particles as m^* is increased. Much of the early work regarding single component coagulation and fragmentation was pioneered by Valentas in the 1960's (Valentas, Bilous and Amundson, 1966; Valentas and Amundson, 1966). For a comprehensive treatment of number density distributions, please refer to Chapter 2.

Table 7-1: Number Density Representations

ϕ	*Definition*	$n(\phi)$	*units*	*# particles*	*total # particles*
v	volume	$n(v)$	$\frac{1}{\text{volume}\cdot\text{m}^3}$	$n(v)dv$	$\int_0^\infty n(v)dv$
m	mass	$n(m)$	$\frac{1}{\text{mass}\cdot\text{m}^3}$	$n(m)dm$	$\int_0^\infty n(m)dm$
$\mathbf{m} = \{m_1, m_2, ..., m_s\}$	mass components	$n(\mathbf{m})$	$\frac{1}{\text{mass}^s\cdot\text{m}^3}$	$n(\mathbf{m})dm_1 dm_2...dm_s$	$\int_0^\infty ... \int_0^\infty \int_0^\infty n(\mathbf{m})dm_1 dm_2 ... dm_s$
$\{\text{m}, \mathbf{x}\} = \{m, x_1, x_2, ..., x_{s-1}\}$	composition	$n(\text{m}, \mathbf{x})$	$\frac{1}{\text{mass}\cdot\text{m}^3}$	$n(m, \mathbf{x})dm dx_1 dx_2...dx_s$	$\int_0^1 ... \int_0^1 \int_0^1 \int_0^\infty n(m, \mathbf{x})dm dx_1 dx_2 ... dx_{s-1}$

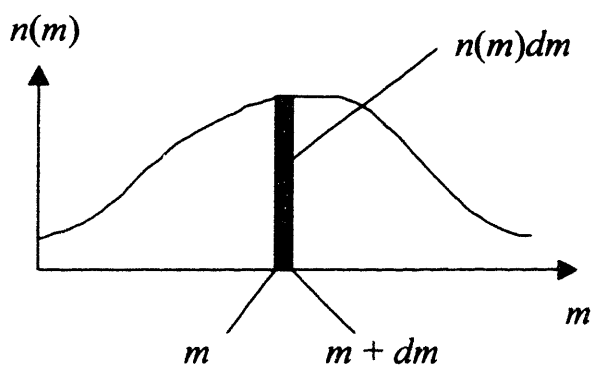

Figure 7-1: Graphical representation of a number density distribution.

For a population with s individual components, as shown in the last two rows of Table 7-1, the population distribution $n(\mathbf{m})$ or $n(m, \mathbf{x})$ requires s degrees of freedom to be completely specified. These degrees of freedom may be specified as individual component mass amounts m_i, as in the third row where $\mathbf{m}$ is a vector $\mathbf{m} = \{m_1, m_2, ..., m_s\}$. Alternatively, the s degrees of freedom may

also be specified by s - 1 mass fractions x_i and total particle mass, m:

$$m = \sum_i m_i$$
$$x_i = \frac{m_i}{m} \tag{7.2}$$

The population distribution now takes the form $n(m, \mathbf{x})$ where $\mathbf{x} = \{x_1, x_2, ..., x_{s-1}\}$. In the next sections, unless specifically noted, all populations will be specified by individual component masses, $n(\mathbf{m})$.

7.3 Multicomponent Governing Equations

7.3.1 Coagulation

As discussed in Chapter 5, the coagulation kernel $\beta(\mathbf{l}, \mathbf{m})$ is defined as the rate per unit of control space at which population members of composition $\mathbf{l}$ and $\mathbf{m}$ coagulate to form a population member of composition $\mathbf{l} + \mathbf{m}$. The units of the coagulation kernel are *space/time*. The relevant units of space vary from one system to another. For a point model or system, space has no dimension, however, for an atmospheric volume, space will be 3-dimensional and have units of $length^3$. The contribution to population members of a given composition $\mathbf{m}$ due to coagulation is given by:

$$\frac{\partial n(\mathbf{m})}{\partial t} = \frac{1}{2}\int_0^{m_s}\cdots\int_0^{m_2}\int_0^{m_1}\beta(\mathbf{m}-\mathbf{c}, \mathbf{c})n(\mathbf{m}-\mathbf{c})n(\mathbf{c})dc_1 dc_2 \ldots dc_s \tag{7.3}$$

where the coagulation event represented within the integral is illustrated in Figure 3. The factor of 1/2 is used to account for the fact that the integral expression double counts collisions (see Chapter 5). For the simple case of two particles with composition $\mathbf{q}$ and $\mathbf{s}$ colliding, the integral will count two collisions in each dimension of integration - one where $\mathbf{c} = \mathbf{q}$ and $\mathbf{m} - \mathbf{c} = \mathbf{s}$ and another when $\mathbf{c} = \mathbf{s}$ and $\mathbf{m} - \mathbf{c} = \mathbf{q}$. The decrease in population members of a given size $\mathbf{m}$ due to agglomeration with particles of other sizes (as shown in Figure 4) is given by:

$$\frac{\partial n(\mathbf{m})}{\partial t} = -n(\mathbf{m})\int_0^{\infty}\cdots\int_0^{\infty}\int_0^{\infty}\beta(\mathbf{m}, \mathbf{c})n(\mathbf{c})dc_1 dc_2 \ldots dc_s \tag{7.4}$$

Naturally, these integral expressions are only applicable when the population contains a large

number of particles. Although individual particles behave stochastically, when large numbers of particles are present individual effects average out and these deterministic equations may be used (Gueron, 1998). For a system affected only by coagulation, the full dynamic population balance includes contributions from both Equations (7.3) and (7.4).

$$\frac{\partial n(\mathbf{m})}{\partial t} = \frac{1}{2}\int_0^{m_s}\cdots\int_0^{m_2}\int_0^{m_1}\beta(\mathbf{m}-\mathbf{c},\mathbf{c})n(\mathbf{m}-\mathbf{c})n(\mathbf{c})dc_1dc_2\ldots dc_s - n(\mathbf{m})\int_0^{\infty}\cdots\int_0^{\infty}\int_0^{\infty}\beta(\mathbf{m},\mathbf{c})n(\mathbf{c})dc_1dc_2\ldots dc_s \tag{7.5}$$

In the special case of a single-component system, Equation (7.5) reduces to the governing equation for number density.

$$\frac{\partial n(m)}{\partial t} = \frac{1}{2}\int_0^{m}\beta(c, m-c)n(c)n(m-c)dc - n(m)\int_0^{\infty}\beta(m, c)n(c)dc \tag{7.6}$$

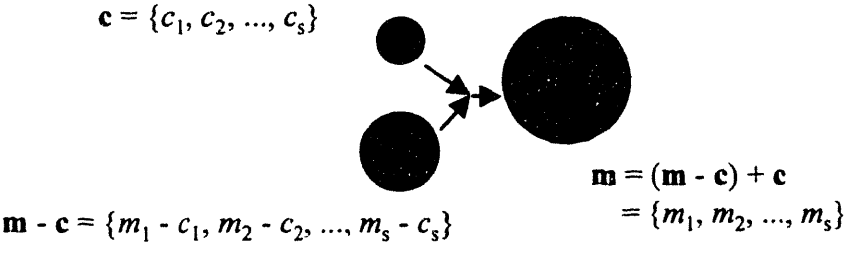

$$\frac{\partial n(\mathbf{m})}{\partial t} = \frac{1}{2}\int_0^{m_s}\cdots\int_0^{m_2}\int_0^{m_1}\beta(\mathbf{m}-\mathbf{c},\mathbf{c})n(\mathbf{m}-\mathbf{c})n(\mathbf{c})dc_1dc_2\ldots dc_s$$

Figure 7-2: Coagulating particles creating a particle size m.

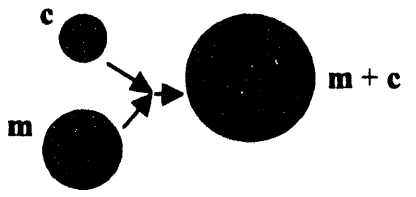

$$\frac{\partial n(\mathbf{m})}{\partial t} = -n(\mathbf{m}) \int_0^{\infty} \cdots \int_0^{\infty} \int_0^{\infty} \beta(\mathbf{m}, \mathbf{c}) n(\mathbf{c}) dc_1 dc_2 \ldots dc_s$$

Figure 7-3: Coagulating particles removing particles size m.

7.3.2 Fragmentation

The multicomponent fragmentation expression is defined in Equation (7.7):

$$\frac{\partial n(\mathbf{m})}{\partial t} = \int_{x_s}^{\infty} \cdots \int_{x_2}^{\infty} \int_{x_1}^{\infty} n(\mathbf{x}) g(\mathbf{x}) v(\mathbf{x}) \gamma(\mathbf{x}, \mathbf{m}) dx_1 dx_2 \ldots dx_s - g(\mathbf{m}) n(\mathbf{m}) \tag{7.7}$$

where $g(\mathbf{x})$ is fragmentation frequency of particles size $\mathbf{x}$, $v(\mathbf{x})$ is the number of smaller fragments created, and $\gamma(\mathbf{x}, \mathbf{m})$ is a density function describing the fractional distribution of fragments from particles size $\mathbf{x}$ into particles size $\mathbf{m}$. The function $v(\mathbf{x})$ is restrained by the expression:

$$v(\mathbf{m}) = \frac{m}{\int_0^{m_s} \cdots \int_0^{m_2} \int_0^{m_1} \gamma(\mathbf{m}, \mathbf{x}) \left(\sum_i x_i \right) dx_1 dx_2 \ldots dx_s} \tag{7.8}$$

which essentially enforces a mass balance on the fragments. For a more detailed review of the multicomponent fragmentation governing equations, please refer to Chapter 5.

7.3.3 Growth

In a multicomponent system, a growth rate is defined for each component as the rate of change of mass in that component per unit time.

$$G_i(\mathbf{m}) = \frac{dm_i}{dt} \tag{7.9}$$

The overall growth rate for a particle is then the sum of these individual component growth rate expressions:

$$\frac{\partial n(\mathbf{m})}{\partial t} = -\sum_i \frac{\partial n((\mathbf{m})G_i(\mathbf{m}))}{\partial m_i} \tag{7.10}$$

7.4 Review of Multicomponent Numerical Solution Methods

In general, complete specification of a multicomponent aerosol system requires knowledge of the time variable, the size variable and, when s is the number of species, s - 1 composition variables. Thus, a total of s + 1 independent variables exist in an s-component dynamic system. In order to generate a full numerical solution with p node points along the axis of each independent variable, a total of p^s node points are required to determine the full multidimensional surface representing the multidimensional number density function $n(m_1, m_2, ..., m_s)$. Accordingly, p^s equations are required for numerical integration. Because the number of equations scales exponentially with the number of components, solving all but the simplest of systems requires a prohibitive amount of computation (Kim and Seinfeld, 1990). Thus, although this method is straightforward and can accurately represent any multicomponent system, it is not suitable for any more than two or three components due to its poor scaling as the number of components is increased. Furthermore, the independent variables typically range over several orders of magnitude which complicates the issue of node placement and scaling along each axis.

When coagulation or fragmentation processes are active in a system, a number of integral terms must be incorporated into the general dynamic equation, transforming it from a partial differential equation into a partial integro-differential system. For multicomponent systems, the coagulation term is expressed as a multidimensional integral, which further adds to the complexity of the problem and increases its computational intensity, as shown in Table 7-2.

Several methods have been previously employed in an attempt to address the difficulties associated with multicomponent particulate systems (see Table 7-2). The distribution splitting method (Toon et al., 1988) proposed that multiple species be represented by a series of mixed and pure-component distributions. For instance, a two-component system would be represented by four distributions: one distribution each representing the number density of each pure component, another number density representing the mixed particles, and a final function describing the composition of the mixed particles (see Figure 7-4). This method allows limited representation of variation in composition at each size point in the overall population. For the two component case,

Table 7-2: Comparison of Multicomponent Population Balance Methods

Method	*Equation Scaling*	*# Equations p = 10, s = 4, n = 2*	*Reference*
Full s-dimensional surface	p^s	10,000	Kim & Seinfeld (1992)
Distribution Splitting	$p \cdot s \cdot 2^{s-1}$	320	Toon et al. (1988)
Multicomponent Sectionalization	$p \cdot s$	40	Gelbard & Seinfeld (1980)
Species Mass Distribution	$p \cdot s$	40	Pilinis (1990)
Split Distribution Method	$p(s \cdot n)^a$	80	-

a. "n" represents the number of terms in the composition expansion, as explained in later sections.

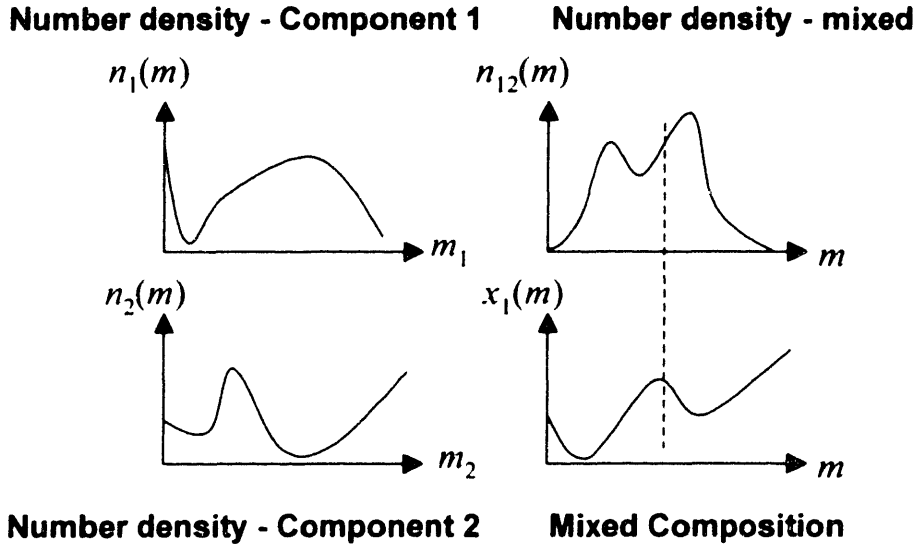

Figure 7-4: Distribution splitting method for representation of multicomponent systems.

three different compositions are possible at any given mass point: pure component 1, pure component 2, and the composition given at that mass point in the mixed composition distribution. Solution time unfortunately scales as $s \cdot 2^{s-1}$ with the number of species s in the system. For more detail on the scaling of the distribution splitting method, please refer to Appendix H.

Another method which has been employed is the multicomponent sectionalization method (Gelbard and Seinfeld, 1980). This method effectively discretizes the representation space along size and composition coordinates. While this method treats coagulation effects well, it does not conserve the number of particles in the system and poses significant difficulties in modeling all

but the most elementary growth processes. The species mass distribution method addresses the number conservation caveat of the multicomponent sectionalization method by implementing a continuous analog of the multicomponent sectionalization method (Pilinis, 1990; Katoshevski and Seinfeld, 1997). The main assumption this technique, known as the internally mixed assumption (IMA), is that all particles of the same mass have the same composition, leading to a uniform composition distribution as shown in Figure 7-5. This assumption states that particles of the same

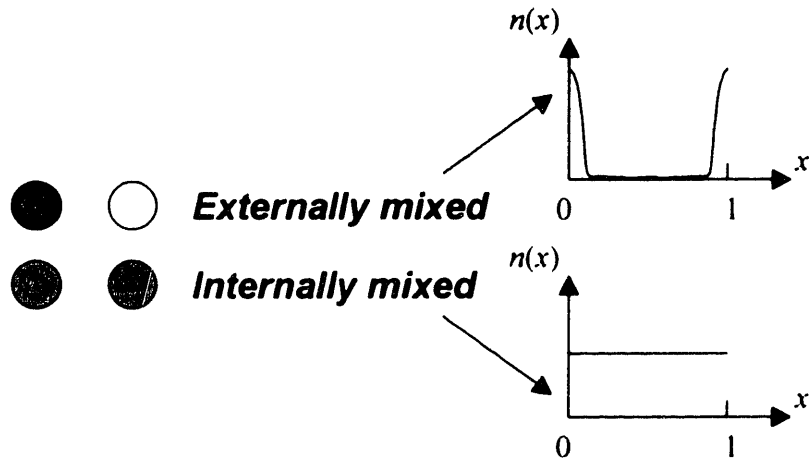

Figure 7-5: Externally mixed aerosols have particles with very different compositions while internally mixed aerosol particles have uniform composition.

size all have the same composition (Fernández-Díaz et al., 1999) and effectively reduces the governing equation set to $p \cdot s$ equations representing each species in the system at p node points. The sacrifice for this reduction in complexity, of course, is the lack of ability to account for compositional variations at each size range of the population. In fact, the representation used by the species mass distribution is even more restrictive than the distribution splitting method and not much better than a lumped one-component representation. For example, in the two-component case the distribution splitting method allows particles of mass m to take on one of three compositions: pure component 1, pure component 2, or mixed component 1 and 2 (at some fixed mixed composition), while the species mass distribution method will restrict all of the particles of mass m to one mixed composition.

In the past, the inability of measurement methods to simultaneously resolve size and composition variations within a population of particles has made the internally mixed assumption difficult

to verify. Recent evidence, however, suggests that particles of the same size but very different compositions coexist in atmospheric aerosols (Noble and Prather, 1996), as shown in Figure 7-6.

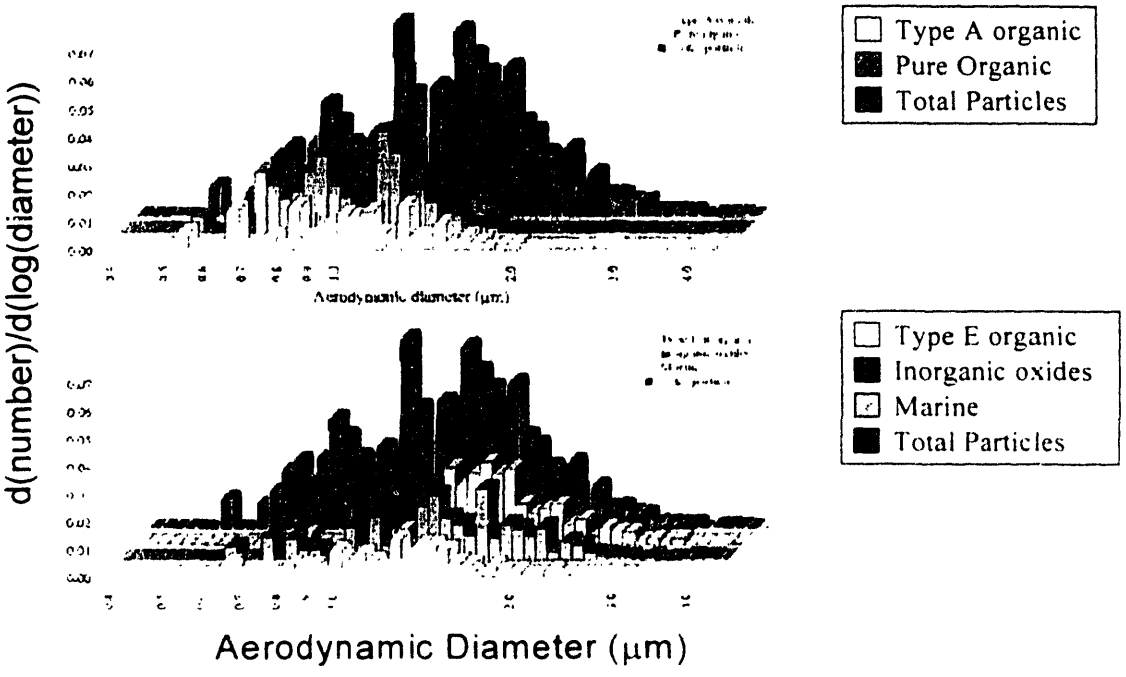

Figure 7-6: Data collected in study of aerosol compositions (Noble and Prather, 1996) showing the large variations in composition within every size segment of the distribution.

The assumptions of these various methods for treating multicomponent aerosol systems are summarized in Figure 7-7, which shows condensed versions of the coagulation production terms of the governing equations. In general, these methods preselect the representation for the system, forcing the user into either a representation which either has adequate representation of the multicomponent system but unsatisfactory solution time (full multidimensional representation) or a representation with satisfactory solution time but an inability to adequately describe the multicomponent system.

In order to address the need for a flexible method which could incorporate varying degrees of resolution for multicomponent systems with tractable solution times, Resch (1995) developed the distribution splitting method. This method uses a Wiener expansion (Tatang, 1994), or polynomial chaos expansion (PCE), to compactly represent the composition at each size range of the

number density distribution. The representation of the multicomponent problem is now "split" into two separate distributions: 1) the number distribution as a function of population member size, and 2) the composition distribution at each size. This implementation has been tested using an analytical solution from Gelbard and Seinfeld (1978) which applies to systems with an exponential initial distribution, constant coagulation kernel, and growth rate proportional to the mass of the particle. This growth law corresponds to a physical system which is limited by volume-based reaction within the particle, and therefore is most efficiently solved when the number density distribution is log-rescaled, as shown in Chapter 6. For clarity, a complete and rigorous presentation of the assumptions and derivations for the split composition distribution method is presented in the following sections. Starting with the basic multicomponent population balance for coagulation, the set of differential equations used in numerical implementations is developed.

Results are presented and compared to a two-component analytical solution.

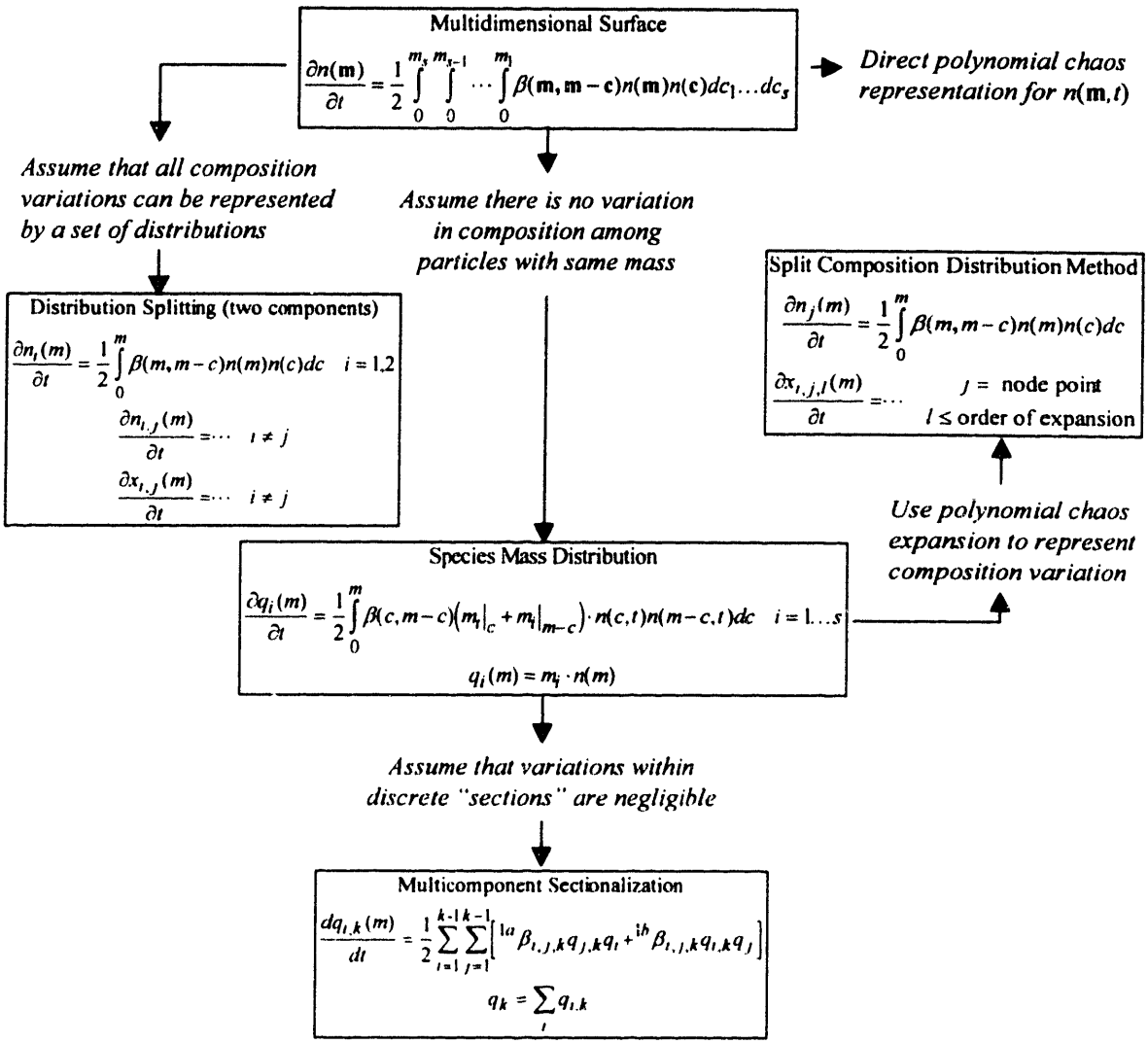

Figure 7-7: Dynamic population balance numerical solution methods summary.

7.4.1 Overview of methods

The species mass distribution concept is based upon the notion that it is possible to explain the evolution of a number density distribution by tracking the mass distributions of the components in the system. The mass distribution is defined similar to the number density distribution, except where the number density describes the number of particles between mass m and $m + dm$, the mass distribution describes the total mass of particles in the size range between m and $m + dm$.

In the general case where the number density is described by $n(\mathbf{m})$ or $n(m, \mathbf{x})$, the mass distri-

bution of a species is a daunting quantity to calculate, involving multidimensional moments over complex integration limits. For example:

$$q_i(m) = \int_0^1 \cdots \int_0^{\infty} \int_0^{\infty} n(m, \mathbf{x}) m x_i \cdot dx_1 dx_2 \ldots dx_{s-1} \tag{7.11}$$

where $q_i(m)$ is the species mass distribution for component i. However, in the case where the particles are assumed to be perfectly internally mixed, this expression is greatly simplified:

$$q_i(m) = n(m) \cdot m_i \tag{7.12}$$

Figure 7-8 depicts and example of a species mass distribution.

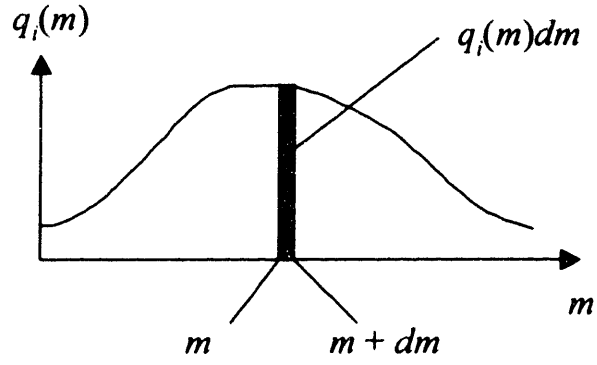

Figure 7-8: Example of a species mass distribution.

Because all of the particles have the same composition, the total mass of component i in the mass range $(m, m + dm)$ is simply the product of that component mass multiplied by the number of particles. This method severely restricts the system by requiring that all particles of the same mass have the same composition, producing a large reduction in the complexity of the solution by essentially assuming a uniform composition distribution among particles of a given size. Instead of solving the governing equations for an s-dimensional system where s is the number of species, the governing set of equations is reduced to a set of s one-dimensional governing equations for the individual mass distributions.

The split composition distribution method essentially relaxes the internally mixed assumption by introducing a probabilistic representation of the variation in particle composition at each particle mass, as shown in Figure 7-9. These probabilistic representations are defined by a random

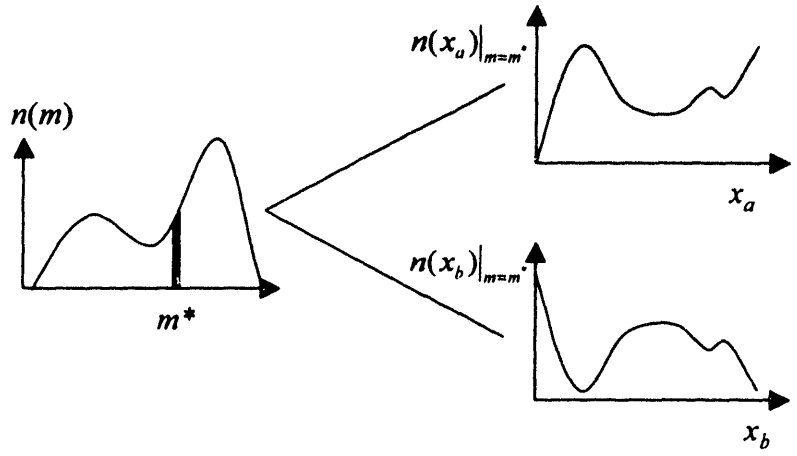

Figure 7-9: Example of a species mass distribution.

variable expansion, the Wiener expansion. Because this expansion converges rapidly, this method can describe a wide range of systems with just a few new differential equations describing the evolution of the moments of these distributions at the each node point in the system. Furthermore, this technique allows the gradual addition of more expansion terms when necessary to meet the desired accuracy. In contrast, full s-dimensional representations scale as p^s where p is the number of node points and s is the number of species. The following sections derive the governing equations for these methods.

7.5 Derivation of the Species Mass Distribution Method

7.5.1 Species mass distribution representation

One method of representing a multicomponent mixture, known as the species mass distribution method, was introduced by Pilinis (1990). The basic assumption behind this method is that all particles of the same size have the same composition.

If the total number of particles between mass m and $m + dm$ is $n(m, t)dm$, then $m_i \cdot n(m)dm$ is the total mass of species i contained in these particles. The number of particles in the population segment multiplied by the mass of component i each particle gives the total mass of component i in particles in that population segment. In order to express this as a distribution, we equate this quantity to the species mass distribution $q_i(m)dm$, defined as the total mass of component i contained in particles ranging in size from m to $m + dm$.

$$q_i(m)dm = m_i \cdot n(m)dm \tag{7.13}$$

This is referred to as the species mass distribution for component i. Here the left side represents the total mass of species i contained by particles between sizes m and $m + dm$. The right side therefore represents the total number of particles between sizes m and $m + dm$ multiplied by m_i, the amount of species i contained in each particle size m. Inherent in this definition is the assumption that all particles of size m contain the same amount of species i, m_i. Dividing both sides of Equation (7.13) through by dm produces the transformation from number density to species mass distribution:

$$q_i(m) = m_i \cdot n(m) \tag{7.14}$$

Naturally, the sum of the individual species masses in a particle must equal the total mass of the particle:

$$m = \sum_i m_i \tag{7.15}$$

and it follows therefore that the sum of the species mass distributions over all species in the system produces the total mass distribution:

$$\begin{aligned} q(m) &= \sum_i q_i(m) \\ &= \sum_i m_i \cdot n(m) \\ &= n(m)\sum_i m_i \\ q(m) &= n(m)m \end{aligned} \tag{7.16}$$

From Equations (7.14) and (7.16) we can write the relation:

$$\frac{q_i(m)}{m_i} = n(m) = \frac{q(m)}{m} \tag{7.17}$$

Thus the individual species mass distributions coupled with the internally mixed assumption completely define the system. The only dependent variable which is not directly specified by the species mass distributions is m_i, however m_i can be calculated using the individual species mass distributions. Starting with the relation given in Equation (7.17):

$$\frac{q_i(m)}{m_i} = \frac{q(m)}{m}$$
$$m_i = \frac{m \cdot q_i(m)}{q(m)} \tag{7.18}$$

Finally, recalling that the total mass distribution is the sum of the individual species mass distributions, as show in the first line of Equation (7.16), we can produce m_i as a function of individual species mass distributions and the independent variable m only.

$$m_i = \frac{m \cdot q_i(m)}{\sum_i q_i(m)} \tag{7.19}$$

The multicomponent general dynamic equation based on individual species balances will thus take the form:

$$\frac{\partial q_i(m)}{\partial t} = \left.\frac{\partial q_i(m)}{\partial t}\right|_{\text{coagulation}} + \left.\frac{\partial q_i(m)}{\partial t}\right|_{\text{fragmentation}} + \left.\frac{\partial q_i(m)}{\partial t}\right|_{\text{growth}} + \left.\frac{\partial q_i(m)}{\partial t}\right|_{\text{sources \& sinks}} \tag{7.20}$$

Each of the contributions from growth, coagulation, and sources and sinks are derived in the following sections.

7.5.2 Coagulation removal term for species mass balance

When particles are lost due to coagulation, each particle lost removes the amount of mass m_i of species i from the mass distribution in the range $(m, m + dm)$. Thus, the coagulation removal term is simply the coagulation rate multiplied by the mass of component i contained in each particle:

$$\frac{\partial q_i(m)}{\partial t} = -m_i\big|_m n(m) \int_0^\infty \beta(m, c) n(c) dc \tag{7.21}$$

Recalling that $q_i(m) = m_i n(m) = m_i\big|_m n(m)$ produces

$$\frac{\partial q_i(m)}{\partial t} = -q_i(m)\int_0^\infty \beta(m,c)n(c)dc \tag{7.22}$$

Finally, because $n(c) = \frac{q(c)}{c}$, we have:

$$\boxed{\frac{\partial q_i(m)}{\partial t} = -q_i(m)\int_0^\infty \beta(m,c)\frac{q(c)}{c}dc} \tag{7.23}$$

Note that in practice this integral cannot be extended to include the point $c = 0$ because $q(c)/c$ is undefined at this point.

7.5.3 Coagulation production term for species mass balance

When two particles coagulate to form a larger particle, the amount of species i that is added to the species mass distribution is equal to the sum of the species masses in the two original particles. Because the mass of species i is a function of m:

$$m_i|_m = m_i|_a + m_i|_{m-a} \tag{7.24}$$

where the masses of the two coagulating particles are a and m - a. Using this fact, the coagulation contribution to the species mass distribution will be the product of the number of particles added and the mass per particle added to the range (m, $m + dm$) of the species mass distribution:

$$\frac{\partial q_i(m)}{\partial t} = \frac{1}{2}\int_0^m (m_i|_a + m_i|_{m-a})\beta(a, m-a)n(a)n(m-a)da \tag{7.25}$$

Substituting $n(a) = \frac{q_i(a)}{m_i|_a}$ and $n(m-a) = \frac{q(m-a)}{m-a}$ yields:

$$\frac{\partial q_i(m)}{\partial t} = \frac{1}{2}\int_0^m (m_i|_a + m_i|_{m-a})\beta(a, m-a)\frac{q_i(a)}{m_i|_a}\frac{q(m-a)}{m-a}da \tag{7.26}$$

which simplifies to:

$$\frac{\partial q_i(m)}{\partial t} = \frac{1}{2}\int_0^m \left(1 + \frac{m_i|_{m-a}}{m_i|_a}\right)\beta(a, m-a)q_i(a)\frac{q(m-a)}{m-a}da \tag{7.27}$$

One pathological case for this expression occurs in the event that $m_i|_a = 0$. Noting that both the

sum $m_i|_m = m_i|_a + m_i|_{m-a}$ and the coagulation kernel are symmetrical expressions, the integration range in Equation (7.25) can be reduced as follows (see Appendix C for more details):

$$\frac{\partial q_i(m)}{\partial t} = \int_0^{\frac{m}{2}} (m_i|_a + m_i|_{m-a}) \beta(a, m-a) n(a) n(m-a) da \tag{7.28}$$

A set of similar substitutions would lead us to the governing equation:

$$\frac{\partial q_i(m)}{\partial t} = \int_0^{\frac{m}{2}} \left(1 + \frac{m_i|_{m-a}}{m_i|_a}\right) \beta(a, m-a) q_i(a) \frac{q(m-a)}{m-a} da \tag{7.29}$$

The advantage of this, of course, is that the computational requirements of the coagulation kernel are roughly reduced by a factor of two. Because the coagulation kernel is often the most costly term to evaluate in terms of computation time, this reduction in integration range often translates into a large reduction in solution time with no loss of accuracy.

Pilinis instead uses the symmetrical nature of the integral to eliminate the $m_i|_a$ terms:

$$\boxed{\frac{\partial q_i(m)}{\partial t} = \int_0^{m} \beta(a, m-a) q_i(a) \frac{q(m-a)}{m-a} da} \tag{7.30}$$

Starting off by breaking the original coagulation production expression from Equation (7.25) into two terms yields:

$$\begin{aligned} \frac{\partial q_i(m)}{\partial t} &= \frac{1}{2} \int_0^{m} \beta(a, m-a)(m_i|_a + m_i|_{m-a}) n(a) n(m-a) da \\ &= \frac{1}{2} \left\{ \int_0^{m} \beta(a, m-a) m_i|_a n(a) n(m-a) da + \int_0^{m} \beta(a, m-a) m_i|_{m-a} n(a) n(m-a) da \right\} \end{aligned} \tag{7.31}$$

Recalling that $m_i|_{m-a} n(m-a) = q_i(m-a)$ and that $n(a) = \frac{q(a)}{a}$, substitutions are made into the second integral:

$$\frac{\partial q_i(m)}{\partial t} = \frac{1}{2}\left\{\int_0^m \beta(a, m-a) m_i\big|_a n(a) n(m-a) da + \int_0^m \beta(a, m-a) m_i\big|_{m-a} n(a) n(m-a) da\right\}$$
$$= \frac{1}{2}\left\{\int_0^m \beta(a, m-a) m_i\big|_a n(a) n(m-a) da + \int_0^m \beta(a, m-a) q_i(m-a)\frac{q(a)}{a} da\right\} \tag{7.32}$$

Similarly, $m_i\big|_a n(a) = q_i(a)$ and $n(m-a) = \frac{q(m-a)}{m-a}$ are substituted into the first integral:

$$\frac{\partial q_i(m)}{\partial t} = \frac{1}{2}\left\{\int_0^m \beta(a, m-a) m_i\big|_a n(a) n(m-a) da + \int_0^m \beta(a, m-a) q_i(m-a)\frac{q(a)}{a} da\right\}$$
$$= \frac{1}{2}\left\{\int_0^m \beta(a, m-a) q_i(a)\frac{q(m-a)}{m-a} da + \int_0^m \beta(a, m-a) q_i(m-a)\frac{q(a)}{a} da\right\} \tag{7.33}$$

Next, transform the second integral using a change of integration variable $c = m - a$.

$$\frac{\partial q_i(m)}{\partial t} = \frac{1}{2}\left\{\int_0^m \beta(a, m-a) m_i\big|_a n(a) n(m-a) da + \int_0^m \beta(a, m-a) q_i(m-a)\frac{q(a)}{a} da\right\}$$
$$= \frac{1}{2}\left\{\int_0^m \beta(a, m-a) q_i(a)\frac{q(m-a)}{m-a} da + \int_m^0 \beta(m-c, c) q_i(c)\frac{q(m-c)}{m-c}(-dc)\right\} \tag{7.34}$$

where the integration limits are changed because now $a = m$ when $c = 0$ and $a = 0$ when $c = m$. Also, $da = -dc$ because m is constant and $a = m - c$. Reversing the limits of the second integral results in:

$$\frac{\partial q_i(m)}{\partial t} = \frac{1}{2}\left\{\int_0^m \beta(a, m-a)q_i(a)\frac{q(m-a)}{m-a}da + \int_m^0 \beta(m-c, c)q_i(c)\frac{q(m-c)}{m-c}(-dc)\right\}$$

$$= \frac{1}{2}\left\{\int_0^m \beta(a, m-a)q_i(a)\frac{q(m-a)}{m-a}da - \int_m^0 \beta(m-c, c)q_i(c)\frac{q(m-c)}{m-c}dc\right\} \tag{7.35}$$

$$= \frac{1}{2}\left\{\int_0^m \beta(a, m-a)q_i(a)\frac{q(m-a)}{m-a}da + \int_0^m \beta(m-c, c)q_i(c)\frac{q(m-c)}{m-c}dc\right\}$$

Changing the dummy variable of integration in the second integral from c to a and applying the symmetry property of the coagulation kernel

$$\frac{\partial q_i(m)}{\partial t} = \frac{1}{2}\left\{\int_0^m \beta(a, m-a)q_i(a)\frac{q(m-a)}{m-a}da + \int_0^m \beta(m-c, c)q_i(c)\frac{q(m-c)}{m-c}dc\right\}$$

$$= \frac{1}{2}\left\{\int_0^m \beta(a, m-a)q_i(a)\frac{q(m-a)}{m-a}da + \int_0^m \beta(m-a, a)q_i(a)\frac{q(m-a)}{m-a}da\right\} \tag{7.36}$$

$$= \frac{1}{2}\left\{\int_0^m \beta(a, m-a)q_i(a)\frac{q(m-a)}{m-a}da + \int_0^m \beta(a, m-a)q_i(a)\frac{q(m-a)}{m-a}da\right\}$$

results in an expression which is easily summed to yield the coagulation production expression due to Pilinis:

$$\frac{\partial q_i(m)}{\partial t} = \frac{1}{2}\left\{\int_0^m \beta(a, m-a) q_i(a) \frac{q(m-a)}{m-a} da + \int_0^m \beta(a, m-a) q_i(a) \frac{q(m-a)}{m-a} da\right\}$$

$$= \frac{1}{2}\left\{2\int_0^m \beta(a, m-a) q_i(a) \frac{q(m-a)}{m-a} da\right\} \tag{7.37}$$

$$= \int_0^m \beta(a, m-a) q_i(a) \frac{q(m-a)}{m-a} da$$

7.5.4 Fragmentation loss term for the species mass balance

The loss of species *i* from the population segment (*m*, *m* + *dm*) due to the fragmentation of particles will be equal to the product of the rate particle fragmentation and the mass of species *i* contained in each of these fragmenting particles, m_i:

$$\frac{\partial q_i(m)}{\partial t} = -g(m) n(m) m_i\big|_m \tag{7.38}$$

Using the relation $q_i(m) = m_i\big|_m n(m)$, Equation (7.38) reduces to the fragmentation loss term for the species mass balance method:

$$\boxed{\frac{\partial q_i(m)}{\partial t} = -g(m) q_i(m)} \tag{7.39}$$

7.5.5 Fragmentation production term for the species mass balance

The increase of species *i* in the population segment covering the interval (*m*, *m* + *dm*) due to the fragmentation of larger particles is equal to the product of two quantities:

1.) the number of fragments created in the interval (*m*, *m* + *dm*)

2.) the amount of species *i* contained in these fragments.

Fragmentation is assumed to distribute all species evenly among the resulting fragments, which are also referred to as daughter particles. Thus, the mass fractions x_i in the fragments particles are the same as in the original particle. If the original particle has mass *c*, then the mass fraction of the fragments is given by:

$$x_i = \frac{m_i|_c}{c} \tag{7.40}$$

Thus every daughter particle of size m will contain an amount of species i equal to the product $m \cdot x_i$. Inserting this into the integrand of the one-component expression for fragmentation production yields the species mass distribution expression for fragmentation production:

$$\begin{aligned} \frac{\partial q_i(m)}{\partial t} &= \int_m^\infty g(c)n(c)v(c)\gamma(c,m)m \cdot x_i|_c \, dc \\ &= \int_m^\infty g(c)n(c)v(c)\gamma(c,m)m\frac{m_i|_c}{c} \cdot dc \end{aligned} \tag{7.41}$$

Substituting the relationship $q_i(c) = m_i|_c \, n(c)$ yields the species mass distribution expression for fragmentation production:

$$\boxed{\frac{\partial q_i(m)}{\partial t} = \int_m^\infty g(c)q_i(c)v(c)\gamma(c,m)\frac{m}{c}dc} \tag{7.42}$$

7.5.6 Growth term for species mass balance

The species mass distribution growth equations can directly be derived from analyzing a distribution segment, just as the growth term was developed for the number density distribution in Chapter 4. The mass of component i in a small slice of the population distribution would be influenced by the amount of component i contained in smaller particles which grew into the current size range, by the amount of component i contained in particles in the current size range which grew to a larger size, and by the change in the amount of component i in the current size range, as shown in Figure 7-10. This is very similar to the single-component expression except that now the mass flux of condensing species into the population segment, $n(m) \cdot dm_i/dt$, also affects the species mass distribution. Note also that the growth rate, dm_i/dt, denoted G_i, is summed over all species to produce the total growth rate for the particle.

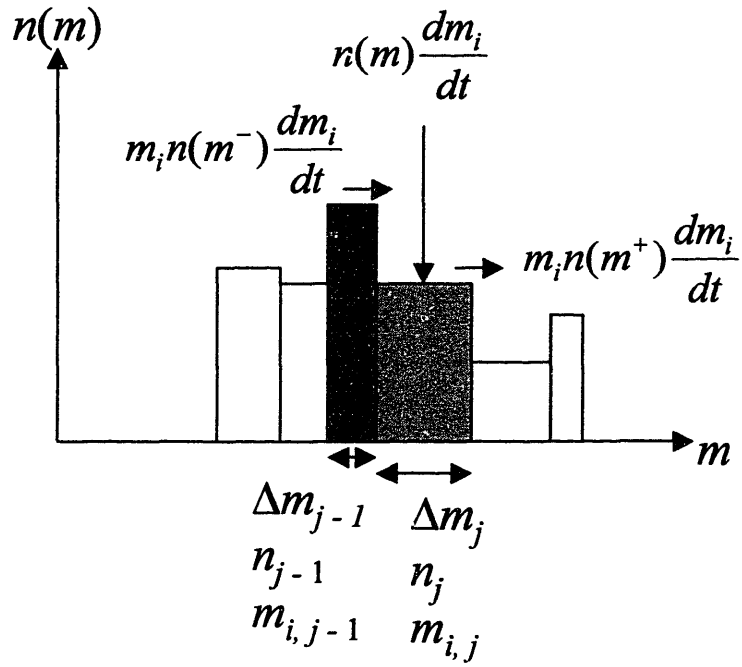

Figure 7-10: Discrete mass species distribution under growth.

Expressing the cumulative effects of these phenomena in a discrete formulation:

$$m_{i,j}n(m_j)\Delta m_j\Big|_{new} - m_{i,j}n(m_j)\Delta m_j\Big|_{old} = \underbrace{m_{i,j-1}n(m_{j-1})\frac{\sum_i \Delta m_{i,j-1}}{\Delta t_{j-1}}\Delta t}_{\text{mass gained from smaller particles grown to size } m_j} - \underbrace{m_{i,j}n(m_j)\frac{\sum_i \Delta m_{i,j}}{\Delta t_j}\Delta t}_{\text{mass gained from size } m_j \text{ particles grown to larger size}} + \underbrace{n(m_j)\frac{\Delta m_{i,j}}{\Delta t_j}\Delta m_{i,j}\Delta t}_{\text{mass gained from particles size } m_j \text{ increasing component } m_i \text{ content}} \quad (7.43)$$

Note that in the last term, $\Delta m_{i,j}$ represents the growth rate of component i in interval j, while the width of the interval is $\Delta m_{i,j}$. Dividing this expression through by Δt yields:

$$m_{i,j}n(m_j)\Delta m_j\big|_{t+1} - m_{i,j}n(m_j)\Delta m_j\big|_t = m_{i,j-1}n(m_{j-1})\left(\sum_i \frac{\Delta m_{i,j-1}}{\Delta t}\right)\Delta t$$
$$- m_{i,j-1}n(m_j)\left(\sum_i \frac{\Delta m_{i,j}}{\Delta t}\right)\Delta t + n(m_j)\Delta m_j \frac{\Delta m_{i,j}}{\Delta t}\Delta t$$

$$\frac{m_{i,j}n(m_j)\Delta m_j\big|_{t+1} - m_{i,j}n(m_j)\Delta m_j\big|_t}{\Delta t} = m_{i,j-1}n(m_{j-1})\left(\sum_i \frac{\Delta m_{i,j-1}}{\Delta t}\right) \tag{7.44}$$
$$- m_{i,j-1}n(m_j)\left(\sum_i \frac{\Delta m_{i,j}}{\Delta t}\right) + n(m_j)\Delta m_j \frac{\Delta m_{i,j}}{\Delta t}$$

Taking the limit of this expression as $\Delta t \to 0$ yields a differential governing equation and converts the $\Delta m/\Delta t$ expressions into growth rates:

$$\frac{dm_i n(m_j)\Delta m_j}{dt} = m_{i,j-1}n(m_{j-1})\sum_i G_{i,j-1} - m_{i,j-1}n(m_j)\sum_i G_{i,j} + n(m_j)\Delta m_j G_{i,j} \tag{7.45}$$

Dividing this expression through by Δm_j and taking the limit as this interval approaches zero yields the species mass balance expression for growth:

$$\frac{dm_i n(m_j)}{dt} = \frac{m_{i,j-1}n(m_{j-1})\sum_i G_{i,j-1} - m_{i,j-1}n(m_j)\sum_i G_{i,j}}{\Delta m_j} + n(m_j)G_{i,j}$$

$$\frac{\partial m_i n(m)}{\partial t} = -\frac{\partial\left(m_i n(m)\sum_i G_i(m)\right)}{\partial m} + n(m)G_i(m) \tag{7.46}$$

Finally, recognizing that $q_i(m) = m_i\big|_m n(m)$ and that $: n(m) = \dfrac{\sum_i q_i(m)}{m}$ yields an expression in terms of species mass balances $q_i(m)$.

$$\boxed{\frac{\partial q_i(m)}{\partial t} = -\frac{\partial\left(\partial q_i(m)\sum_j G_j(m)\right)}{\partial m} + \frac{\sum_j q_j(m)}{m}G_i(m)} \tag{7.47}$$

Note that the dummy variable for the summations has been changed from i to j to emphasize the distinction with i used in the other terms.

7.5.7 Sources & sink terms for the species mass balance

In order to specify the effect of sources and sinks on an individual species mass distribution, it is necessary to specify both the increase in number of particles as a function of time as well as the change in their composition with time:

$$\frac{\partial q_i(m)}{\partial t} = m_i(m)\Big|_{\text{source}} \cdot \frac{\partial n(m)}{\partial t}\Big|_{\text{source}} \tag{7.48}$$

In essence, this expression states that the rate of mass accumulation is the product of the number of new particles entering the system and their compositions.

7.6 Split Composition Distribution Method

In order to address the need for a multicomponent representation which can be tailored to the needs of various systems, the split composition distribution was proposed by Resch (1995). This method essentially models the overall number density distribution and then superimposes a representation describing the composition distribution of particles at each mass segment of the number density distribution. This is essentially accomplished by substituting a random variable $x_i(\omega)$ for the composition into the species mass distribution equations where:

$$m_i = m \cdot x_i(\omega) \tag{7.49}$$

This essentially relaxes the internally mixed assumption and allows variation within the sub-population of particles. The basis behind this approach is to treat the particles at each specific size as a sub-population. Within each of these sub-populations, the probability density function of $x_i(\omega)$ describes the composition variation of the particles, as shown in Figure 7-11. This probability density function is essentially the number density function normalized by the number of particles in the number density distribution segment $(m, m + dm)$. Please refer to Chapter 2 for more information on the relation between number density distributions and probability density distributions.

Because these particle systems are generally assumed to contain a large number of particles, the law of large numbers can be applied to $n(m)$ and the probability density function for composition to determine the number of particles at any combination of mass and composition. In this sense, the split composition distribution representation fully defines the multidimensional system. For instance, integrating $n(m)$ over the mass range between $m = 1.0 \times 10^{-15}$ and $m + dm = 1.01 \times 10^{-15}$ might reveal that $N(1.0 \times 10^{-15} < m < 1.01 \times 10^{-15}) = 10^3$. If we wanted to know the num-

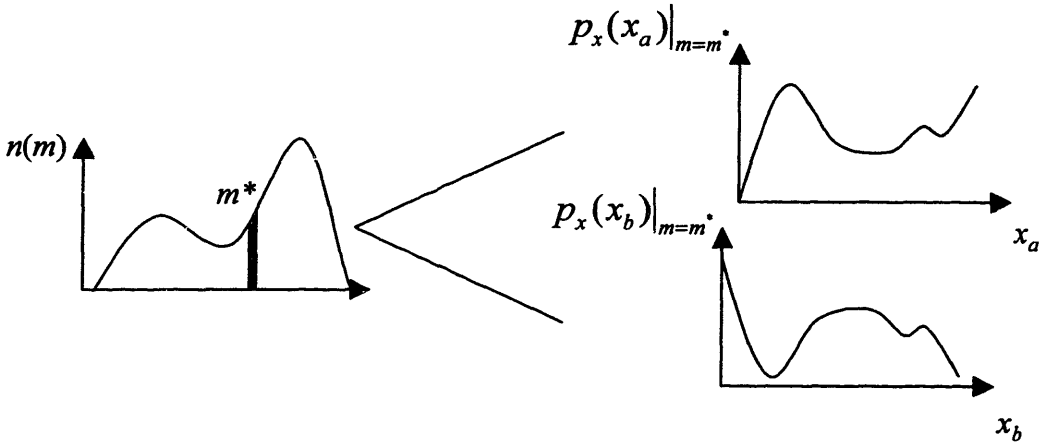

Figure 7-11: Discrete mass species distribution under growth.

ber of particles within this mass range which had compositions between $x_a = 0.5$ and 0.501, this quantity could be calculated as follows:

$$N(1.0\times10^{-15} < m < 1.01\times10^{-15}, 0.5 < x_a < 0.501) = \int_{1.0\times10^{-15}}^{1.01\times10^{-15}} n(m)\left(\int_{0.5}^{0.501} p_x[x_a(m)]dx_a\right)dm \quad (7.50)$$

For more information on probability density functions, please refer to Drake (1967), Papoulis (1991) or Appendix D.

The split composition distribution method thus produces the following set of governing equations:

1.) an overall number density equation
2.) s - 1 "relaxed" species mass distributions, where s is the number of species

If there are p node points for the number density equations, this will contribute p equations to the system of ODEs representing the split composition distribution model. If p node points are similarly used to represent each probability density function for the composition, then the "relaxed" species mass distributions will be two-dimensional functions in (x_i, m) space. If p node points are used along each of these dimensions, then p^2 node points will be needed for each of the "relaxed" species mass distributions - in the case where the compositions are assumed to be independent of one another. Thus, the complete solution will require the simultaneous numerical integration of $p + (s - 1) \cdot p^2$ ODEs. If no assumptions are made regarding the correlation of the compositions, then a full set of p^s governing equations may be needed.

In order to reduce the set of governing ODEs, an orthogonal expansion of random variables is employed to describe $x_i(\omega)$ for each species. This expansion is known as the Wiener expansion or polynomial chaos expansion (PCE) and was developed by Norbert Wiener (Wiener, 1938; Wang, 1999). Because this orthogonal expansion converges quickly, a wide range of probability density functions can be represented with very few expansion terms. Recent applications of this technique have been developed for uncertainty analysis and representation of uncertain random variables (Tatang, 1994; Wang, 1999), but the representation is also well-suited for describing the distribution of compositions among particles.

7.6.1 Wiener expansion

In order to represent the composition distribution, an expansion is used which was developed by Norbert Wiener (Wiener, 1938). This expansion uses a set of orthogonal basis functionals of standard probability density functions to represent distributions. In general, these probability density functions can be any continuous distribution, including lognormal, gaussian, exponential distributions, etc. Depending on the basis function used, the expansion will have a different domain and a different set of orthogonal functionals. By changing the basis function, the expansion can be tailored to better fit the particular requirements of a given application (Wang, 1999).

In the split composition distribution method, independent Gaussian probability distributions of mean zero and standard deviation one ($\xi_i(\omega) \sim N(0, 1)$) are used as basis functions. For this set of basis probability density functions, the orthogonal functionals of the Wiener expansion consist of Hermite polynomial functionals of Gaussian random variables. Thus, a two-dimensional Wiener expansion describing a two-dimensional random variable is given by:

$$\begin{aligned} x_i(\omega) = {} & x_{i,0} + x_{i,1}\xi_1(\omega) + x_{i,2}\xi_2(\omega) + x_{i,3}[\xi_1(\omega)^2 - 1] \\ & + x_{i,4}\xi_1(\omega)\xi_2(\omega) + x_{i,5}[\xi_2(\omega)^2 - 1] + \ldots \end{aligned} \tag{7.51}$$

where the $x_{i,j}$ are coefficients of the expansion. Depending on the type of system represented and the required accuracy, different probability density functions may be used and a varying number of terms included in the expansion. When a two-term Wiener expansion is used to represent the composition distribution of each component in the system:

$$x_i = x_{i,0} + x_{i,1}\xi_1(\omega) \tag{7.52}$$

then the composition distribution of each component i is Gaussian with mean $x_{i,0}$ and standard

deviation $x_{i,1}$(see Figure 7-12). This is easy to confirm by directly calculating the mean and vari-

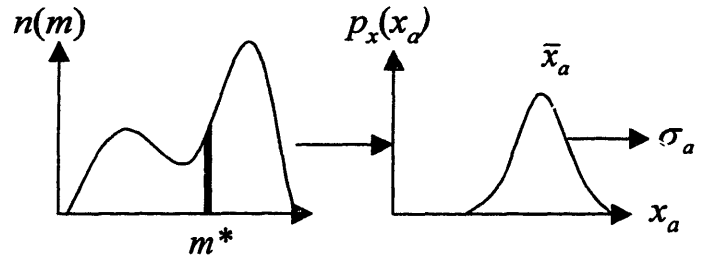

Figure 7-12: Two-term Wiener expansion based on Gaussian random variables.

ance of the expansion:

$$\begin{aligned}
\bar{x}_i &= E[x_i] = \int_{-\infty}^{\infty} (x_{i,0} + x_{i,1}\xi_1) dP(\xi_1) \\
&= \int_{-\infty}^{\infty} (x_{i,0} + x_{i,1}\xi_1) f(\xi_1) d\xi_1 \\
&= \int_{-\infty}^{\infty} (x_{i,0} + x_{i,1}\xi_1) \frac{1}{\sigma\sqrt{2\pi}} e^{\frac{-\xi_1^2}{2\sigma^2}} d\xi_1 \\
&= x_{i,0}
\end{aligned} \tag{7.53}$$

$$\begin{aligned}
\sigma^2 &= E[(x_i - \bar{x}_i)^2] = \int_{-\infty}^{\infty} (x_{i,0} + x_{i,1}\xi_1 - x_{i,0})^2 dP(\xi_1) \\
&= \int_{-\infty}^{\infty} (x_{i,1}\xi_1)^2 \frac{1}{\sigma\sqrt{2\pi}} e^{\frac{-\xi_1^2}{2\sigma^2}} d\xi_1 \\
&= x_{i,1}^2
\end{aligned} \tag{7.54}$$

Note that these evaluations are conveniently defined by the moment generating property of Gaussian random variables (see Appendix D). For convenience, all random variables have been expressed in the form ξ in lieu of $\xi(\omega)$.

Solving for these two coefficients of the expansion completely determine the probability density function for each species. In the case where there are *s* species and *n* expansion terms in a

system with p node points, the total number of ODEs specifying the system is $p(1 + s \cdot n)$. Solution of the overall number density expression contributes p equations, while the composition distribution equations contribute $p \cdot s \cdot n$ equations.

7.7 Derivation of Split Composition Distribution Method Governing Equations

Derivation of the split composition distribution method governing equations involves the following steps:

1. decide how many terms will be included in the Wiener expansion for the system
2. substitute the Wiener expansion into the species mass distribution governing equations\
3. minimize the error in the composition equations by forcing the expansion to be orthogonal to the basis functions. This step produces a set of governing ODEs for composition.

The following sections derive the form of the split composition distribution governing equations for a system where the Wiener expansion for each species is given in Equation (7.52).

7.7.1 Coagulation

Coagulation has the ability both produce and usurp particles of any given size. Starting off with the governing equation for coagulation loss as given in Equation (7.22):

$$\frac{\partial q_i(m)}{\partial t} = -q_i(m) \int_0^\infty \beta(m, c) n(c) dc \tag{7.55}$$

and substituting $q_i(m) = n(m) \cdot m \cdot x_i(m)$ yields:

$$\frac{\partial n(m) m \cdot x_i(m)}{\partial t} = -n(m) m \cdot x_i(m) \int_0^\infty \beta(m, c) n(c) dc \tag{7.56}$$

For this derivation the Wiener expansion is:

$$x_i(m, \omega) = x_{i,0}(m) + x_{i,1}(m) \xi_i(\omega) \tag{7.57}$$

This notation emphasizes that the parameters of the random variable $x_i(m, \omega)$ are a function of particle size m. Substituting the Wiener expansion into the governing equation produces:

$$\frac{\partial n(m)m \cdot [x_{i,0}(m) + x_{i,1}(m)\xi_i(\omega)]}{\partial t} = -n(m)m \cdot [x_{i,0}(m) + x_{i,1}(m)\xi_i(\omega)] \cdot \int_0^\infty \beta(m,c)n(c)dc \tag{7.58}$$

Henceforth ξ_i will be understood to mean $\xi_i(\omega)$ for the sake of clarity. The error of this governing equation is minimized by taking its inner product with respect to the two basis functions for this expansion, 1 and ξ_i. First starting with the left-hand side expression and taking the inner product with respect to 1 and ξ_i.

$$\begin{aligned} \int_{-\infty}^{\infty} \frac{\partial n(m)m \cdot [x_{i,0}(m) + x_{i,1}(m)\xi_i]}{\partial t} p_{\xi_i}(\xi_i)d\xi_i &= \frac{\partial n(m)m \cdot x_{i,0}(m)}{\partial t} \\ \int_{-\infty}^{\infty} \frac{\partial n(m)m \cdot [x_{i,0}(m) + x_{i,1}(m)\xi_i]}{\partial t} \xi_i p_{\xi_i}(\xi_i)d\xi_i &= \frac{\partial n(m)m \cdot x_{i,1}(m)}{\partial t} \end{aligned} \tag{7.59}$$

These expressions are trivial to evaluate because the inner products are essentially moments of the Gaussian probability density function. As shown in Appendix E, the moments are given by the formula:

$$\begin{aligned} E[\xi^n] &= \int_{-\infty}^{\infty} f(\xi)\xi^n d\xi = \int_{-\infty}^{\infty} \frac{1}{\sigma\sqrt{2\pi}} e^{\frac{-\xi^2}{2\sigma^2}} \xi^n d\xi \\ &= \begin{cases} 0 & n = 2k+1 \\ 1 \cdot 3 \cdot \ldots (n-1)\sigma^n & n = 2k \end{cases} \end{aligned} \tag{7.60}$$

Applying the same inner products to the right hand sides of Equation (7.58) yields:

$$\begin{aligned} \langle -n(m)m \cdot [x_{i,0}(m) + x_{i,1}(m)\xi_i] \int_0^\infty \beta(m,c)n(c)dc, 1 \rangle &= -n(m)m \cdot x_{i,0}(m) \int_0^\infty \beta(m,c)n(c)dc \\ \langle -n(m)m \cdot [x_{i,0}(m) + x_{i,1}(m)\xi_i] \int_0^\infty \beta(m,c)n(c)dc, \xi_i \rangle &= -n(m)m \cdot x_{i,1}(m) \int_0^\infty \beta(m,c)n(c)dc \end{aligned} \tag{7.61}$$

The two differential equations which specify the evolution of $x_{i,0}$ and $x_{i,1}$ are thus:

$$\begin{aligned}\frac{\partial n(m)m\cdot x_{i,0}(m)}{\partial t} &= -n(m)m\cdot x_{i,0}(m)\int_0^\infty \beta(m,c)n(c)dc \\ \frac{\partial n(m)m\cdot x_{i,1}(m)}{\partial t} &= -n(m)m\cdot x_{i,1}(m)\int_0^\infty \beta(m,c)n(c)dc\end{aligned} \tag{7.62}$$

The coagulation production term is derived in a similar fashion. Starting with Equation (7.25) and then converting all m_i's and $q_i(m)$'s to $n(m)$, m, and x_i yields:

$$\begin{aligned}\frac{\partial q_i(m)}{\partial t} &= \frac{1}{2}\int_0^m (m_i|_a + m_i|_{m-a})\beta(a,m-a)n(a)n(m-a)da \\ \frac{\partial n(m)m\cdot x_i}{\partial t} &= \frac{1}{2}\int_0^m (a\cdot x_i|_a + (m-a)x_i|_{m-a})\beta(a,m-a)n(a)n(m-a)da\end{aligned} \tag{7.63}$$

Next, substituting the Wiener expansion results in:

$$\begin{aligned}\frac{\partial n(m)m\cdot[x_{i,0}(m)+x_{i,1}(m)\xi_i]}{\partial t} = \frac{1}{2}\int_0^m &\{a\cdot[x_{i,0}(a)+x_{i,1}(a)\xi_i] \\ &+(m-a)[x_{i,0}(m-a)+x_{i,1}(m-a)\xi_i]\} \\ &\cdot\beta(a,m-a)n(a)n(m-a)da\end{aligned} \tag{7.64}$$

Taking the inner products of this expression with respect to 1 and dx results in the expression for coagulation production:

$$\begin{aligned}\frac{\partial n(m)m\cdot x_{i,0}(m)}{\partial t} &= \frac{1}{2}\int_0^m \{a\cdot x_{i,0}(a)+(m-a)x_{i,0}(m-a)\} \\ &\quad\cdot\beta(a,m-a)n(a)n(m-a)da \\ \frac{\partial n(m)m\cdot x_{i,1}(m)}{\partial t} &= \frac{1}{2}\int_0^m \{a\cdot x_{i,1}(a)+(m-a)x_{i,1}(m-a)\} \\ &\quad\cdot\beta(a,m-a)n(a)n(m-a)da\end{aligned} \tag{7.65}$$

Introducing the Wiener expansion into the governing equations actually means that the number density $n(m)$ is no longer deterministic and can also be described by a Wiener expansion. If

necessary, the number density distribution can be expanded to include multiple terms; by treating $n(m)$ as a deterministic quantity, implicitly the assumption has been made that $n(m)$ is adequately described by the zero-order Wiener expansion:

$$n(m) = n_{i,0}(m) \tag{7.66}$$

which is equivalent to assuming that the *expected value* of the number density distribution is sufficient to describe the solution.

7.7.2 Fragmentation

Just as with coagulation, fragmentation affects the number density distribution through both fragmentation loss and production mechanisms. The fragmentation loss mechanism is given by Equation (7.39); converting this expression in terms of $n(m)$, m, and x_i results in:

$$\begin{aligned} \frac{\partial q_i(m)}{\partial t} &= -g(m)q_i(m) \\ \frac{\partial n(m)m \cdot x_i}{\partial t} &= -g(m)n(m)m \cdot x_i \end{aligned} \tag{7.67}$$

Substituting the Wiener expansion yields:

$$\frac{\partial n(m)m \cdot [x_{i,0}(m) + x_{i,1}(m)\xi_i]}{\partial t} = -g(m)n(m)m \cdot [x_{i,0}(m) + x_{i,1}(m)\xi_i] \tag{7.68}$$

Finally, taking the inner product of this expression with respect to the basis functions 1 and ξ_i results in the expression for fragmentation loss:

$$\boxed{\begin{aligned} \frac{\partial n(m)m \cdot x_{i,0}(m)}{\partial t} &= -g(m)n(m)m \cdot x_{i,0}(m) \\ \frac{\partial n(m)m \cdot x_{i,1}(m)}{\partial t} &= -g(m)n(m)m \cdot x_{i,1}(m) \end{aligned}} \tag{7.69}$$

The fragmentation production term is given by Equation (7.42).

$$\frac{\partial q_i(m)}{\partial t} = \int_m^\infty g(c)q_i(c)v(c)\gamma(c, m)\frac{m}{c}dc \tag{7.70}$$

Converting the $q_i(m)$ terms to $n(m)$, m, and x_i yields:

$$\frac{\partial n(m)m \cdot x_i}{\partial t} = \int_m^\infty g(c)n(c)c \cdot x_i|_c \nu(c)\gamma(c,m)\frac{m}{c}dc \tag{7.71}$$

Next, substituting the Wiener expansion produces:

$$\frac{\partial n(m)m \cdot [x_{i,0}(m) + x_{i,1}(m)\xi_i]}{\partial t} = \int_m^\infty g(c)n(c)c \cdot [x_{i,0}(c) + x_{i,1}(c)\xi_i]\nu(c)\gamma(c,m)\frac{m}{c}dc \tag{7.72}$$

Finally, taking the inner product with respect to the basis functions 1 and ξ_i results in the governing expression for fragmentation production:

$$\boxed{\begin{aligned}\frac{\partial n(m)m \cdot x_{i,0}(m)}{\partial t} &= \int_m^\infty g(c)n(c)c \cdot x_{i,0}(c)\nu(c)\gamma(c,m)\frac{m}{c}dc \\ \frac{\partial n(m)m \cdot x_{i,1}(m)}{\partial t} &= \int_m^\infty g(c)n(c) \cdot x_{i,1}(c)\nu(c)\gamma(c,m)\frac{m}{c}dc\end{aligned}} \tag{7.73}$$

7.7.3 Growth

Unlike fragmentation and coagulation, growth is often a strong function of composition in many applications. Therefore, any variation in composition should produce some variation in the growth rate, depending on the system.

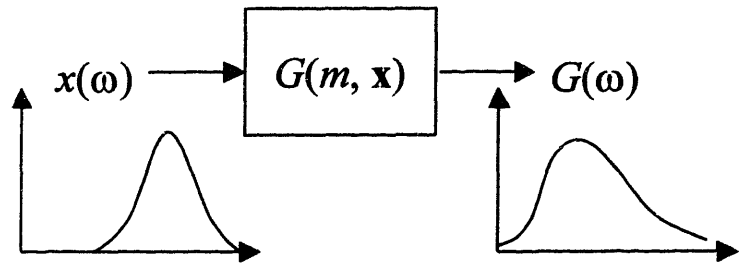

Figure 7-13: Random variable representations for both the composition and the growth rate, which is a function of composition.

Figure 7-13 depicts a sample system where a distribution of composition at some mass point m in the system results in a growth rate which is also a distribution described by a random variable. As a result, $G_i(m)$ can be described by a Wiener expansion of the same form as $x(\omega)$, but with different coefficients:

$$G_i(m,\omega) = g_{i,0}(m) + g_{i,1}(m)\xi_i \tag{7.74}$$

where the ξ_1 used in this expansion is the same ξ_1 used in the Wiener expansion for $x(\omega)$. The problem of determining the growth rate can be viewed as a parametric uncertainty problem. In general, parametric uncertainty problems use some deterministic model in conjunction with a random input to describe the output of the system. Because the input is a random variable, the output is also described by a random variable. In the growth problem, the varying input is given by $x(\omega)$ while the system model is the growth rate law for species i, $G_i(m, \mathbf{x})$. The output of this model is thus described the random variable $G_i(m, \omega)$. Using the uncertainty analysis methods developed by Tatang (1994) and Wang (1999), it is possible to solve for the coefficients $g_{i,0}(m)$ and $g_{i,1}(m)$ as a function of the coefficients of the $x_{i,0}(m)$ and $x_{i,1}(m)$ in the Wiener expansion for the composition.

In order to calculate the growth term in the split composition distribution method, we start off with the species mass distribution expression for growth:

$$\frac{\partial q_i(m)}{\partial t} = -\frac{\partial\left(\partial q_i(m)\sum_j G_j(m)\right)}{\partial m} + \frac{\sum_j q_j(m)}{m} G_i(m) \tag{7.75}$$

Substituting $q_i(m) = n(m) \cdot m \cdot x_i$ into this expression yields:

$$\frac{\partial n(m) \cdot m \cdot x_i(m)}{\partial t} = -\frac{\partial\left(n(m) \cdot m \cdot x_i(m)\sum_j G_j(m)\right)}{\partial m} + \frac{\sum_j n(m) \cdot m \cdot x_j(m)}{m} G_i(m) \tag{7.76}$$

Next, replacing the expressions x_i and $G_i(m)$ with the appropriate Wiener expansions produces:

$$\begin{aligned}
&\frac{\partial n(m) \cdot m \cdot [x_{i,0}(m) + x_{i,1}(m)\xi_i]}{\partial t} = \\
&-\frac{\partial\left[n(m) \cdot m \cdot [x_{i,0}(m) + x_{i,1}(m)\xi_i]\sum_j (g_{j,0}(m) + g_{j,1}(m)\xi_j)\right]}{\partial m} \\
&+ n(m)\left(\sum_j x_{j,0}(m) + x_{j,1}(m)\xi_j\right)(g_{i,0}(m) + g_{i,1}(m)\xi_i)
\end{aligned} \tag{7.77}$$

Finally, taking the inner product with respect to the basis functions 1 and ξ_i results in the final

form of the governing equations:

$$\begin{aligned}
\frac{\partial n(m) m \cdot x_{i,0}(m)}{\partial t} &= -\frac{\partial\left[n(m) \cdot m\left(x_{i,0}(m)\sum_j g_{j,0}(m) + x_{i,1}(m) \cdot g_{i,1}(m)\right)\right]}{\partial m} \\
&\quad + n(m)\left[g_{i,0}(m)\sum_j x_{j,0}(m) + x_{i,0}(m) \cdot g_{i,1}(m)\right] \\
\frac{\partial n(m) m \cdot x_{i,1}(m)}{\partial t} &= -\frac{\partial\left[n(m) \cdot m\left(x_{i,0}(m) \cdot g_{i,1}(m) + x_{i,1}(m)\sum_j g_{j,0}(m)\right)\right]}{\partial m} \\
&\quad + n(m)\left[x_{i,1}(m) \cdot g_{i,0}(m) + g_{i,1}(m)\sum_j x_{j,0}(m)\right]
\end{aligned} \tag{7.78}$$

In the case where the coagulation or fragmentation rates were also strong functions of composition, the corresponding coagulation and/or fragmentation kernels would also be random variables and would require treatment similar to the growth expression. Conversely, in systems where the growth rate is *not* a strong function of composition $g_{i,1}(m) \approx 0$ and the growth rate is deterministic.

7.7.4 Sources & sinks

Starting with the species mass balance expression for sources:

$$\frac{\partial q_i(m)}{\partial t} = m_i(m)\Big|_{\text{source}} \cdot \frac{\partial n(m)}{\partial t}\Big|_{\text{source}} \tag{7.79}$$

we first substitute $q_i(m) = n(m) \cdot m \cdot x_i(m)$ to produce:

$$\frac{\partial n(m) \cdot m \cdot x_i(m)}{\partial t} = m \cdot x_i\Big|_{\text{source}} \cdot \frac{\partial n(m)}{\partial t}\Big|_{\text{source}} \tag{7.80}$$

Because the split composition distribution method allows variation in the particle composition, substituting the Wiener expansion results in:

$$\frac{\partial n(m) \cdot m[x_{i,0}(m) + x_{i,1}(m)\xi_i]}{\partial t} = m \cdot (x_{i,0}(m)\Big|_{\text{source}} + x_{i,1}(m)\xi_i\Big|_{\text{source}}) \cdot \frac{\partial n(m)}{\partial t}\Big|_{\text{source}} \tag{7.81}$$

Taking the inner product of this expression with respect to the basis functions 1 and ξ_i produces the split composition distribution method governing equation:

$$\boxed{\begin{aligned} \frac{\partial n(m)\cdot m\cdot x_{i,0}(m)}{\partial t} &= m\cdot x_{i,0}(m)\big|_{\text{source}}\cdot\left.\frac{\partial n(m)}{\partial t}\right|_{\text{source}} \\ \frac{\partial n(m)\cdot m\cdot x_{i,1}(m)}{\partial t} &= m\cdot x_{i,1}(m)\xi_i\big|_{\text{source}}\cdot\left.\frac{\partial n(m)}{\partial t}\right|_{\text{source}} \end{aligned}} \tag{7.82}$$

7.7.5 Full set of governing equations

The equations outlined in the sections above generate a solution for the quantities $(m)\cdot m\cdot x_{i,0}(m)$ and $n(m)\cdot m\cdot x_{i,1}(m)$. In order to fully define the solution and solve for the moments of the composition distribution $x_{i,0}(m)$ and $x_{i,1}(m)$, a solution is needed for $n(m)$. This solution is generated by the solution of the overall number density distribution governing equations as given for a one-component system in Chapter 4, where the overall growth rate in the system is simply the sum of the mean growth rates:

$$G(m) = \sum_i \overline{G}_i(\omega) \tag{7.83}$$

7.8 Analytical solution

Analytical solutions to the multicomponent population balance exist only under very restrictive conditions. For systems with simultaneous coagulation and growth, an analytical solution exists under the following conditions (Kim and Seinfeld, 1992):

1. the initial multicomponent number density distribution follows an exponential distribution:

$$n_0(m_1, m_2, \ldots, m_s) = N_0 \frac{e^{\left(-\frac{m_1}{m_{10}}\right)}}{m_{10}} \frac{e^{\left(-\frac{m_2}{m_{20}}\right)}}{m_{20}} \cdots \frac{e^{\left(-\frac{m_s}{m_{s0}}\right)}}{m_{s0}} \tag{7.84}$$

2. the growth rate is proportional to the mass of each component in the particle:

$$G_i(m) = c_i \cdot m \tag{7.85}$$

3. the coagulation kernel $\beta(x, y)$ is constant:

$$\beta(x, y) = \beta_0 \tag{7.86}$$

Note that this form of the growth rate law corresponds to a system where growth is limited by volume-based reaction (see Chapter 6).

Under these conditions, the resulting multicomponent number density distribution is:

$$n(\mathbf{m},\tau) = \frac{4N_0}{(\tau+2^2)}\prod_{i=1}^{s}\frac{1}{m_{i0}}\exp\left(-\frac{m_i}{m_{i0}}e^{-\Lambda_i r}-\Lambda_i r\right)\sum_{k=0}^{\infty}\frac{1}{(k!)^s}\left[\frac{\tau}{2+\tau}\prod_{j=1}^{s}\frac{m_j}{m_{j0}}e^{-\Lambda_j r}\right]^k \tag{7.87}$$

where:

- N_0 is the initial number of particles in the population,
- m_{i0} is a parameter defining the initial distribution of component i.
- m_j is mass amount of component j.
- τ is defined as:

$$\tau = N_0\beta_0 t \tag{7.88}$$

- β_0 is the constant value of the coagulation kernel.
- Λ_i is defined as follows:

$$\Lambda_i = \frac{c_i}{N_0\beta_0} \tag{7.89}$$

In a system where the growth rate is zero, this solution reduces to:

$$n(\mathbf{m},\tau) = \frac{4N_0}{(\tau+2^2)}\prod_{i=1}^{s}\frac{1}{m_{i0}}\exp\left(-\frac{m_i}{m_{i0}}\right)\sum_{k=0}^{\infty}\frac{1}{(k!)^s}\left[\frac{\tau}{2+\tau}\prod_{j=1}^{s}\frac{m_j}{m_{j0}}\right]^k \tag{7.90}$$

7.9 Summary

In an effort to practically address the needs of multicomponent population balance problems, Pilinis (1990) introduced the species mass distribution method. While this method successfully reduces the governing set of equations enough to produce a tractable solution, in practice the internally mixed assumption restricts this method to the extent that it is almost a pseudo-one-component solution. Take, for instance, a system undergoing fragmentation of particles and consider

two portions of the corresponding species mass distributions, as shown in Figure 7-14.

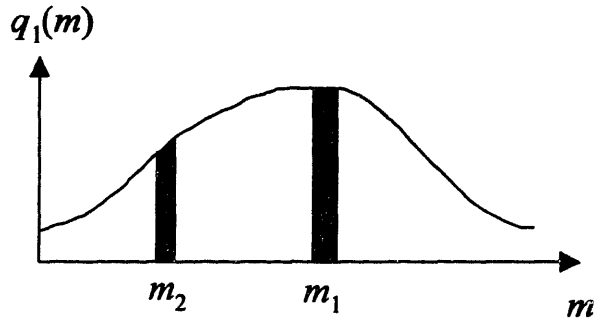

Figure 7-14: Two portions of a species mass distribution undergoing fragmentation.

In general, particles at m_1 will not have the same composition as particles at m_2. However, particles of mass m_2 can be produced from particles of size m_1. These new fragments of mass m_2 will not have the same composition as the other particles at mass m_2, however the internally mixed assumption requires that all of these particle have the same composition. To meet this requirement, the representation essentially averages the composition of the new fragments with the other fragments at size m_2. In practice, however, this is an artifact of the representation because no mechanisms exists which averages the composition of new fragments with the fragments. As a result, the true physics of this process are not well-represented by the species mass distribution.

References

[1] Fernández-Díaz, J. M.; Rodriguez Braña, M. A.; Arganza García, B.; González-Pola Muñiz, C.; Garcia Nieto, P. J. *Analytic Solution of the Aerosol Rigorous General Dynamic Equation without Coagulation in Multidimension,* Aerosol Science and Technology **31**, 3-16, 1999.

[2] Gelbard, Fred M.; Seinfeld, John. H. *Coagulation and Growth of a Multicomponent Aerosol.* Joural of Colloid and Interface Science **3**, 472, 1978.

[3] Gueron, Shay. *The Steady-State Distributions of Coagulation-Fragmentation Processes*, Journal of Mathematical Biology, **37**, 1, 1998.

[4] Katoshevski, David; Seinfeld, John. H. *Analytical Solution of the Multicomponent Aerosol General Dynamic Equation - without Coagulation,* Aerosol Science and Technology, **24**(7), 541-549, 1997.

[5] Katoshevski, David; Seinfeld, John H. *Analytical - Numerical Solution of the Multicomponent Aerosol General Dynamic Equation - with Coagulation,* Aerosol Science and Technology, **24**(7), 550-556, 1997.

[6] Kim, Yong P.; Seinfeld, John H. *Simulations of multicomponent aerosol condensation by the moving sectional method,* Journal of Colloid and Interface Science, **135**, 185, 1990.

[7] Pilinis, Christodoulos *Derivation and Numerical Solution of the Species Mass Distribution Equations for Multicomponent Particulate Systems,* Atmospheric Environment, **24A**(7), 1923-1928, 1990.

[8] Resch, Timothy J. *A Framework for the Modeling of Suspended Multicomponent Particulate Systems with Applications to Atmospheric Aerosols,* Ph.D. Thesis, Massachusetts Institute of Technology, 1995.

[9] Tatang, Menner A. *Direct Incorporation of Uncertainty in Chemical and Environmental Systems,* Ph. D. Thesis, Massachusetts Institute of Technology, 1994.

[10] Toon, O. B.; Turco, R. P. et al. *A Multidimensional model for aerosols: Description of computational analogs*, Journal of Atmospheric Science, **45**, 2123, 1988.

[11] Valentas, Kenneth J.; Amundson, Neal R. *Breakage and Coalescence in Dispersed Phase Systems,* Industrial and Engineering Chemistry Fundamentals, **5,** 533-542, 1966.

[12] Valentas, Kenneth J.; Bilous, Olegh; Amundson, Neal R. *Analysis of Breakage in Dispersed Phase Systems,* Industrial and Engineering Chemistry Fundamentals, **5**, 271-279, 1966.

[13] Wang, Cheng *Parametric Uncertainty Analysis for Complex Engineering Systems,* MIT Thesis, 1999.

[14] Wiener, Norbert *The Homogeneous Chaos*, American Journal of Mathematics, **60,** 897-936, 1938.

Chapter 8: Numerical Implementation and Solution of the Split Distribution Method

Analytical solutions to multicomponent population balance problems only exist for a limited number of highly restricted conditions. As a result, numerical solutions are needed for the majority of applications. However, analytical solutions do have utility for verifying the results of numerical solutions. This chapter develops the numerical solution for the analytical solution presented at the end of Chapter 7 for systems with coagulation and growth, and compares the results of this solution to the analytical results.

8.1 Rescaled equations

As discussed in Chapter 6, the form of the growth rate law affects how the governing equations should be scaled. For a solution with evenly spaced elements and a growth law of the form:

$$G_i(m) = c_i \cdot m_i \tag{8.1}$$

Rescaling the governing equations to $n(w)$ results in the optimal time step for the numerical solution. The following exponential scaling is used, based on the maximum and minimum particle sizes in the domain range of the solution, m_{max} and m_{min}:

$$\begin{aligned} \gamma &= \ln\left(\frac{m_{\max}}{m_{\min}}\right) \\ m &= m_{\min} e^{\gamma w} \qquad m_0 = m_{\min} \\ \frac{dm}{dw} &= \gamma m_0 e^{\gamma w} = \gamma m \end{aligned} \tag{8.2}$$

The following sections detail the development of the governing equations in $n(w)$ and their implementation in a numerical solution using the orthogonal collocation on finite elements method.

8.2 Coagulation

8.2.1 Coagulation removal

In order to derive the rescaled split composition distribution equations, we start with the governing equations scaled for $n(m)$. These equations include the overall number density equation:

$$\frac{\partial n(m)}{\partial t} = -n(m)\int_0^\infty \beta(m,a)n(a)da \tag{8.3}$$

as well as the governing equations for composition:

$$\begin{aligned}\frac{\partial n(m)m\cdot x_{i,0}(m)}{\partial t} &= -n(m)m\cdot x_{i,0}(m)\int_0^\infty \beta(m,a)n(a)da \\ \frac{\partial n(m)m\cdot x_{i,1}(m)}{\partial t} &= -n(m)m\cdot x_{i,1}(m)\int_0^\infty \beta(m,a)n(a)da\end{aligned} \tag{8.4}$$

First, the governing equation for overall number density will be transformed, followed by the governing equations for composition.

Development of the term for the governing equation for coagulation loss in the overall number density equation starts with the substitution of $n(m) = n(w)\frac{dw}{dm} = \frac{n(w)}{\gamma m}$:

$$\frac{\partial\left[\frac{n(w)}{\gamma m}\right]}{\partial t} = -\frac{n(w)}{\gamma m}\int_0^\infty \beta(m(w),a)n(a)da \tag{8.5}$$

Where m in the coagulation kernel has been replaced by $m(w)$. Multiplying both sides of this expression by γm yields:

$$\frac{\partial n(w)}{\partial t} = -n(w)\int_0^\infty \beta(m(w),a)n(a)da \tag{8.6}$$

The integration limits also need to be adjusted to account for the fact that the solution domain is $(m_{\min}, m_{\max})$:

$$\frac{\partial n(w)}{\partial t} = -n(w)\int_{m_{\min}}^{m_{\max}} \beta(m(w),a)n(a)da \tag{8.7}$$

To complete the transformation, the dummy integration variable must also be transformed to an logarithmic scale. This is accomplished by the transformation:

$$a = m_0 e^{\gamma v} \tag{8.8}$$

This transformation yields the relationship $n(a)da = n(v)dv$ which completes the rescaling of the governing equations:

$$\boxed{\frac{\partial n(w)}{\partial t} = -n(w)\int_0^1 \beta(m(w), c(v))n(v)dv} \tag{8.9}$$

Table 8-1 summarizes the variable transformations used in rescaling the governing equations.

Table 8-1: Original and rescaled distribution variables.

Original	*Rescaled*	*Relation*
m	w	$m = m_0 e^{\gamma w}$
a	v	$a = m_0 e^{\gamma v}$

In order to derive the form of the governing equations for composition, the same general procedure is used. First, substituting $n(m) = n(w)\frac{dw}{dm} = \frac{n(w)}{\gamma m}$ into Equation (8.4) produces:

$$\begin{aligned}
\frac{\partial \frac{n(w)}{\gamma m} m \cdot x_{i,0}(m(w))}{\partial t} &= -\frac{n(w)}{\gamma m} m \cdot x_{i,0}(m(w)) \int_0^\infty \beta(m(w), a)n(a)da \\
\frac{\partial \frac{n(w)}{\gamma m} m \cdot x_{i,1}(m(w))}{\partial t} &= -\frac{n(w)}{\gamma m} m \cdot x_{i,1}(m(w)) \int_0^\infty \beta(m(w), a)n(a)da
\end{aligned} \tag{8.10}$$

Canceling out m's and multiplying through by γ results in a simplified expression:

$$\begin{aligned}
\frac{\partial n(w)x_{i,0}(w)}{\partial t} &= -n(w) \cdot x_{i,0}(w) \int_0^\infty \beta(m(w), a)n(a)da \\
\frac{\partial n(w) \cdot x_{i,1}(w)}{\partial t} &= -n(w) \cdot x_{i,1}(w) \int_0^\infty \beta(m(w), a)n(a)da
\end{aligned} \tag{8.11}$$

where the $x(m(w))$ terms have been expressed as $x(w)$. Again, the integration limits are adjusted to affect the solution domain:

$$\frac{\partial n(w)x_{i,0}(w)}{\partial t} = -n(w)\cdot x_{i,0}(w)\int_{m_{min}}^{m_{max}}\beta(m(w),a)n(a)da$$
$$\frac{\partial n(w)\cdot x_{i,1}(w)}{\partial t} = -n(w)\cdot x_{i,1}(w)\int_{m_{min}}^{m_{max}}\beta(m(w),a)n(a)da \tag{8.12}$$

Finally, the dummy integration variable must also be rescaled by substituting $n(a)da = n(v)dv$

$$\boxed{\begin{aligned}\frac{\partial n(w)x_{i,0}(w)}{\partial t} &= -n(w)\cdot x_{i,0}(w)\int_0^1\beta(m(w),a(v))n(v)dv\\ \frac{\partial n(w)\cdot x_{i,1}(w)}{\partial t} &= -n(w)\cdot x_{i,1}(w)\int_0^1\beta(m(w),a(v))n(v)dv\end{aligned}} \tag{8.13}$$

8.2.2 Coagulation production

A similar procedure is followed to convert the governing equations for coagulation production, which include both the overall number density expression:

$$\frac{\partial n(m)}{\partial t} = \frac{1}{2}\int_0^m\beta(m-a,a)n(m-a)n(a)da \tag{8.14}$$

as well as the governing equations for composition:

$$\begin{aligned}\frac{\partial n(m)m\cdot x_{i,0}(m)}{\partial t} &= \frac{1}{2}\int_0^m\{a\cdot x_{i,0}(a)+(m-a)x_{i,0}(m-a)\}\\ &\quad\cdot\beta(a,m-a)n(a)n(m-a)da\\ \frac{\partial n(m)m\cdot x_{i,1}(m)}{\partial t} &= \frac{1}{2}\int_0^m\{a\cdot x_{i,1}(a)+(m-a)x_{i,1}(m-a)\}\\ &\quad\cdot\beta(a,m-a)n(a)n(m-a)da\end{aligned} \tag{8.15}$$

Again, the overall number density expression will be treated first, followed by the governing equations for composition. First, $n(m) = n(w)\frac{dw}{dm} = \frac{n(w)}{\gamma m}$ is substituted into the expression.

$$\frac{\partial\left[\frac{n(w)}{\gamma m}\right]}{\partial t} = \frac{1}{2}\int_0^m \beta(m-a,a)n(m-a)n(a)da \tag{8.16}$$

This expression is simplified by multiplying both sides of the equation by γm. The integration limits are also changed to reflect the fact that the smallest possible coagulating particles have mass m_{min} and that therefore the largest coagulating particles can have mass m - m_{min}.

$$\begin{aligned}\frac{\partial n(w)}{\partial t} &= \gamma m\frac{1}{2}\int_0^m \beta(m(w)-a,a)n(m(w)-a)n(a)da \\ &= \gamma m\frac{1}{2}\int_{m_{min}}^{m-m_{min}} \beta(m(w)-a,a)n(m(w)-a)n(a)da\end{aligned} \tag{8.17}$$

Applying the symmetry property to this integral to eliminate the double-counting correction factor ½ and reduce the integration range results in:

$$\begin{aligned}\frac{\partial n(w)}{\partial t} &= \gamma m\int_{m_{min}}^{\frac{m-m_{min}}{2}} \beta(m(w)-a,a)n(m(w)-a)n(a)da \\ &= \gamma m_0 e^{\gamma w}\int_{m_{min}}^{\frac{m-m_{min}}{2}} \beta(m(w)-a,a)n(m(w)-a)n(a)da\end{aligned} \tag{8.18}$$

In order to convert the dummy variable to an exponential scale, it is necessary to derive conversions for $n(m - a)$ as well as $n(a)$. Because logarithmic-scaled mass variables are being used, it is necessary to write the rescaled versions of $n(m - a)$ and $n(a)$ in a manner that conserves mass, as shown in Figure 8-1. In order to account for this nonlinear relationship between the logarithmic-scaled particle masses, a new variable u is introduced to represent the mass of the second coagu-

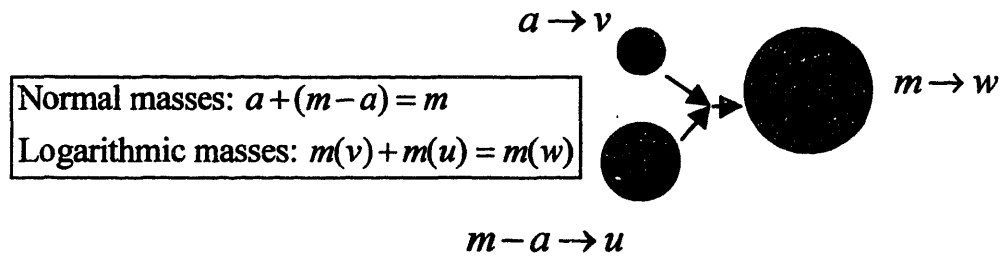

Figure 8-1: Graphical representation of a number density distribution.

lating particle, as shown in Table 8-2. Using these variables, it is possible to use the mass balance

Table 8-2: Exponential Variables Transformation Summary

Particle	*Normal Size Variable*	*Exponential Size Variable*	*Scaling Relation*
Small Coagulation Particle #1	a	v	$a = m_0 e^{\gamma v}$
Small Coagulation Particle #2	$m - a$	u	$m - a = m_0 e^{\gamma u}$
Large Coagulation Particle	m	w	$m = m_0 e^{\gamma w}$

on the coagulating particles to solve for u as a function of w and v.

$$\begin{aligned} m(u) &= m-a \\ m(u) &= m(w)-m(v) \\ m_0 e^{\gamma u} &= m_0 e^{\gamma w} - m_0 e^{\gamma v} \\ u &= \frac{1}{\gamma}\ln(e^{\gamma w} - e^{\gamma v}) \end{aligned} \tag{8.19}$$

The transformation for $n(a)$ is given by $n(a) = n(v)\frac{dv}{da} = \frac{n(v)}{m_0 \gamma e^{\gamma v}}$. However, a transformation is still needed from $n(m - a)$ to $n(u)$.

In general, transformations are defined by equating two segments of corresponding number density distributions. Starting with the basic identity $n(s)ds = n(u)du$ where define $s = m - a$ and $m(u) = m(w) - m(v)$. Because $ds/da = -1$, we can write:

$$\begin{aligned} n(s)ds &= n(u)du \\ -n(m-a)da &= n(u)du \\ n(m-a)da &= -n(u)du \end{aligned} \tag{8.20}$$

Note that u is a function of v and w. Because $n(a)$ has been converted to $n(v)$, the integration variable must be a function of v. This is easily accomplished by differentiating Equation (8.19) with respect to the variable to be used in the coagulation interval, v:

$$\begin{aligned} \frac{du}{dv} &= \frac{1}{\gamma}\frac{-\gamma e^{\gamma v}}{e^{\gamma v w} - e^{\gamma v}} \\ du &= \frac{1}{\gamma}\frac{-\gamma e^{\gamma v}}{e^{\gamma v w} - e^{\gamma v}}dv = \frac{-e^{\gamma v}}{e^{\gamma v w} - e^{\gamma v}}dv \end{aligned} \tag{8.21}$$

This yields the desired conversion for $n(m - a)da$:

$$\begin{aligned} n(m-a)da &= -n(u)du \\ n(m-a)da &= -n(u)\frac{-e^{\gamma v}}{e^{\gamma v w} - e^{\gamma v}}dv \\ n(m-a)da &= n(u)\frac{e^{\gamma v}}{e^{\gamma v w} - e^{\gamma v}}dv \end{aligned} \tag{8.22}$$

Substituting these expressions into the governing equation for coagulation production will also require a change of integration limits. The limit at $m_{\min}$ convert to 0:

$$m(v) = m_0 e^{\gamma v} \rightarrow \gamma v = \ln\left(\frac{m_0}{m_0}\right) = 0 \rightarrow v = 0 \tag{8.23}$$

and the limit at $(m - m_{\min})/2$ converts as follows:

$$\begin{aligned} m(v) &= \frac{m - m_{\min}}{2} \rightarrow m_0 e^{\gamma v} = \frac{m_0 e^{\gamma w} - m_0}{2} \\ e^{\gamma v} &= \frac{e^{\gamma w} - 1}{2} \\ v &= \frac{1}{\gamma}\ln\left[\frac{e^{\gamma w} - 1}{2}\right] \end{aligned} \tag{8.24}$$

Substituting these integration limits and variable transformations yields the rescaled overall number density governing equation:

$$\frac{\partial n(w)}{\partial t} = \gamma m_0 e^{\gamma w} \int_0^{\frac{1}{\gamma}\ln\left[\frac{e^{\gamma w}-1}{2}\right]} \beta[m(u), m(v)]\frac{n(v)}{m_0 \gamma e^{\gamma v}}\frac{e^{\gamma v}}{e^{\gamma v w} - e^{\gamma v}}dv \tag{8.25}$$

Simplifying this expression results in the final form of the overall number density governing

equation for coagulation production:

$$\frac{\partial n(w)}{\partial t} = \int_0^{\frac{1}{\gamma}\ln\left[\frac{e^{\gamma w}-1}{2}\right]} \beta[m(u), m(v)]n(u)n(v)\frac{e^{\gamma w}}{e^{\gamma v w}-e^{\gamma v}}dv \tag{8.26}$$

The same transformations are used for the governing equations for composition:

$$\begin{aligned}\frac{\partial\frac{n(w)}{\gamma m}m\cdot x_{i,0}(w)}{\partial t} &= \int_0^{\frac{1}{\gamma}\ln\left[\frac{e^{\gamma w}-1}{2}\right]} \{m_0 e^{\gamma v}\cdot x_{i,0}(v) + m_0 e^{\gamma u}x_{i,0}(u)\} \\ &\quad \cdot \beta[m(u), m(v)]\frac{n(v)}{m_0\gamma e^{\gamma v}}\frac{e^{\gamma v}}{e^{\gamma v w}-e^{\gamma v}}n(u)dv \\ \frac{\partial\frac{n(w)}{\gamma m}m\cdot x_{i,1}(w)}{\partial t} &= \int_0^{\frac{1}{\gamma}\ln\left[\frac{e^{\gamma w}-1}{2}\right]} \{m_0 e^{\gamma v}\cdot x_{i,1}(v) + m_0 e^{\gamma u}x_{i,1}(u)\} \\ &\quad \cdot \beta[m(u), m(v)]\frac{n(v)}{m_0\gamma e^{\gamma v}}\frac{e^{\gamma v}}{e^{\gamma v w}-e^{\gamma v}}n(u)dv\end{aligned} \tag{8.27}$$

Simplifying these expressions yields:

$$\begin{aligned}\frac{\partial n(w)x_{i,0}(w)}{\partial t} &= \int_0^{\frac{1}{\gamma}\ln\left[\frac{e^{\gamma w}-1}{2}\right]} \{e^{\gamma v}\cdot x_{i,0}(v) + e^{\gamma u}x_{i,0}(u)\} \\ &\quad \cdot \beta[m(u), m(v)]n(v)\frac{1}{e^{\gamma v w}-e^{\gamma v}}n(u)dv \\ \frac{\partial n(w)x_{i,1}(w)}{\partial t} &= \int_0^{\frac{1}{\gamma}\ln\left[\frac{e^{\gamma w}-1}{2}\right]} \{e^{\gamma v}\cdot x_{i,1}(v) + e^{\gamma u}x_{i,1}(u)\} \\ &\quad \cdot \beta[m(u), m(v)]n(v)\frac{1}{e^{\gamma v w}-e^{\gamma v}}n(u)dv\end{aligned} \tag{8.28}$$

8.3 Growth

The growth expression for the overall number density equation is transformed as follows (see Chapter 6):

$$\frac{\partial n(w)}{\partial t} = -\frac{\partial (n(w)G(w))}{\partial w} \tag{8.29}$$

$G(w)$ is given by:

$$G(w) = \sum_i \overline{G}_i(w) = \sum_i g_{i,0}(w) \tag{8.30}$$

where the $\overline{G}_i(w)$ is the expected value of the growth rate for species i. These values can be surmised from comparing the Wiener expansions for $G_i(m)$ and $G_i(m)$, as developed in the following section.

8.3.1 Derivation of rescaled growth rate Wiener expansion

In Chapter 7, the form of the Wiener expansion for $G_i(m)$ was derived:

$$G_i(m, \omega) = g_{i,0}(m) + g_{i,1}(m)\xi_i \tag{8.31}$$

For the growth rate law of the current system where $G_i(m) = c_i \cdot m_i = c_i \cdot m \cdot x_i$, substituting the Wiener expansion for x:

$$x_i(m) = x_{i,0}(m) + x_{i,1}(m)\xi_i \tag{8.32}$$

produces the expression for $G_i(m, \omega)$:

$$\begin{aligned} G_i(m, \omega) &= c_i \cdot m \cdot [x_{i,0}(m) + x_{i,1}(m)\xi_i] \\ &= c_i \cdot m \cdot x_{i,0}(m) + c_i \cdot m \cdot x_{i,1}(m)\xi_i \end{aligned} \tag{8.33}$$

Comparing this expression and Equation (8.31) reveals that:

$$\begin{aligned} g_{i,0}(m) &= c_i \cdot m \cdot x_{i,0}(m) \\ g_{i,1}(m) &= c_i \cdot m \cdot x_{i,1}(m) \end{aligned} \tag{8.34}$$

Starting off with the growth rate law given in Equation (8.31), the growth rate can be first transformed to $G_i(m)$.

$$\begin{aligned} G_i(w) &= \frac{dm_i}{dt} \cdot \frac{dw}{dm} \\ &= G_i(m)\frac{dw}{dm} \\ &= \frac{G_i(m)}{\gamma m} = \frac{c_i \cdot m \cdot x_i}{\gamma m} \end{aligned} \tag{8.35}$$

Simplifying this expression yields the final form of the growth rate expression:

$$G_i(w) = \frac{c_i}{\gamma} x_i \tag{8.36}$$

Substituting the Wiener expansion for x_i into this expression produces

$$\begin{aligned} G_i(w) &= \frac{c_i}{\gamma}[x_{i,0}(w) + x_{i,1}(w)\xi_i] \\ &= \frac{c_i}{\gamma} x_{i,0}(w) + \frac{c_i}{\gamma} x_{i,1}(w)\xi_i \end{aligned} \tag{8.37}$$

Comparing this expression to the Wiener expansion for $G_i(m)$:

$$G_i(w) = g_{i,0}(w) + g_{i,1}(w)\xi_i \tag{8.38}$$

reveals that the coefficients are:

$$\begin{aligned} g_{i,0}(w) &= \frac{c_i}{\gamma} x_{i,0}(w) \\ g_{i,1}(w) &= \frac{c_i}{\gamma} x_{i,1}(w) \end{aligned} \tag{8.39}$$

Incidentally, this is the same result that would have been reached using the same transformation as for $G_i(m)$ on the coefficients of the expansion. These transformations are defined in the same manner as for $G_i(m)$:

$$\begin{aligned} g_{i,0}(w) &= g_{i,0}(m) \cdot \frac{dw}{dm} \\ g_{i,1}(w) &= g_{i,1}(m) \cdot \frac{dw}{dm} \end{aligned} \tag{8.40}$$

Substituting the expressions for the coefficients from the $G_i(m, \omega)$ expansion:

$$g_{i,0}(w) = c_i \cdot m \cdot x_{i,0}(m) \cdot \frac{1}{\gamma m} = \frac{c_i}{\gamma} \cdot x_{i,0}(m)$$
$$g_{i,1}(w) = c_i \cdot m \cdot x_{i,1}(m) \cdot \frac{1}{\gamma m} = \frac{c_i}{\gamma} \cdot x_{i,1}(m) \tag{8.41}$$

produces the identical coefficients for the Wiener expansion and verifies the transform given in Equation (8.40).

8.3.2 Governing equations for composition

Because transformations have been already been defined for $n(m)$ and the coefficients of the growth rate Wiener expansion, these expressions can be directly substituted into the split composition distribution governing equations:

$$\frac{\partial n(m) m \cdot x_{i,0}(m)}{\partial t} = -\frac{\partial\left[n(m) \cdot m\left(x_{i,0}(m)\sum_j g_{j,0}(m) + x_{i,1}(m) \cdot g_{i,1}(m)\right)\right]}{\partial m}$$
$$+ n(m)\left[g_{i,0}(m)\sum_j x_{j,0}(m) + x_{i,0}(m) \cdot g_{i,1}(m)\right]$$
$$\frac{\partial n(m) m \cdot x_{i,1}(m)}{\partial t} = -\frac{\partial\left[n(m) \cdot m\left(x_{i,0}(m) \cdot g_{i,1}(m) + x_{i,1}(m)\sum_j g_{j,0}(m)\right)\right]}{\partial m} \tag{8.42}$$
$$+ n(m)\left[x_{i,1}(m) \cdot g_{i,0}(m) + g_{i,1}(m)\sum_j x_{j,0}(m)\right]$$

which produces the rescaled governing equations.

$$\frac{\partial n(w)\frac{dw}{dm}m \cdot x_{i,0}(w)}{\partial t} = -\frac{\partial\left[n(w)\frac{dw}{dm} \cdot m\left(x_{i,0}(w)\sum_j g_{j,0}(w)\frac{dm}{dw} + x_{i,1}(w) \cdot g_{i,1}(w)\frac{dm}{dw}\right)\right]}{\partial w}\frac{\partial w}{\partial m}$$

$$+ n(w)\frac{dw}{dm}\left[g_{i,0}(w)\frac{dm}{dw}\sum_j x_{j,0}(w) + x_{i,0}(w) \cdot g_{i,1}(w)\frac{dm}{dw}\right]$$

$$\frac{\partial n(w)\frac{dw}{dm}m \cdot x_{i,1}(w)}{\partial t} = -\frac{\partial\left[n(w)\frac{dw}{dm} \cdot m\left(x_{i,0}(w) \cdot g_{i,1}(w)\frac{dm}{dw} + x_{i,1}(w)\sum_j g_{j,0}(w)\frac{dm}{dw}\right)\right]}{\partial w}\frac{\partial w}{\partial m} \tag{8.43}$$

$$+ n(w)\frac{dw}{dm}\left[x_{i,1}(w) \cdot g_{i,0}(w)\frac{dm}{dw} + g_{i,1}(w)\frac{dm}{dw}\sum_j x_{j,0}(w)\right]$$

Multiplying through by *dm/dw* terms leaves:

(8.44)

$$\frac{\partial n(w)m \cdot x_{i,0}(w)}{\partial t} = -\frac{\partial\left[n(w)\frac{dw}{dm} \cdot m\left(x_{i,0}(w)\sum_j g_{j,0}(w)\frac{dm}{dw} + x_{i,1}(w) \cdot g_{i,1}(w)\frac{dm}{dw}\right)\right]}{\partial w}$$

$$+ n(w)\left[g_{i,0}(w)\frac{dm}{dw}\sum_j x_{j,0}(w) + x_{i,0}(w) \cdot g_{i,1}(w)\frac{dm}{dw}\right]$$

$$\frac{\partial n(w)m \cdot x_{i,1}(w)}{\partial t} = -\frac{\partial\left[n(w)\frac{dw}{dm} \cdot m\left(x_{i,0}(w) \cdot g_{i,1}(w)\frac{dm}{dw} + x_{i,1}(w)\sum_j g_{j,0}(w)\frac{dm}{dw}\right)\right]}{\partial w}$$

$$+ n(w)\left[x_{i,1}(w) \cdot g_{i,0}(w)\frac{dm}{dw} + g_{i,1}(w)\frac{dm}{dw}\sum_j x_{j,0}(w)\right]$$

Finally, canceling the remaining extra *dm/dw* terms and dividing through by *m* results in the final

form of the governing equations.

$$\frac{\partial n(w)x_{i,0}(w)}{\partial t} = -\frac{1}{m_0 e^{\gamma w}}\frac{\partial\left[n(w)\cdot m\left(x_{i,0}(w)\sum_j g_{j,0}(w) + x_{i,1}(w)\cdot g_{i,1}(w)\right)\right]}{\partial w}$$
$$+\frac{n(w)}{m_0 e^{\gamma w}}\left[g_{i,0}(w)\frac{dm}{dw}\sum_j x_{j,0}(w) + x_{i,0}(w)\cdot g_{i,1}(w)\frac{dm}{dw}\right]$$

$$\frac{\partial n(w)m\cdot x_{i,1}(w)}{\partial t} = -\frac{1}{m_0 e^{\gamma w}}\frac{\partial\left[n(w)\cdot m\left(x_{i,0}(w)\cdot g_{i,1}(w) + x_{i,1}(w)\sum_j g_{j,0}(w)\right)\right]}{\partial w}$$
$$+\frac{n(w)}{m_0 e^{\gamma w}}\left[x_{i,1}(w)\cdot g_{i,0}(w)\frac{dm}{dw} + g_{i,1}(w)\frac{dm}{dw}\sum_j x_{j,0}(w)\right]$$

(8.45)

8.3.3 Combined system of governing equations

The combined system of governing equations for a system are assembled by collecting each of the relevant terms describing all of the desired mechanisms for each set of equations needed to fully specify the system. In this particular instance, there are three sets of equations are needed to describe the system:

- one overall number density equation
- s composition equations describing the evolution of $x_{i,0}$, the mean composition for each component in the system
- another set of s composition equations describing the evolution of $x_{i,1}$, the standard deviation of composition for each component in the system

This system of equations can be expressed in the following form:

$$\frac{\partial n(w)}{\partial t} = \left.\frac{\partial n(w)}{\partial t}\right|_{\substack{\text{coagulation}\\\text{loss}}} + \left.\frac{\partial n(w)}{\partial t}\right|_{\substack{\text{coagulation}\\\text{production}}} + \left.\frac{\partial n(w)}{\partial t}\right|_{\text{growth}}$$

$$\frac{\partial n(w)x_{i,0}(w)}{\partial t} = \left.\frac{\partial n(w)x_{i,0}(w)}{\partial t}\right|_{\substack{\text{coagulation}\\\text{loss}}} + \left.\frac{\partial n(w)x_{i,0}(w)}{\partial t}\right|_{\substack{\text{coagulation}\\\text{production}}} + \left.\frac{\partial n(w)x_{i,0}(w)}{\partial t}\right|_{\text{growth}} \quad (8.46)$$

$$\frac{\partial n(w)x_{i,1}(w)}{\partial t} = \left.\frac{\partial n(w)x_{i,1}(w)}{\partial t}\right|_{\substack{\text{coagulation}\\\text{loss}}} + \left.\frac{\partial n(w)x_{i,1}(w)}{\partial t}\right|_{\substack{\text{coagulation}\\\text{production}}} + \left.\frac{\partial n(w)x_{i,1}(w)}{\partial t}\right|_{\text{growth}}$$

where each of the terms in these equations have been derived in the preceding sections. Note that the last two sets of equations actually add s equations each because $i = 1, 2, ..., s$.

In general, this system can be completely described by a *state vector* of variables, $\mathbf{n}$. For this system, the state vector is fully described by $n(w)$, $n(w) \cdot x_{i,0}$ and $n(w) \cdot x_{i,1}$ where the latter two terms can be divided by $n(w)$ to reveal the mean and standard deviation of the composition, respectively. Reviewing the governing equations reveals that the right hand side terms belong to two groups:

1. functions of the state variables
2. first derivatives of functions of the state variables

Accordingly, if all of the right hand side terms are lumped into these two groups, the governing equations can generally be expressed as:

$$\begin{aligned} \frac{\partial \mathbf{n}(w)}{\partial t} &= f[\mathbf{n}(w)] + \frac{\partial g[\mathbf{n}(w)]}{\partial w} \\ \frac{\partial \mathbf{n}(w)}{\partial t} - f[\mathbf{n}(w)] - \frac{\partial g[\mathbf{n}(w)]}{\partial w} &= 0 \end{aligned} \quad (8.47)$$

Note that the integral terms are lumped under $f[\mathbf{n}(w)]$.

8.4 Numerical Solution

As first shown in the crystallizer example of Chapter 4, the method for implementing the numerical solution follows the following steps:

1. Propose an approximate solution
2. Formulate an error expression

3. Minimize the error expression

This procedure essentially takes a set of partial differential equations (PDEs) governing a system and then converts this system to a set of ordinary differential equations. In general, if the approximate solution is written as $\mathbf{n}^*(w)$, then the error expression is the difference between the right and left sides of Equation (8.47):

$$R(w) = \frac{\partial \mathbf{n}^*(w)}{\partial t} - f[\mathbf{n}^*(w)] - \frac{\partial g[\mathbf{n}^*(w)]}{\partial w} \tag{8.48}$$

This function $R(w)$ is referred to as the residual or error function. In order to optimize the solution and ensure that the approximate solution $\mathbf{n}^*(w)$ matches the true solution as closely as possible, we seek to minimize this residual over the solution domain $w = (w_{min}, w_{max})$. Depending on the form chosen for the approximation, a number of different techniques may be employed to minimize the residual, including finite element, finite differences, and orthogonal collocation on finite elements (see Appendices A and B for more examples and discussion). Also, depending on the independent variable used for the spatial or size coordinate, w may be substituted for m, $\ln(m)$, etc. For the most general case, then, we write $R(\phi)$ to denote the system:

$$R(\phi) = \frac{\partial \mathbf{n}^*(\phi)}{\partial t} - f[\mathbf{n}^*(\phi)] - \frac{\partial g[\mathbf{n}^*(\phi)]}{\partial \phi} \tag{8.49}$$

and emphasize that ϕ can take on any one of a number of forms depending on the application and scaling of the independent variable.

For this particular implementation, the orthogonal collocation on finite elements method will be employed. This method proposes an approximate solution in the form of a cubic spline over a number of solution subdomains which are referred to as elements (see Figure 8-2).

8.4.1 Cubic spline representation for orthogonal collocation on finite elements

Orthogonal collocation on finite elements uses a series of polynomial representation functions over local element domains illustrated in Figure 8-2. Typically, the polynomials for orthogonal collocation on finite elements are represented by spline curves. When a cubic spline representation is chosen, $n(\phi)$ is fully determined by four coefficients active on each element i:

$$n(\phi) = f_i(\eta) = \alpha_{i,0} + \eta\alpha_{i,1} + \eta^2\alpha_{i,2} + \eta^3\alpha_{i,3} \tag{8.50}$$

Note that η is a local variable on each element and is equal to $\phi - \phi_i$ within element i. Two condi-

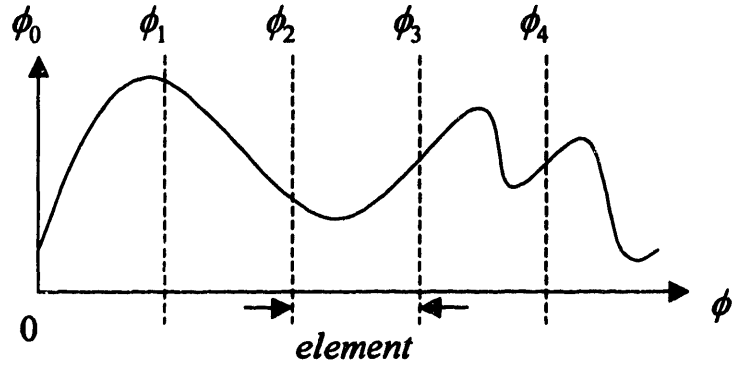

Figure 8-2: Element subdomains with a cubic spline fit over each element.

tions are imposed at the boundary of adjacent elements: 1) continuity, and 2) continuity of the first derivative. Continuity is an obvious requirement and continuity of the first derivative imposes continuity of particle flux due to growth between two elements, a necessary condition for any implementation which aspires to describe growth processes:

$$\text{Flux out of element } i \;=\; \text{Flux into element } i+1 \Leftrightarrow -G\frac{\partial n(\phi)}{\partial \phi}\bigg|_{\phi^-} = -G\frac{\partial n(\phi)}{\partial \phi}\bigg|_{\phi^+} \tag{8.51}$$

Using the notation from Equation (8.50), these continuity condition is:

$$\alpha_{i,0} + \eta\alpha_{i,1} + \eta^2\alpha_{i,2} + \eta^3\alpha_{i,3}\Big|_{\eta=1} = \alpha_{i+1,0} + \eta\alpha_{i+1,1} + \eta^2\alpha_{i+1,2} + \eta^3\alpha_{i+1,3}\Big|_{\eta=0} \tag{8.52}$$

which reduces to:

$$\boxed{\alpha_{i,0} + \alpha_{i,1} + \alpha_{i,2} + \alpha_{i,3} = \alpha_{i+1,0}} \tag{8.53}$$

In order to apply a continuity condition for the first derivative, we must apply the chain rule to the derivatives of each element:

$$\frac{dn(\phi)}{d\phi} = \frac{df_i(\eta)}{d\eta}\frac{d\eta}{d\phi} \tag{8.54}$$

where the function η on each element is a function of ϕ defined by:

$$\eta = \frac{\phi - \phi_{i-1}}{\phi_i - \phi_{i-1}} \tag{8.55}$$

and it follows that $d\eta/d\phi$ is the inverse element width:

$$\frac{d\eta}{d\phi} = \frac{1}{\phi_i - \phi_{i-1}} \tag{8.56}$$

As a result, equating the first derivative between two element requires that:

$$\left.\frac{df_i(\eta)}{d\eta}\frac{d\eta}{d\phi}\right|_{\eta=1} = \left.\frac{df_{i+1}(\eta)}{d\eta}\frac{d\eta}{d\phi}\right|_{\eta=0} \tag{8.57}$$

The derivatives for f_1 and f_{i+1} can be calculated from Equation (8.50):

$$\frac{df_i(\eta)}{d\eta} = \alpha_{i,1} + 2\eta\alpha_{i,2} + 3\eta^2\alpha_{i,3} \tag{8.58}$$

Substituting this expression and Equation (8.56) into Equation (8.57) yields the continuity expression for the derivatives at the element boundaries:

$$\begin{aligned}
\left.\frac{df_i(\eta)}{d\eta}\frac{1}{\phi_i - \phi_{i-1}}\right|_{\eta=1} &= \left.\frac{df_{i+1}(\eta)}{d\eta}\frac{1}{\phi_{i+1} - \phi_i}\right|_{\eta=0} \\
\left.\alpha_{i,1} + 2\eta\alpha_{i,2} + 3\eta^2\alpha_{i,3}\frac{1}{\phi_i - \phi_{i-1}}\right|_{\eta=1} &= \left.\alpha_{i+1,1} + 2\eta\alpha_{i+1,2} + 3\eta^2\alpha_{i+1,3}\frac{1}{\phi_{i+1} - \phi_i}\right|_{\eta=0} \\
\alpha_{i,1} + 2\alpha_{i,2} + 3\alpha_{i,3}\frac{1}{\phi_i - \phi_{i-1}} &= \alpha_{i+1,1}\frac{1}{\phi_{i+1} - \phi_i}
\end{aligned} \tag{8.59}$$

Isolating the element widths results in the final form of the derivative continuity constraint:

$$\boxed{\alpha_{i,1} + 2\alpha_{i,2} + 3\alpha_{i,3} = \frac{\phi_i - \phi_{i-1}}{\phi_{i+1} - \phi_i}\alpha_{i+1,1}} \tag{8.60}$$

Equations (8.53) and (8.60) determine two coefficients on each element. The remaining two coefficients must be determined by two more conditions on each element. These conditions are determined by the value of $n(m)$ at two node points η_k in each element:

$$n(\phi)_{i,k} = f_i(\eta_k) = \alpha_{i,0} + \eta_k\alpha_{i,1} + \eta_k^2\alpha_{i,2} + \eta_k^3\alpha_{i,3} \qquad k = 1, 2 \tag{8.61}$$

First, the continuity restraint from Equation (8.53) can be solved for the coefficient $\alpha_{i,2}$:

$$\alpha_{i,2} = \alpha_{i+1,0} - \alpha_{i,0} - \alpha_{i,1} - \alpha_{i,3} \tag{8.62}$$

which is then substituted into Equation (8.61):

$$\begin{aligned} n(\phi)_{i,k} &= \alpha_{i,0} + \eta_k \alpha_{i,1} + \eta_k^2(\alpha_{i+1,0} - \alpha_{i,0} - \alpha_{i,1} - \alpha_{i,3}) + \eta_k^3 \alpha_{i,3} \\ &= (1-\eta_k^2)\alpha_{i,0} + (\eta_k - \eta_k^2)\alpha_{i,1} + \eta_k^2 \alpha_{i+1,0} + (\eta_k^3 - \eta_k^2)\alpha_{i,3} \end{aligned} \tag{8.63}$$

In order to reduce this expression to contain just the first two coefficients for the two adjacent elements i and $i + 1$, an expression is needed for $\alpha_{i,3}$. This expression is obtained by solving Equations (8.53) and (8.60) for the coefficient $\alpha_{i,3}$ while eliminating $\alpha_{i,2}$. Multiplying Equation (8.53) by 2 and subtracting from Equation (8.60) yields the desired result:

$$\begin{aligned} \alpha_{i,1} + 2\alpha_{i,2} + 3\alpha_{i,3} &= \frac{\phi_i - \phi_{i-1}}{\phi_{i+1} - \phi_i}\alpha_{i+1,1} \\ \underline{-2(\alpha_{i,0} + \alpha_{i,1} + \alpha_{i,2} + \alpha_{i,3}) &= -2\alpha_{i+1,0}} \\ -2\alpha_{i,0} - \alpha_{i,1} + \alpha_{i,3} &= -2\alpha_{i+1,0} + \frac{\phi_i - \phi_{i-1}}{\phi_{i+1} - \phi_i}\alpha_{i+1,1} \\ \alpha_{i,3} &= 2\alpha_{i,0} + \alpha_{i,1} - 2\alpha_{i+1,0} + \frac{\phi_i - \phi_{i-1}}{\phi_{i+1} - \phi_i}\alpha_{i+1,1} \end{aligned} \tag{8.64}$$

Finally, substituting this expression into Equation (8.63) results in the final expression:

$$\begin{aligned} n(\phi)_{i,k} &= (1 - 3\eta_k^2 + 2\eta_k^3)\alpha_{i,0} + (\eta_k - 2\eta_k^2 + \eta_k^3)\alpha_{i,1} \\ &\quad + (3\eta_k^2 - 2\eta_k^3)\alpha_{i+1,0} + \frac{\phi_i - \phi_{i-1}}{\phi_{i+1} - \phi_i}(\eta_k^3 - \eta_k^2)\alpha_{1+i,1} \end{aligned} \tag{8.65}$$

Thus for a system with N elements, there are $4 \cdot N$ unknown coefficients. These coefficients are specified by $2 \cdot (N - 1)$ conditions imposed by Equation (8.53) at the boundary between elements, and $2 \cdot N$ more conditions imposed by Equation (8.61). The remaining two degrees of freedom are specified by the boundary conditions. For all of the elements i except the last, this system of equations is therefore given by the following general formula:

$$\begin{aligned} n(\phi)_{i,k} &= (1 - 3\eta_k^2 + 2\eta_k^3)\alpha_{i,0} + (\eta_k - 2\eta_k^2 + \eta_k^3)\alpha_{i,1} \\ &\quad + (3\eta_k^2 - 2\eta_k^3)\alpha_{i+1,0} + \frac{\phi_i - \phi_{i-1}}{\phi_{i+1} - \phi_i}(\eta_k^3 - \eta_k^2)\alpha_{1+i,1} \end{aligned} \qquad \begin{aligned} i &= 2, \ldots, N-1 \quad & k &= 1, 2 \\ i &= 1 & k &= 0, 1, 2 \end{aligned} \tag{8.66}$$

where the node points η_k are placed at the roots of the second order shifted Legendre polynomial on the interval $(0, \phi_i - \phi_{i-1}) = (0, w_i)$ corresponding to the width of the each element. This placement of collocation points minimizes the error in the solution and provides the optimal coefficients for the cubic spline representation (Villadsen and Michelsen, 1978; Finlayson, 1972).

Table 8-3 gives the location of node points for a cubic spline on each element. The points $k = 0$ in the first element and $k = N$ in the last element are placed at the edges of the system boundary and serve as implementation points for the boundary conditions.

Table 8-3: Collocation Point Placement

k	η_k
0	0
1	$\frac{1}{2}-\frac{1}{\sqrt{12}}\approx 0.211$
2	$\frac{1}{2}+\frac{1}{\sqrt{12}}\approx 0.789$
3	1

The optimal solution given by the orthogonal collocation on finite elements method can be understood by analyzing the error, or residual R in the solution of the differential equation:

$$R(w) = \frac{\partial \mathbf{n}(w)}{\partial t} - f[\mathbf{n}(w)] - \frac{\partial g[\mathbf{n}(w)]}{\partial w} \tag{8.67}$$

The cumulative error over the domain of interest (a, b) is represented as:

$$\text{Error} = \int_a^b R(w)dw \tag{8.68}$$

Using a method known as Gaussian quadrature (Stoer and Bulirisch, 1980) this integral can be calculated exactly using a weighted sum of $R(w)$ at specific points w_i - referred to as *collocation points* - located at the roots of the corresponding orthogonal polynomial for the system (see Table 8-3):

$$\text{Error} = \int_a^b R(w)dw = \sum_i R(w_i)w_i \tag{8.69}$$

The error can then be minimized by forcing it to zero. This simply requires that $R(w_i) = 0$ for all node points w_i, and is equivalent to requiring that the PDE given in Equation (8.67) is satisfied at each node point in the system. The new system of ODEs now takes the form:

$$\begin{aligned}
\frac{dn(w_j)}{dt} &= f[n(\mathbf{w})]\big|_{m=m_j} + \frac{d}{dw}(g[n(\mathbf{w})])\big|_{m=m_j} \qquad \forall j = 1\ldots 2N+2 \\
\frac{dn(w_j)x_{i,0}(w_j)}{dt} &= f_0[n(\mathbf{w}), x_{i,0}(\mathbf{w}), x_{i,1}(\mathbf{w})]\big|_{m=m_j} \qquad \forall j = 1\ldots 2N+2 \\
&\quad + \frac{d}{dw}g_0[n(\mathbf{w}), x_{i,0}(\mathbf{w}), x_{i,1}(\mathbf{w})]\big|_{m=m_j} \\
\frac{dn(w_j)x_{i,1}(w_j)}{dt} &= f_1[n(\mathbf{w}), x_{i,0}(\mathbf{w}), x_{i,1}(\mathbf{w})]\big|_{m=m_j} \qquad \forall j = 1\ldots 2N+2 \\
&\quad + \frac{d}{dw}g_1[n(\mathbf{w}), x_{i,0}(\mathbf{w}), x_{i,1}(\mathbf{w})]\big|_{m=m_j}
\end{aligned} \tag{8.70}$$

where the $n(w_j)$ and its associated products with the compositions $x_{i,0}(w_j)$ and $x_{i,1}(w_j)$ are the elements of the state vector. Note that the each line of Equation (8.70) represents a series of equations describing the evolution of $n(w_j)$, $n(w_j) \cdot x_{i,0}(w_j)$, and $n(w_j) \cdot x_{i,1}(w_j)$, respectively, at the node points $j = 1, 2, \ldots, 2 \cdot N + 2$ where N is the number of elements in the solution domain.

Using the Equation (8.66), it is possible to write a matrix expression relating the node point values $n(w_i)$ to the coefficients $\alpha_{i,0}$ and $\alpha_{i,1}$ for $i = 1, 2, \ldots, 2 \cdot N + 2$. Using the general notation of ϕ for w:

$$\mathbf{n}(\phi) = \mathbf{A} \cdot \alpha \tag{8.71}$$

where the **A** matrix is given in Equation (8.72).

$$\mathbf{A} = \begin{bmatrix}
(1-3\eta_0^2+2\eta_0^3) & (\eta_0-2\eta_0^2+\eta_0^3) & (3\eta_0^2-2\eta_0^3) & \frac{\Delta\phi_1}{\Delta\phi_2}(\eta_0^3-\eta_0^2) & & & & & \\
(1-3\eta_1^2+2\eta_1^3) & (\eta_1-2\eta_1^2+\eta_1^3) & (3\eta_1^2-2\eta_1^3) & \frac{\Delta\phi_1}{\Delta\phi_2}(\eta_1^3-\eta_1^2) & & & & & \\
(1-3\eta_2^2+2\eta_2^3) & (\eta_2-2\eta_2^2+\eta_2^3) & (3\eta_2^2-2\eta_2^3) & \frac{\Delta\phi_1}{\Delta\phi_2}(\eta_2^3-\eta_2^2) & & & & & \\
 & & (1-3\eta_1^2+2\eta_1^3) & (\eta_1-2\eta_1^2+\eta_1^3) & (3\eta_1^2-2\eta_1^3) & \frac{\Delta\phi_i}{\Delta\phi_{i+1}}(\eta_1^3-\eta_1^2) & & & \\
 & & (1-3\eta_2^2+2\eta_2^3) & (\eta_2-2\eta_2^2+\eta_2^3) & (3\eta_2^2-2\eta_2^3) & \frac{\Delta\phi_i}{\Delta\phi_{i+1}}(\eta_2^3-\eta_2^2) & & & \\
 & & & \ddots & \ddots & \ddots & & & \\
 & & & & (1-3\eta_2^2+2\eta_2^3) & (\eta_2-2\eta_2^2+\eta_2^3) & (3\eta_2^2-2\eta_2^3) & \frac{\Delta\phi_{N-1}}{\Delta\phi_N}(\eta_2^3-\eta_2^2) & \\
 & & & & & & 1 & \eta_1 & \eta_1^2 \quad \eta_1^3 \\
 & & & & & & 1 & \eta_2 & \eta_2^2 \quad \eta_2^3 \\
 & & & & & & 1 & \eta_3 & \eta_3^2 \quad \eta_3^3
\end{bmatrix} \tag{8.72}$$

For the sake of brevity, $\Delta\phi_i$ has been substituted for the ratio of element widths:

$$\frac{\Delta\phi_i}{\Delta\phi_{i+1}} = \frac{\phi_i - \phi_{i-1}}{\phi_{i+1} - \phi_i} \tag{8.73}$$

Likewise, the first two coefficients of each cubic spline function can be recovered using the values at the node points and the inverse of the **A** matrix:

$$\alpha = \mathbf{A}^{-1} \cdot \mathbf{n}(\phi) \tag{8.74}$$

and the remaining two coefficients can easily be solved using Equation (8.53). Because all position-dependent expressions are isolated in the **A** matrix, the first and second derivatives with respect to ϕ can be found by differentiating individual terms in the **A** matrix:

$$\begin{aligned} \frac{\partial \mathbf{n}(\phi)}{\partial \phi} &= \frac{\partial \mathbf{A}}{\partial \phi} \cdot \alpha = \mathbf{B} \cdot \alpha \\ \frac{\partial^2}{\partial \phi^2}\mathbf{n}(\phi) &= \frac{\partial^2}{\partial \phi^2}\mathbf{A} \cdot \alpha = \mathbf{C} \cdot \alpha \end{aligned} \tag{8.75}$$

Re-substituting the second relationship into Equation (2) yields two matrices, $\mathbf{B} \cdot \mathbf{A}^{-1}$ and $\mathbf{C} \cdot \mathbf{A}^{-1}$ which act as first and second derivative linear operators. These operators are convenient in evaluating derivatives such as those common in growth terms.

$$\begin{aligned} \frac{\partial \mathbf{n}(\phi)}{\partial \phi} &= \mathbf{B} \cdot \alpha = \mathbf{B}\mathbf{A}^{-1}\mathbf{n}(\phi) \\ \frac{\partial^2}{\partial \phi^2}\mathbf{n}(\phi) &= \mathbf{C} \cdot \alpha = \mathbf{C}\mathbf{A}^{-1}\mathbf{n}(\phi) \end{aligned} \tag{8.76}$$

Equations (8.77) and (8.78) illustrate these matrix representations in full.

$$\mathbf{n}(\phi) = \begin{bmatrix} n(\phi)_{1,0} \\ n(\phi)_{1,1} \\ n(\phi)_{1,2} \\ \vdots \\ \vdots \\ n(\phi)_{i,1} \\ n(\phi)_{i,2} \\ n(\phi)_{i+1,1} \\ n(\phi)_{i+1,2} \\ \vdots \\ n(\phi)_{N,1} \\ n(\phi)_{N,2} \\ n(\phi)_{N,3} \end{bmatrix} \qquad \alpha = \begin{bmatrix} \alpha_{1,0} \\ \alpha_{1,1} \\ \alpha_{2,0} \\ \alpha_{2,1} \\ \\ \alpha_{i,0} \\ \alpha_{i,1} \\ \alpha_{i+1,0} \\ \alpha_{i+1,1} \\ \vdots \\ \alpha_{N,0} \\ \alpha_{N,1} \\ \alpha_{N,2} \\ \alpha_{N,3} \end{bmatrix} \tag{8.77}$$

$$\mathbf{B}=\begin{bmatrix}
\frac{(-6\eta_0+6\eta_0^2)}{\Delta\phi_1} & \frac{(1-4\eta_0+3\eta_0^2)}{\Delta\phi_1} & \frac{(6\eta_0-6\eta_0^2)}{\Delta\phi_1} & \frac{1}{\Delta\phi_2}(3\eta_0^2-2\eta_0) & & & & & & \\
\frac{(-6\eta_1+6\eta_1^2)}{\Delta\phi_1} & \frac{(1-4\eta_1+3\eta_1^2)}{\Delta\phi_1} & \frac{(6\eta_1-6\eta_1^2)}{\Delta\phi_1} & \frac{1}{\Delta\phi_2}(3\eta_1^2-2\eta_1) & & & & & & \\
\frac{(-6\eta_2+6\eta_2^2)}{\Delta\phi_1} & \frac{(1-4\eta_2+3\eta_2^2)}{\Delta\phi_1} & \frac{(6\eta_2-6\eta_2^2)}{\Delta\phi_1} & \frac{1}{\Delta\phi_2}(3\eta_2^2-2\eta_2) & & & & & & \\
 & & \frac{(-6\eta_1+6\eta_1^2)}{\Delta\phi_i} & \frac{(1-4\eta_1+3\eta_1^2)}{\Delta\phi_i} & \frac{(6\eta_1-6\eta_1^2)}{\Delta\phi_i} & \frac{1}{\Delta\phi_{i+1}}(3\eta_1^2-2\eta_1) & & & & \\
 & & \frac{(-6\eta_2+6\eta_2^2)}{\Delta\phi_i} & \frac{(1-4\eta_2+3\eta_2^2)}{\Delta\phi_i} & \frac{(6\eta_2-6\eta_2^2)}{\Delta\phi_i} & \frac{1}{\Delta\phi_{i+1}}(3\eta_2^2-2\eta_2) & & & & \\
 & & & \ddots & \ddots & \ddots & & & & \\
 & & & & \frac{(-6\eta_2+6\eta_2^2)}{\Delta\phi_{N-1}} & \frac{(1-4\eta_2+3\eta_2^2)}{\Delta\phi_{N-1}} & \frac{(6\eta_2-6\eta_2^2)}{\Delta\phi_{N-1}} & \frac{1}{\Delta\phi_N}(3\eta_2^2-2\eta_2) & & \\
 & & & & & & 0 & \frac{1}{\Delta\phi_N} & \frac{2\eta_1}{\Delta\phi_N} & \frac{3\eta_1^2}{\Delta\phi_N} \\
 & & & & & & 0 & \frac{1}{\Delta\phi_N} & \frac{2\eta_2}{\Delta\phi_N} & \frac{3\eta_2^2}{\Delta\phi_N} \\
 & & & & & & 0 & \frac{1}{\Delta\phi_N} & \frac{2\eta_3}{\Delta\phi_N} & \frac{3\eta_3^2}{\Delta\phi_N}
\end{bmatrix} \tag{8.78}$$

$$\mathbf{C}=\begin{bmatrix}
\frac{(-6+12\eta_0)}{\Delta\phi_1^2} & \frac{(-4+6\eta_0)}{\Delta\phi_1^2} & \frac{(6\eta_0-6\eta_0^2)}{\Delta\phi_1^2} & \frac{(6\eta_0-2)}{\Delta\phi_1\Delta\phi_2} & & & & & & \\
\frac{(-6+12\eta_1)}{\Delta\phi_1^2} & \frac{(-4+6\eta_1)}{\Delta\phi_1^2} & \frac{(6\eta_1-6\eta_1^2)}{\Delta\phi_1^2} & \frac{(6\eta_1-2)}{\Delta\phi_1\Delta\phi_2} & & & & & & \\
\frac{(-6+12\eta_2)}{\Delta\phi_1^2} & \frac{(-4+6\eta_2)}{\Delta\phi_1^2} & \frac{(6\eta_2-6\eta_2^2)}{\Delta\phi_1^2} & \frac{(6\eta_2-2)}{\Delta\phi_1\Delta\phi_2} & & & & & & \\
 & & \frac{(-6+12\eta_1)}{\Delta\phi_i^2} & \frac{(-4+6\eta_1)}{\Delta\phi_i^2} & \frac{(6\eta_1-6\eta_1^2)}{\Delta\phi_i^2} & \frac{(6\eta_1-2)}{\Delta\phi_i\Delta\phi_{i+1}} & & & & \\
 & & \frac{(-6+12\eta_2)}{\Delta\phi_i^2} & \frac{(-4+6\eta_2)}{\Delta\phi_i^2} & \frac{(6\eta_2-6\eta_2^2)}{\Delta\phi_i^2} & \frac{(6\eta_2-2)}{\Delta\phi_i\Delta\phi_{i+1}} & & & & \\
 & & & \ddots & \ddots & \ddots & & & & \\
 & & & & \frac{(-6+12\eta_2)}{\Delta\phi_{N-1}^2} & \frac{(-4+6\eta_2)}{\Delta\phi_{N-1}^2} & \frac{(6\eta_2-6\eta_2^2)}{\Delta\phi_{N-1}^2} & \frac{(6\eta_2-2)}{\Delta\phi_{N-1}\Delta\phi_N} & & \\
 & & & & & & 0 & 0 & \frac{2}{\Delta\phi_N^2} & \frac{6\eta_1}{\Delta\phi_N^2} \\
 & & & & & & 0 & 0 & \frac{2}{\Delta\phi_N^2} & \frac{6\eta_2}{\Delta\phi_N^2} \\
 & & & & & & 0 & 0 & \frac{2}{\Delta\phi_N^2} & \frac{6\eta_3}{\Delta\phi_N^2}
\end{bmatrix} \tag{8.79}$$

Note that this method provides a compact representation for imbedding the calculations for the cubic splines and its derivatives in a matrix which does not vary with time. This provides for fast and easy interpolation between the nodepoints and derivative calculations, operations which are necessary for the calculation of coagulation and growth terms, respectively.

8.5 Results

Using the method of orthogonal collocation on finite elements, the equations for coagulation and growth were written out at each node point as shown in the previous section. This system of differential equations was then numerically integrated using a Runge-Kutta timestep algorithm.

8.5.1 Coagulation only

As a start, the solution was tested for coagulation only with a constant coagulation kernel. Figure 8-3 compares the overall number density results to the analytical solution, starting from a two-component exponential distribution as the initial condition.

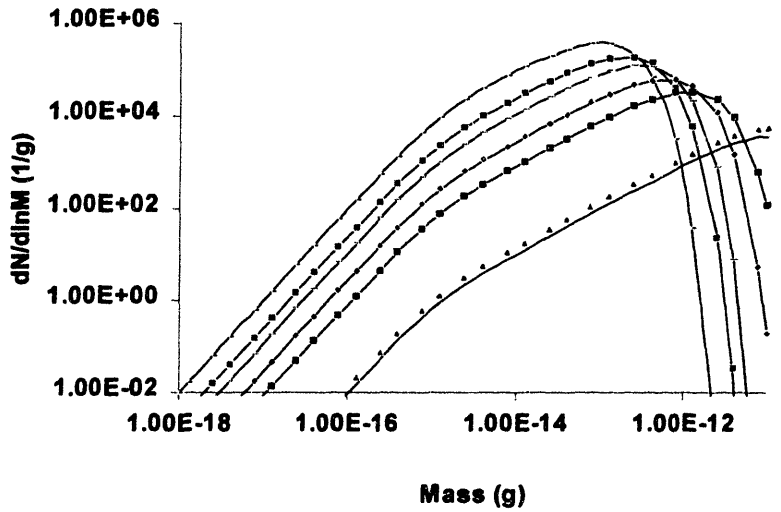

Figure 8-3: Comparison of analytical and two-component number density results.

The parameter values used in this calculation are given in Table 8-4.

Table 8-4: Parameter values

Symbol	*Value*	*Units*
N_0	10^6	cm^{-3}
β_0	10^{-7}	cm^3/s
m_{10}	10^{-16}	g
m_{10}	10^{-18}	g

The results for composition are shown in Figure 8-4. The solution for both $n(m)$ and the mole

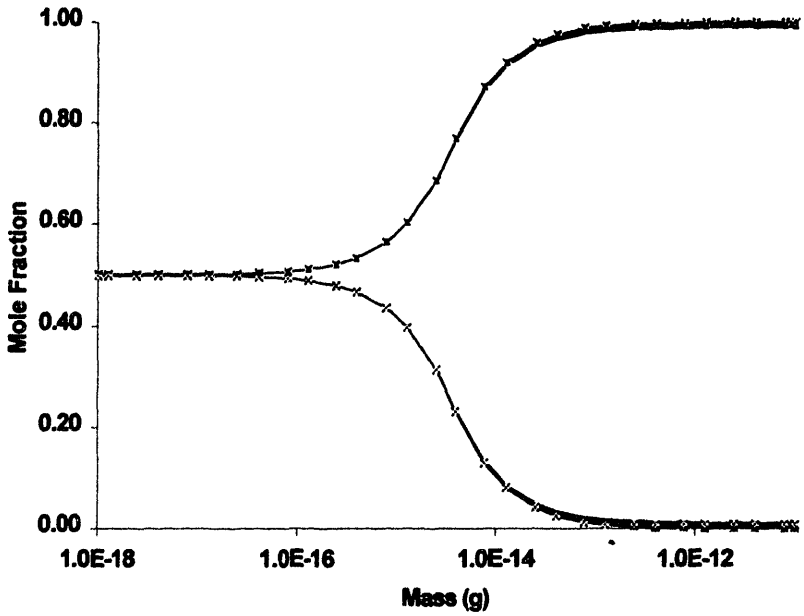

Figure 8-4: Mole fraction comparison of analytical and numerical results for two-component system.

fraction closely match the analytical results, indicating that the first-order Wiener expansion is a reasonable approximation for this particular problem.

Note that because the analytical solution given in Chapter 7 is given in terms of $n(m_1, m_2)$, the number density distribution must be converted to $n(m)$ and the mean mole fractions must be calculated in order to compare with the experimental results. Appendix H presents the full method used for deriving the transformed results.

8.5.2 Growth only

Because the rescaled growth rate is constant, it is trivial to test the overall number density solution for growth in the one-component case. For the growth rate law:

$$G(m) = \gamma m \tag{8.80}$$

where $\gamma = \ln(m_{max}/m_{min})$, the growth-only solution was calculated for an initially lognormal distribution. The numerical and analytical results for this system are compared in Figure 8-5,

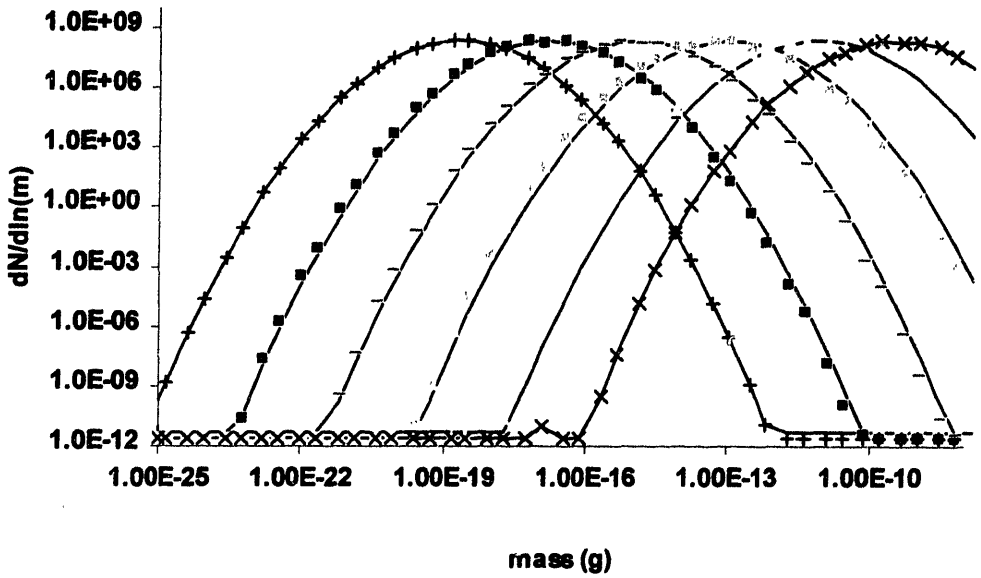

Figure 8-5: Single-component solution for a lognormal initial distribution with growth rate law $G(m) = \gamma \cdot m$.

which shows very good agreement. For more detailed comparison and analysis of multicomponent results, please refer to Resch (1995).

References

[1] Finlayson, Bruce A. *The Method of Weighted Residuals and Variational Principles, with Application in Fluid Mechanics, Heat and Mass Transfer*, Academic Press, 1972.

[2] Resch, Timothy J. *A Framework for the Modeling of Suspended Multicomponent Particulate Systems with Applications to Atmospheric Aerosols,* Ph.D. Thesis, Massachusetts Institute of Technology, 1995.

[3] Stoer, J.; Bulirisch, R. *Introduction to Numerical Analysis,* 2nd edition, translated by R. Bartels, W. Gautschi, and C. Witzgall, Springer-Verlag, 1993.

[4] Villadsen, John; Michelsen, Michael L. *Solution of Differential Equation Models by Polynomial Approximation,* Prentice-Hall, 1978.

Chapter 9: Aerosol Mass Spectrometer Experimental System

A novel measurement system has been developed by Aerodyne Research, Inc. to simultaneously measure aerosol size and composition (Jayne et al., 2000).

9.1 Experimental System

The experimental system consists of a heated bath, injector, and flow tube, as depicted in Figure 9-1.

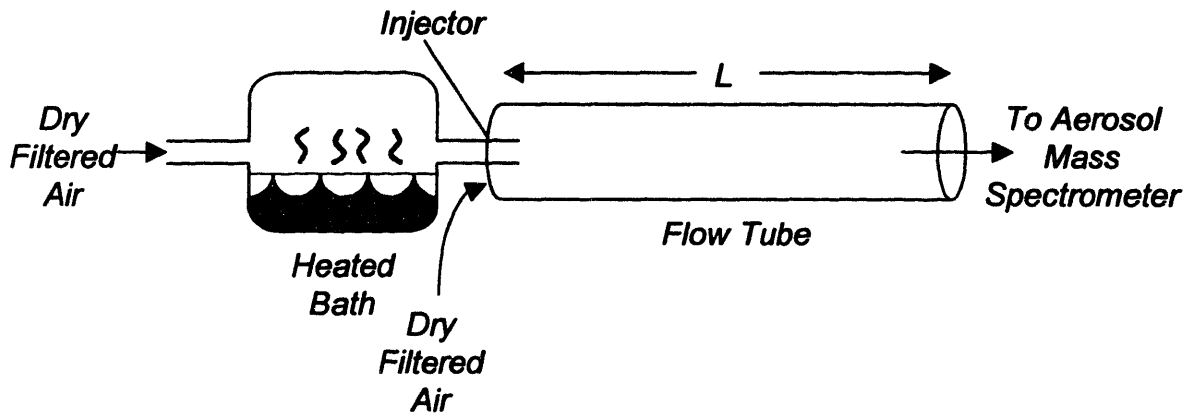

Figure 9-1: Laminar flow through a cylinder with constant wall temperature T_w and uniform initial temperature T_0.

Dry, filtered air enters the heated bath where it absorbs vapor from the heated liquid. The air then exits the heated bath and flows through an injector into a flow tube. The air from the injector is introduced into the center of a laminar flow at a flowrate which matches the average laminar flowrate over the injector cross-section, as shown in Figure 9-2. The gas from the injector then

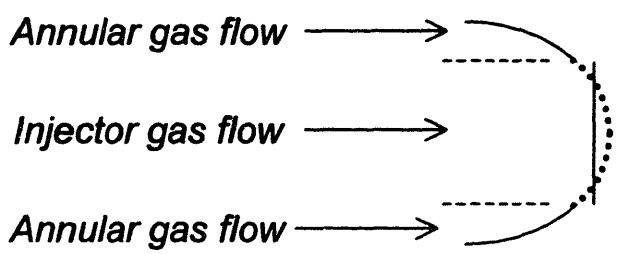

Figure 9-2: Matching of injector gas flowrate with average laminar flowrate over injected cross-section.

cools as it passes through the flow tube, undergoing nucleation, growth, coagulation, and diffusion. The injected gas is assumed to quickly take on a laminar flow profile without significant mixing with the annular gas flow. Upon exiting the flow tube, a sample from the central injected flow region is withdrawn for sampling by the aerosol mass spectrometer. Table 9-1 summarizes some of the base case operating parameters for the experimental system.

Table 9-1: Summary of parameters for experimental flow tube system.

Symbol	*Definition*	*Value*	*Units*
L	flow tube length	25	cm
D	flow tube diameter	2.5	cm
D_0	injector diameter	1.1	cm
v_T	total flowrate	14.8	cm^3/s
v_I	injector flowrate	3.7	cm^3/s
t_f	flow time through tube	3.0	s
u	superficial velocity	8.3	cm/s

For this analysis, the bath will be treated as containing pure H_2SO_4 at a temperature of 137°C.

9.2 Scale Analysis

A number of different physical processes may act on the injected stream of H_2SO_4 after it enters the flow tube. As the gas progresses down the flow tube toward the aerosol mass spectrometer inlet, it cools down. This causes the gas phase H_2SO_4 to nucleate into small particles which can then grow and/or coagulate with other particles. The H_2SO_4 vapor will also diffuse out of the center injected flow region out towards the flow tube wall. Some of the H_2SO_4 particles will also migrate out toward the flow tube wall due to Brownian diffusion. The following scale analysis compares the magnitude of these processes.

9.2.1 Loss of H_2SO_4 due to flow tube wall deposition

One potential sink of gas phase H_2SO_4 is the molecular diffusion from the center injection region out to the flow tube wall, as illustrated in Figure 9-3.

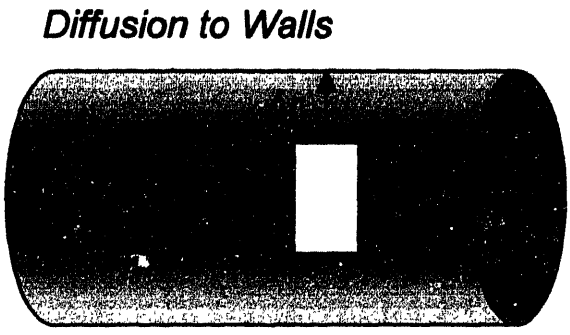

Figure 9-3: Diffusion of gas phase H_2SO_4 in the flow tube. H_2SO_4 vapor diffuses from the central flow of injected gas from the heated bath to the walls.

Gas which diffuses to the wall is assumed to be deposited on the wall and removed from the gas phase. The gaseous phase H_2SO_4 concentration at the wall is assumed to be zero. The concentration in the central flow will be highest when the gas is first injected into the flow tube. The gas which exits the bath through the injector is assumed to be saturated with the liquid H_2SO_4 in the bath; its vapor pressure is given by the Antoine equation (Reid, Prausnitz, and Poling, 1987).

$$\ln(P_{vp}) = K_1 - \frac{K_2}{T + K_3} \tag{9.1}$$

The concentration of H_2SO_4 then follows directly from the ideal gas law.

$$C = \frac{P_{vp} W}{RT} \tag{9.2}$$

Table 9-2 summarizes the data used in the Antoine equation and subsequent conversion to concentration, as measured experimentally in the H_2SO_4 bath (note that P_{vp} needs to be converted

from N/m^2 to N/cm^2 for use in the concentration equation). In order to determine the time scale

Table 9-2: Parameters for calculation of gas phase H_2SO_4 concentration

Symbol	*Definition*	*Value*	*Units*
K_1	1st Antoine equation parameter	32.21	-
K_2	2nd Antoine equation parameter	11709.73	K
K_3	3rd Antoine equation parameter	17.98	K
T	temperature	410	K
P_{vp}	vapor pressure	127.11	N/m^2
W	molecular weight	98.07	g/mol
R	ideal gas constant	831.4	N·cm/mol/K
T	temperature	410	K
C	concentration	3.66×10^{-6}	g/cm^3

(Deen, 1998) of diffusion, the ranges of each appropriate variable in the system are substituted into the governing equation for radial diffusion:

$$\frac{\partial C}{\partial t} = \frac{1}{r}\frac{\partial}{\partial r}\left(Dr\frac{\partial C}{\partial r}\right) \tag{9.3}$$

which will result in a number of expressions ΔC, Δt, Δr, D:

$$\frac{\Delta C}{\Delta t} = \frac{1}{r}\frac{1}{\Delta r}\left(Dr\frac{\Delta C}{\Delta r}\right) \tag{9.4}$$

Table 9-3 summarizes the basis for calculating the values in Equation (9.4).

Table 9-3: Calculation of characteristic ranges for radial diffusion

Symbol	*Maximum Value*	*Minimum Value*	Δ	*Units*
C	3.66×10^{-6}	0	3.66×10^{-6}	g/cm^3
r	1.25	0.55	0.7	cm
t	τ	0	τ	s

Using the fact that the $\Delta t = \tau$, it is possible to solve Equation (9.4) and produce a generic expression for the characteristic radial diffusion time.

$$\frac{\Delta C}{\Delta t} = \frac{1}{r}\frac{1}{\Delta r}\left(Dr\frac{\Delta C}{\Delta r}\right)$$

$$\frac{\Delta C}{\tau} = \frac{1}{r}\frac{1}{\Delta r}\left(Dr\frac{\Delta C}{\Delta r}\right) \qquad (9.5)$$

$$\tau = \frac{(\Delta r)^2}{D}$$

The diffusivity of H_2SO_4 is determined from a set of experimental results in a similar system (Pöschl et al., 1998) where the diffusivity of H_2SO_4 through N_2 gas was determined as a function of total system pressure.

$$D = \frac{D_p}{P} \qquad D_p = 66.8 \text{ torr } \frac{cm^2}{s} \qquad (9.6)$$

Assuming that the diffusivity of H_2SO_4 through dry air is similar to the diffusivity through nitrogen gas, the diffusivity of H_2SO_4 can be calculated using Equation (9.6) and the fact that the experimental system is at atmospheric pressure, 760 torr.

$$D = \frac{66.8 \text{ torr } \frac{cm^2}{s}}{760 \text{ torr}} \qquad (9.7)$$

$$D = 0.0879\frac{cm^2}{s}$$

Substituting the appropriate values into Equation (9.5) and solving for τ yields the characteristic diffusion time.

$$\tau = \frac{0.7^2}{0.0879}$$
$$\tau = 5.57 \text{ s} \tag{9.8}$$

Thus a first order estimate would assume exponential decay of concentration in the central flow region with a decay constant of τ. Because the residence time in the flow tube is 3.0 s, we have:

$$\frac{C}{C_0} = e^{-t/\tau} = e^{-3.0/5.57}$$
$$\frac{C}{C_0} = 0.58 \tag{9.9}$$

where C_0 represents the initial concentration of a gas packet entering the flow tube and C represents its concentration at time t. Under the current system, approximately 58% of the entering H_2SO_4 vapor will remain when the gas exits the flow tube. However, the following sections will reveal that this is an upper limit for H_2SO_4 vapor deposition. In fact, H_2SO_4 is also usurped by nucleation and growth, reducing the total fraction of H_2SO_4 deposited on the flow tube walls.

9.2.2 Loss of particles due to flow tube wall deposition

The flow tube wall also acts as a particle sink due to diffusion from the central flow region to the walls, where the particles are deposited. According to Friedlander (2000), the diffusivity of particles in a gas is described by the set of relations in Equation (9.10).

$$D = \frac{kT}{f}$$
$$f = \frac{3\pi\mu D_p}{K} \tag{9.10}$$
$$\kappa = 1 + \frac{2\lambda}{D_p}\left[A_1 + A_2 \exp\left(\frac{-A_3 D_p}{\lambda}\right)\right]$$

where λ represents the mean free path of air as given in Atkins (1994).

$$\lambda = \frac{kT}{\sqrt{2}\sigma P} \tag{9.11}$$

The third expression in Equating (9.10) represents a slip correction factor. Substituting into Equation (9.5) produces the characteristic particle diffusion time as a function of particle diameter, temperature, and gas viscosity.

$$\tau = \frac{(\Delta r)^2 3\pi\mu D_p}{kT\kappa} \tag{9.12}$$

Using a 2nd order polynomial fit to interpolate air viscosity data from Incroprera and DeWitt (1996) in addition to the parameters for Equation (9.10) given in Friedlander (2000), the variables used to calculate the characteristic diffusion time can be summarized as in Table 9-4.

Table 9-4: Summary of parameters for calculating particle diffusivity

Symbol	*Definition*	*Value*	*Units*
Δr	distance from central flow region to wall	0.7	cm
k	Boltzmann constant	1.38×10^{-21}	$\frac{N \cdot cm}{K}$
T	temperature	410	K
λ	mean free path of air	$\frac{kT}{\sqrt{2}\sigma P}$	cm
σ	collision cross-section of air	4.24×10^{-19}	m^2
P	atmospheric pressure	101,325	$\frac{N}{m^2}$
μ	viscosity of air	2.35×10^{-9}	$\frac{N \cdot s}{cm^2}$
D_p	particle diameter	*varies*	cm
A_1	1st slip correction factor coefficient	1.257	-
A_2	2nd slip correction factor coefficient	0.4	-
A_3	3rd slip correction factor coefficient	0.55	-

Note: the collision cross-section of air was obtained by taking a composition average of the cross-sections of N_2 and O_2 (4.0×10^{-19} m^2 and 4.3×10^{-19} m^2), respectively:

$$\sigma = 0.79\sigma_{N_2} + 0.21\sigma_{O_2} \tag{9.13}$$

Figure 9-4 plots n/n_0, the fraction of original particles remaining in the central flow region after 3.0 s in the flow tube..

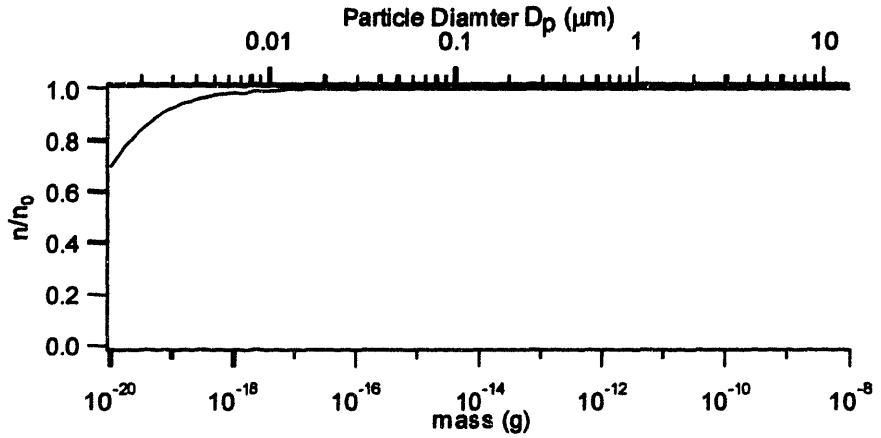

Figure 9-4: Fraction of original particles remaining in the central flow after 3.0 s in the flow tube.

The largest particles diffuse slower than the smaller particles, explaining why the vast majority of the larger particles are not deposited on the flow tube wall. Figure 9-5 plots diffusivity as a function of particle size.

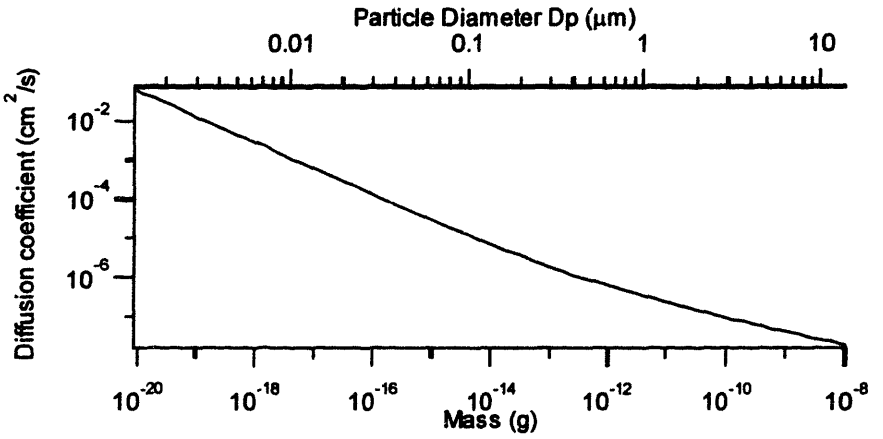

Figure 9-5: Particle diffusivity due to Brownian motion as a function of particle size.

9.3 Temperature Profile - Graetz Problem

It is possible to solve for the temperature profile in the flow tube using theoretical results for the temperature profile of a fluid under laminar flow in a circular tube with constant wall temperature, as shown in Figure 9-6.

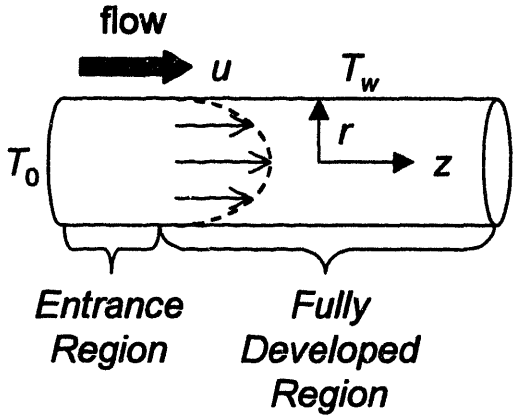

Figure 9-6: Laminar flow through a cylinder with constant wall temperature T_w and uniform initial temperature T_0.

In general, there are two important temperature profile regions in any laminar flow heat transfer problem in a cylinder: the entrance region and the fully developed region. For a fully developed flow, the Nusselt number is constant and directly relates the heat transfer coefficient, fluid conductivity, and diameter. For cylinders with a constant wall temperature T_w, this correlation takes the following form (Incropera and DeWitt, 1996):

$$Nu = \frac{hD}{k} = 3.66 \tag{9.14}$$

The length of the entrance region for these is given by the following set of relations:

$$Re = \frac{\rho u_0 D}{\mu}$$
$$\frac{\left(\frac{z}{D}\right)}{Re \cdot Pr} = Gz^{-1} = 0.05 \tag{9.15}$$

where Gz is the Graetz number. Note that the density refers to the density of air, and is calculated by an expression very similar to Equation (9.2).

$$\rho = \frac{PW}{RT} \tag{9.16}$$

Table 9-5 summarizes the parameters used in calculating the density of air. The molecular weight of air was calculated assuming that the composition of air consists of 78 mol% N_2, 21 mol% O_2,

and 1 mol% Ar.

Table 9-5: Data for calculation of the density of air

Symbol	*Description*	*Value*	*Units*
P	ambient pressure	10.13	Nc/m^2
W	molecular weight of air	28.59	g/mol
R	ideal gas constant	831.4	N·cm/mol/K
T	temperature	410	K
ρ	density	8.50×10^{-4}	g/cm^3

Table 9-6 summarizes the values of the parameters to be used in the calculation of the entrance length. Note that the Prandtl number, *Pr*, was linearly interpolated for air from data in Incropera and DeWitt (1996).

Table 9-6: Parameters used in calculating the length of the entrance region

Symbol	*Description*	*Value*	*Units*
ρ	density	8.50×10^{-4}	g/cm^3
u_0	superficial velocity	8.33	cm/s
D	diameter	2.5	cm
μ	viscosity	2.35×10^{-4}	$\frac{g}{cm \cdot s}$
Re	Reynolds number	75.3	-
Pr	Prandtl number	0.687	-
z	entrance length	6.47	cm

Solving Equation (9.15) for z results in an entrance length of 6.47 cm, much less than the total length of the flow tube. Because the entrance length represents such a minor fraction of the total flow tube length, the Nusselt number for the fully developed region will be used to determine the temperature profile of the entire flow tube. This temperature profile can be derived by performing a heat balance on a length segment Δz of the pipe, as shown in Figure 9-7.

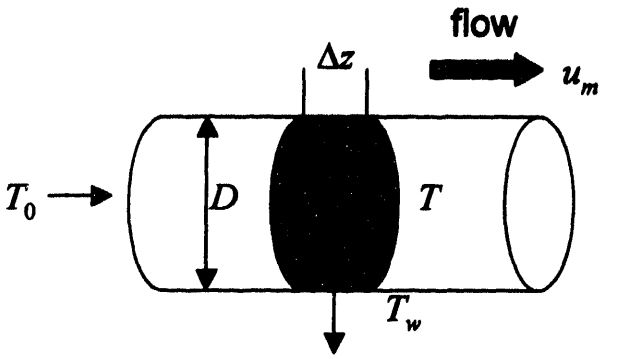

Figure 9-7: Heat balance on a segment Δz of the flow tube.

The heat balance on this segment matches the temperature change to the heat lost due to convection at the flow tube surface.

$$\begin{aligned} m \cdot C_p \frac{dT}{dt} &= -hA\Delta T \\ \Delta z \pi \rho \frac{D^2}{4} C_p \frac{dT}{dt} &= -h\Delta z \pi D(T - T_w) \end{aligned} \tag{9.17}$$

Recall that for gases, density is a function of pressure:

$$\rho = \frac{PW}{RT} \tag{9.18}$$

Substituting this relation and simplifying yields the heat balance:

$$\begin{aligned} \frac{\Delta z \pi PWD^2 C_p}{4RT} \frac{dT}{dt} &= -h\Delta z \pi D(T - T_w) \\ \frac{PWDC_p}{4RT} \frac{dT}{dt} &= -h(T - T_w) \\ \frac{dT}{dt} &= \frac{-4hRT(T - T_w)}{PWDC_p} \end{aligned} \tag{9.19}$$

Rearranging this expression yields an easily integrable form produces:

$$\frac{dT}{T(T-Tw)dt} = \frac{-4hR}{PWDC_p}$$

$$\frac{-1}{T_w T}\frac{dT}{dt} + \frac{1}{T_w(T-T_w)}\frac{dT}{dt} = \frac{-4hR}{PWDC_p} \tag{9.20}$$

$$\int_{T_0}^{T}\frac{-1}{T_w T}dT + \int_{T_0}^{T}\frac{1}{T_w(T-T_w)}dT = \int_{0}^{t}\frac{-4hR}{PWDC_p}dt$$

which yields the temperature profile in the flow tube.

$$T = \frac{T_w}{1-\left(\frac{T_0-T_w}{T_0}\right)\exp\left(\frac{-4hRT_w t}{PWDC_p}\right)} \tag{9.21}$$

Finally, using the superficial velocity to recall that $z = t \cdot u_0$, the temperature profile can be converted to a function of distance along the flow tube.

$$\boxed{T = \frac{T_w}{1-\left(\frac{T_0-T_w}{T_0}\right)\exp\left(\frac{-4hRT_w z}{PWDC_p u_0}\right)}} \tag{9.22}$$

Note that Equation (9.14) is used to calculate the heat transfer coefficient, *h*. Table 9-7 summa-

rizes the parameters used to calculate the temperature profile.

Table 9-7: Summary of parameters for temperature profile calculation

Symbol	*Definition*	*Value*	*Units*
T_0	initial temperature	410	K
T_w	wall temperature	298	K
k	conductivity of air	0.0345	$\frac{W}{m \cdot K}$
h	heat transfer coeffi-cient	5.05	$\frac{W}{m^2 \cdot K}$
R	ideal gas constant	8.314	$\frac{J}{mol \cdot K}$
P	ambient pressure	101,325	N/m^2
W	molecular weight	0.02859	kg/mol
D	flow tube diameter	0.025	m
C_p	heat capacity of air	1015.4	$\frac{J}{kg \cdot K}$
z	position in flow tube	varies	cm
u_0	superficial velocity	8.33	cm/s

Figure 9-8 graphs the temperature profile of the flow tube.

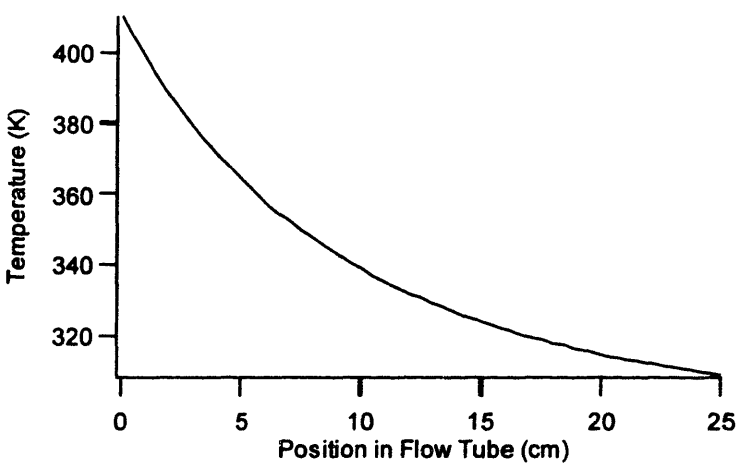

Figure 9-8: Temperature profile in the flow tube.

As the flow tube cools, the gas phase H_2SO_4 will naturally become supersaturated, which drives the particle creation and growth mechanisms. These mechanisms and their effects on the particle size distribution will be discussed in the following sections.

9.4 Nucleation

The primary source of particles in this system is nucleation. In general, nucleation may occur on small "seed" particles distributed through the gas phase or it may occur when tiny clusters of condensing gas molecules grow into a particle. The latter case is known as homogeneous nucleation; it is the dominant particle generation mechanism in the flow tube.

Friedlander (2000) states the following relation for the nucleation rate:

$$\frac{dN_0}{dt} = 2\left[\frac{P_i}{\sqrt{2\pi W_m kT}}\right](n_i v_m^{2/3})\sqrt{\frac{\sigma v_m^{2/3}}{kT}}\exp\left[\frac{-16\pi\sigma^3 v_m^2}{3(kT)^3 \ln\left(\frac{P_i}{P_{vp}}\right)}\right] \tag{9.23}$$

Table 9-8 summarizes the parameters used in the nucleation expression.

Table 9-8: Nucleation rate calculation parameters

Symbol	*Definition*	*Value*	*Units*
$\frac{dN_0}{dt}$	rate of particle nucleation	varies	$\frac{\#\ \text{particles}}{\text{cm}^3 \cdot \text{s}}$
P_i	gas phase H_2SO_4 pressure	0.0127	N/cm^2
W_m	mass of an H_2SO_4 molecule	1.63×10^{-25}	kg
k	Boltzmann constant	1.38×10^{-23}	J/K
T	temperature	varies	K
n_i	concentration of H_2SO_4 molecules	2.24×10^{16}	$\frac{\#\ \text{molecules}}{\text{cm}^3}$
v_m	volume of an H_2SO_4 molecule	3.93×10^{-23}	cm^3
σ	surface tension	5.95×10^{-6}	J/cm^2
P_{vp}	vapor pressure	varies	N/cm^2

Figure 9-9 graphs the homogeneous nucleation rate as a function of flow tube position assuming

the temperature profile from the Graetz problem..

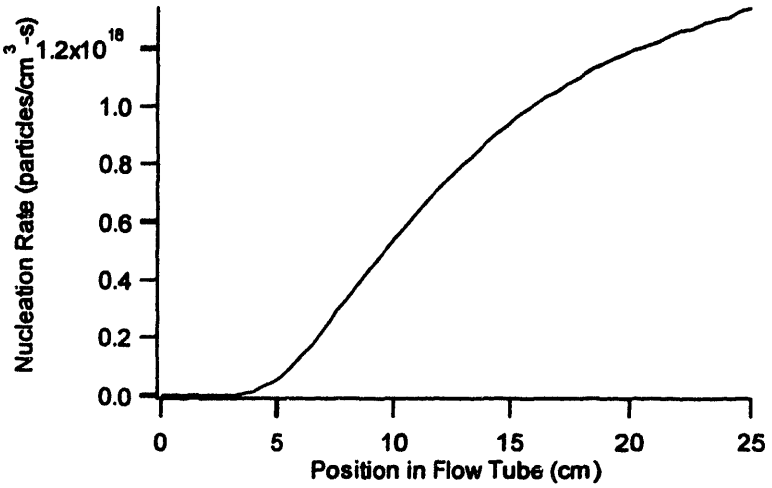

Figure 9-9: Nucleation rate as a function of position.

The gas phase concentration of H_2SO_4 molecules, n_i, is calculated from the gas phase concentration using the molecular mass and Avagadro's number.

$$n_i = \frac{CN_A}{W}$$

$$n_i = \frac{3.66\times10^{-6}\frac{g}{cm^3}6.024\times10^{23}\frac{molecules}{mol}}{98.07\frac{g}{mol}} \tag{9.24}$$

$$n_i = 2.24\times10^{16}\frac{molecules}{mol}$$

The details of the calculations for determining the surface tension and molecular volume of H_2SO_4 are included in the following sections.

9.4.1 Surface tension of H_2SO_4

The surface tension of H_2SO_4 is calculated according to the group-contribution "parachor" method described in Reid, Prausnitz, and Poling (1987). According to this method, the surface tension is given by:

$$\sigma = [P\cdot(\rho_l-\rho_v)]^4 \tag{9.25}$$

where P is the parachor and ρ_l and ρ_v are the liquid and gas phase densities, respectively. The

parachor calculation is summarized in Table 9-9.

Table 9-9: Parachor calculation summary

Group	*Number of Groups*	*Individual Contribution*	*Total Contribution*
S	1	49.1	49.1
-OH	2	29.8	58.6
-O	2	20.0	40.0
		TOTAL	**147.7**

Using this value of the parachor, Table 9-10 summarizes the calculation of the surface tension.

Table 9-10: Surface tension calculation parameters

Symbol	*Definition*	*Value*	*Units*
P	parachor	147.7	-
ρ_l	liquid density	0.0188	mol/cm^3
ρ_v	vapor density density	3.72×10^{-8}	mol/cm^3
σ	surface tension	59.45	g/s^2

Note that in the nucleation expression the surface tension σ is given in terms of J/cm^2, which requires a conversion factor of 10^{-7}.

9.4.2 Molecular volume of H_2SO_4

The molecular volume of H_2SO_4 is determined by assuming that the atom farthest from the central sulfur atom will determine the molecular radius. Because all of the O and S atoms in the molecule are sp^3 hybridized, all of the angles are 109.5° (Atkins, 1994). Thus, the radius of the molecule should be determined by the distance between the S and H atoms. Placing one of the S-

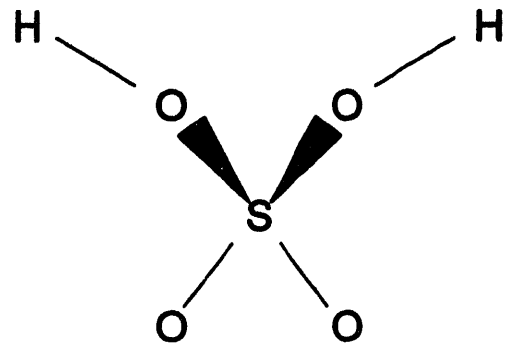

Figure 9-10: Structure of the H_2SO_4 molecule.

O-H groups in cartesian coordinates makes for ready evaluation of this distance.

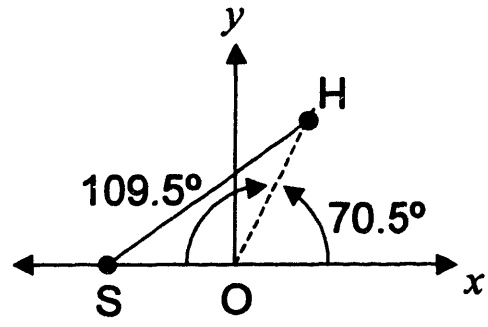

Figure 9-11: Placement of S-O-H bond in cartesian coordinates.

Consulting the *CRC Handbook of Chemistry and Physics* (Lide and Frederikse, 1996) reveals the bond lengths, as summarized in Table 9-11.

Table 9-11: Bond lengths in H_2SO_4

Bond	*Length* (Å)
S-O	1.574
O-H	0.970

which allow quick calculation of the *x-y* coordinates of the S and H molecules.

Table 9-12: Coordinates of S and H atoms in H_2SO_4 radius calculation

Atom	*Coordinate*	*Formula*	*Value*
H	*x*	0.970cos(70.5)	0.324
H	*y*	0.970sin(70.5)	0.914
S	*x*	-1.574	-1.574
S	*y*	0	0

Applying the distance formula results in the radius of the H_2SO_4 molecule.

$$\begin{aligned} d &= \sqrt{(0.324-(-1.574))^2+(0.914-0)^2} \\ d &= 2.11 \end{aligned} \tag{9.26}$$

With a molecular radius of 2.11Å, the molecular volume is easily calculated as follows.

$$\begin{aligned} v &= \frac{4}{3}\pi r^3 = \frac{4}{3}\pi(2.11)^3 \\ v &= 37.35 \end{aligned} \tag{9.27}$$

Converting the molecular volume from $Å^3$ to cm^3 yields 3.93×10^{-23} cm^3.

9.5 Growth

Particles which have nucleated also grow under the supersaturated conditions of the flow tube. Assuming a diffusion-limited growth law, as given in Equation (9.5):

$$\begin{aligned} K &= 2\pi D(c_\infty - c_s)\left(\frac{6}{\rho\pi}\right)^{1/3} \\ G(m) &= Km^{1/3} \end{aligned} \tag{9.28}$$

where *W* has been omitted because the concentrations will now be expressed in g/cm^3. Using a method of characteristics analysis (see Chapter 6), it is possible to predict the growth of particles, assuming a constant degree of supersaturation, which fixes *K*. Specifically, the mass of the particles is given as a function of time and initial particle size by the Equation (9.25).

$$t - t_0 = \frac{3}{2K}(m^{2/3} - m_0^{2/3})$$
$$m = \left(\frac{2K}{3}(t - t_0) + m_0^{2/3}\right)^{3/2} \tag{9.29}$$

Because the nucleation rate can also be calculated (see section 9.4), it is possible to approximate the number density distribution of particles exiting the flow tube under conditions of varying nucleation rate and constant supersaturation. Table 9-13 summarizes the calculation of K for this system.

Table 9-13: Calculation of growth rate constant

Symbol	*Description*	*Value*	*Units*
D	diffusivity of H_2SO_4 in air	0.0879	cm^2/s
c_∞	bulk concentration of H_2SO_4	4.85×10^{-6}	g/cm^3
c_s	equilibrium concentration of H_2SO_4	1.03×10^{-9}	g/cm^3
ρ	liquid H_2SO_4 density	1.841	g/cm^3
K	growth constant	2.71×10^{-6}	$g^{2/3}/s$

Take a differential section of air traveling through the length of the flow tube, as shown in Figure 9-12. As the position of the segment moves from z_a to z_b, the residence time of the seg-

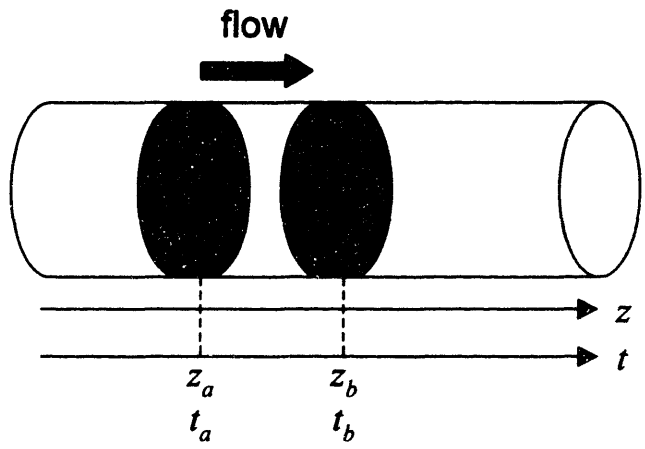

Figure 9-12: Differential segment of air as it transverses the flow tube.

ment varies from t_a to t_b, where:

$$t_a = \frac{z_a}{u_0}$$
$$t_b = \frac{z_b}{u_0} \tag{9.30}$$

Over this time segment, a number N_0 of new particles will nucleate within this differential segment of air. If $n_0(t)$ represents the nucleation rate per cm^3 of air as a function of time, then N_0 represents the total number of nucleated particles over this time span.

$$N_0 = \int_{t_a}^{t_b} n_0(t^*)dt^* \tag{9.31}$$

Assuming constant supersaturation, these newly nucleated particles will follow a characteristic curve over time as they grow from size m_0 at time t^* when they nucleate. Thus, the largest particles in this segment will be the ones which nucleated at time t_a and the smallest particles will be the ones which nucleated at time t_b.

$$m_a = \left(\frac{2K}{3}(t - t_a) + m_0^{2/3}\right)^{3/2}$$
$$m_b = \left(\frac{2K}{3}(t - t_b) + m_0^{2/3}\right)^{3/2} \tag{9.32}$$

Notice the data we now have describe a "bin" into which this population segment fits, as shown in Figure 9-13.

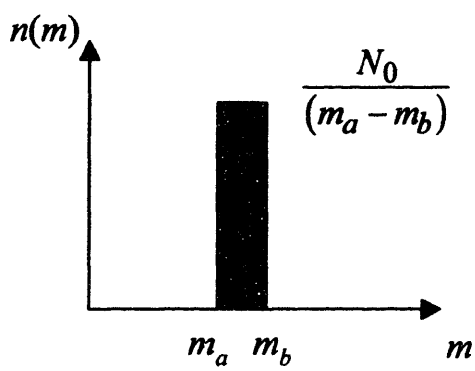

Figure 9-13: Bin defined by nucleating and growing particles.

In fact, if the total residence time in the flow tube is divided up into many tiny segments (t_a, t_b), then this same procedure may be used to approximate the entire number density distribution of particles when the gas segment exits the flow tube, as shown in Figure 9-14. Using this data, it is

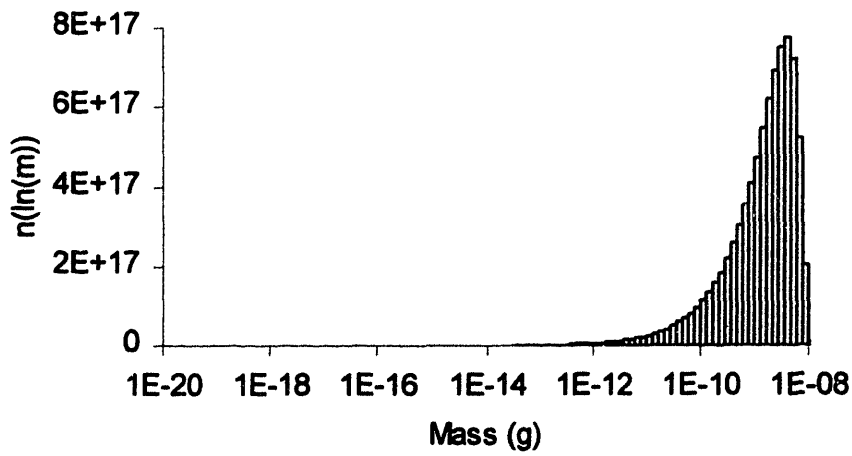

Figure 9-14: Size distribution resulting from nucleation and growth at constant supersaturation over the full residence time in the flow tube.

possible to compare the relative contributions of coagulation and growth to determine if coagulation is a significant process in this system.

A quick order of magnitude analysis and comparison with Figure 9-9 reveals that 10^{18} particles/ cm^3 have nucleated in this system and grown to a size of approximately 10^{-9} g, which means that the total mass of all particles should be somewhere on the order of 10^9 g/cm^3! This obviously indicates that all of the gas phase H_2SO_4 is taken up into particles well before 3 second limit. In order to obtain a realistic result, it is necessary to iteratively solve this system for the maximum amount of time that particles can nucleate and grow before all of the gas phase H_2SO_4 is taken up. Iteratively solving the nucleation and growth problem reveals that all of the gas phase H_2SO_4 is usurped by nucleation and adsorption at roughly 0.17685 seconds. The results of this analysis are

presented in Figure 9-15.

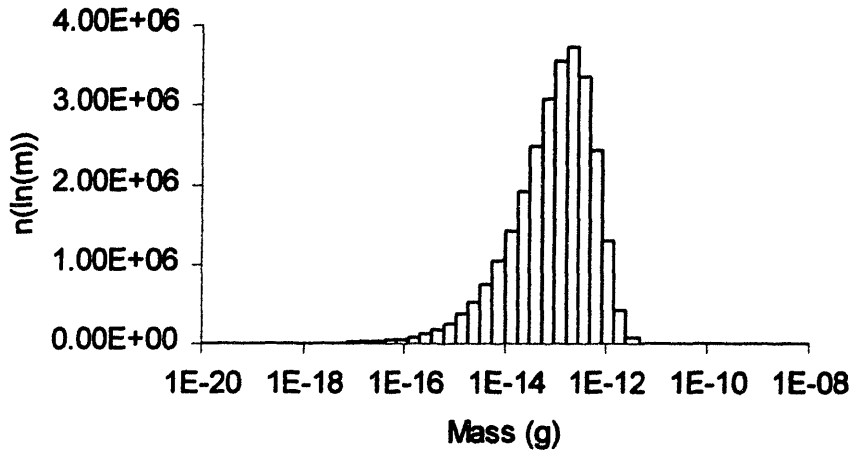

Figure 9-15: Size distribution resulting from nucleation and growth at constant maximum supersaturation over 0.18 seconds in the flow tube.

These results further reinforce the analysis of H_2SO_4 lost to the flow tube wall. Inserting a characteristic adsorption time for the gas phase of 0.18 seconds into Equation (9.9):

$$\frac{C}{C_0} = e^{-t/\tau} = e^{-0.18/5.57}$$
$$\frac{C}{C_0} = 0.968 \tag{9.33}$$

reveals that less than 3.2% of the gas phase H_2SO_4 is lost to wall deposition.

9.6 Comparison of Coagulation and Growth Rates

Given the data presented in Figure 9-15 and the fact that coagulation scales roughly with the square of number density, the highest coagulation rate will occur near the peak of the graph - somewhere near 10^{-13} g. Calculating the rate at which self-coagulation removes particles from this bin involves employing the following formula:

$$\text{rate} = \beta(m, m) \cdot N(m)\Delta m \cdot N(m)\Delta m \tag{9.34}$$

The coagulation kernel β is calculated based on the Brownian coagulation kernel:

$$\beta(r_1, r_2) = \frac{2kT}{3\mu}\left(\frac{1}{r_1} + \frac{1}{r_2}\right)(r_1 + r_2) \tag{9.35}$$

where r_1 and r_2 are the radii of the two coagulating particles. Data on the peak bin is summarized in Table 9-14.

Table 9-14: Data for peak bin and coagulation calculation

Symbol	*Definition*	*Value*	*Units*
m_a	lower bin range	1.58×10^{-13}	g
m_b	upper bin range	2.75×10^{-13}	g
N_0	number of particles in bin	2.01×10^{6}	-
r_1, r_2	mean bin radius	3.02×10^{-5}	cm
ρ	particle density	1.841	g/cm^3
k	Boltzmann constant	1.38×10^{-21}	$\frac{N \cdot cm}{K}$
T	temperature	410	K
μ	viscosity of air	2.35×10^{-9}	$\frac{N \cdot s}{cm^2}$
rate	coagulation rate	2594	$\frac{particles}{s \cdot cm^3}$

Growth out of this bin can be thought of as a rate process describing the rate at which particles leave the bin. Expressing the rate as the total number of particles divided by some rate constant Δt:

$$\text{rate} = \frac{N_0}{\Delta t} \tag{9.36}$$

A simple manipulation reveals that this is equivalent to the product of the growth rate and the number density.

$$\begin{aligned} \text{rate} &= \frac{N_0}{\Delta t} = \frac{N_0}{\Delta m}\frac{\Delta m}{\Delta t} \\ \text{rate} &= \frac{N_0}{\Delta m} G(m) \end{aligned} \tag{9.37}$$

Recalling that $G(m) = K \cdot m^{1/3}$ and calculating the new value of $K = 1.43\times10^{-6}$ based on the

shorter final supersaturation, we can use $\Delta m = m_b - m_a = 1.17\times10^{-13}$ to estimate the rate of particles leaving the bin due to growth is:

$$\text{rate} = \frac{N_0}{\Delta m} K m^{1/3}$$

$$\text{rate} = \frac{2.01\times10^{6}}{1.03\times10^{-13}} 1.43\times10^{-6} (2.17\times10^{-13})^{1/3} \qquad (9.38)$$

$$\text{rate} = 1.67\times10^{9}$$

where m is taken to be the midpoint of the mass interval. The relative rates of coagulation and growth reveal that coagulation is an insignificant process compared to growth in this system.

9.7 Variation of Nucleation and Growth Results with Temperature

Using the analysis presented in section 9.5, it is possible to predict the variation in the number density as the initial bath temperature T_0 of the system is varied. Figure 9-16 plots results comparing the number density distributions when the bath temperature is 350 K and 410 K.

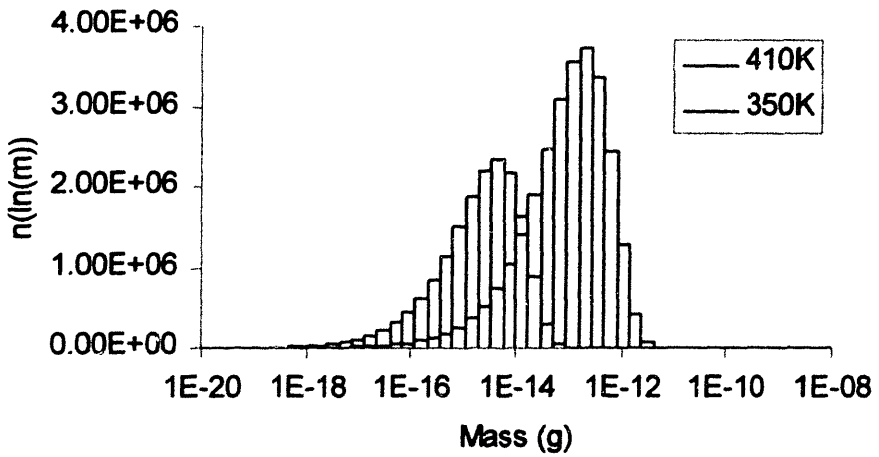

Figure 9-16: Comparison of the size distributions in the flow tube as a function of temperature.

These results indicated that a smaller total number of particles are nucleated at lower temperatures, and that these particles grow to a smaller particle size, as expected.

References

[1] Atkins, Peter W. *Physical Chemistry,* 5th Ed., W. H. Freeman and Company, 1994.

[2] Crank, John. *Mathematics of Diffusion,* 2nd Ed., Oxford University Press, 1975.

[3] Deen, William M. *Analysis of Transport Phenomena,* Oxford University Press, 1998.

[4] Friedlander, Sheldon K. *Smoke Dust, and Haze: Fundamentals of Aerosol Dynamics,* 2nd Ed., Oxford University Press, 2000.

[5] Incropera, Frank P.; DeWitt, David P. *Fundamentals of Heat and Mass Transfer,* 4th Ed., John Wiley & Sons, 1996.

[6] Jayne, John T.; Leard, Danna C.; Zhang, Xuefang; Davidovits, Paul; Smith, Kenneth A.; Kolb, Charles E.; and Worsnop, Douglas R. *Development of an Aerosol Mass Spectrometer for Size and Composition Analysis of Submicron Particles,* Aerosol Science and Technology, **33**(1-2), 49-70, 2000.

[7] Jaeger, J. C.; Carslaw, Horatio S. *Conduction of Heat in Solids,* 2nd Ed., Oxford University Press, 1986.

[8] Kays, W. M.; Crawford, M. E. *Convective Heat and Mass Transfer,* McGraw-Hill, 1980.

[9] Lide, David R.; Frederikse, H. P. R. *CRC Handbook of Chemistry and Physics,* CRC Press, 1996.

[10] Pöschl, Ulrich; Canagaratna, Majula; Jayne, John T.; Molina, Luisa T.; Worsnop, Douglas R.; Kolb, Charles E.; and Molina, Mario J. *Mass Accomodation Coefficient of H_2SO_4 Vapor on Aqueous Sulfuric Acid Surfaces and Gaseous Diffusion Coefficient of H_2SO_4 in N_2/H_2O,* Journal of Physical Chemistry A: Molecules, **102**(49), 10082-10089, 1998.

[11] Reid, Robert C.; Prausnitz, John M.; and Poling, Bruce E. *The Properties of Gases and Liquids,* 4th Ed., McGraw-Hill, 1987.

Chapter 10: Solution and Scale Analysis of Simultaneous Coagulation, Growth, and Nucleation

10.1 Introduction

The practical solution of population balance systems often requires a solution over many orders of magnitude. For instance, consider the following experimental data describing the mass distribution of aerosol particles formed in the aerosol mass spectrometer system described in Chapter 9. Clearly, this system is capable of producing particles up to 10^{-11} g in size. The largest

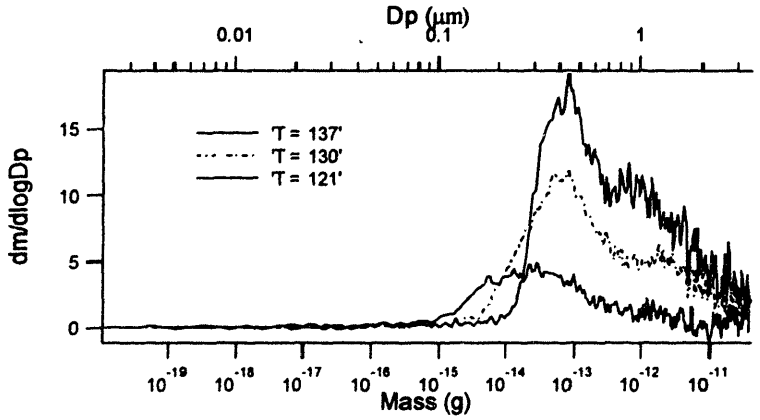

Figure 10-1: Sample mass distribution data from aerosol mass spectrometer experimental system.

particles contain the most mass per particle, and therefore decreasing the upper solution range from 10^{-11} g will result in a physically inaccurate model, much as in the crystallizer model discussed in Chapter 4 and presented in Pantelides and Oh (1996).

Because the system is undergoing nucleation, a comprehensive model must include particles down to the typical nucleus size. For H_2SO_4, experimental results have shown that the typical nucleus diameter is in the range of 2 - 10 nm (Berndt et al., 2000), which requires a minimum particle mass of approximately 10^{-20} g. For this system, the growth rate uses a diffusion-limited growth law:

$$G(m) = Km^{1/3}$$
$$K = 2\pi D(c_\infty - c_s)\left(\frac{6}{\rho\pi}\right)^{1/3} \tag{10.1}$$

which is the most common physical mechanism for particle growth. As a result, any practical solution which aspires to describe the formation of particles in this system must be able to solve the population balance including the growth law given in Equation (10.1) over roughly 9 orders of magnitude in particle mass. Examination of the growth rate expression reveals that the growth rate can be expected to vary over at least three orders of magnitude, without including the variations expected over time as gas phase concentrations change.

In spite of these requirements, all of the numerical solutions which have been developed in the literature fail to solve diffusion-based growth population balances over any significant range of particle sizes. In fact, the only numerical solutions which do solve the population balance equation for growth over more than just two orders of magnitude use the growth rate law:

$$G(m) = Km \tag{10.2}$$

which yields characteristic curves of constant slope when the node points are log scaled (see Chapter 6). This is equivalent to a constant growth rate over the logarithmic range of particle sizes and results in a system of equations which is trivial to solve. Solutions which include surface reaction-limited or diffusion-limited growth laws are much more difficult to solve and - up to now - solutions have only been produced for two or fewer orders of magnitude. Table 10-1 summarizes the results presented in the literature for a variety of population balance models and

experimental systems.

Table 10-1: Summary of population balance solutions including growth

Reference	*System*	*Growth law*	$G(m)$	*Orders of magnitude* $\log(m_{max}/m_{min})$
Chung et al. (1999)	crystallization	Constant	K	2
Resch (1995)	aerosol	Volume reaction	Km	6
Pilinis (1990)	aerosol	Volume reaction	Km	9
Kim and Seinfeld (1991)	aerosol	Volume reaction	Km	5
Alvarez et al. (1992)	polymerization	Volume reaction	Km	1
Katoshevski and Seinfeld (1997)	aerosol	Surface reaction	$Km^{2/3}$	2
Pantelides and Oh (1996)	crystallizer	Diffusion	$Km^{1/3}$	1

This chapter outlines the development and implementation of novel scaling methods which overcome the limitations in current implementations to develop optimal solutions for a variety of growth rate laws over many orders of magnitude. In addition, the scaling requirements of coagulation and growth processes are developed.

10.2 Scaling of Numerical Solution Methods

The growth term is mathematically identical to a convection equation and therefore must adhere to the Courant condition (Strang, 1986):

$$G(\phi)\Delta t \leq \Delta\phi \tag{10.3}$$

where $G(\phi)$ is the growth rate in the ϕ coordinate, Δt is the maximum allowable time step, and $\Delta\phi$ is the spacing between node points in the solution domain. Depending on the scaling system chosen, this results in a different maximum time step. Because growth is assumed to be diffusion-limited, the growth expressions for m and w solution coordinates are:

$$\begin{aligned} G(m) &= Km^{1/3} \\ G(w) &= \frac{K}{\gamma m^{2/3}} \end{aligned} \tag{10.4}$$

These two functions are plotted over the proposed solution domain in Figure 10-2. Note that the

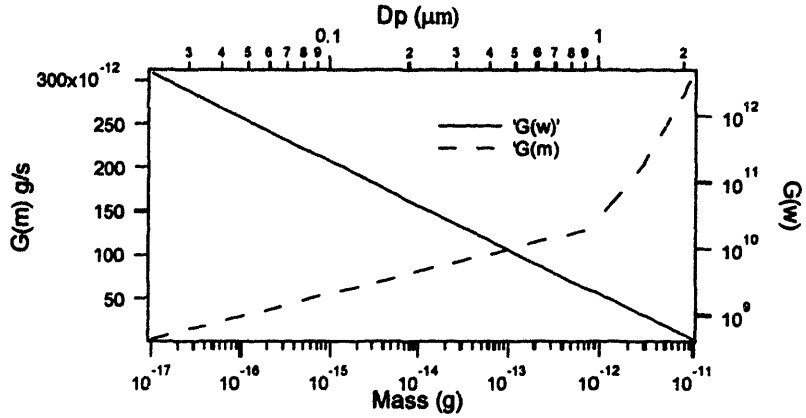

Figure 10-2: Comparison of rescaled growth rate expressions in *m* and *w* scaling systems.

mass-based growth rate varies over only two orders of magnitude, while the *w*-scaled growth rate varies over roughly four orders of magnitude. Using 14 elements spaced along this solution domain results in the element boundary placement shown in Figure 10-3. Even though the node

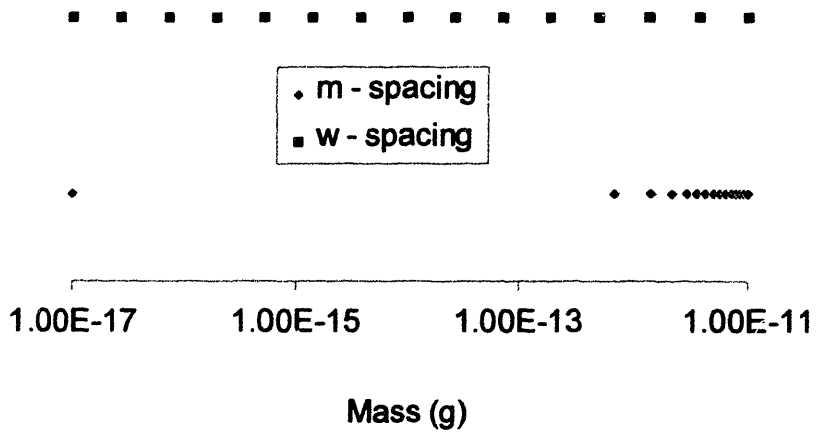

Figure 10-3: Comparison of element spacing for *m* and *w* scaling methods.

points are unevenly placed, the element boundaries are evenly spaced in their respective scaling systems, yielding the minimum time step functions over the domain range shown in Figure 10-4. Note that the *m* - scaling has maximum time steps on the order of 10^{-3}, and can thus be expected

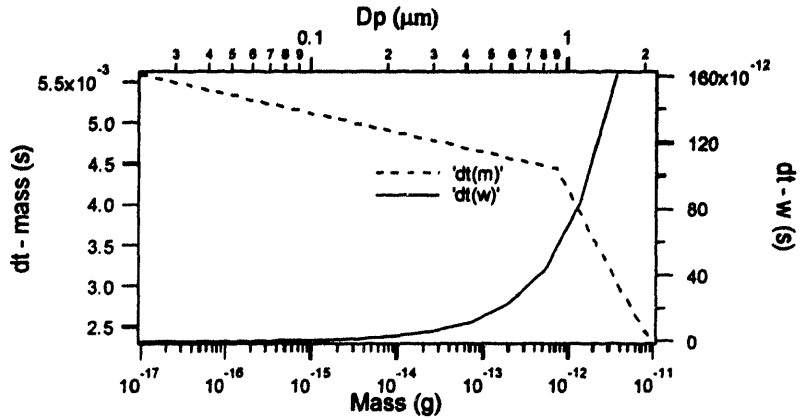

Figure 10-4: Minimum time step variation over the solution domain range for *w* and *m* scaling systems.

to complete each second of numerical integration with several thousand time steps. The *w* - scaling, however, generates minimum time steps on the order of 10^{-14} s, thus requiring an exorbitant number of timesteps to solve. Note also that the *m* - scaling method places a large number of elements in the upper size range, as shown in Figure 10-3, leaving only one element to cover the most important part of the solution range. In contrast, *w* - scaling offers uniform scaling over the solution domain and desirable node point resolution, but at the expense of intractable solution times. It is readily apparent that neither of these scaling methods are appropriate, and therefore a new scaling method must be formulated.

10.3 The R - Scaling Method

The Courant condition offers a very limited range of possibilities for reducing the number of time steps required for numerical integration:

$$\Delta t \leq \frac{\Delta \phi}{G(\phi)} \tag{10.5}$$

In general, the growth rate $G(\phi)$ is determined by the physics of the system; this leaves only one degree of freedom - $\Delta\phi$ or Δt - in the Courant condition. Simply put, *because the physics of the system determine the growth law and the Courant condition is necessary to enforce stability, choosing the time step determines the solution node placement and vice versa.* However, the numerical integration routine is forced to use the same value of Δt for all points in the solution domain. By choosing a variable node point placement $\Delta\phi$, it is possible to construct a node-point scaling which results in a constant time step:

$$\tau \approx \frac{\Delta\phi}{G(\phi)} \tag{10.6}$$

This can be accomplished if $\Delta\phi$ has the same functional form of $G(\phi)$. For the case where $\phi = m$ and the growth law is diffusion-limited:

$$\tau = \frac{\Delta m}{K m^{1/3}} \tag{10.7}$$

In order to find an optimal scaling method, a new scaling coordinate λ is needed such that the node points are evenly spaced:

$$\frac{\Delta\lambda}{G(\lambda)} = \tau \tag{10.8}$$

where τ represents a constant timestep value. In essence, this is equivalent to specifying that $G(\lambda)$ is constant in the new scaling coordinate. Setting the value of this constant to $1/\gamma$ yields:

$$G(\lambda) = \frac{1}{\gamma} \tag{10.9}$$

However, recall the relationship:

$$\begin{aligned} G(\lambda) &= \frac{d\lambda}{dt} = \frac{dm}{dt} \cdot \frac{d\lambda}{dm} \\ G(\lambda) &= G(m)\frac{d\lambda}{dm} \end{aligned} \tag{10.10}$$

Substituting this expression into Equation (10.9) yields a new basis for defining a transform between m and the new scaling coordinate λ:

$$\begin{aligned} G(m)\frac{d\lambda}{dm} &= \frac{1}{\gamma} \\ d\lambda &= \frac{dm}{\gamma m^{1/3}} \end{aligned} \tag{10.11}$$

Integrating this expression yields the functional relationship underlying this transformation:

$$\begin{aligned} \int_0^{\lambda} d\lambda &= \int_{m_{\min}}^{m} \frac{dm}{\gamma m^{1/3}} \\ \lambda &= \frac{3}{2\gamma}(m^{2/3} - m_{\min}^{2/3}) \end{aligned} \tag{10.12}$$

The scaling factor γ is defined by setting $\lambda = 1$ when $m = m_{max}$:

$$1 = \frac{3}{2\gamma}(m_{max}^{2/3} - m_{min}^{2/3})$$
$$\gamma = \frac{3}{2}(m_{max}^{2/3} - m_{min}^{2/3}) \tag{10.13}$$

Spacing the elements evenly along the coordinate λ results in a constant timestep, with the following element boundaries, plotted here for comparison with w and m scaling.

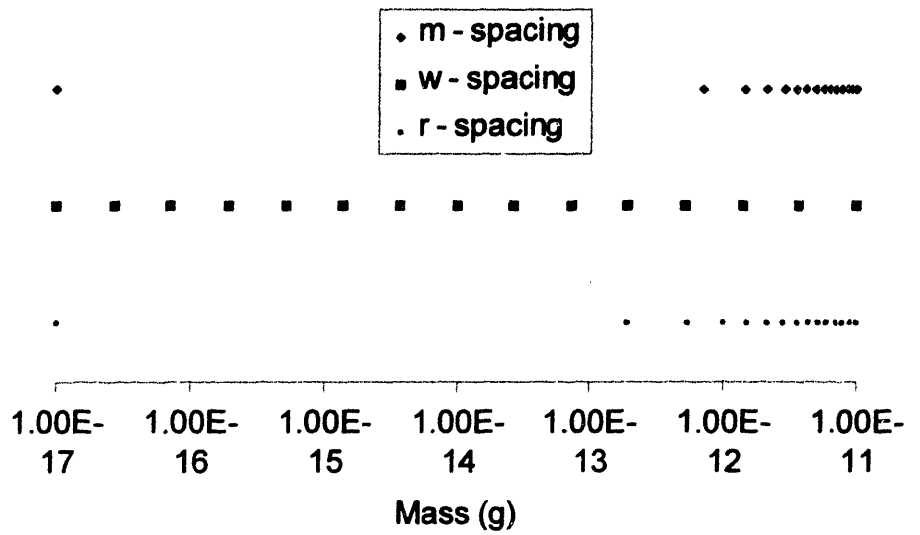

Figure 10-5: *r* - scaled node point placement in comparison with *w* and *m* spacing.

As shown in Figure 10-5, this new scaling method provides more even spacing, and therefore better resolution than the m - spacing method, while minimizing the solution time required at this resolution. This is made possible by the fact that both Δm and $G(m)$ have the same functional form, as shown in Figure 10-6. Because the shape of these function match very closely, the timestep, which is determined by the ratio of these two functions, is almost constant. Figure 10-7 shows a plot of the maximum time step as a function of particle size. Because the maximum timestep allowable in the numerical integration algorithm is the *lowest* maximum timestep over the entire solution domain, it is evident that this new r - scaling method has a maximum timestep comparable to the m - scaling method and many orders of magnitude faster than the w -scaling method. Thus this new scaling method offers fast solution times with increased resolution by optimizing the timestep with respect to the Courant condition.

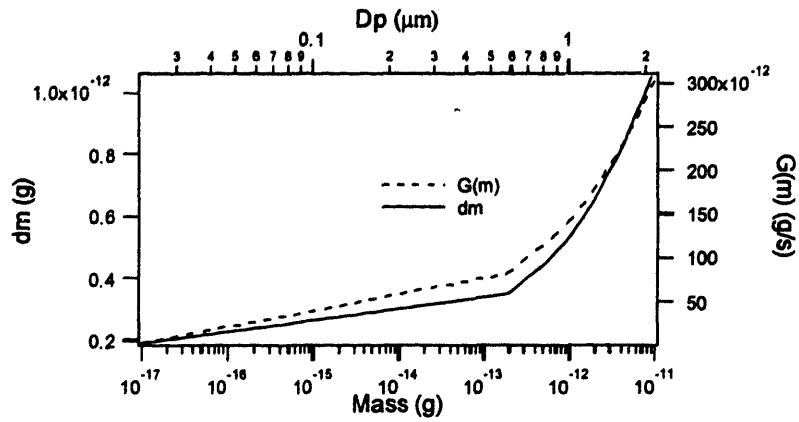

Figure 10-6: Comparison of node spacing *dm* and growth rate function *G(m)* over the solution domain using *r* - spacing.

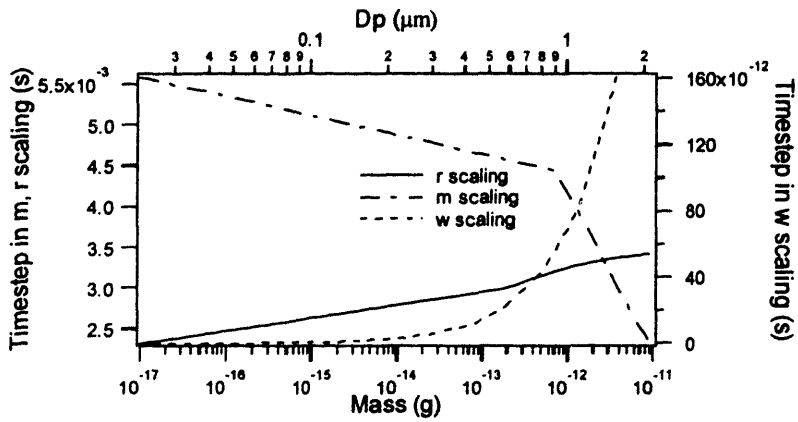

Figure 10-7: λ - scaled node point placement in comparison with *w* and *m* spacing.

10.4 Hybrid Scaling Methods

The *r* - scaling method presents a method for optimizing the resolution and solution time for a given growth kernel. In general, an optimal scaling method can be derived using the same method as shown in the previous example for the *r* - scaling method. This can be accomplished by substituting the growth law into Equation (10.7) and proceeding with the derivation as outlined.

Although this method yields the optimal results for resolution and timestep, demanding applications may require a larger number of node points and/or more orders of magnitude in the final solution. While the *r* - scaling method offers better spatial resolution than *w* - scaling, applications requiring more node points in the lower range of the logarithmic size range will need to add

a large number of node points before adequate resolution is achieved in the size domain (see Figure 10-5). For these cases, hybrid scaling systems can be constructed which combine the benefits of the various scaling methods over different ranges of the solution domain. For instance, when a system requires the solution of a diffusion-based growth equation over very many orders of magnitude, a hybrid method can be employed which combines the ability of *w* - scaling to offer high resolution over many orders of magnitude and the ability of *r* - scaling to offer fast solution times.

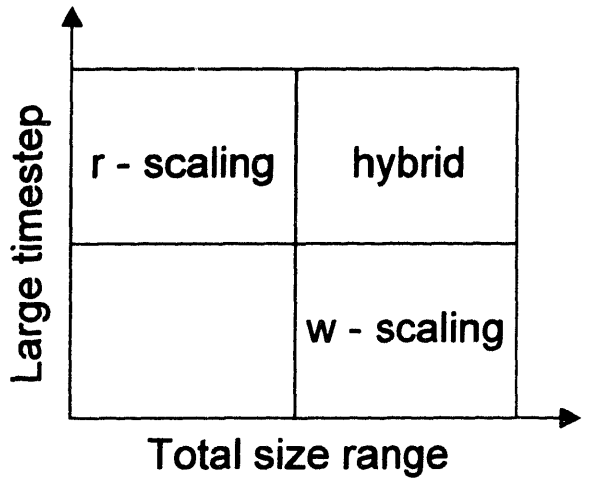

Figure 10-8: λ - scaled node point placement in comparison with *w* and *m* spacing.

Examining Figure 10-4 reveals that the time step for the *w* - scaling method is most restrictive in the lower size range. This occurs because $G(w) = K/\gamma \cdot m^{-2/3}$ and thus the rescaled growth rate is largest in the smallest size range. However, because Δw is constant, this means that the Courant condition will produce the smallest maximum timestep in the smallest size ranges, where $G(w)$ is largest:

$$\Delta t \leq \frac{\Delta w}{G(w)} \tag{10.14}$$

Because the *r* scaling method has a constant time step over the entire domain range, it can be effectively employed over the lower size ranges, while the *w* scaling method can be employed to efficiently cover the upper particle size ranges with relatively few extra node points.

In the case of a system requiring a solution over the domain (10^{-20} g, 10^{-8} g), a total of 14 total finite elements can be used, with the first elements scaled using the *r* system over the range from 10^{-20} to 10^{-14} and the remaining elements using the *w* scaling system to cover the remainder of the

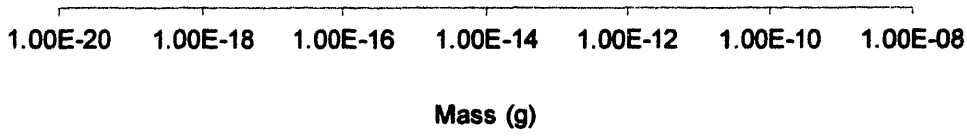

Figure 10-9: Node point placement for a hybrid scheme combining *r* - scaling in the lower solution range with *w* scaling in the upper solution range.

solution domain. The node spacing for this scheme is illustrated in Figure 10-9. Using this scaling scheme, a solution was generated for the known analytical solution of an initial lognormal distribution and the growth rate $G(m) = m$. Figure 10-10 shows the results of this numerical solution

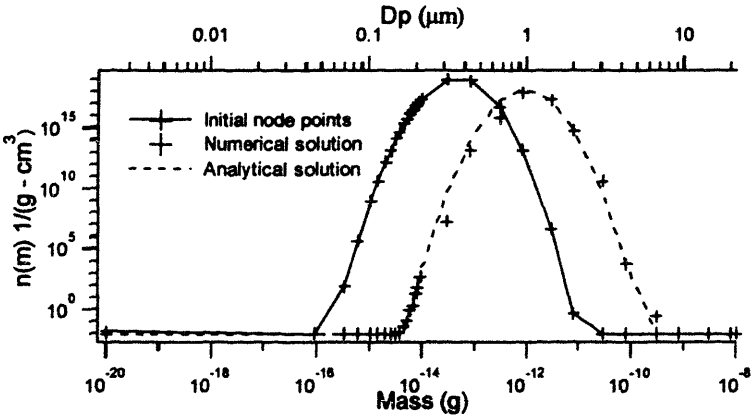

Figure 10-10: Comparison of analytical and numerical results for a hybrid solution of an initially lognormal distribution with growth rate $G(m) = m$.

for a final solution time of 3.0 s. Solution time was approximately 20 s on a 333 MHz personal computer, and the close agreement between numerical and analytical results indicates that the solution is both accurate and fast. Figure 10-11 plots the node spacing and growth rate as a func-

tion of particle size. The resulting minimum time step is a function of particle size, as shown in

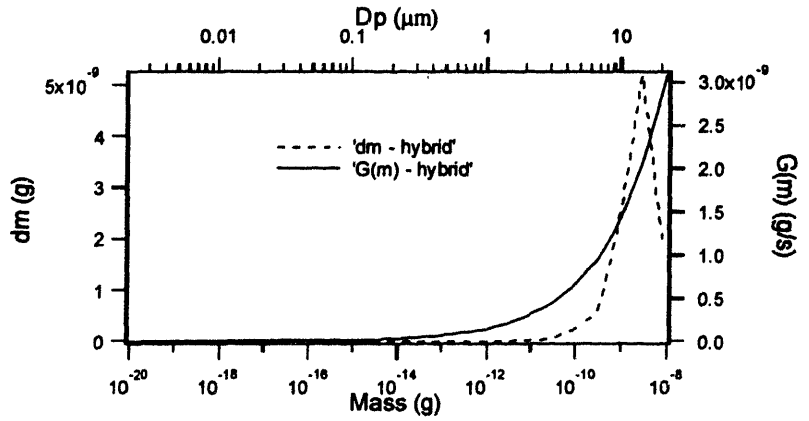

Figure 10-11: Growth rate and node spacing as a function of particle size for hybrid spacing method using diffusion-limited growth law.

Figure 10-12. Note that the *w* - scaled section does *not* limit the timestep; using the *r* scaling

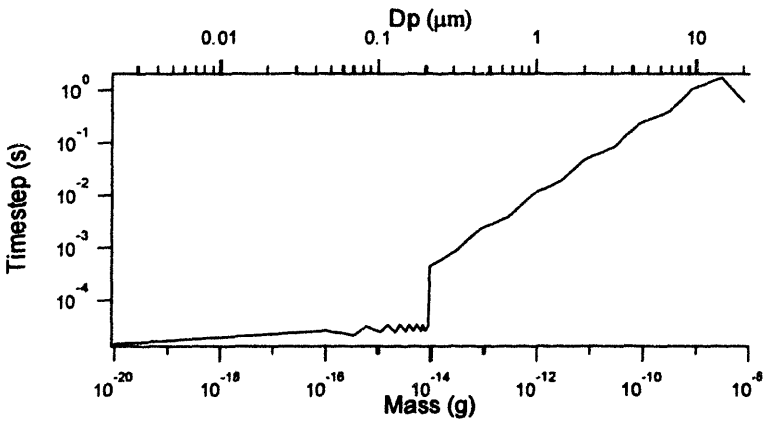

Figure 10-12: Timestep as a function of particle size for hybrid spacing method with diffusion-limited growth law.

method in the lower size ranges results in a maximum timestep on the order of 10^{-5} s which is still much larger than the maximum timestep for pure *w* - scaling of 10^{-14}.

10.5 Solution for Aerosol Mass Spectrometer Experimental System

In an effort to demonstrate the utility of these rescaled growth equations for describing the solution of population balance problems, sample solutions have been developed to compare with

analytical solutions describing the aerosol mass spectrometer experimental system under a variety of conditions. The set of governing equations for this system include the single-component number density governing equation:

$$\frac{\partial n(m)}{\partial t} = \int_0^{\frac{m}{2}} \beta(x, m-x) n(x) n(m-x) dx - n(m) \int_0^{\infty} \beta(m, x) n(x) dx - \frac{\partial (G(m) n(m))}{\partial m} \qquad (10.15)$$

where the growth law is generally assumed to represent diffusion-limited growth, as shown in Equation (10.1):

$$G(m) = Km^{1/3}$$
$$K = 2\pi D(c_\infty - c_s)\left(\frac{6}{\rho\pi}\right)^{1/3} \qquad (10.16)$$

However, because this is an enclosed system, an additional mass balance is needed for the gas phase in order to model the uptake of H_2SO_4 from the gas phase:

$$\frac{\partial C}{\partial t} = -\int_{m_{min}}^{\infty} G(m) n(m) dm - N_0 \cdot m_{min} \qquad (10.17)$$

which occurs due to particle nucleation and growth.

The first term describes the uptake of gas phase H_2SO_4 due to particle growth; the second term describes the rate of uptake due to nucleation. If the gas entering the flow tube is saturated with H_2SO_4 at a temperature of 410 K, it will contain roughly 3.65×10^{-6} g/cm^3 H_2SO_4. Examining Figure 9-15 reveals that these particles can be expected to grow to a size of 10^{-11} g. Summing the particles from all of the bins in this solution reveals that approximately 1.47×10^{7} particles are expected to nucleate. If all of these particles grew to the same size, they would need to reach a size of 2.48×10^{-13} g in order to uptake all of the H_2SO_4 vapor. This represents the absolute minimum upper size limit that can be used for any numerical solution of this problem; anything less will create a situation where particles "escape" the system by growing larger than the maximum size limit and therefore no longer participate in the uptake equation. The resulting vapor concentration will be overestimated, leading to overestimates of number density and nucleation rates similar to the crystallization example (Pantelides and Oh, 1996) shown in Section 4.5.2. Observ-

ing Figure 9-15 also reveals that the number density of particles starts to become significant somewhere around 10^{-17} g, and thus a solution domain of (10^{-17}, 10^{-11}) would be the absolute minimum required for this particular application. In order to generate a solution, a scaling system must be selected for the solution domain.

Using the homogeneous nucleation rate and characteristic solution given in Chapter 9, it is possible to approximate the analytical solution to this system for nucleation and growth. This is essentially accomplished by repeatedly performing the "bins" solution presented in sections 9.5 - 9.7 over small timesteps, using the results of the previous timestep as the input for the next timestep. Figure 10-13 shows the results of this analysis for when the particle size distribution initially contains zero particles and the H_2SO_4 bath temperature is 410 K. Final conditions for

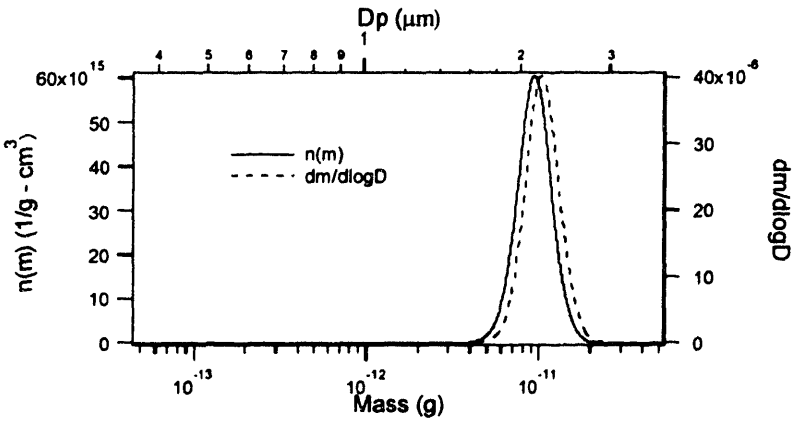

Figure 10-13: Analytical results for nucleation and growth

this simulation where reached when the growth and nucleation rates became negligible. At this final condition, 90% of the initial gas phase H_2SO_4 had been adsorbed by the particles and a total of 3.26×10^5 particles had nucleated. Note that the results predict an almost monodisperse particle size distribution, a significant departure from the observed shape of the number density distribution shown in Figure 10-1 as well as the sample solution with time-varying nucleation rate given in Figure 9-15.

Using the final conditions from the analytical solution, it is possible to estimate characteristic coagulation and growth rates. For coagulation, the distribution can be treated as monodisperse; it follows then that the rate of change in the number density distribution can be approximated by:

$$\text{rate} = \beta(m, m) \cdot N^2 \tag{10.18}$$

Because the particles are well within the continuum coagulation regime, the Brownian diffusion coagulation kernel takes the form:

$$\beta(x, y) = \frac{2kT}{3\mu}\left(\frac{1}{r(x)} + \frac{1}{r(y)}\right)[r(x) + r(y)] \tag{10.19}$$

Where $r(x)$ and $r(y)$ are the radii of particles sized x and y, respectively. Note that in this case $x = y = m$ and so the coagulation rate reduces to:

$$\text{rate} = \frac{8kT}{3\mu} \cdot N^2 \tag{10.20}$$

Each coagulation event will produce a particle with approximate mass $2 \cdot m$. In order to compare the growth rate, it is necessary to determine the rate at which particles of at mass m would grow to the same size, $2 \cdot m$. This rate can be estimated by the following expression:

$$\text{rate} = N \cdot \frac{G(m)}{\Delta m} \tag{10.21}$$

The expression $G(m)/\Delta m$ approximates the frequency (units 1/s) at which particles grow from m to $2 \cdot m$; multiplying this expression by N produces the overall rate. The parameters used in this

calculation and the results are summarized in Table 10-2.

Table 10-2: Calculation of growth rate constant

Symbol	*Description*	*Value*	*Units*
k	Boltzmann constant	1.38×10^{-21}	$\frac{N \cdot cm}{K}$
T	temperature	410	K
μ	viscosity of air	2.35×10^{-9}	$\frac{N \cdot s}{cm^2}$
m	change in mass	1.0×10^{-11}	g
Δm	change in mass	1.0×10^{-11}	g
K	growth constant	2.51×10^{-8}	$g^{2/3}/s$
N	number of particles	3.26×10^{5}	$\#/cm^3$
$G(m)$	$K \cdot m^{1/3}$	5.4×10^{-12}	g/s
-	coagulation rate	68.23	#/s
-	growth rate	1.76×10^{5}	#/s

Even under these conditions, the growth rate of particles overwhelms the coagulation rate, justifying the lack of coagulation in this solution and suggesting that the discrepancy between experimental and theoretical results must be due to some deficiency in the model physics. This deficiency is most likely in the nucleation rate; the classical homogeneous nucleation rate has been widely criticized in a variety of applications ranging from crystallization to the formation of carbon black (Fabry, Flamant, and Fulcheri, 2001; Leubner, 2000). In particular, the nucleation rate is particularly sensitive to the value σ, which represents the surface tension of H_2SO_4 in the nucleating particles. Figure 10-14 shows results for this solution with initial temperature of 376 K and twice the normal value of σ. Note that the resulting number density distribution still has the same shape as the analytical solution given in Figure 10-13, however it is about two orders of magnitude wider at the base. Although this qualitatively reproduces the trends shown for lower temperatures in the experimental data (see Figure 10-1), it still represents a large departure from

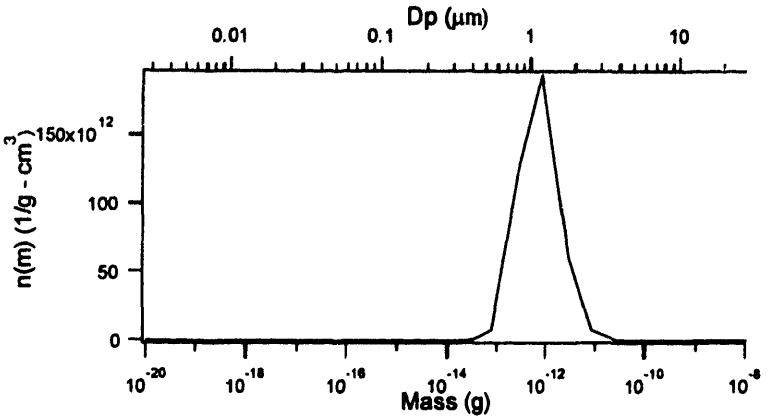

Figure 10-14: Test numerical solution for growth and nucleation with increased σ value.

the experimental data and further emphasizes the need for accurate nucleation models.

In fact, it is possible to analyze the experimental data given in Figure 10-1 and these analytical results to estimate the number of particles. For the experimental data at the highest temperature point (410 K, see Figure 10-1), it is possible to estimate the total number of particles in the distribution using the following pieces of information:

1. the initial gas is initially assumed to be saturated at a concentration of $.65\times10^{-6}$ g/cm^3

2. the mean particle mass lies between 10^{-13} and 10^{-11} g (the area on either side of the mean particle mass in Figure 10-1 will be equal at this point).

If mean particle mass is 10^{-13} g and the total mass of all the particles is $.65\times10^{-6}$ g/cm^3, then there must be $3.65\times10^{-6}/1.0\times10^{-13}$, or 3.65×10^{7} total particles per cm^3. This represents the upper limit total particles. A similar calculation for the case where the mean mass is 10^{-11} g reveals that the lower limit for total particles is 3.65×10^{5}. However, the data in Table 10-2 indicates that 3.26×10^{5} particles are present in the analytical solution. Thus, the experimental system contains up to two orders of magnitude more particles than are produced in the numerical model. However, because the total number of particles are conserved in the nucleation and growth model, this shortfall in particles must be produced by a shortfall in the nucleation rate. In the case where coagulation is occurring at an appreciable rate in the experimental system, this shortfall is even more pronounced. A similar analysis for the case of increased σ results in a mean particle mass of roughly 10^{-12} and therefore a total number density of roughly 3.65×10^{6}, which is closer to the experimental value.

In order to address these discrepancies in nucleation rates, techniques such as parameter estimation and model discrimination can be applied to rigorously optimize such imbedded parameters as σ. Because the hybrid scaling method results in fast solution times, both parameter estimation and model discrimination studies can be completed in a reasonable amount of time.

10.6 Application Examples

10.6.1 Optimal seeding of batch crystallization

In industrial practice, the majority of particle processes do not rely on nucleation for the creation of particles, but instead use seed particles as a starting point for heterogeneous nucleation and growth. Examples of seed-initiated growth processes include colloid processing (Dushkin, 2000) and crystallization. The seed particles represent an initial condition for the growth problem and have a strong influence on the final shape of the particle number density distribution (Chung et al., 1999). In order to determine the optimal seed particle number density distribution, an inversion problem must be solved; this requires a fast and accurate numerical solution of the population balance.

10.6.2 Condensation nucleation counters

The ability to produce nucleation and growth solutions over many of orders of magnitude directly impacts a large range of population balance applications. One example is the application to condensation nucleation counters (CNC's). Direct particle sizing methods can typically only measure particles down to the 10 - 20 nm size range; in order to measure particles smaller than this, condensation nucleation counters are employed (see Figure 10-15). These counters pass the sampled particles through a condenser to increase their size up to the measurable range, then invert a growth model of the condenser to infer the original distribution of particles entering the CNC. By utilizing the scaling methods developed here, the growth model for the CNC can be solved much faster than with conventional methods, allowing decreased computation time for estimating the initial distribution and, as a result, increased sampling rates and/or an increased sample measurement range.

10.7 Summary

Current numerical solutions of population balance models are generally either restricted to a

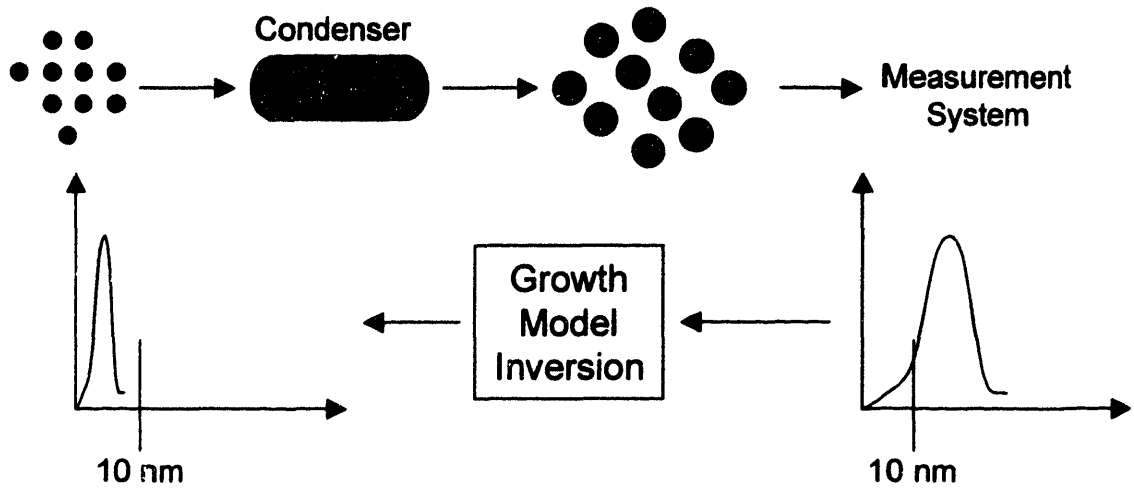

Figure 10-15: Condensation nucleation counter grows particles by passing them through a condenser until they reach a measurable size, then inverts a growth model to estimate the original particle size of the particles.

limited selection of growth laws or limited solution range. This lack of modeling ability generally precludes the accurate and/or fast solution of the entire class of problems involving simultaneous nucleation and growth, and limits the solution domain for these systems to just one or two orders of magnitude. However, using insights into the numerical stability limits of the governing equations for growth, it is possible to develop new node point placement schemes which reduce the solution times and increase the solution domains by orders of magnitude. In particular, the r - scaling method has been developed for growth rate laws of the form:

$$G(m) = K \cdot m^{1/3} \tag{10.22}$$

In addition, hybrid methods have been developed to improve the resolution of the r - scaling method while minimizing the negative impact on the maximum time step, and therefore minimizing the increase in solution times. This same framework can in fact be used to develop optimal node point scaling for any arbitrary growth law by using the relationship:

$$\int_0^{\lambda} d\lambda = \int_{m_{min}}^{m} \frac{dm}{\gamma G(m)} \tag{10.23}$$

which determines the algebraic relationship between the new optimized scaling coordinate λ and the mass-scaled coordinate m. Finally, these scaling methods are trivially extendable to the multicomponent governing equations used in the multicomponent split composition distribution

method (Resch, 1995), where the growth rate expression takes the form:

$$\frac{\partial q_i(m)}{\partial t} = -\frac{\partial\left(\partial q_i(m)\sum_j G_j(m)\right)}{\partial m} + \frac{\sum_j q_j(m)}{m} G_i(m) \tag{10.24}$$

which results in the same stability condition for the timestep:

$$\Delta t \leq \frac{\Delta m}{G(m)} \tag{10.25}$$

References

[1] Alvarez, Jesús; Alvarez, José; Hernández, Martín *A Population Balance Approach for the Description of Particle Size Distributions in Suspensioni Polymerization Reactors.* Chemical Engineering Science **49**(1), 99-113, 1994.

[2] Berndt, T.; Böge, O.; Conrath, T.; Stratmann, F.; Heintzenberg, J. *Formation of New Particles in the system H_2SO_4 (SO_3) / H_2O / (NH_3) - First Results from a Flow-Tube Study,* Journal of Aerosol Science, **31**(Supplement 1), S554-S555, 2000.

[3] Chung, Serena H.; Ma, David L.; Braatz, Richard D. *Optimal Seeding in Batch Crystallization.* Canadian Journal of Chemical Engineering, **77**, 590-596, 1999.

[4] Dushkin, C. D.; Saita, S.; Yoshie, K., Yamaguchi, Y. *The Kinetics of Growth of Semiconductor Nanocrystals in a Hot Amphiphile Matrix,* Advances in Colloid and Interface Science, **88**, 37-78, 2000.

[5] Fabry, Frédéric; Flamant, Gilles; Fulcheri, Laurent *Carbon Black Processing by Thermal Plasma. Analysis of the Particle Formation Mechanism,* Chemical Engineering Science, **56**, 2123-2132, 2001.

[6] Katoshevski, David; Seinfeld, John. H. *Analytical Solution of the Multicomponent Aerosol General Dynamic Equation - without Coagulation,* Aerosol Science and Technology, **24**(7), 541-549, 1997.

[7] Katoshevski, David; Seinfeld, John H. *Analytical - Numerical Solution of the Multicomponent Aerosol General Dynamic Equation - with Coagulation,* Aerosol Science and Technology, **24**(7), 550-556, 1997.

[8] Kim, Yong P.; Seinfeld, John H. *Simulations of multicomponent aerosol condensation by the moving sectional method,* Journal of Colloid and Interface Science, **135**, 185, 1990.

[9] Leubner, Ingo H. *Particle Nucleation and Growth Models,* Current Opinion in Colloid & Interface Science **5**, 151-159, 2000.

[10] Pantelides, Constantinos C.; Oh, Min *Process Modelling Tools and Their Application to Particulate Processes,* Powder Technology **87**, 13-20, 1996.

[11] Pilinis, Christodoulos *Derivation and Numerical Solution of the Species Mass Distribution Equations for Multicomponent Particulate Systems,* Atmospheric Environment, **24A**(7), 1923-1928, 1990.

[12] Resch, Timothy J. *A Framework for the Modeling of Suspended Multicomponent Particulate Systems with Applications to Atmospheric Aerosols,* Ph.D. Thesis, Massachusetts Institute of Technology, 1995.

[13] Strang, Gilbert *Introduction to Applied Mathematics*, Wellesley Cambridge Press, 1986.

Chapter 11: Conclusions and Directions for Future Research

11.1 Conclusions

Current numerical solutions of population balance models are generally either restricted to limited selection of growth laws or limited solution range. This lack of modeling ability generally precludes the accurate and/or fast solution of the entire class of problems involving simultaneous nucleation and growth, and limits the solution domain for these systems to just one or two orders of magnitude. However, using insights into the numerical stability limits of the governing equations for growth, it is possible to develop new node point placement schemes which reduce the solution time by orders of magnitude (see Chapter 10). These new solution methods enable a

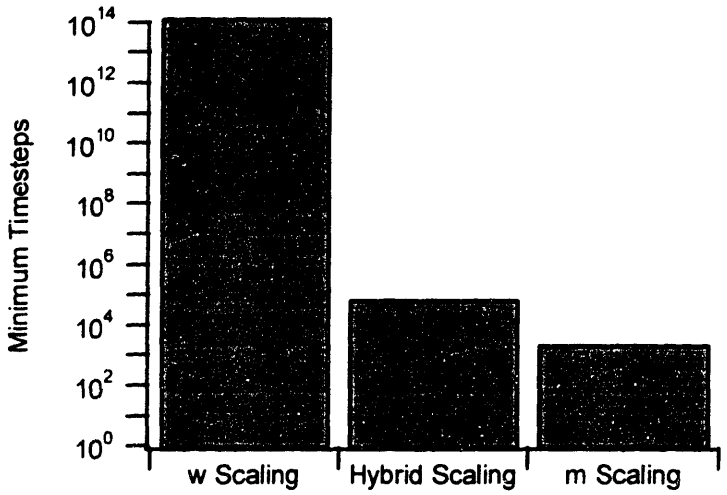

Figure 11-1: Minimum number of timesteps for 1 second solution time as a function of scaling method.

wide range of applications including:

-fundamental model refinement
-condensation nucleation counters and other measurement systems
-estimation of optimal seed crystal distributions

Because these scaling methods are directly applicable to the split composition distribution method (see Chapters 7 and 8), they can readily be extended to multicomponent systems. In this sense, the combined scaling techniques with the Split Composition Distribution method form a frame-

work for the efficient and accurate solution of multicomponent population balance problems over many orders of magnitude.

Currently the dynamics of particle formation is poorly understood. For instance, classical nucleation theory is widely acknowledged to poorly represent the nucleation processes in a large variety of systems (Berndt et al., 2000; Fabry et al., 2001; Leubner et al., 2000). In order to test and develop new theories of particle nucleation, growth, and coagulation, more accurate models and experimental data are needed. In particular, high time-resolution data is needed for carefully controlled experimental systems, and sophisticated models are needed to study these systems. Furthermore, analytical methods are needed for comparison with numerical results. Chapters 9 and 10 present a case study of an aerosol mass spectrometer experimental system, developing a set of analytical tools to compare with numerical and experimental results. A comparison of analytical and numerical results for this system reveals that relatively monodisperse distributions are produced under conditions of nucleation and growth only, and that coagulation is insignificant under these conditions. However, comparison of the resulting experimental and numerical/analytical number density distributions reveals that the models underpredict the number of particles in the system. Because particle growth conserves the number of particles in the system, this shortfall in particles can only be due to an underprediction of the nucleation rate.

In the past, the inability of models to cover a large range of particle size prevented the development of models which could attempt to reproduce the results of these systems. The development of new scaling methods has enabled accurate modeling these experimental systems, creating the opportunity for refinement of classical nucleation theory by model discrimination and parameter estimation techniques.

Finally, the development and implementation of population balance models has been poorly treated in the literature. For the first time, this work presents all the relevant topics for understanding population balance models in one coherent document. Specifically, the following topics are presented to clarify the modeling of population balance systems:

1. number density distributions and scaling transformations
2. governing equations for single and multicomponent systems
3. implementation of these governing equations in a numerical model

In order to make these concepts clear, the concept of number density distributions is rigorously

defined in Chapter 2. The basic properties of these number density distributions forms the foundation behind the derivations of scaling transformations in Chapter 3, where the conditions for the existence of a scaling transformation are developed. This analysis enables the development of multicomponent scaling transformations, presented in this work for the first time.

The basic definition of a number density distribution is then used in Chapters 4 and 5 to derive the single- and multi-component governing equations for processes including coagulation, growth, fragmentation, and sources. The derivation also identifies a method for reducing the integration range of the multicomponent coagulation integral by a factor of ½, which significantly reduces the computational load on aerosol models.

11.2 Directions for Future Research

In order to make the most use of the advances in current methods, several directions for future research exist.

11.2.1 Testing and refinement of theoretical models

Up to now, the lack of efficient solution methods and controlled experimental systems have prohibited the development of solution methods which accurately describe simultaneous nucleation, growth, and coagulation. However, these three processes control the formation of new particles in all particulate processes. In spite of this, it is widely acknowledged that classical homogeneous nucleation theory fails to accurately describe a wide range of processes. By using the methods contained in this work, the combined coagulation, growth, and nucleation models can be efficiently solved, allowing the testing and refinement of these physical mechanisms. Using carefully controlled experimental systems such as aerosol mass spectrometer and flow tube developed by Aerodyne (see Chapter 9), experimental results can now be directly compared with numerical solutions. Using the scale analysis tools developed in chapters 6, 9, and 10, experiments can be designed to decouple the effects of nucleation, growth, and coagulation.

11.2.2 Numerical analysis of the coagulation and fragmentation kernels

While a wealth of numerical stability and error analysis is available to describe hyperbolic terms describing particle growth, little analysis is available to describe the stability and error conditions of the integral terms. This analysis desperately needs to be performed to establish concrete stability limits for systems involving coagulation and fragmentation.

11.2.3 Improvements in the split composition distribution method

Up to this point, the convergence properties of the Wiener expansion in the split composition distribution have not been studied. Higher-resolution multicomponent number density experimental data is needed to determine:

1. which set of basis functions is most appropriate for the Wiener expansion
2. the rate of convergence for the Wiener expansion as new terms are added.

These data will provide the basis for testing the split composition distribution method against experimental results, and determine the ability of this method to accurately describe the full range of possibilities between internally mixed and externally mixed aerosols.

11.2.4 Development of fully integrated population balance solution

In spite of the utility of the split composition distribution method for multicomponent systems, it has yet to find widespread use. This can largely be attributed to the difficulty in understanding the Wiener expansion methods for describing composition variations. While this document has attempted to present the split composition method clearly, the level of programming skills and mathematical understanding required to manipulate this method effectively is far too high. Furthermore, the programming tools which have been developed for the split composition distribution method use antiquated programming approaches and are difficult to maintain for even an expert user. An object-oriented programming framework for population balances will improve maintainability and facilitate the development of new algorithms and modeling techniques. Finally, the implementation of an imbedded algorithm to generate the governing equations for the Wiener expansion terms will enable the widespread use of the split composition distribution method.

References

[1] Berndt, T.; Böge, O.; Conrath, T.; Stratmann, F.; Heintzenberg, J. *Formation of New Particles in the system H_2SO_4 (SO_3) / H_2O / (NH_3) - First Results from a Flow-Tube Study,* Journal of Aerosol Science, **31**(Supplement 1), S554-S555, 2000.

[2] Fabry, Frédéric; Flamant, Gilles; Fulcheri, Laurent *Carbon Black Processing by Thermal Plasma. Analysis of the Particle Formation Mechanism,* Chemical Engineering Science, **56**,

2123-2132, 2001.

[3] Leubner, Ingo H. *Particle Nucleation and Growth Models,* Current Opinion in Colloid & Interface Science **5**, 151-159, 2000.

Appendix A: Case Study of a Pressure Swing Adsorption System

A.1 Introduction

Since the inception of pressure swing adsorption (PSA) systems and their subsequent implementation in industrial processes beginning with Skarstrom's cycle (Skarstrom, 1960), a prolific number of new PSA cycles have been developed (Jasra et al., 1991; Ruthven et al., 1994; Yang, 1987) in parallel with a family of model simulations for these processes (Ruthven et al., 1994; Yang, 1987). Today, PSA processes are not only used in industrial applications, but also in military, commercial and home applications. Among air separation applications alone, PSA systems are widely used to produce oxygen for the crew in military aircraft (Teague and Edgar, 1999), to provide an on-board source of enriched air on scuba diving vessels (Rossier, 1999), and to provide oxygen at home for persons with lung diseases. Modern PSA systems often operate on a complex cycle and rely on a complex system of valves to control flow throughout the cycle. Modeling efforts use this information to decouple individual adsorption beds, allowing accurate description of the process with a relatively simple model.

Recently, a new PSA process has been developed which operates without any valves. While this process promises to offer reduced maintenance and increased reliability, the lack of an externally-controlled pressure cycle results in a much more complex process model than conventional models require. This paper presents a model which meets the rigorous demands of dynamically describing this valveless process. While some modern PSA models have described complex cycles (Malek and Farooq, 1997), most of these models do not employ strict conservation of mass across system boundaries (Teague and Edgar, 1999). This model combines a complex process cycle with rigorous implementation of boundary conditions to accurately solve for pressure histories in the adsorption beds. Results indicate that strict conservation of mass is the most critical criterion for accurately describing the dynamics of such a complex PSA cycle.

From the very first PSA patents in the late 1920's and early 1930's (Hasche and Dargan, 1931; Finlayson and Sharp, 1932; Perley, 1933) up until the current day, essentially all PSA systems have used valves. The valving systems used in modern PSA systems channel air through networks of adsorption beds in order to repeatedly saturate, regenerate, and sometimes equalize

adsorption beds. A PSA process operating on a complex cycle may have more then 30 valves (Malek and Farooq, 1997) and 10 or more adsorption beds (Fuderer and Rudelstorfer, 1976). While valves allow precise control of flow and pressure in the process, they also require maintenance and proper control algorithms. From a modeling perspective, valves have the added benefit of simplifying many PSA process models by decoupling the interactions between adsorption beds. Many studies such as Malek and Farooq (1997) use this decoupling to simplify process models, allowing the adsorption beds to be simulated individually using boundary information from columns at other stages of the PSA cycle. However, PSA cycles which contain equalizing columns cannot be completely decoupled and present several challenges: 1) properly coupling flow between the equalizing columns, 2) rigorously conserving mass, and 3) solving for the correct pressure equalization profile. While recent models have taken into account the effects multiple components (Chlendi, Tondeur, and Rolland, 1995) or nonisothermal conditions in a multibed process (Malek and Farooq, 1997), these models make assumptions which fail to conserve mass (Malek and Farooq, 1997; Budner et al., 1999) by assuming a pressure relationship between two equalizing adsorption beds of the form given in Equation (A.1).

$$\frac{dP_1}{dt} = -k(P_1 - P_2) \quad P_1 > P_2 \tag{A.1}$$

This assumption is made to avoid the added computational cost associated with implementing rigorous flow boundary conditions between the adsorption beds, however, it leads to incorrect results, including false pressure and velocity profiles, and incorrect product purity information.

A novel new PSA process has been developed and is currently used for medical oxygen as well as a variety of commercial applications (Hill, 1992). While this cycle is essentially a Skarstrom cycle with one equalization step added (see Figure A-1) the process is fundamentally different in how the individual adsorption beds are connected. Unlike conventional PSA processes, flow between adsorption beds is not controlled by valves, but rather through a set of open orifices which connect the adsorption beds at their product side to a common product collection vessel and a channeled rotor (see Figure A-2). Because the channeled rotor is the only moving part within the PSA unit, this process exhibits much higher reliability than conventional processes (Hill, 1992). Two banks of six beds each operate in parallel on a six-stage cycle to produce oxygen from a compressed air inlet stream. While this open-orifice configuration significantly sim-

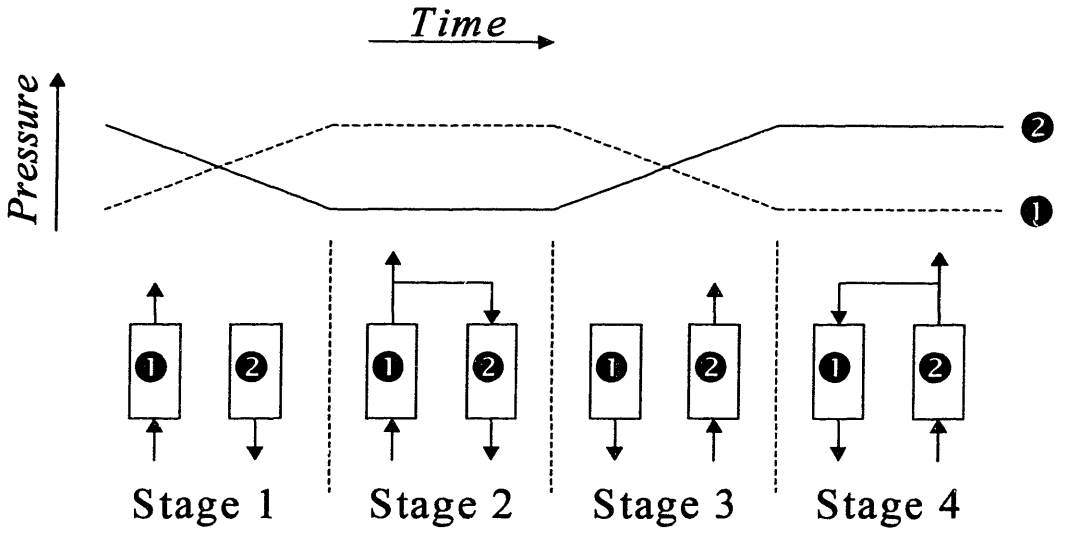

Figure A-1: Pressure swing adsorption cycle with one equalization stage.

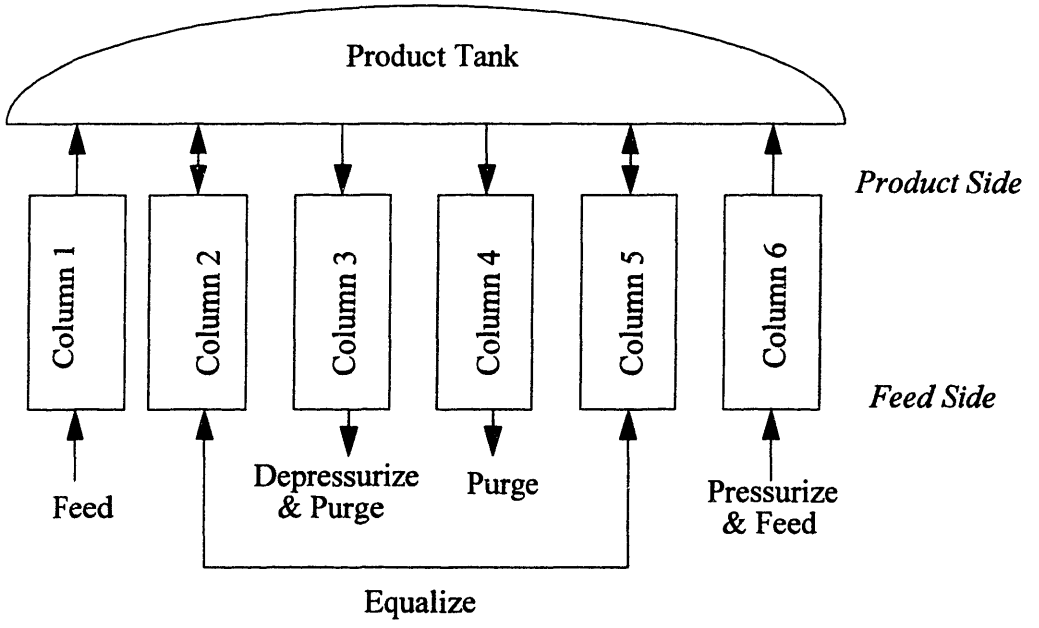

Figure A-2: Arrangement of adsorption beds in PSA unit.

plifies the mechanics and controls for this PSA system, it also opens many new degrees of freedom in its conceptual model and greatly increases the complexity of numerical solution. Typical PSA models rely on well-defined control of the overall PSA cycle to decouple the various adsorption columns. In many cases, this reduces the model to include just one adsorption column which needs to reach a cyclic steady state. Furthermore, the system of equations is often a linear set of differential algebraic equations (Ruthven et al., 1994). In contrast, because this new pro-

cess has continuously connected product tanks and adsorption beds with dynamically varying boundary conditions, the model for this PSA system requires simultaneous solution of a system of equations including all of the adsorption columns and the product tank. In addition, two columns in the process are always equalizing, requiring the solution of an additional nonlinear set of equations to rigorously determine the pressures in these beds. Finally, the time-scales over which the adsorption columns pressurize and depressurize differ greatly from the time scales characteristic of the product tank, creating a system of stiff nonlinear differential algebraic equations (DAEs).

A mathematical model for this new PSA process is presented and solved under a variety of process conditions. The existence of multiple steady states is demonstrated and the rationale behind the existence of these steady states explained. Experimental results are compared with the simulation output under a range of conditions.

A.2 PSA Process Description

The PSA process consists of twelve pressure swing adsorption (PSA) beds, or columns, arranged such that two banks of six columns are simultaneously performing the same PSA cycle (see Figure A-2). At the end of each cycle, the columns rotate to new positions, as shown in Table A-1. Flow on the product side of the columns is restricted by an orifice, while flow on the feed

Table A-1: Column Rotation

Old Position		New Position
Column 1	→	Column 2
Column 2	→	Column 3
Column 3	→	Column 4
Column 4	→	Column 5
Column 5	→	Column 6
Column 6	→	Column 1

side of the columns is channeled through a rotor. The rotor exposes each adsorption bed to high pressure feed air, ambient air, and a pressure-equalizing adsorption bed as it moves through the PSA cycle. A sample pressure profile through all six positions is sketched in Figure A-3.

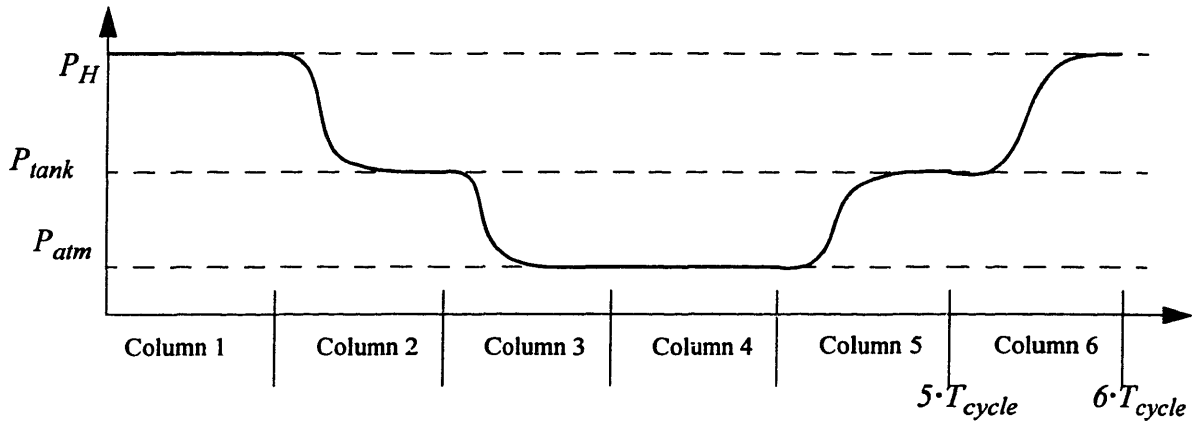

Figure A-3: Example pressure profile over process cycle.

An adsorption column which starts off in the "Column 1" position is being fed at high pressure. When it reaches the Column 2 position it will equalize in pressure with the bed in the Column 5 position. During the next step as Column 3, it will blow down to atmospheric pressure and then purge through its entire tenure as Column 4. Upon reaching the Column 5 position, the adsorption bed will gain pressure as it equalizes with Column 2. Finally, the column will completely repressurize and start high pressure feed while at the Column 6 position before returning back to the Column 1 position. Table A-2 summarizes the cycling process for each column.

Table A-2: PSA Cycle Summary

Column	Stage 1	Stage 2	Stage 3	Stage 4	Stage 5	Stage 6
1	High Pressure Feed	Equalization	Blowdown & Purge	Purge	Equalization	Pressurization & Feed
2	Equalization	Blowdown & Purge	Purge	Equalization	Pressurization & Feed	High Pressure Feed
3	Blowdown & Purge	Purge	Equalization	Pressurization & Feed	High Pressure Feed	Equalization
4	Purge	Equalization	Pressurization & Feed	High Pressure Feed	Equalization	Blowdown & Purge
5	Equalization	Pressurization & Feed	High Pressure Feed	Equalization	Blowdown & Purge	Purge
6	Pressurization & Feed	High Pressure Feed	Equalization	Blowdown & Purge	Purge	Equalization

Product gas flows into the product tank from the feed columns. Some of this product gas is withdrawn as product at a regulated flowrate; the remaining gas exits as it purges columns 3 and 4.

A.3 Mathematical Model

Pressure gradients across orifices govern the flowrate in each column. Flow through each orifice is described by the orifice equation (Geankoplis, 1993) and shown in Equation (A.2):

$$u_0 = \frac{C_0}{\sqrt{1-\left(\frac{D_0}{D_1}\right)^4}}\sqrt{\frac{2(P_1-P_2)}{\rho}} \tag{A.2}$$

where the diagram in Figure A-4 clarifies some of the variable names.

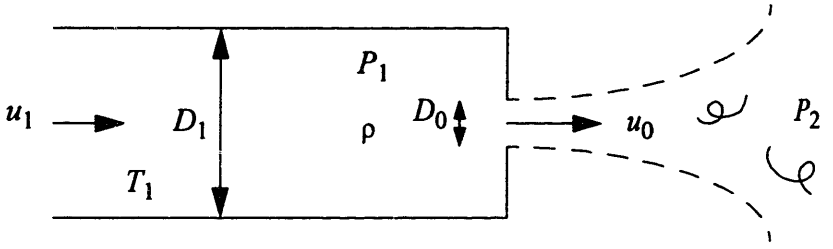

Figure A-4: Orifice configuration and relevant variables.

In order to conserve mass across all orifices, the mass flowrate is required to be constant according to the relationship given in Equation (A.3), in conjunction with the requirement that the composition of the gas is identical on both sides of the orifice.

$$u_0 P_0 A_0 = u_1 P_1 A_1 \tag{A.3}$$

P_1, D_1, T_1, ρ, and u_1 are the pressure, diameter, temperature, density, and superficial velocity of the gas in the tube, respectively. u_0 is the superficial velocity of gas through the orifice, D_1 is the orifice diameter, and P_2 is the pressure of the gas at the outlet. Pressure is assumed to equilibrate instantaneously throughout the entire column, as confirmed with preliminary calculations using the Ergun equation. A generalized Langmuir isotherm, commonly referred to as a competitive Langmuir isotherm, is used to describe adsorbent equilibrium.

$$\frac{q_i^*}{q_{is}} = \frac{b_i c_i}{1+\sum_j b_j c_j} \tag{A.4}$$

The following assumptions are used in the development of the mathematical model:

1. The adsorption column is assumed to be isothermal. This was justified by experimental results confirming that no significant heating of product gas occurred.

2. The ideal gas law applies to this system.

3. Columns which are depressurizing or pressurizing follow either a logistic growth or exponential model pressure profile. These are just two of many possible pressure profiles that could be used. The logistic growth model is useful because it is a second order model with derivatives of zero as $t \to 0$ or $t \to \infty$. The differential equation and algebraic solution of the logistic growth model for the $N_0 > K/2$ case along with the shape of the solution for both cases are shown in Figure A-5. Specifically, stage 2 columns follow an exponential pressure decay, while columns in stages

$$N_0 > \frac{K}{2}:$$

$$\frac{dN}{dt} = rN\left(1 - \frac{N}{k}\right)$$

$$N(t) = \frac{N_0 K e^{rt}}{K + N_0(e^{rt} - 1)}$$

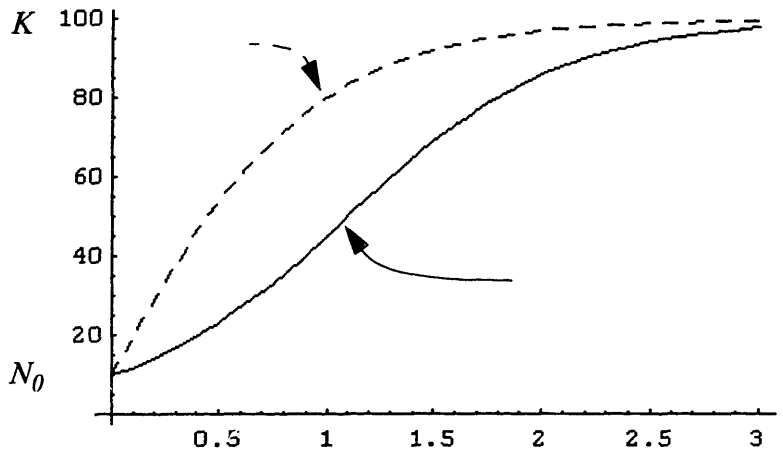

Figure A-5: Logistic growth model used for pressure profile in columns.

four and six follow a logistic growth model. Stage 5 columns require special treatment and will be addressed later.

4. The composition of air is assumed to be as shown in Table A-3.

Table A-3: Air Composition

Component	Mole Fraction
N_2	0.78
O_2	0.22

Two equations govern the behavior of a pressure swing adsorption column with two components: the mass balance and the component balance for one species, listed respectively in Equations (A.5) and (A.6).

$$\varepsilon\left\{-D_L\frac{\partial^2 C}{\partial z^2}+\frac{\partial}{\partial z}(uC)+\frac{\partial C}{\partial t}\right\}+(1-\varepsilon)\sum_{j=1}^{n}\frac{\partial \bar{q}_j}{\partial t}=0 \tag{A.5}$$

$$\varepsilon\left\{-D_L\frac{\partial^2 c_i}{\partial z^2}+\frac{\partial}{\partial z}(uc_i)+\frac{\partial c_i}{\partial t}\right\}+(1-\varepsilon)\frac{\partial \bar{q}_i}{\partial t}=0 \tag{A.6}$$

The linear driving force (LDF) model (Glueckauf and Coates, 1947; Glueckauf, 1955) is used as a lumped mass transfer model, where the rate of mass transfer is proportional to the difference between the concentration on the adsorbent and the equilibrium concentration, q_i^*.

$$\frac{\partial \bar{q}_i}{\partial t}=k_i(q_i^*-\bar{q}_i) \tag{A.7}$$

Substituting the generalized Langmuir isotherm yields the solid phase component balance.

$$\begin{aligned}\frac{\partial x_{O_2}}{\partial t}&=k_{O_2}\left(\frac{\beta_{O_2}y_{O_2}}{1+\beta_{O_2}y_{O_2}+\beta_{N_2}y_{N_2}}-x_{O_2}\right)\\ \frac{\partial x_{N_2}}{\partial t}&=k_{N_2}\left(\frac{\beta_{N_2}y_{N_2}}{1+\beta_{O_2}y_{O_2}+\beta_{N_2}y_{N_2}}-x_{N_2}\right)\end{aligned} \tag{A.8}$$

The gas phase component balance for this case is derived by manipulating Equation (A.6).

$$\frac{\partial y}{\partial t}=D_L\frac{\partial^2 y}{\partial z^2}-u\frac{\partial y}{\partial z}+\frac{\psi}{P}\left((y-1)\frac{\partial x_{O_2}}{\partial t}+y\gamma_s\frac{\partial x_{N_2}}{\partial t}\right) \tag{A.9}$$

Likewise, the gas phase mass balance is derived from Equation (A.5).

$$\frac{\partial u}{\partial z}=-\frac{1}{P}\frac{\partial P}{\partial t}-\frac{\psi}{P}\left(\frac{\partial x_{O_2}}{\partial t}+\gamma_s\frac{\partial x_{N_2}}{\partial t}\right) \tag{A.10}$$

A different mass balance and composition balance are required to describe the evolution of pressure and composition within the product tank, which is assumed to be well-mixed.

$$\frac{dP_T}{dt}=\frac{RT}{V_T}\sum_{i=1}^{6}\frac{u_{Ni}A_iP_i}{RT}-\frac{v_{prod}P_{atm}}{V_T}=\frac{\sum_{i=1}^{6}u_{Ni}A_iP_i}{V_T}-\frac{v_{prod}P_{atm}}{V_T} \tag{A.11}$$

$$\frac{dy_T}{dt} = \frac{1}{P_T V_T}\left(\sum_{i=1}^{6} u_{Ni} A_i P_i y_{Ni} - v_{prod} P_{atm} y_T\right) - \frac{y_T dP_T}{P_T dt} \tag{A.12}$$

In these governing equations, P_T, V_T, y_T, and T are product tank pressure, volume, mole fraction of oxygen, and temperature, respectively. A_i is the cross-sectional area of each bed which is open to flow, v_{prod} is the volumetric product flowrate, P_{atm} is the ambient (atmospheric) pressure, and u_{Ni} and y_{Ni} denote the composition and flowrate at the orifice of column i.

To completely specify the governing equations, two boundary conditions are required for the gas phase composition Equations (A.9) and (A.12), while one boundary condition is required to solve the velocity Equations (A.10) and (A.11). The composition boundary conditions are treated as follows. At all boundaries where gas is flowing into a column, the boundary composition is set at the composition of the incoming gas; at all boundaries where gas is flowing out of a column, the system is treated as being convection-dominated and the dispersive term is dropped. Naturally, the velocity boundary conditions are given by Equation (A.2), which specifies the velocity at the orifice. However mass must be conserved in the flow between columns 2 and 5 when they are equalizing. This is accomplished by requiring that the pressure-adjusted flowrate leaving column 2 is equal to the pressure-adjusted flowrate entering column 5.

$$P_2 u|_{z=0,\,\text{column 2}} = -P_5 u|_{z=0,\,\text{column 5}} \tag{A.13}$$

This additional condition overspecifies the boundary conditions for column 5, as illustrated in Figure A-6.

In order to meet this extra condition, an additional degree of freedom - pressure - must be granted to the equations governing column 5. Because the pressure in column 5 is not explicitly given by any of the governing equations, the nonlinear system of equations relating bed pressure to outlet velocity must be solved independently. However, inspection of Equation (A.10) reveals that as *dP/dt* varies in the adsorption bed, the inlet velocity will vary monotonically. That is, the faster the pressure increases in an adsorption bed, the faster air will need to enter the bed. Using this fact, it is possible to implement an efficient and stable interval halving search which converges rapidly to the correct pressure in the repressurizing adsorption bed.

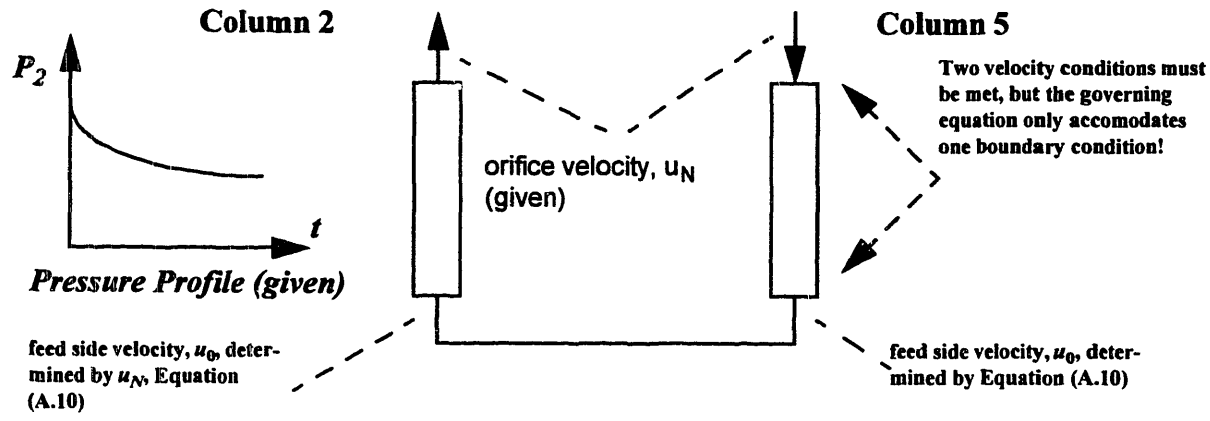

Figure A-6: Simultaneous calculation of pressure and velocity in equalizing columns 2 & 5.

A.4 Numerical Implementation

The governing partial differential equations were converted to a set of ordinary differential equations by the method of orthogonal collocation on finite elements (see Figure A.7), which represents the solution as a series of cubic splines on elements representing subdomains of the entire solution domain. By solving the system of governing equations at nodes within each element placed at the root of the local orthogonal polynomial, the error in the solution is minimized (Villadsen and Michelsen, 1978; Finlayson, 1972). Using matrices $\mathbf{BA^{-1}}$ and $\mathbf{CA^{-1}}$ to represent operator matrices for the first and second derivatives, respectively, the system of converted ordinary differential equations may be represented in matrix form.

$$\frac{dx_{O_2,i}}{dt} = k_{O_2}\left(\frac{\beta_{O_2} y_i}{1+\beta_{O_2} y_i + \beta_{N_2}(1-y_i)} - x_{O_2}\right)$$

$$\frac{dx_{N_2,i}}{dt} = k_{N_2}\left(\frac{\beta_{N_2}(1-y_i)}{1+\beta_{O_2} y_i + \beta_{N_2}(1-y_i)} - x_{N_2}\right) \qquad i = 1, \ldots, N \qquad \text{(A.14)}$$

$$\frac{dy_i}{dt} = D_L \sum_{j=1}^{N} y_j (\mathbf{CA^{-1}})_{i,j} - u_i \sum_{j=1}^{N} y_i (\mathbf{BA^{-1}})_{i,j} + \frac{\psi}{P}\left((y_i - 1)\frac{dx_{O_2,i}}{dt} + y_i \gamma_s \frac{dx_{N_2,i}}{dt}\right) \qquad i = 1 \text{(A.15)}$$

$$\sum_{j=1}^{N-1} u_i (\mathbf{BA^{-1}})_{i,j} = -\frac{1}{P}\frac{dP}{dt} - \frac{\psi}{P}\left(\frac{dx_{O_2,i}}{dt} + \gamma_s \frac{dx_{N_2,i}}{dt}\right) - u_N (\mathbf{BA^{-1}})_{i,N} \qquad \text{(A.16)}$$

The above system of equations describes one PSA bed only; the full set of equations is a block diagonal system consisting of the above set of equations for each bed, augmented by terms and equations describing the connectivity of each bed. The DASSL time step integration package is used to numerically integrate the system of differential equations, using a backwards differentiation formula (BDF) method (Petzold, 1982). Note that at each time step, several challenges exist:

1) because the pressure of the product tank varies freely, columns which are pressurizing or depressurizing may experience a change in flow direction through the orifice. Controls are necessary to monitor flow direction and ensure that the correct boundary conditions are maintained.

2) for each time step, many evaluations of the differential algebraic equation system are required. To evaluate the algebraic equations governing velocity, the convergence algorithm to properly match flowrates between equalizing beds 2 and 5 must be employed.

The model was run through a successive substitution convergence algorithm (see Figure A.8) until it reached cyclic steady state. Although successive substitution typically converges slower than more sophisticated algorithms, it is known for its stability, a characteristic that is highly valued in this application. In addition, evidence supporting the existence of multiple steady states in such this system requires a consistent set of initial conditions to ensure that the same steady state is reached at convergence. Typically, between 30 and 70 cycles are necessary to reach convergence, which requires between 20 minutes and an hour to simulate on a 333 MHz personal computer.

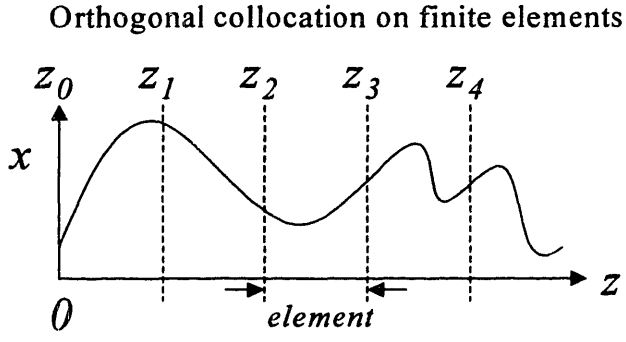

Figure A-7: Orthogonal collocation on finite elements.

A.5 Methods

Langmuir isotherm parameters were fitted using data from the adsorbent manufacturer, UOP,

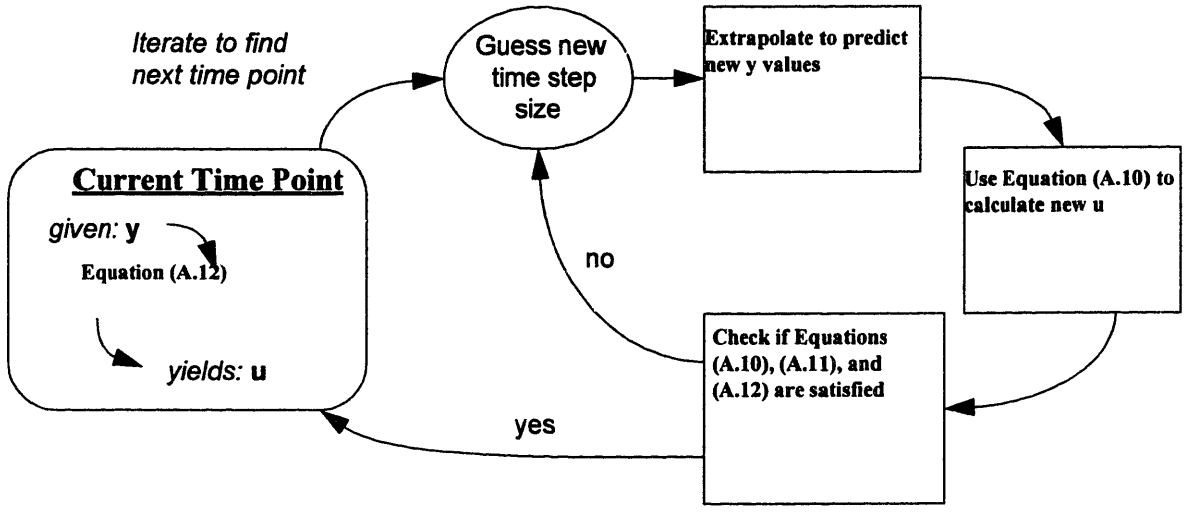

Figure A-8: Time step integration schematic.

for 5A zeolite. The parameters corresponding to the fitted isotherms are summarized in Table A-4. Note that H is the Henry's law coefficient for each component and is equal to $q_s^{\cdot} \cdot b$. In order

Table A-4: Oxygen and Nitrogen Adsorption Parameters

Component	q_s (mol/m^3)	b (m^3/mol)	H
Oxygen	4841	0.001036	5.018
Nitrogen	3055	0.003800	11.61

to maintain the most robust model possible, the velocity between equalizing columns is fixed as a function of the pressure difference between the two columns, as shown in Equation (A.17).

$$U = f(P_2, P_5)$$

$$U_2 = \frac{-Min\left\{2.0\times10^7,\ 0.1P_2\sqrt{Max(1.0-\dot{P}_5/P_2),\ 0.0}\right\}}{P_2} \tag{A.17}$$

Note that the negative sign denotes that the direction of flow is *out* of the bottom of column 2. For P_2 held constant at 130,000 Pa, the velocity out of the feed side of column 2 will vary as shown in Figure A-9.

Note that positive velocities between the two equalizing columns are not physical and are there-

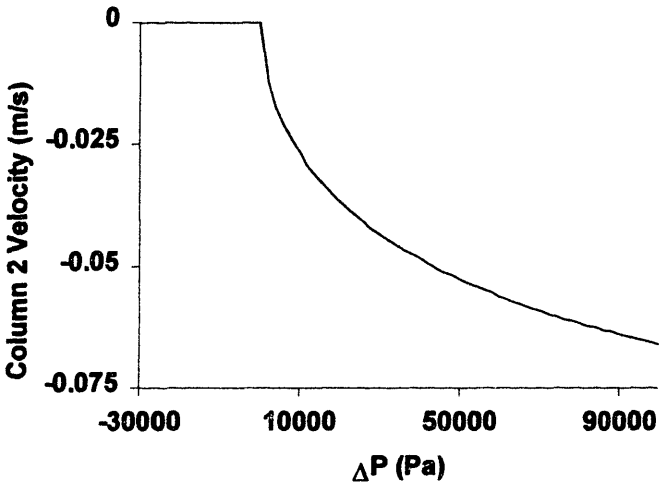

Figure A-9: Column 2 feed side velocity as a function of pressure difference with column 5.

fore eliminated to prevent numerical oscillations in velocity between the two columns. Orifices between the beds and product tanks were also characterized, with an orifice coefficient of 0.61.

A base case was established to represent the performance of the PSA unit with 14.5" adsorp-

tion beds under the most basic set of input parameters, as listed in Table A-5. Note again the feed

Table A-5: Base Case Input Parameter Values

Name	Description	Value	Units	Reference	Page
C_0	orifice discharge coefficient	0.6139	-	Experiment	
D_{tube}	tube diameter	1.438	in.	-	-
D_L	axial dispersion coefficient	2.02×10^{-3}	m^2/s	Ruthven et al., (1994)[a]	186
D_0	orifice diameter	0.029	in	-	-
ε	void fraction	0.37	-	-	-
L	column (bed) length	14.5	in	-	-
$K_{O_{22}}$	oxygen mass transfer coefficient	62.0	s^{-1}	Ruthven et al., (1994)	186
K_{N_2}	nitrogen mass transfer coefficient	19.7	s^{-1}	Ruthven et al., (1994)	186
q_{O_2s}	oxygen saturation concentration	4841	mol/m^3	Table A-4	
q_{N_2s}	nitrogen saturation concentration	3055	mol/m^3	Table A-4	
H_{O_2}	Henry's law O_2 coefficient	5.02	-	Table A-4	
H_{N_2}	Henry's law N_2 coefficient	11.6	-	Table 4	
M_w	gas phase molecular weight	3.18×10^{-2}	kg/mol	95% O_2	
P_{atm}	atmospheric pressure	30.2	psia	-	-
P_H	atmospheric pressure	14.7	psia	-	-
T	temperature	298	K	-	-
T_{cycle}	cycle time	2.5	s	-	-
V_T	tank volume	5.0×10^{-4}	m^3	-	-
y_{feed}	feed composition	0.22	-	-	-

a.This value is used to give a Peclet number of 500.

composition of $y_A = 0.22$ is used to represent the lumped mole fraction of both oxygen and argon. In order to check that solution included a sufficient number of finite elements to reach convergence, models were solved with both 5 finite elements and 10 finite elements. The results of one such run are summarized in Table A-6. Comparison of results with 5 and 10 elements indicates

Table A-6: Product Purity Comparison for 5 and 10 Finite Elements

Flowrate (lpm)	2.08	3.22	4.48	5.80	7.00	8.14
5 elements	0.939	0.935	0.93	0.924	0.918	0.912
10 elements	0.938	0.933	0.928	0.923	0.917	0.912

that 5 elements sufficiently represent the solution and thus 5 elements were used for all model solutions.

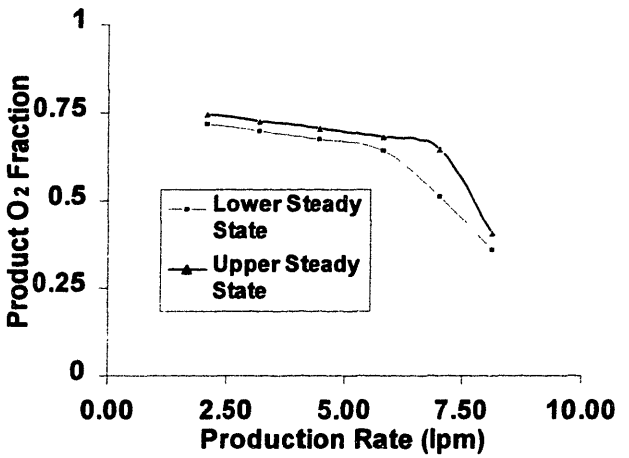

Figure A-10: Existence of multiple steady states as a function of production rate.

Initial condition effects were studied by using two different initial oxygen mole fractions, 0.22 and 0.95. It was found that under some conditions, differing initial conditions would result in different cyclic steady states, as shown in Figure A-10. The existence of multiple steady states is not uncommon for a complex nonlinear system, and can be explained by analyzing the amount of oxygen entering and leaving the PSA unit under different conditions. The product O_2 removed is related to the O_2 product purity linearly through the flowrate.

$$\text{Product } O_2 \text{ Removed} = O_2 \text{ Product Purity} \cdot \text{ Product Flowrate} \qquad \text{(A.18)}$$

Note that the shape of the "O_2 fed - O_2 purged" curve (see Figure A.11), can be deduced from computational results. First, whenever the starting composition is $y = 0.22$, the solution is at a higher composition. Therefore, the amount of O_2 removed from the system must be less than the amount of O_2 entering the system in this regime, in order to drive the model towards the stable steady state. Likewise, at y=1.0, the stable steady state solution is always at a lower composition value, indicating that the amount of O_2 removed under these conditions is greater than the amount entering the unit. Therefore, due to the linearity of the O_2 removed line, there must be *at least one* intermediate unsteady state corresponding to the point where the lines cross in between the two stable steady states. This does not preclude the existence of more steady states (more crossings of the product O_2 removed line). Also, under some operating conditions the two steady states will approach each other and merge, as illustrated in Figure A-12, to yield a set of conditions with one unique steady state.

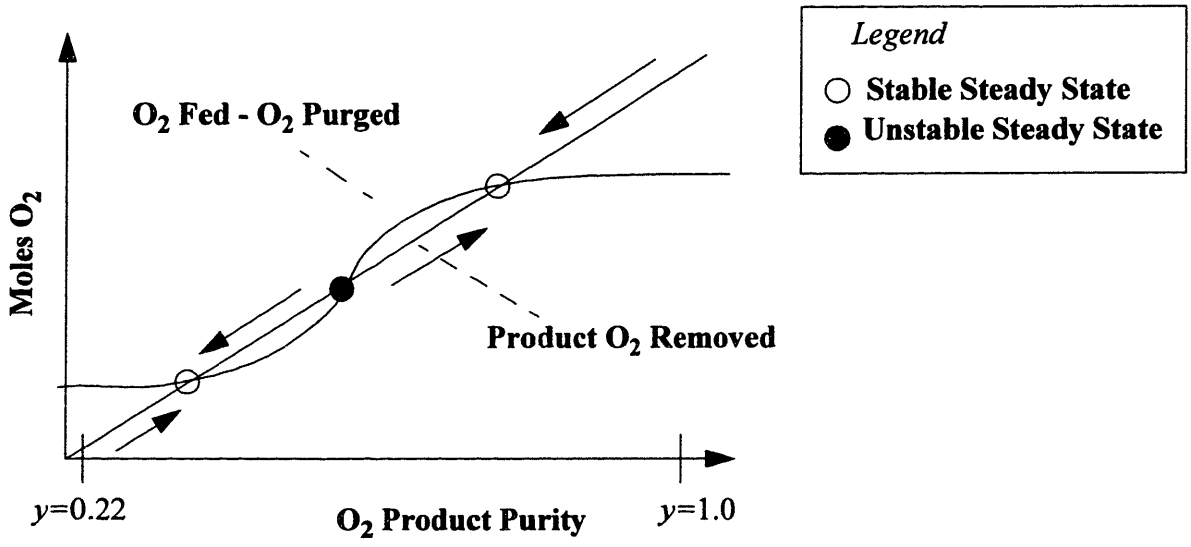

Figure A-11: Multiple steady state analysis of total O_2 balance around PSA unit comparing O_2 generated and O_2 removed.

An analogous explanation of multiple steady states in continuously stirred tank reactors (CSTR's) can be found in Fogler (1999). In order to ensure that all simulation results were reaching the same steady state, initial conditions of $y = 0.22$ were used in all simulations.

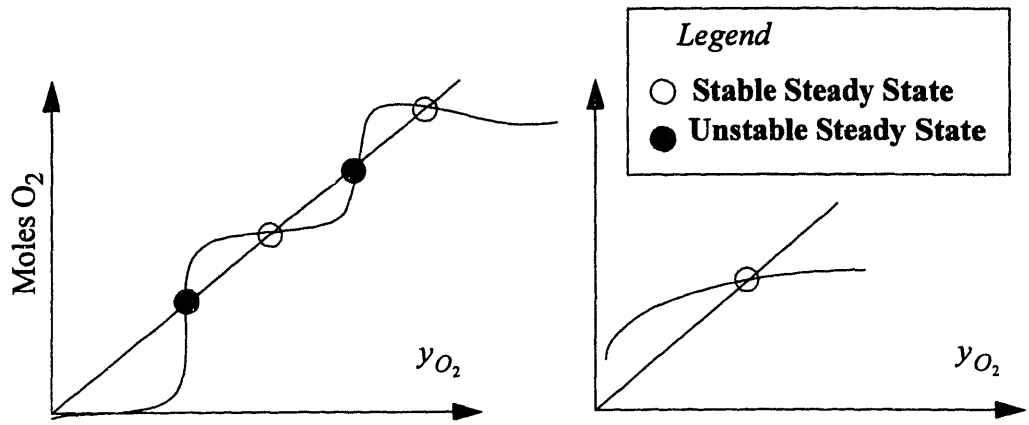

Figure A-12: Special cases of oxygen generation and removal resulting in varying numbers of stable and unstable steady states.

A.6 Results and Discussion

The base case gas phase compositions of the system throughout the steady state cycle are illustrated in Figure A-13. The corresponding product purities over the a range of production flowrates is as follows shown in Figure A.14. As can be seen from Figure A-14, the base case product purity does not degrade with increasing production rate as the experimental data indicates. Average inlet flowrates for this case range between 1.87×10^{-3} and 1.94×10^{-3} m^3/s, where experimental data report inlet flowrates ranging between 4.13×10^{-4} and 1.01×10^{-3} m^3/s. In spite of the rigorous orifice characterization and use of actual experimental values for many parameters, the inlet flowrate is still far too high. Similar results were observed with a PSA unit with reduced length 7.5" adsorption beds (see Figure A-15).

In order to reconcile these discrepancies, the effects of several important effects were studied: void fraction ε, bed efficiency, mass transfer coefficients, pressure drops between beds, orifice coefficient, and cycle time. As shown in Figure A-16, void fraction has little effect on breakthrough under base case operating conditions. It is also possible that a significant portion of adsorbent particle interiors are not active due to the amount of binder used in creating the adsorbent pellets (Breck, 1973; Teague and Edgar, 1999). In order to incorporate the effect of inactive binder in adsorbent pellets, the parameter ψ is multiplied by an "active adsorbent fraction" η, yielding Equation A.19.

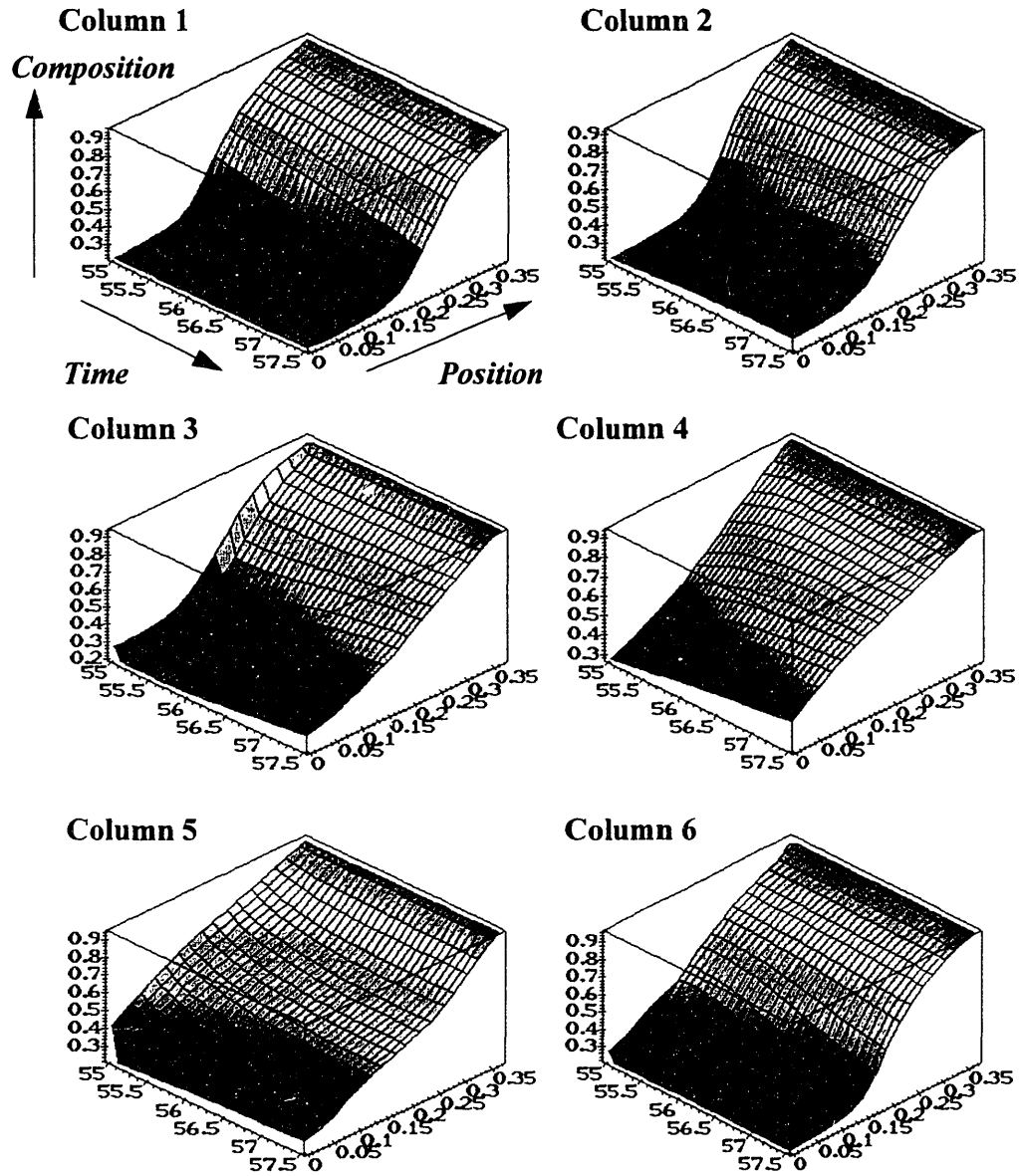

Figure A-13: Gas phase composition profiles for each column over the entire process cycle.

$$\frac{\partial u}{\partial z} = -\frac{1}{P}\frac{\partial P}{\partial t} - \frac{\eta\psi}{P}\left(\frac{\partial x_{O_2}}{\partial t} + \gamma_s \frac{\partial x_{N_2}}{\partial t}\right) \tag{A.19}$$

Furthermore, the value of $\psi = \frac{1-\varepsilon}{\varepsilon} R_g T_0 q_{O_2 s}$ in Equation (A.9) can be pre-multiplied by another factor "λ" to represent the fraction of active adsorbent which participates in mass transfer to the bulk, resulting in Equation (A.20).

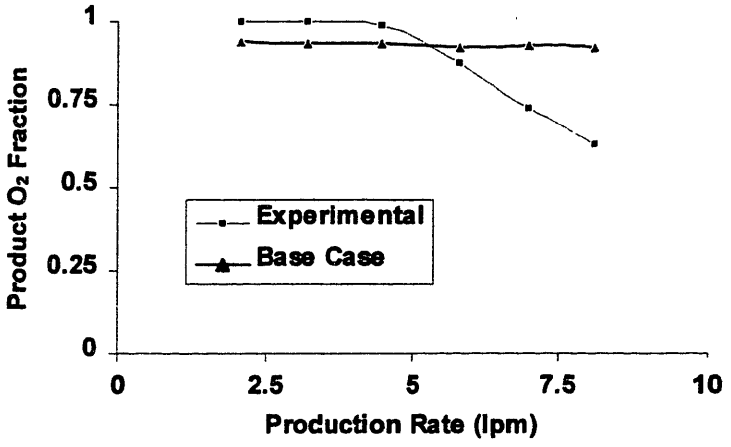

Figure A-14: Base case product purity as a function of product flowrate.

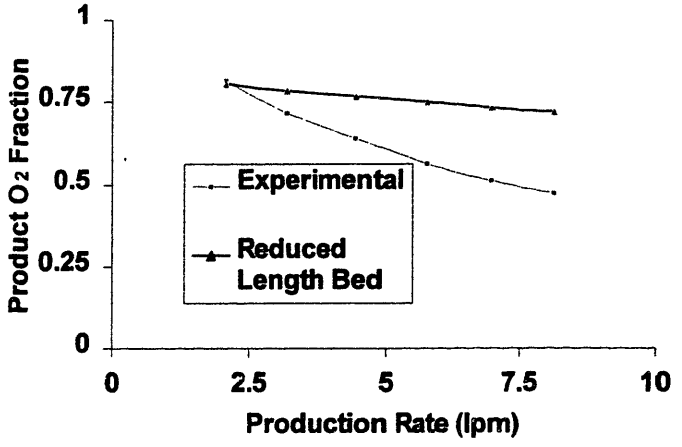

Figure A-15: Product purity as a function of product flowrate with reduced length adsorption beds.

$$\frac{\partial y}{\partial t} = D_L \frac{\partial^2 y}{\partial z^2} - u\frac{\partial y}{\partial z} + \frac{\lambda \eta \psi}{P}\left((y-1)\frac{\partial x_{O_2}}{\partial t} + y\gamma_s \frac{\partial x_{N_2}}{\partial t}\right) \tag{A.20}$$

This realistically emulates the conditions where some portion of the adsorbent particles are unable to effectively participate in mass transfer to the bulk gas. One example of how this could occur is shown in Figure A-17. Gas deep within the pores will still adsorb and desorb as the PSA systems cycles from high to low pressures, but it is effectively isolated from the bulk gas and unable to participate in mass transfer. Decreasing either of these efficiency factors decreases the

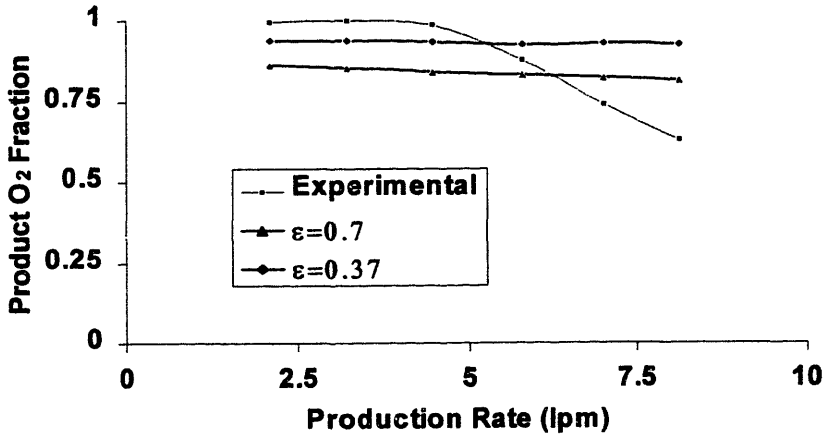

Figure A-16: Product purity as a function of production rate under varying adsorbent bed void fractions.

product purity uniformly as a function of product flowrate (see Figure A-18), yet neither make breakthrough more pronounced. Similarly, decreasing mass transfer decreased product purity, but still did not produce breakthrough as illustrated in Figure A-19.

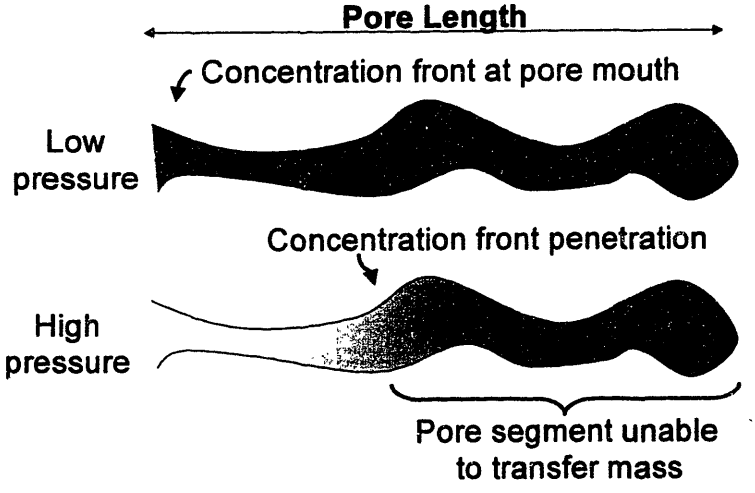

Figure A-17: Isolated pore regions with restricted mass transfer to bulk gas.

Increased pressure drops though adsorption bed connections were emulated by concurrently increasing the purge pressure and decreasing the feed pressure in the stem. Pressure drops were varied from 1 to 4 psi, but revealed only minor effects (see Figure A-20).

The effect of cycle times on the product purity was investigated at a flowrate of 5.80 lpm in the 14.5" bed PSA unit. Results are graphically summarized in Figure A-21. As cycle time

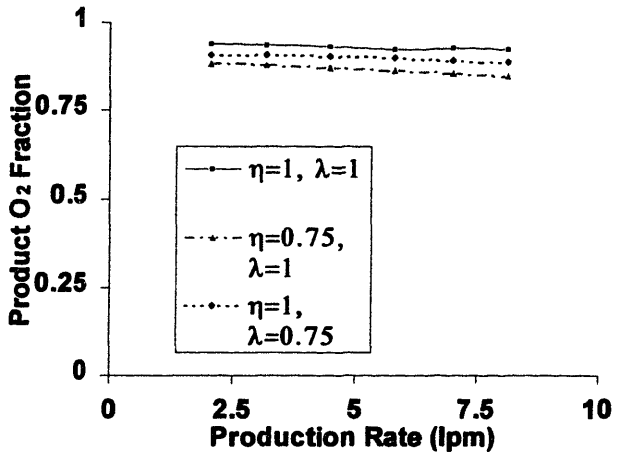

Figure A-18: Product purity vs. product flowrate at varying adsorbent efficiencies.

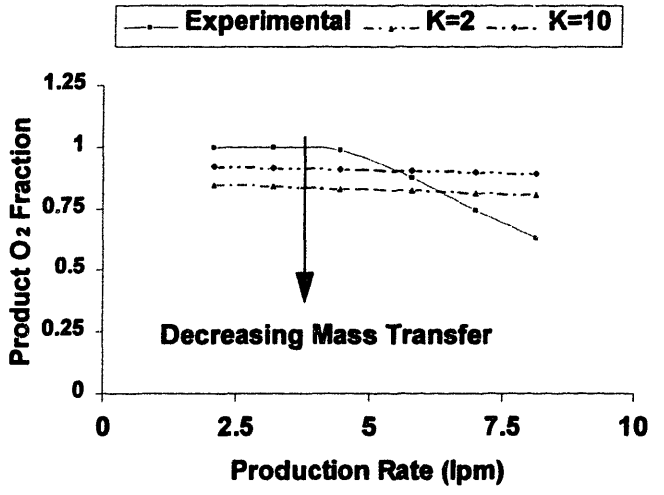

Figure A-19: Effects of mass transfer coefficient on product purity as a function of product flowrate.

increases, the amount of breakthrough and resulting degradation in product purity is very evident at increased cycle times. The similarity of these two curves can be related through the dimensionless time parameter $\tau = t \cdot u / L$. As the cycle time increases, the dimensionless time parameter increases at constant velocity u (as determined by the orifice) and tube length L. Likewise, at constant cycle time t and tube length L, the experimental data could be interpreted as representing an increasing velocity in the tube and therefore an increasing τ. This suggests that if the correct adsorption bed orifice flowrates could be reproduced in the model, then experimental and model

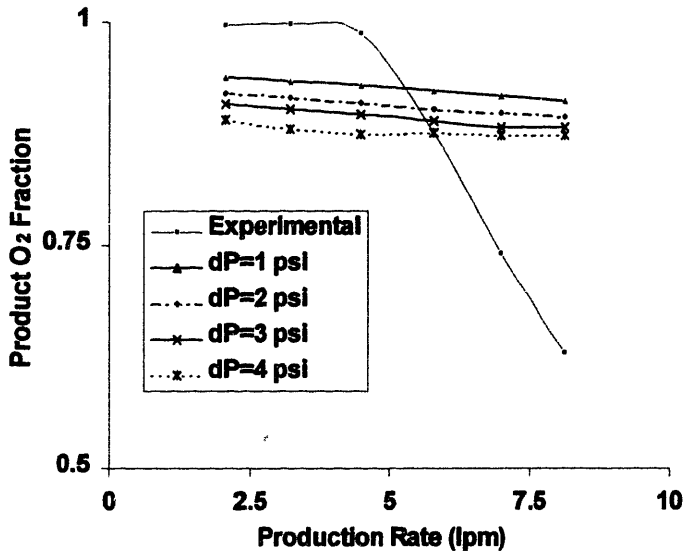

Figure A-20: Product purity effects of increased pressure losses across adsorption beds.

results would match well. However absorption bed orifice flowrate measurements are essentially impossible to obtain from this PSA unit. Instead, overall inlet flowrates must be compared under varying conditions (see Table A-7). This comparison reveals that the inlet flowrates most closely

Table A-7: Effect of parameters on inlet flowrate, product flowrate = 5.08 m^3/s

Model	Inlet Flowrate (m^3/s)
Base Case	1.91×10^{-3}
Reduced C_0	1.70×10^{-3}
Reduced C_0, Pressure drop = 3 psi	9.64×10^{-4}
$\varepsilon = 0.95$	6.52×10^{-4}

match experimental values when the orifice coefficient is reduced, indicating that additional flow restrictions exist in the PSA unit. However, by lumping these resistances into the orifice coefficient, satisfactory results can be obtained.

More restricted orifices affect the internal PSA unit dynamics in two ways. First, they directly affect the amount of gas entering the PSA unit. Second, more restricted orifices prevent gas from

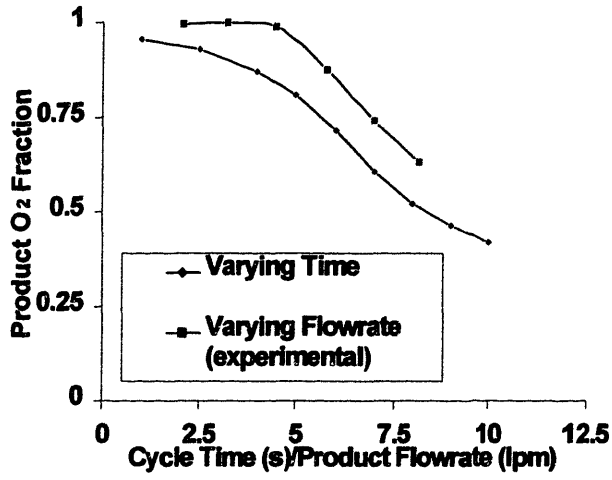

Figure A-21: Similarity of product purity as a function of cycle time and product flowrate.

columns 2 & 5 from flowing into the product chamber, reducing the amount of gas available for purge. It is thus observed that much more restricted orifices ($C_0 \approx 0.2$) reproduce the observed breakthrough effects for the PSA unit, as shown in Figure A-22.

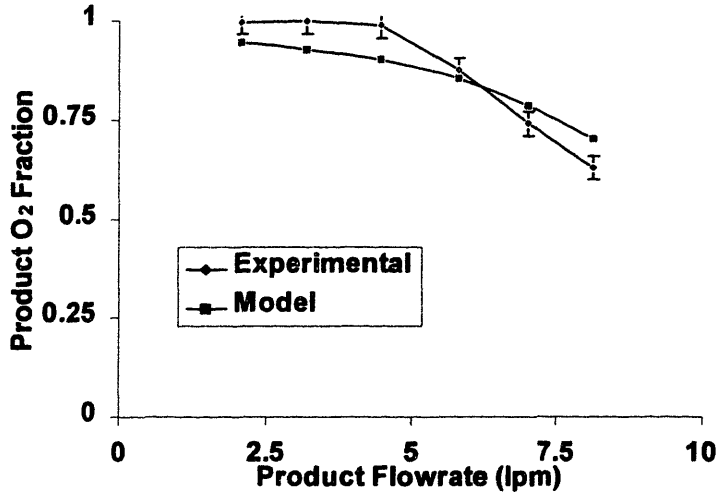

Figure A-22: Comparison between experimental and numerical product purity as a function of product flowrate.

According to the dimensionless cycle time τ, more pronounced breakthrough curves would be expected if the individual adsorption bed cycle time increased. Because cycle time t and bed length L are constant, τ can only increase with superficial velocity u in the bed. One would expect that less restricted orifices would increase velocity u and generate results in accord with experi-

mental data. The pressure in the product tank would decrease as more product is drawn off at higher production rates, causing an increase in orifice velocity and a decrease in product purity by breakthrough. Instead, more restricted orifices yielded the correct product purity and inlet flowrate results. This can be explained by analyzing the effects of product tank pressure on purity. The overall mass balance on the system reveals that under base case conditions, the inlet flowrate in the PSA model is higher than in experimental results. Because product flowrate is the same in both the model and experimental results, this means that the base case *purge* rate was too high. Restricting orifices to match inlet flowrates produced correct purity results because of two effects. First, reducing the overall inlet flowrate decreased the amount of purge gas (product flowrates are unaffected), resulting in adsorption beds which break through more easily. Second, decreasing inlet flowrate increases the effects of drawing more product from the unit. Drawing more product at lower inlet flowrates creates a more pronounced decrease in product tank pressure and the corresponding increase in velocity u and breakthrough.

A.7 Conclusions

Results indicate that parameters directly affecting the dimensionless time parameter τ of the adsorbent beds dictate the performance of the system and dominate the product purity of the PSA unit. A number of other parameters including void fraction, adsorbent efficiency, pressure drops, and mass transfer have a minimal effect on product purity. Specifically, changing cycle time, bed length and orifice velocity within the columns influences τ. Further analysis revealed that the relationships between these flowrates and other measurable quantities, such as inlet flowrate, are complex and depend on a variety of process parameters. Hence, for any PSA process operating at this level of complexity, it is critical that the entire model be implemented with rigor. Boundary conditions which properly conserve mass and convergence algorithms which accurately solve equalizing adsorption bed pressure histories are crucial. Any deviation from this level of rigor will lead to false results and invalidate any useful comparisons that could be made between predicted model performance and observed experimental results.

In addition, using a more complex model requires a deeper process understanding. For instance, this model required use of specific initial conditions to ensure that the same steady state was reached. In similar complex PSA models, it is crucial to ensure that 1) the convergence algorithm is stable, and 2) if the converged steady state is dependent on initial conditions. Failure to

do so will again result in false or misleading model results which will confound efforts to reconcile experimental and simulated model results.

A.8 Summary

A mathematical model has been developed to describe a novel new PSA process which controls flow between six adsorption beds via orifices and a channeled rotor instead of solenoid valves. Orifice-restricted flows pose several new challenges which increase both the conceptual and computational complexity of the model. First, unlike previously developed PSA models, effects between the various adsorption beds cannot be decoupled due to the continuous interconnection of all adsorption beds through orifices to a product collection tank. Continuous coupling of all adsorption beds and the product tank requires that all of these individual subunits are incorporated into one comprehensive dynamic model, greatly increasing the size and complexity of the set of differential equations in comparison with conventional models. Second, because flow conditions are unknown, a separate nonlinear algebraic set of equations must be solved to rigorously determine the correct pressure profile in the equalizing columns. Unlike models with decoupled adsorption beds, this model requires that mass conservation is enforced at all times. If this condition were not enforced, model results would indicate that the PSA unit was either creating or destroying oxygen and/or nitrogen. Third, flows between individual columns and the product collection chamber may also change directions, which requires dynamic monitoring and maintenance of boundary conditions within the time-step integration algorithm. Finally, the existence of multiple steady states restricts the sets of initial conditions that can be used in order to achieve consistent and repeatable results. By using orthogonal collocation on finite differences implementation for this complex system, a fast and accurate model was created, which was subsequently used in a thorough study of the PSA unit.

A.9 Notation

A_i = cross-sectional area of an adsorption bed

b_i = Langmuir isotherm coefficient for component i

c_i = gas phase concentration of component i

C_0 = orifice discharge coefficient

ε = void fraction

γ_s = ratio of saturation concentrations $\frac{q_{O_2 s}}{q_{O_2 s}}$

η = active adsorbent fraction

k_i = mass transfer coefficient for component *i*.

L = adsorbent bed length

λ = fraction of the total adsorbent available to participate in mass transfer

P_T, P_{atm}, P_i = pressure of product tank, atmosphere, and column *i*, respectively

$$\psi = \frac{1-\varepsilon}{\varepsilon} R_g T_0 q_{O_2 s}$$

q_{is} = saturation concentration of gas on an adsorbent particle

q_i^* = equilibrium concentration of gas on adsorbent

$\bar{q}_i$ = average concentration in adsorbent particle

$x_{O2,i}$, $x_{N2,i}$ = concentration of oxygen and nitrogen, respectively, on adsorbent particles at position *i* in the adsorbent bed

y = gas phase oxygen concentration

y_T = gas phase oxygen concentration in product tank

z = axial position in the adsorbent bed

References

[1] Breck, D. W. *Zeolite Molecular Sieves*, Wiley, 1974.

[2] Budner, Z.; Podstawa, W.; Gawdzik, A. "Study and Modelling of the Vacuum Swing Adsorption (VSA) Process Employed in the Production of Oxygen." *Chem. Eng. Res. Des.*, **77**, 405, 1999.

[3] Chlendi, M.; Tondeur, D.; Rolland, F. "A Method to Obtain a Compact Representation of Process Performances from a Numerical Simulator: Example of Pressure Swing Adsorption for Pure Hydrogen Production," *Gas Sep. Purif.*, **9**, 125, 1995.

[4] Finlayson, Bruce A. *The Method of Weighted Residuals and Variational Principles, with Application in Fluid Mechanics, Heat and Mass Transfer*, Academic Press, New York, 1972.

[5] Finlayson, D.; Sharp, A. J. "Improvements in or Relating to the Treatment of Gaseous Mixtures for the Purpose of Separating Them into Their Components or Enriching Them with Respect to One or More of Their Components," British Patent No. 365,092, 1932.

[6] Fogler, H. Scott, *Elements of Chemical Reaction Engineering,* 3rd. ed., Prentice-Hall, Englewood Cliffs, N. J., 1999.

[7] Fuderer, A.; Rudelstorfer, E. "Selective Adsorption Processes," U.S. Patent No. 3.846,849, 1976.

[8] Geankoplis, C. J. *Transport Processes and Unit Operations* Prentice-Hall, Englewood Cliffs, N. J., 1993.

[9] Glueckauf, E.; Coates, J. E. "Theory of Chromatography. Part IV. The Influence of Incomplete Equilibrium on the Front Boundary of Chromatograms and on the Effectiveness of Separation," *J. Chem. Soc.*, 1315, 1947.

[10] Glueckauf, E. "Theory of Chromatography. Part 10.-Formulae for the diffusion into spheres and their application to chromatography," *Trans. Faraday Soc.*, **51,** 1540, 1955.

[11] Hasche, R. L;. Dargan, W. N. "Separation of Gases," U.S. Patent No. 1,794,377 1931.

[12] Hill, C., "Fluid Fractionator," U. S. Patent No. 5,112,367, 1992.

[13] Jasra, R. V.; Choudray, N. V.; Bhat, S. G. T. "Separation of Gases by Pressure Swing Adsorption," *Sep. Sci. Tech.*, **26**, 885, 1991.

[14] Malek, A.; Farooq, S. "Study of a Six-Bed Pressure Swing Adsorption Process," *AIChE J.*, **43**, 2509, 1997.

[15] Perley, G. A., "Method of Making Commericial Hydrogen," U.S. Patent No. 1,896,916, 1933.

[16] Petzold, Linda R., "A Description of DASSL: A Differential/Algebraic System Solver," SAND82-8637, Sandia National Laboratries, September, 1982.

[17] Press, W. H.; Teukolsky, S. A. ; Vetterling, W. T.; Flannery, B. P. *Numerical Recipes in C: The Art of Scientific Computing,* 2nd ed. Cambridge University Press, 1993.

[18] Rossier, R. N., *Unnatural Gas,* Alert Diver, Nov.-Dec. 1999.

[19] Ruthven, D.; Farooq, M., S.; Knaebel, K. S. *Pressure Swing Adsorption,* VCH Publishers, New York, 1994.

[20] Sirkar, S. *Pressure Swing Adsorption Technology,* Adsorption: Science and Technology, A. E. Rodrigues, M. D. Levan, and D. Tondeur, eds., NATO ASI Series E158, Kluwer Academix Publishers, Dordrecht, The Netherlands, p. 285, 1989.

[21] Skarstrom, C. W. "Method and Apparatus for Fractionating Gaseous Mixtures by Adsorption," U. S. Patent No. 2,944,627, 1960.

[22] Teague, K. G.; Edgar, T. F. "Predictive Dynamic Model of a Small Pressure Swing Adsorption Air Separation Unit," *Ind. Eng. Chem. Res.*, **38,** 3761, 1999.

[23] Villadsen, J.; Michelsen, M. L. *Solution of Differential Equation Models by Polynomial Approximation*, Prentice-Hall, Englewood Cliffs, N. J., 1978.

[24] Yang, R. T. *Gas Separation by Adsorption Processes,* Butterworths, Boston, 1987.

Appendix B: Numerical Solution of Mathematical Models

B.1 Background

Many models are expressed in the mathematical form:

$$\begin{aligned} y' + \alpha + \beta L(y) + \gamma L(L(y)) &= 0 \\ f(\alpha, \beta, \gamma, y) &= 0 \end{aligned} \tag{B.1}$$

Specifically, when L is the differential operator with respect to some spatial variable, for example, x, equation (B.1) is:

$$\frac{\partial y}{\partial t} = \alpha + \beta \frac{\partial y}{\partial x} + \gamma \frac{\partial^2 y}{\partial x^2} \tag{B.2}$$

Corresponding initial and boundary conditions are required to fully specify the problem:

$$\begin{aligned} y|_{x=0} &= f(x) \\ ay|_{x=0} + b\left.\frac{\partial y}{\partial x}\right|_{x=0} &= c \end{aligned} \tag{B.3}$$

The boundary condition given in equation (B.3) is commonly referred to as the *Robin* boundary condition. Special cases of this occur when a or b are zero. When $a = 0$, a constant flux is specified at the boundary; this is called a *Neumann* boundary condition. If $b = 0$, a constant boundary value is specified; this is referred to as a *Dirichlet* boundary condition. This form of differential equation is widely used in many applications, including fluid dynamics, statics, heat and mass transfer, and particulate systems.

There are several numerical solution methods for this equation. Each method, however, generates a system of equations that solves for the value of the unknown variable at a finite number of points in the system. Thus, the solution is obtained for a *discretized* system. This is accomplished by using the values in the system at the present time to approximate the time derivative term. A time step algorithm is then used to determine the value of the unknown variable at these nodes for the next time step. The value of the unknown function at other points is determined either by interpolation or a linear combination of polynomials. For example, in solving for a function in a two-dimensional field, the solution points might be chosen as shown in Figure B-1:

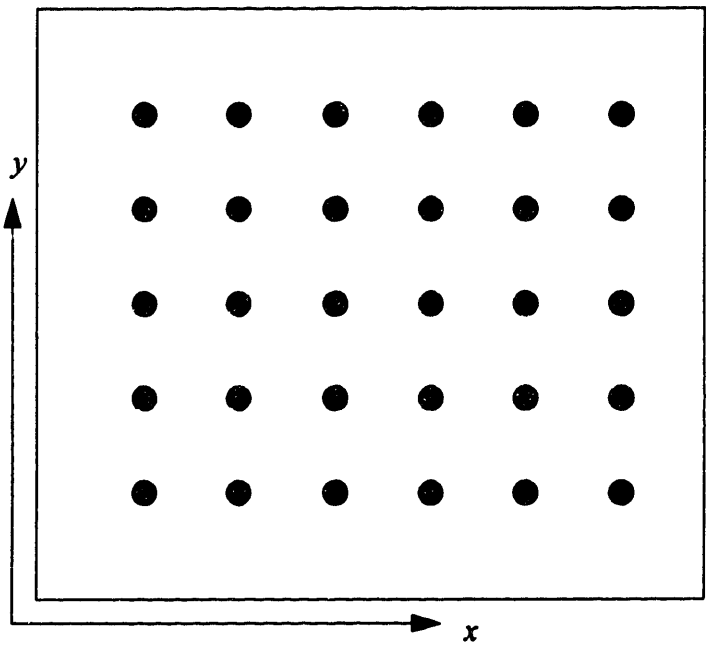

Figure B-1: Sample node point placement in a two-dimensional solution.

B.2 Finite Difference Methods

Finite difference schemes directly approximate the derivative terms. Where the derivative is defined as:

$$f'(x) = \lim_{\Delta x \to 0} \frac{f(x + \Delta x) - f(x)}{\Delta x} \tag{B.4}$$

the simplest form of finite difference approximation is analogous. For a one-dimensional discret-

ization, let the values at the nodes be y_i, where $i = 0, 1, ..., N$:

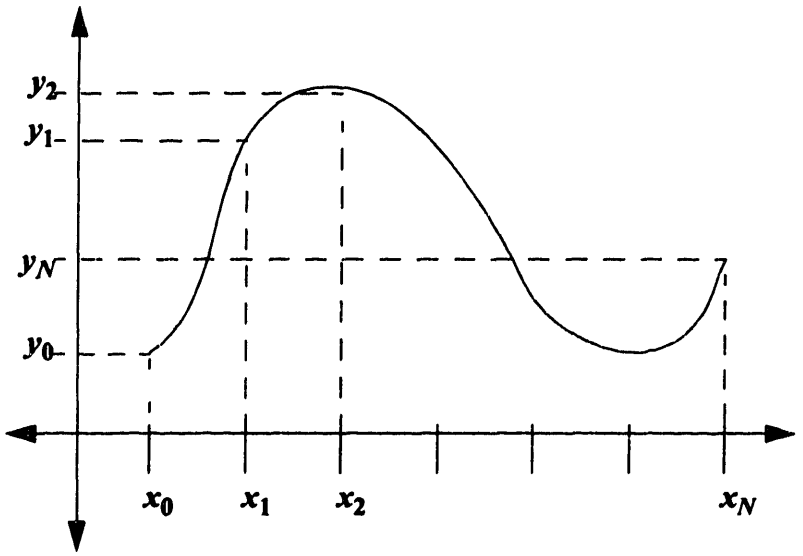

Figure B-2: Correspondence between node points and solution values in a one-dimensional system.

These values of y_i and x_i are then used to determine the first derivative at each node using an analogous definition of derivative:

$$\left.\frac{\partial y}{\partial x}\right|_i = \frac{y_{i+1}-y_i}{x_{i+1}-x_i} = \frac{f(x_{i+1})-f(x_i)}{x_{i+1}-x_i} \tag{B.5}$$

B.2.1 Accuracy determination

Many different linear combinations of these points may be used; this affects the accuracy of the solution. The accuracy is determined by generating a Taylor expansion of the function at each node and then substituting this into the derivative formula. The formula for a Taylor series expansion of a function $f(x)$ around the point x_0 is:

$$f(x) = f(x_0) + (x-x_0)f'(x_0) + \frac{(x-x_0)^2}{2!}f''(x_0) + \ldots + \frac{(x-x_0)^n}{n!}f^{(n)} + \ldots \tag{B.6}$$

For the numerical differentiation formula given by equation (B.6), the accuracy is determined as

follows. Let $\Delta x = x_{i+1} - x_i$.

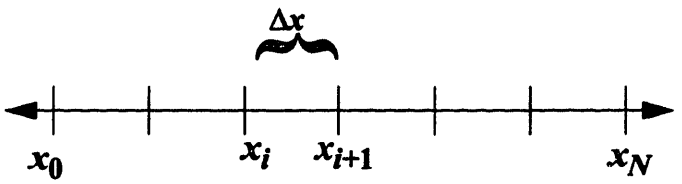

Figure B-3: Node point placement in a one-dimensional system.

Performing a Taylor expansion at the node x_{i+1} around the node x_i results in:

$$f(x_{i+1}) = f(x_i) + \Delta x f'(x_i) + \frac{\Delta x^2}{2} f''(x_i) + \ldots \tag{B.7}$$

Substituting this expression into equation (B.5) yields:

$$f'(x_i) = \frac{f(x_i) + \Delta x f'(x_i) + \frac{\Delta x^2}{2} f''(x_i) + \ldots - f(x_i)}{\Delta x} = f'(x_i) + \frac{\Delta x}{2} f''(x_i) + \ldots \tag{B.8}$$

Thus the largest error term is $\frac{\Delta x}{2} f''(x_i)$ and the expression is $O(\Delta x)$ accurate.

It is possible to construct differentiation formulas that are more accurate. This generally requires using more node values. Richardson extrapolation (Bender and Orszag, 1978) is one method for finding more accurate differentiation formulas, however, more accurate approximations can also be found by performing Taylor expansions at neighboring nodes and then generating a solvable system of equations. For example, in order to generate a more accurate first derivative for a system with uniformly spaced points, one would begin by performing Taylor expansions at the points x_{i+1} and x_{i-1}:

$$\begin{aligned} f(x_{i+1}) &= f(x_i) + \Delta x_1 f'(x_i) + \frac{\Delta x_1^2}{2} f''(x_i) + \frac{\Delta x_1^3}{3!} f^{(3)}(x_i) + \ldots \\ f(x_{i-1}) &= f(x_i) - \Delta x_2 f'(x_i) + \frac{\Delta x_2^2}{2} f''(x_i) - \frac{\Delta x_2^3}{3!} f^{(3)}(x_i) + \ldots \end{aligned} \tag{B.9}$$

where the points x, x_{i+1} and x_{i-1} are unevenly spaced, as shown in Figure B-4:

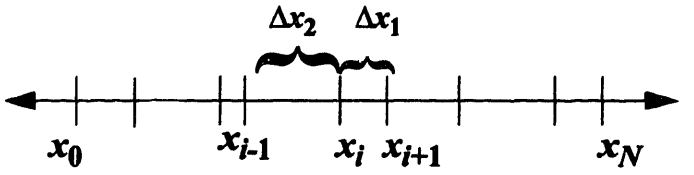

Figure B-4: Uneven node point placement in a one-dimensional system.

Now the differentiation formula must be some linear combination of $f(x_i)$ and the expansions for $f(x_{i+1})$ and $f(x_{i-1})$. Let the coefficients for this linear combination be A, B, and C:

$$\begin{aligned} f'(x_i) = {} & Bf(x_i) + Af(x_i) + A\Delta x_1 f'(x_i) + A\frac{\Delta x_1^2}{2}f''(x_i) + A\frac{\Delta x_1^3}{3!}f^{(3)}(x_i) + \ldots \\ & + Cf(x_i) - C\Delta x_2 f'(x_i) + C\frac{\Delta x_2^2}{2}f''(x_i) - C\frac{\Delta x_2^3}{3!}f^{(3)}(x_i) + \ldots \end{aligned} \tag{B.10}$$

In order to solve the following system for the best approximation to the first derivative, the $f(x_i)$ terms must cancel:

$$Bf(x_i) + Af(x_i) + Cf(x_i) = 0 \tag{B.11}$$

Likewise, the sum of the $f'(x_i)$ terms must be $f'(x_i)$:

$$A\Delta x_1 f'(x_i) - C\Delta x_2 f'(x_i) = f'(x_i) \tag{B.12}$$

Finally, to obtain higher-order accuracy, the $f''(x_i)$ terms must also cancel:

$$A\frac{\Delta x_1^2}{2}f''(x_i) + C\frac{\Delta x_2^2}{2}f''(x_i) = 0 \tag{B.13}$$

This system of equations can be expressed in matrix form:

$$\begin{bmatrix} 1 & 1 & 1 \\ \Delta x_1 & 0 & -\Delta x_2 \\ \dfrac{\Delta x_1^2}{2} & 0 & \dfrac{\Delta x_2^2}{2} \end{bmatrix} \begin{bmatrix} A \\ B \\ C \end{bmatrix} = \begin{bmatrix} 0 \\ 1 \\ 0 \end{bmatrix} \tag{B.14}$$

The appropriate coefficients A, B, and C can then be determined by simple matrix inversion.

In the special case where $\Delta x_1 = \Delta x_2 = \Delta x$, the system of equations looks like:

$$\begin{bmatrix} 1 & 1 & 1 \\ \Delta x & 0 & -\Delta x \\ 1 & 0 & 1 \end{bmatrix} \begin{bmatrix} A \\ B \\ C \end{bmatrix} = \begin{bmatrix} 0 \\ 1 \\ 0 \end{bmatrix} \tag{B.15}$$

and the solution is $A = 1/2\Delta x$, $B = 0$, $C = -1/2\Delta x$. In fact, substituting these coefficients into Equation (B.10) yields:

$$f'(x_i) = f'(x_i) + \frac{\Delta x^2}{2 \cdot 3!} f^{(3)}(x_i) + \ldots \tag{11.1}$$

and the approximation is now $O(\Delta x^2)$ accurate. Note that in the case of unevenly spaced nodes, this error term would be $O([max(\Delta x_1, \Delta x_2)]^2)$ accurate.

Second derivative approximations can be built up in a similar fashion. As an example, the linear combination method could be used to cancel our all terms but the f'' terms. Likewise, "the derivative of the first derivative" could also be found. Using the linear combination of nodes method, the following coefficients give accuracy $O(\Delta x^2)$ for the second derivative in the case of evenly spaced nodes:

Table B-1: Coefficients for Second Derivative

Node	Coefficient
$f(x_{i-1})$	$1/\Delta x^2$
$f(x)$	$-2/\Delta x^2$
$f(x_{i+1})$	$1/\Delta x^2$

This is a *centered* finite difference scheme because nodes on both sides of node x are used in calculating the derivative at node x. This is often impossible for boundary points. In this case, either forward or backward finite difference schemes are used. For calculating the derivative at the node x_0 with equally spaced nodes, the points $f(x_0)$, $f(x_1)$, $f(x_2)$, and $f(x_3)$ are used in obtaining $O(\Delta x^2)$ accuracy:

Table B-2: Coefficients for First Derivative, Left Boundary

Node	Coefficient
$f(x_0)$	$-11/6\Delta x$

Table B-2: Coefficients for First Derivative, Left Boundary

Node	Coefficient
$f(x_1)$	$3/\Delta x$
$f(x_2)$	$-3/2\Delta x$
$f(x_3)$	$-1/3\Delta x$

In summary, numerical difference schemes can be used to approximate a wide range of derivative accuracies. Further information on numerical derivative approximation is available in Stoer and Bulirisch (1993).

Consider the solution for Equation (B.2). After discretizing the system into N evenly spaced points, with $N = 0$ corresponding to $x = 0$ and $N = 10$ corresponding to $x = L$, the system can be expressed in matrix form:

$$\frac{d}{dt}\begin{bmatrix} y_0 \\ y_1 \\ y_2 \\ | \\ y_{N-1} \\ y_N \end{bmatrix} = \begin{bmatrix} \alpha_0 \\ \alpha_1 \\ \alpha_2 \\ | \\ \alpha_{N-1} \\ \alpha_N \end{bmatrix} + \frac{\beta}{\Delta x}\begin{bmatrix} \backslash & \backslash & \backslash & 0 & 0 & 0 & 0 \\ -1 & 0 & 1 & 0 & \dots & \dots & 0 \\ & \backslash & \backslash & \backslash & & & \\ 0 & \dots & -1 & 0 & 1 & \dots & 0 \\ & & & \backslash & \backslash & \backslash & \\ 0 & \dots & \dots & 0 & -1 & 0 & 1 \\ 0 & 0 & 0 & 0 & \backslash & \backslash & \backslash \end{bmatrix}\begin{bmatrix} y_0 \\ y_1 \\ y_2 \\ | \\ y_{N-1} \\ y_N \end{bmatrix} + \frac{\gamma}{\Delta x^2}\begin{bmatrix} \backslash & \backslash & \backslash & 0 & 0 & 0 & 0 \\ 1 & -2 & 1 & 0 & \dots & \dots & 0 \\ & \backslash & \backslash & \backslash & & & \\ 0 & \dots & 1 & -2 & 1 & \dots & 0 \\ & & & \backslash & \backslash & \backslash & \\ 0 & \dots & \dots & 0 & 1 & -2 & 1 \\ 0 & 0 & 0 & 0 & \backslash & \backslash & \backslash \end{bmatrix}\begin{bmatrix} y_0 \\ y_1 \\ y_2 \\ | \\ y_{N-1} \\ y_N \end{bmatrix} \tag{B.16}$$

Note that in this case, $\Delta x = L/10$.

B.2.2 Boundary conditions

The boundary conditions describe the behavior at the edge of the domain that is being modeled, and are necessary to fill in the rows for y_0 and y_N in equation (B.16). Taking the most general case of a mixed boundary condition, given by equation (B.3), the boundary conditions at y_0 and y_N may be written:

$$\begin{aligned} a_0 y_0 + b_0 \left.\frac{\partial y}{\partial x}\right|_{x=0} &= c_0 \\ a_L y_N + b_L \left.\frac{\partial y}{\partial x}\right|_{x=L} &= c_L \end{aligned} \tag{B.17}$$

These expressions can be solved for $\partial y / \partial x$ and substituted into the model equation at y_0 and y_N:

$$\frac{d}{dt}\begin{bmatrix} y_0 \\ y_1 \\ y_2 \\ | \\ y_{N-1} \\ y_N \end{bmatrix} = \begin{bmatrix} \alpha_0 + \frac{c_0}{b_0} \\ \alpha_1 \\ \alpha_2 \\ | \\ \alpha_{N-1} \\ \alpha_N + \frac{c_L}{b_L} \end{bmatrix} + \frac{\beta}{\Delta x}\begin{bmatrix} \frac{-a_0}{b_0} & \backslash & \backslash & 0 & 0 & 0 & 0 \\ -1 & 0 & 1 & 0 & \dots & \dots & 0 \\ & \backslash & \backslash & \backslash & & & \\ 0 & \dots & -1 & 0 & 1 & \dots & 0 \\ & & & \backslash & \backslash & \backslash & \\ 0 & \dots & \dots & 0 & -1 & 0 & 1 \\ 0 & 0 & 0 & 0 & \backslash & \backslash & \frac{-a_L}{b_L} \end{bmatrix}\begin{bmatrix} y_0 \\ y_1 \\ y_2 \\ | \\ y_{N-1} \\ y_N \end{bmatrix} + \frac{\gamma}{\Delta x^2}\begin{bmatrix} \backslash & \backslash & \backslash & 0 & 0 & 0 & 0 \\ 1 & -2 & 1 & 0 & \dots & \dots & 0 \\ & \backslash & \backslash & \backslash & & & \\ 0 & \dots & 1 & -2 & 1 & \dots & 0 \\ & & & \backslash & \backslash & \backslash & \\ 0 & \dots & \dots & 0 & 1 & -2 & 1 \\ 0 & 0 & 0 & 0 & \backslash & \backslash & \backslash \end{bmatrix}\begin{bmatrix} y_0 \\ y_1 \\ y_2 \\ | \\ y_{N-1} \\ y_N \end{bmatrix} \tag{B.18}$$

Using the values of y at each iteration, the value of dy/dt is determined. A time step algorithm is then used to integrate dy/dt with respect to time.

B.3 Method of Weighted Residuals

Another method for solving these types of equations is the method of weighted residuals. In the method of weighted residuals, the first step is to form a residual, usually denoted R, representing the deviation of the numerical solution from the true solution. Using the example given in Equation (B.1):

$$R = y' + \alpha + \beta L(y) + \gamma L(L(y)) \tag{B.19}$$

The goal then is to generate a solution such that this residual is zero over the domain of the solution. To accomplish this, the solution is first approximated by some representation:

$$y(t) \approx \sum_{i=0}^{N} y_i(t)\phi_i(x) \tag{B.20}$$

At each point in time, the solution is now the linear combination of some set of representation functions ϕ_i with the coefficients y_i. Substituting this representation into the residual:

$$\begin{aligned} R &= \sum_{i=0}^{N} \phi_i(x) y_i'(t) + \alpha + \beta \sum_{i=0}^{N} y_i(t) L(\phi_i(x)) + \gamma \sum_{i=0}^{N} y_i(t) L(L(\phi_i(x))) \\ R &= \alpha + \sum_{i=0}^{N} [\phi_i(x) y_i'(t) + \beta y_i(t) L(\phi_i(x)) + \gamma y_i(t) L(L(\phi_i(x)))] \end{aligned} \tag{B.21}$$

Now we have a system of $N + 1$ unknowns and only one equation! In order to get a satisfactory solution, we need to find the optimal values for the y_i's which minimize the value of the residual over the entire domain of the solution. This is accomplished by setting the integral of the residual

with some weighting functions, ω_j, to zero:

$$\int_A \left\{ \alpha + \sum_{i=0}^{N} [\phi_i(x) y_i'(t) + \beta y_i(t) L(\phi_i(x)) + \gamma y_i(t) L(L(\phi_i(x)))] \right\} \omega_j dA = 0 \qquad \text{(B.22)}$$

By choosing $N + 1$ different ω_j's, we can now generate the $N + 1$ equations necessary to solve for the y_i coefficients. This is equivalent to setting the inner product of the residual and some weighting to zero, which forces the length of the residual vector in the function space of the weighting function to zero.

Implementations of this method will vary based on: 1) the form of the linear operator 2) choice of representation function, and 3) choice of weighting function. Three of the most well-known implementations of this method are known as Galerkin's method, collocation, and subdomain methods. Examples will be derived for the special case where the linear operator, L, is the differential operator. The resulting form of the differential equation is:

$$\frac{\partial y}{\partial t} + \alpha + \beta \frac{\partial y}{\partial x} + \gamma \frac{\partial^2 y}{\partial x^2} = 0 \qquad \text{(B.23)}$$

This equation represents a convection-diffusion model, and applies to a host of other models. The term α represents a forcing term, while the first derivative term represents convection and the second derivative term represents diffusion. Typical boundary conditions for this equation fit the form given by Equation (B.3):

$$ay + b\frac{\partial y}{\partial x} = c \qquad \text{(B.24)}$$

B.4 Finite Element Methods - Galerkin Approach

The Galerkin method is applied by choosing identical "hat" functions for *both* the representation and the weighting function, where the hat function ϕ_i has value zero at x_{i-1} and x_{i+1} and

value one at x_i where $x_i \in [q, r]$, the spatial domain of the solution (Finlayson, 1972):

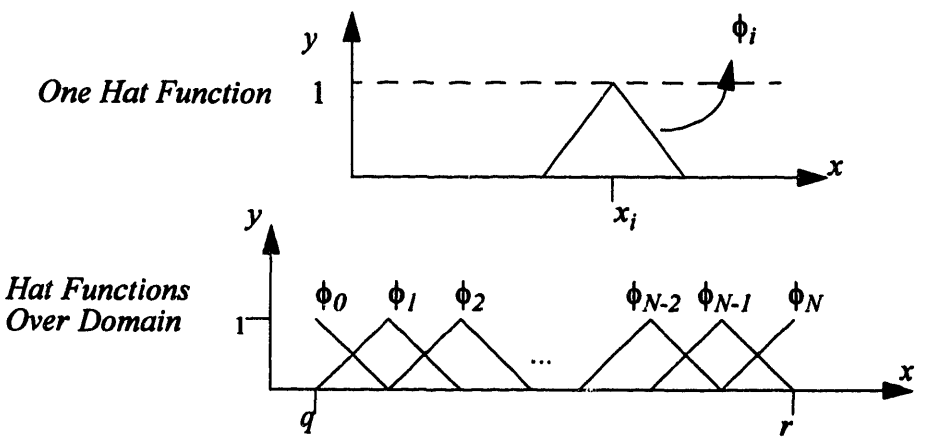

Figure B-5: "Hat" functions used as for both representation and weighting in the Galerkin method.

where

$$y(t) = \sum_{i=0}^{N} y_i(t)\phi_i(x) \tag{B.25}$$

Note that with this representation, the y_i's are easily interpreted as the value of the solution at x_i, since $\phi_i = 1$ at x_i. Thus, for this system, the residual is given by Equation (B.23):

$$R = \frac{\partial y}{\partial t} + \alpha + \beta\frac{\partial y}{\partial x} + \gamma\frac{\partial^2 y}{\partial x^2} \tag{B.26}$$

Substituting the representation for y and setting the integral of the residual with respect to the weighting functions ϕ_j to zero yields:

$$R = \sum_{i=0}^{N} \phi_i\frac{\partial y_i}{\partial t} + \alpha + \beta\sum_{i=0}^{N} y_i\frac{\partial \phi_i}{\partial x} + \gamma\sum_{i=0}^{N} y_i\frac{\partial^2 \phi_i}{\partial x^2}$$

$$\int_q^r \left(\sum_{i=0}^{N} \phi_i\frac{\partial y_i}{\partial t}\phi_j + \alpha\phi_j + \beta\sum_{i=0}^{N} y_i\frac{\partial \phi_i}{\partial x}\phi_j + \gamma\sum_{i=0}^{N} y_i\frac{\partial^2 \phi_i}{\partial x^2}\phi_j \right) dx = 0 \qquad j = 0, \ldots, N \tag{B.27}$$

This integral actually forms a system of equations which can be expressed in matrix form where row $j + 1$ of the matrix system represents the integral of the residual with respect to weighting function ϕ_j. Note that the values of x_1, x_2, x_3 effect the slopes of the hat functions, and therefore

the values of the integrals. This example will be developed term by term for the common case where the x_i's are evenly spaced with a distance of ε from x_i to x_{i+1}.

B.4.1 First term

The $j + 1^{th}$ row of the matrix describing the first term is:

$$\int_q^r \left(\sum_{i=0}^{N} \phi_i \frac{\partial y_i}{\partial t} \phi_j \right) dx = \sum_{i=0}^{N} \frac{\partial y_i}{\partial t} \int_q^r \phi_i \phi_j dx \tag{B.28}$$

The different cases for evaluating this integral are illustrated in Figure B-6, shown in "local" coordinates ε.

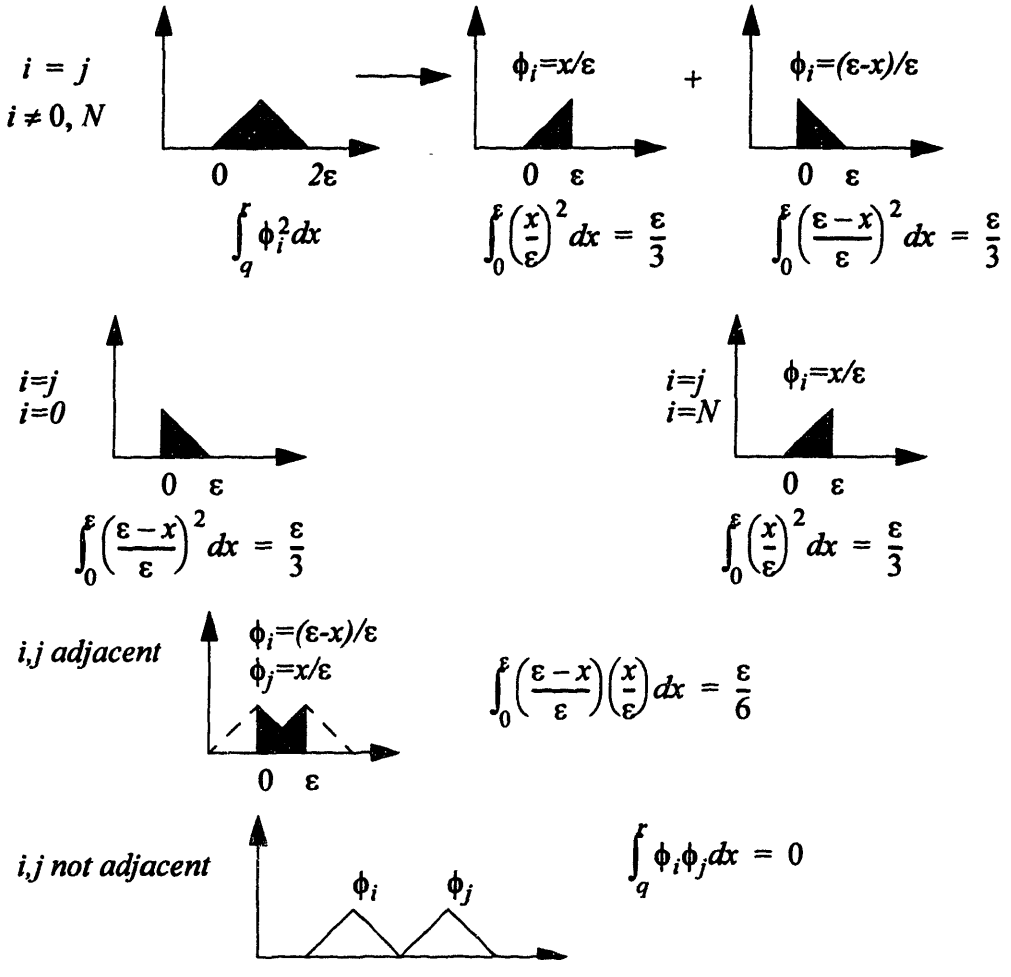

Figure B-6: Galerkin method contributions for the ϕ_i ϕ_j integral.

Using this information, the matrix for the first term is:

$$\frac{1}{6\varepsilon}\begin{bmatrix} 2 & 1 & 0 & 0 & 0 & 0 & 0 \\ 1 & 4 & 1 & 0 & \dots & \dots & 0 \\ & \backslash & \backslash & \backslash & & & \\ 0 & \dots & 1 & 4 & 1 & \dots & 0 \\ & & & \backslash & \backslash & \backslash & \\ 0 & \dots & \dots & 0 & 1 & 4 & 1 \\ 0 & 0 & 0 & 0 & 0 & 1 & 2 \end{bmatrix} \frac{d}{dt}\begin{bmatrix} y_0 \\ y_1 \\ y_2 \\ | \\ y_{N-1} \\ y_N \end{bmatrix} = \frac{1}{6\varepsilon}A\frac{d}{dt}\mathbf{y} \tag{B.29}$$

B.4.2 Second term

The second term is much easier to evaluate. Assuming that α is constant with respect to x:

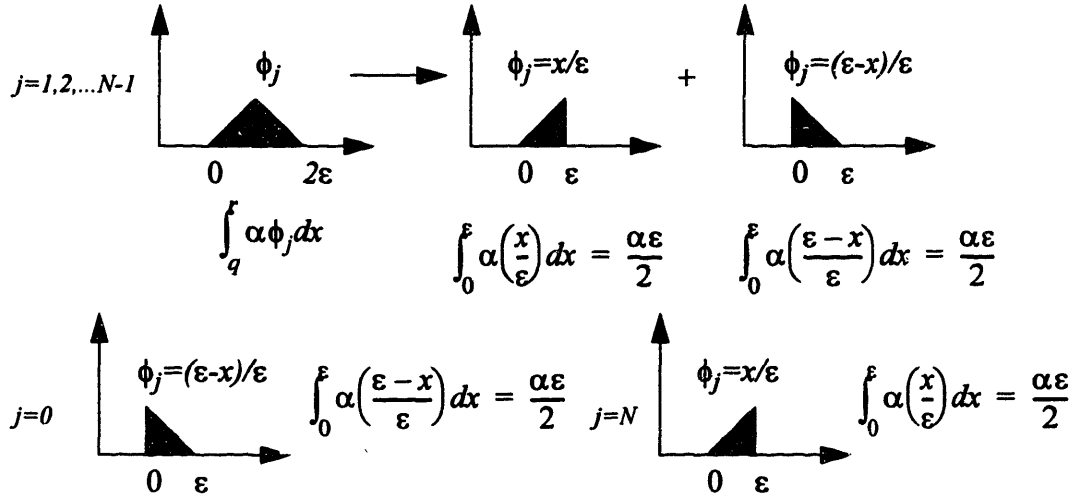

Figure B-7: Galerkin method contributions for the $\alpha\phi_j$ integral.

Knowing these integrals, the contribution of the second term, α, can be expressed as a forcing vector with $N + 1$ rows:

$$\begin{bmatrix} \alpha\frac{\varepsilon}{2} \\ \alpha\varepsilon \\ | \\ \alpha\varepsilon \\ \alpha\frac{\varepsilon}{2} \end{bmatrix} = \mathbf{f} \tag{B.30}$$

B.4.3 Third term

The $j + 1^{th}$ row of the matrix describing the contribution of the third term is (assuming that β

is constant with respect to x):

$$\int_q^r \beta \sum_{i=0}^{N} y_i \frac{\partial \phi_i}{\partial x} \phi_j dx = \beta \sum_{i=0}^{N} y_i \int_q^r \frac{\partial \phi_i}{\partial x} \phi_j dx \tag{B.31}$$

Figure B-8 summarizes the values these integrals take on:

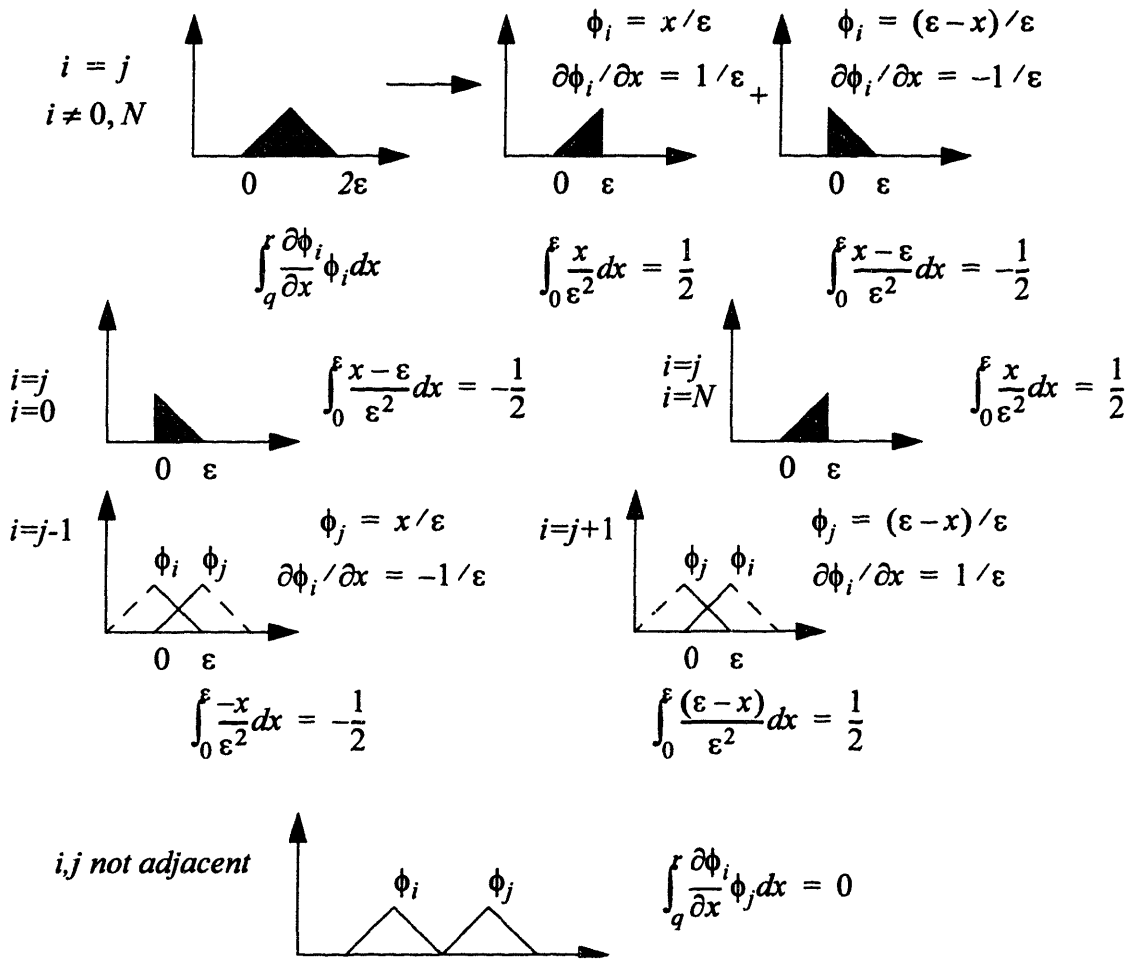

Figure B-8: Galerkin method contributions for the $(\partial\phi_i/\partial x)\phi_j$ integral.

Now the contribution matrix for these terms can be written as:

$$\frac{\beta}{2}\begin{bmatrix} -1 & 1 & 0 & 0 & 0 & 0 & 0 \\ -1 & 0 & 1 & 0 & \dots & \dots & 0 \\ & \backslash & \backslash & \backslash & & & \\ 0 & \dots & -1 & 0 & 1 & \dots & 0 \\ & & & \backslash & \backslash & \backslash & \\ 0 & \dots & \dots & 0 & -1 & 0 & 1 \\ 0 & 0 & 0 & 0 & 0 & -1 & 1 \end{bmatrix}\begin{bmatrix} y_0 \\ y_1 \\ y_2 \\ | \\ y_{N-1} \\ y_N \end{bmatrix} = \mathbf{By} \tag{B.32}$$

B.4.4 Fourth term

The $j + 1^{th}$ row of the matrix expressing the contribution of the fourth term is (assuming that γ is constant with respect to x):

$$\int_q^r \gamma \sum_{i=0}^{N} y_i \frac{\partial^2 \phi_i}{\partial x^2} \phi_j dx = \gamma \sum_{i=0}^{N} y_i \int_q^r \frac{\partial^2 \phi_i}{\partial x^2} \phi_j dx \tag{B.33}$$

There is a severe problem with this contribution as it is expressed in Equation (B.33). Since the hat functions are linear, their first derivatives will be constants and their second derivative will be zero. Thus the second derivative of ϕ_i in Equation (B.33) should be zero and therefore there should be no contribution from the fourth term! Furthermore, up to this time no heed has been paid at all to the incorporation of boundary conditions in this problem, as given in Equation (B.24). Stating these boundary conditions explicitly:

$$\begin{aligned} a_r y|_r + b_r \left.\frac{\partial y}{\partial x}\right|_r &= c_r \rightarrow \left.\frac{\partial y}{\partial x}\right|_r = \frac{c_r - a_r y|_r}{b_r} \\ a_q y|_q + b_q \left.\frac{\partial y}{\partial x}\right|_q &= c_q \rightarrow \left.\frac{\partial y}{\partial x}\right|_q = \frac{c_q - a_q y|_q}{b_q} \end{aligned} \tag{B.34}$$

One elegant mathematical manipulation can make the boundary conditions easy to incorporate at the same time that it eliminates the problem caused by taking the second derivative of a linear function. Integrating the integral in Equation (B.33) by parts yields:

$$\int_q^r \frac{\partial^2 \phi_i}{\partial x^2} \phi_j dx = \left. \phi_j \frac{\partial \phi_i}{\partial x} \right|_q^r - \int_q^r \frac{\partial \phi_i}{\partial x} \frac{\partial \phi_j}{\partial x} dx \tag{B.35}$$

Substituting this expression back into Equation (B.33) produces:

$$\gamma \sum_{i=0}^{N} y_i \int_q^r \frac{\partial^2 \phi_i}{\partial x^2} \phi_j dx = \gamma \sum_{i=0}^{N} y_i \phi_j \frac{\partial \phi_i}{\partial x}\bigg|_q^r - \gamma \sum_{i=0}^{N} y_i \int_q^r \frac{\partial \phi_i}{\partial x} \frac{\partial \phi_j}{\partial x} dx \tag{B.36}$$

The first term in Equation (B.36) allows the easy incorporation of boundary conditions:

$$\gamma \sum_{i=0}^{N} y_i \phi_j \frac{\partial \phi_i}{\partial x}\bigg|_q^r = \gamma \phi_j \frac{\partial y}{\partial x}\bigg|_q^r \tag{B.37}$$

The only terms where this expression will be nonzero is when $j = 0$ or N:

$$\begin{aligned} j = 0 \rightarrow \gamma \phi_j \frac{\partial y}{\partial x}\bigg|_q^r &= -\gamma \frac{\partial y}{\partial x}\bigg|_q = -\gamma \left(\frac{c_q - a_q y|_q}{b_q} \right) = -\gamma \frac{c_q}{b_q} + \gamma \frac{a_q}{b_q} y_0 \\ j = N \rightarrow \gamma \phi_j \frac{\partial y}{\partial x}\bigg|_q^r &= \gamma \frac{\partial y}{\partial x}\bigg|_r = \gamma \left(\frac{c_r - a_r y|_r}{b_r} \right) = \gamma \frac{c_r}{b_r} - \gamma \frac{a_r}{b_r} y_N \end{aligned} \tag{B.38}$$

These terms are easily incorporated into the matrix system. Note that when b_q or b_r are zero (Dirichlet boundary condition), the corresponding expression is undefined. This happens when the boundary condition specifies the value of y. When a boundary condition specifies the value of y at the boundary, the row of the matrix system describing that boundary is eliminated. Since y is known at that boundary, the system has one less unknown and one less equation. The column of the matrices which were multiplied by that value of y become a forcing vector. This will be illustrated later.

The only contributions left to describe are due to the second term in Equation (B.36), as illus-

trated in Figure B-9.

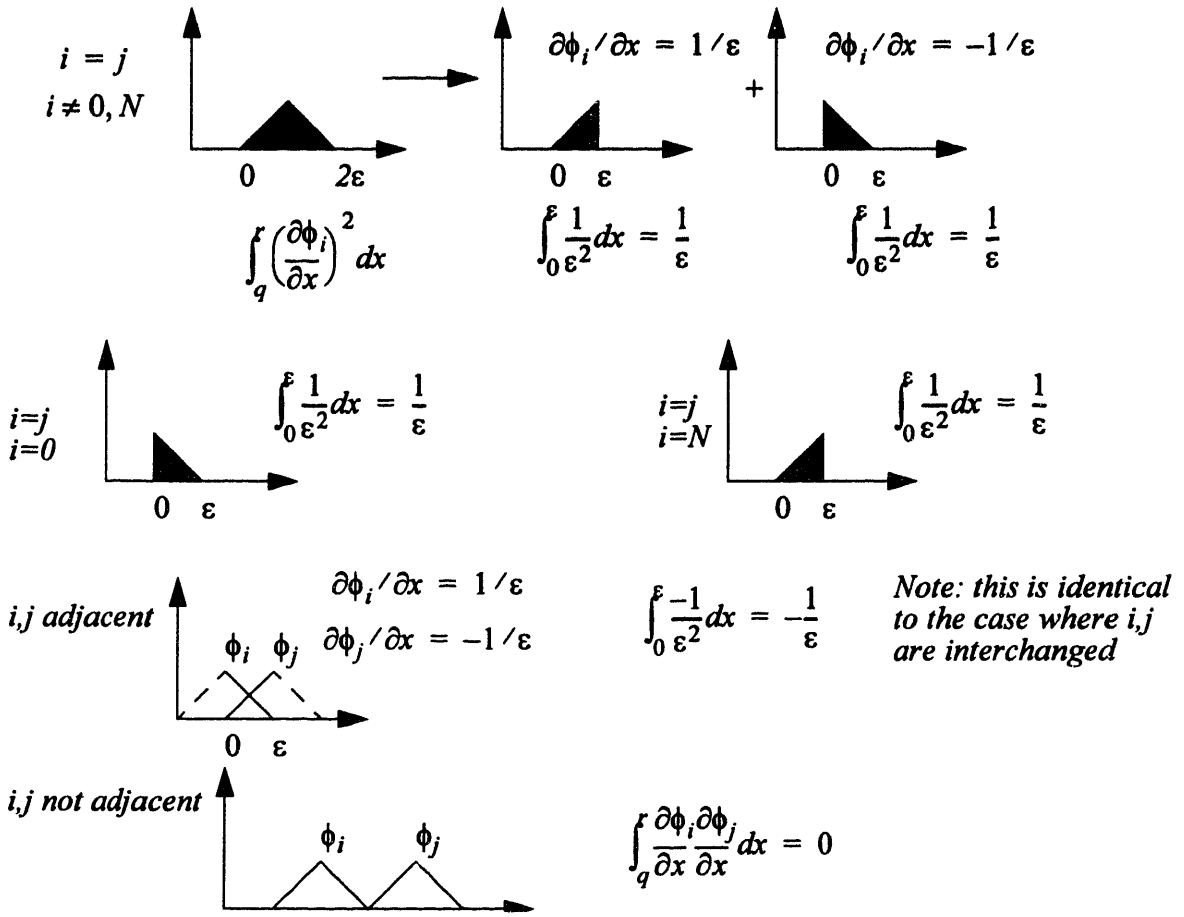

Figure B-9: Galerkin method contributions for the $(\partial\phi_i/\partial x)(\partial\phi_j/\partial x)$ integral.

Writing out these contributions in matrix form:

$$\frac{\gamma}{\varepsilon}\begin{bmatrix} 1 & -1 & 0 & 0 & 0 & 0 & 0 \\ -1 & 2 & -1 & 0 & \dots & \dots & 0 \\ & \ddots & \ddots & \ddots & & & \\ 0 & \dots & -1 & 2 & -1 & \dots & 0 \\ & & & \ddots & \ddots & \ddots & \\ 0 & \dots & \dots & 0 & -1 & 2 & -1 \\ 0 & 0 & 0 & 0 & 0 & -1 & 1 \end{bmatrix}\begin{bmatrix} y_0 \\ y_1 \\ y_2 \\ \vdots \\ y_{N-1} \\ y_N \end{bmatrix} = \mathbf{Cy} \tag{B.39}$$

The entire formulation is the set of matrix equations:

$$\frac{1}{6\varepsilon}\mathbf{A}\frac{\mathrm{d}}{\mathrm{d}t}\mathbf{y} + \mathbf{f} + \mathbf{By} + \mathbf{Cy} = 0 \rightarrow \frac{\mathrm{d}}{\mathrm{d}t}\mathbf{y} = 6\varepsilon\mathbf{A}^{-1}((\mathbf{B}+\mathbf{C})\mathbf{y} + \mathbf{f}) \tag{B.40}$$

Where A is exactly as given by Equation (B.29). The remaining terms, $(\mathbf{B} + \mathbf{C})\mathbf{y} + \mathbf{f}$, including the boundary effects for non-Dirichlet boundaries are:

$$\begin{bmatrix} \frac{\gamma}{\varepsilon}-\frac{\beta}{2}+\gamma\frac{a_q}{b_q}\left(\frac{\beta}{2}-\frac{\gamma}{\varepsilon}\right) & 0 & 0 & 0 & 0 & 0 \\ -\frac{\beta}{2}-\frac{\gamma}{\varepsilon} & \left(2\frac{\gamma}{\varepsilon}\right) & \frac{\beta}{2}-\frac{\gamma}{\varepsilon} & 0 & \cdots & 0 \\ & \ddots & \ddots & \ddots & & \\ 0 & \cdots & -\frac{\beta}{2}-\frac{\gamma}{\varepsilon} & \left(2\frac{\gamma}{\varepsilon}\right) & \frac{\beta}{2}-\frac{\gamma}{\varepsilon} & 0 \\ & & & \ddots & \ddots & \ddots \\ 0 & \cdots & 0 & -\frac{\beta}{2}-\frac{\gamma}{\varepsilon} & \left(2\frac{\gamma}{\varepsilon}\right) & \frac{\beta}{2}-\frac{\gamma}{\varepsilon} \\ 0 & 0 & 0 & 0 & -\frac{\beta}{2}-\frac{\gamma}{\varepsilon} & \left(\frac{\beta}{2}+\frac{\gamma}{\varepsilon}-\gamma\frac{a_r}{b_r}\right) \end{bmatrix} \begin{bmatrix} y_0 \\ y_1 \\ y_2 \\ \vdots \\ y_{N-1} \\ y_N \end{bmatrix} + \begin{bmatrix} \alpha\frac{\varepsilon}{2}-\gamma\frac{c_q}{b_q} \\ \alpha\varepsilon \\ \vdots \\ \alpha\varepsilon \\ \alpha\frac{\varepsilon}{2}+\gamma\frac{c_r}{b_r} \end{bmatrix} \tag{B.41}$$

As an example if a Dirichlet boundary condition were given that $y = y_0$ at $x = r$, the system would look like:

$$\begin{bmatrix} \left(2\frac{\gamma}{\varepsilon}\right) & \frac{\beta}{2}-\frac{\gamma}{\varepsilon} & & & & \\ \ddots & \ddots & \ddots & & & \\ & -\frac{\beta}{2}-\frac{\gamma}{\varepsilon} & \left(2\frac{\gamma}{\varepsilon}\right) & \frac{\beta}{2}-\frac{\gamma}{\varepsilon} & & \\ & & \ddots & \ddots & \ddots & \\ 0 & 0 & 0 & -\frac{\beta}{2}-\frac{\gamma}{\varepsilon} & \left(2\frac{\gamma}{\varepsilon}\right) & \frac{\beta}{2}-\frac{\gamma}{\varepsilon} \\ 0 & 0 & 0 & 0 & -\frac{\beta}{2}-\frac{\gamma}{\varepsilon} & \left(\frac{\beta}{2}+\frac{\gamma}{\varepsilon}-\gamma\frac{a_r}{b_r}\right) \end{bmatrix} \begin{bmatrix} y_1 \\ y_2 \\ \vdots \\ y_{N-1} \\ y_N \end{bmatrix} + \begin{bmatrix} \alpha\varepsilon + y_0\left(-\frac{\beta}{2}-\frac{\gamma}{\varepsilon}\right) \\ \vdots \\ \alpha\varepsilon \\ \alpha\frac{\varepsilon}{2}+\gamma\frac{c_r}{b_r} \end{bmatrix} \tag{B.42}$$

References

[1] Bender, C.; Orszag, S. *Advanced Mathematical Methods for Scientists and Engineers,* McGraw-Hill, New York, 1978.

[2] Finlayson, Bruce A. *The Method of Weighted Residuals and Variational Principles, with Applications in Fluid Mechanics, Heat and Mass Transfer,* Academic Press, 1972.

[3] Stoer, J.; Bulirisch, R. *Introduction to Numerical Analysis,* 2nd Edition, translated by R. Bartels, W. Gautschi, and C. Witzgall, Springer-Verlag, New York, 1993.

Appendix C: Multicomponent Coagulation Production Expression

C.1 Introduction

The mechanism of coagulation, also referred to as agglomeration, affects a wide variety of physical systems including aerosols, soot formation, polymer condensation, and other particulate processes.

C.1.1 Number density distribution definition

The state of a population balance system is typically defined by a number density distribution which describes the number of particles possessing a given combination of properties. For "single-component" number density distributions, the number density distribution gives the number of particles as a function of a single particle property such as mass, volume, diameter, etc. Figure C-1 illustrates a typical number density distribution based on particle mass. For a single-compo-

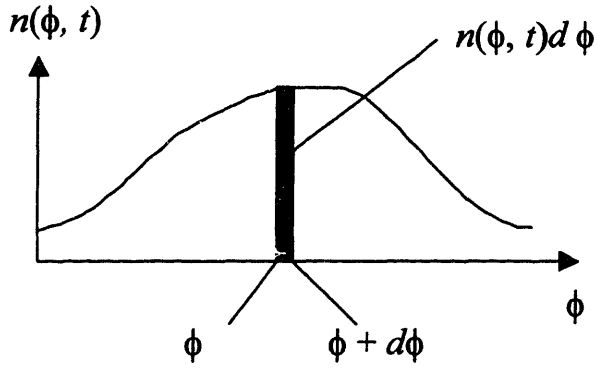

Figure C-1: Example number density distribution as a function of property ϕ.

nent system, the number density is formally defined as follows.

DEFINITION

*The **number density** function of particles is given by $n(\phi, t)$ such that $n(\phi, t)d\phi$ is the number particles in the size range $[\phi, \phi + d\phi]$ at time t.*

Note that $n(\phi)$ represents the number *density* of particles; in order to find the total number of particles it is necessary to integrate over a segment of the density distribution:

$$N(a < \phi < b) = \int_a^b n(\phi) d\phi \tag{C.1}$$

In a typical implementation, the total number of particles is expressed per unit volume of the system. For instance, in an aerosol system N might be expressed in units of particles/cm^3. It follows then from Equation (C.1) that $n(\phi)$ has units of $1/([\phi] \cdot \text{cm}^3)$. If ϕ were mass in g, then the units of $n(\phi)$ would be $1/(\text{g} \cdot \text{cm}^3)$. The foundation of modern population balance problems for single-component systems can be traced back to Valentas and Amundson (1966) and Valentas, Bilous, and Amundson (1966).

For multicomponent systems, more than one particle property is of interest and ϕ becomes a vector of properties, ϕ. This leads to the following expanded definition for multicomponent number density distributions:

DEFINITION

*The **number density** function of population members with s attributes is completely specified by the vector $\phi = \{\phi_1, \phi_2, \phi_3, \ldots, \phi_s\}$ is given by $n(\phi)$ such that $n(\phi)d\phi$ is the number of population members in the attribute range $[\phi_1, \phi_1 + d\phi_1][\phi_2, \phi_2 + d\phi_2][\phi_3, \phi_3 + d\phi_3] \ldots [\phi_s, \phi_s + d\phi_s]$.*

For a system where the only attributes of interest are component masses, s will be the number of species in the system. Again, it is important to emphasize that this expression is a density function and that the total number of particles is produced by integrating over a multidimensional segment of the distribution.

$$N(a_1 < \phi_1 < b_1, a_2 < \phi_2 < b_2, \ldots, a_s < \phi_s < b_s) = \int_{a_s}^{b_s} \cdots \int_{a_2}^{b_2} \int_{a_1}^{b_1} n(\phi) d\phi_1 d\phi_2 \ldots d\phi_s \tag{C.2}$$

Of course, in the case where $s = 1$, Equation (C.2) reduces to Equation (C.1). The units of N will still be the number of particles per cm^3 of system volume. Accordingly, the number density function $n(\phi)$ will have units $1/([\phi_1][\phi_2] \ldots [\phi_s] \cdot \text{cm}^3)$. If $n(\phi)$ describes an aerosol system with s components where $\phi_1 = m_1$, the mass of component 1 in grams, $\phi_2 = m_2$, the mass of component 2 in grams, etc., then the number density is written as $n(\mathbf{m})$ and the units are $1/(\text{g}^s \cdot \text{cm}^3)$.

C.2 Coagulating Particles Mass Balance

Because the process of coagulation conserves mass, in the one-component case two particles of

mass a and b will combine to form a new particle of mass $a + b$, as illustrated in Figure C-2

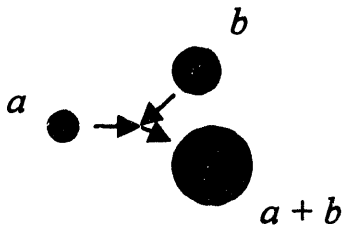

Figure C-2: Masses of coagulating particles *a* and *b* to form a particle of mass *a* + *b*.

For a multicomponent system, the individual component masses are tracked separately. The mass of the two particles are vectors **a** and **b** where $\mathbf{a} = \{a_1, a_2, ..., a_s\}$ and $\mathbf{b} = \{b_1, b_2, ..., b_s\}$. The particle which is created by this coagulation event has mass $\mathbf{c} = \{c_1, c_2, ..., c_s\}$, as shown in Figure C-3. Table C-1 summarizes the relationship beween the component masses of the coagulating particles.

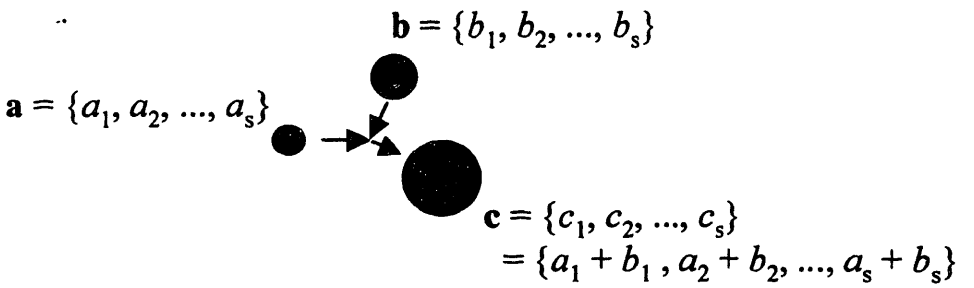

Figure C-3: Particle masses in multicomponent coagulation.

Table C-1: Individual component masses in multicomponent coagulation

Particle	*a*	*b*	*c*
Mass of component 1	a_1	b_1	c_1
Mass of component 2	a_2	b_2	c_2
Mass of component *s*	a_s	b_s	c_s
Total particle mass	$\sum_i a_i$	$\sum_i b_i$	$\sum_i c_i$

In fact, using the information in Table C-1, the multicomponent coagulation of particles **a** and **b** is

much more accurately depicted in Figure C-4. It is important to note that each of the individual

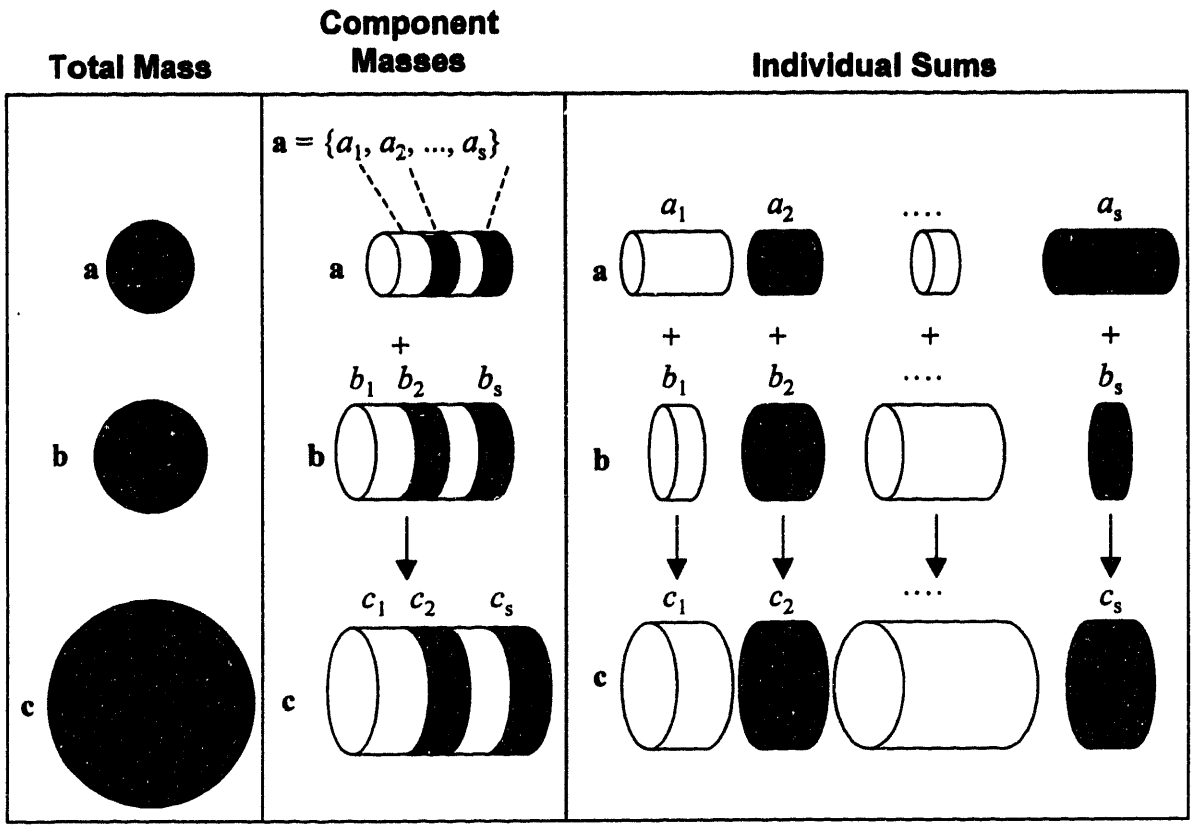

Figure C-4: Multicomponent coagulation particle masses and relation to total mass.

component masses can vary independent of the other masses. Thus, although particle *b* is much larger than particle *a*, particle *a* actually contains much more of component *s* than particle *b* and is therefore the largest contributor to the final amount of component *s* in particle *c*.

C.3 Coagulation Kernel

Most particle systems contain a large enough number of particles that coagulation events can be described as a rate process, as opposed to isolated stochastic events. Because coagulation is a binary process, we would expect that the overall coagulation rate follows a first-order rate law in the concentration of particles size *a* and *b*.

$$\text{rate} = k \cdot [a] \cdot [b] \tag{C.3}$$

The single-component form of this coagulation kernel is formally defined as follows.

DEFINITION

The coagulation kernel $\beta(a, b)$ is the rate function for the first-order rate process where particles of mass $c = a + b$ are formed due to the coagulation of two particles of masses a and b.

$$\text{rate} = \beta(a, b) \cdot [a] \cdot [b] \tag{C.4}$$

It follows that the coagulation kernel should have units *space/time*, or cm^3/s for the aerosol example. Note that the coagulation kernel is a symmetrical function by definition as no distinction is made between the coagulating particles:

$$\beta(a, b) = \beta(b, a) \tag{C.5}$$

Using the definition of the coagulation kernel, it is possible to describe the evolution of a number density distribution. In general, coagulation will affect the number density of particles size m in two ways:

1.) coagulation loss: when a particle of size m coagulates with any other particle in the system, a particle of mass m is lost and $n(m)$ decreases.

2.) coagulation production: when two smaller particle coagulate to form a larger particle of size m, the number density $n(m)$ increases.

The multicomponent coagulation kernel is defined similar to the single-component coagulation kernel

DEFINITION

The multicomponent coagulation kernel $\beta(\mathbf{a}, \mathbf{b})$ is the rate function for the first-order process by which particles of compositions $\mathbf{a}$ and $\mathbf{b}$ will collide and coagulate into one larger member with composition $\mathbf{c} = \mathbf{a} + \mathbf{b}$.

Just as with the one-component case, the units of the coagulation kernel are *space* • $time^{-1}$ and are the same as for the single-component case. Also, because there is no distinction between particles a and b, the multicomponent coagulation kernel must also be a symmetrical function:

$$\beta(\mathbf{a}, \mathbf{b}) = \beta(\mathbf{b}, \mathbf{a}) \tag{C.6}$$

Just as in the single-component case, the number density $n(\mathbf{m})$ can be affected by both loss and production of particles of mass $\mathbf{m}$ due to coagulation. Using the definitions of number density distribution and the coagulation kernel, the following sections derive the proper expressions describing the evolution of the multicomponent number density distribution due to coagulation.

C.3.1 Coagulation loss of particles

In the single-component case, particles of mass m are lost when a particle of mass m coagulates with any other particle. The rate at which particles of mass m are lost due to coagulation with particles of mass u is a function of the number of particles of mass m, the number of particles of mass u, and the coagulation kernel:

$$\frac{dn(m)dm}{dt} = -\beta(m, u)n(m)dm \cdot n(u)du \tag{C.7}$$

This expression follows directly from the first-order rate law given in Equation (C.4). Because $n(u)$ and $n(m)$ are density functions, the expressions $n(m)dm$ and $n(u)du$ represent the concentration of particles in the size ranges $(m, m + dm)$ and $(u, u + du)$, respectively. Both of these expressions have units of $1/cm^3$. Note the consistency of the units in this expression, as shown in Table C-2.

Table C-2: Units of variables in coagulation loss expression

Symbol	*Definition*	*Units*
$n(m)$	number density	$\frac{1}{g \cdot cm^3}$
dm	(differential) mass range	g
$n(u)$	number density	$\frac{1}{g \cdot cm^3}$
du	(differential) mass range	g
$\beta(m, u)$	coagulation kernel	$\frac{cm^3}{s}$

Dividing Equation (C.7) through by dm produces the rate of change in number density $n(m)$:

$$\frac{dn(m)}{dt} = -\beta(m, u)n(m)n(u)du \tag{C.8}$$

This expression only accounts for the loss of particles of size m due to coagulation with particles in the differential size range $(u, u + du)$. In order to produce the total loss rate of particles size m, it is necesssary to account for all possible values of u, which requires an integral:

$$\frac{dn(m)}{dt} = -\int_0^\infty \beta(m,u)n(m)n(u)du \tag{C.9}$$

Recognizing that $n(m)$ is constant within the integral produces the final form of the single-component coagulation loss expression:

$$\boxed{\frac{dn(m)}{dt} = -n(m)\int_0^\infty \beta(m,u)n(u)du} \tag{C.10}$$

For multicomponent systems, the total loss expression due to coagualtion for particles of mass **m** coagulating with particles of mass **u** is a multidimensional integral which accounts for *all* of the combinations with which particles of mass **m** may coagulate.

$$\frac{dn(m_1, m_2, \ldots m_s)}{dt} = -n(\mathbf{m})\int_0^\infty \ldots \int_0^\infty \int_0^\infty \beta(\mathbf{m},\mathbf{u})n(\mathbf{u})du_1 du_2 \ldots du_s \tag{C.11}$$

C.3.2 Coagulation production of particles: one-component case

For one-component systems, the production of particles of mass m occurs when any two particles of masses summing to m coagulate. If these two particles have masses a and b, then $a + b = m$. Because of this restriction, there is only one degree of freedom in choosing the size of the coagulating particles - as soon as the mass of particle a is chosen then the mass of particle b is given by $b = m - a$. Figure C-5 illustrates this relationship, where the mass of the two components are the a and b axes and the line $b = m - a$ defines the relationship between the masses of the two coagulating particles.

Incorporating this restraint into the single-component rate law for coagulation given in Equation (C.4) yields the expression for the rate of production of particles size m from particles size a and $m - a$.

$$\begin{aligned} \frac{dn(m)dm}{dt} &= \beta(a,b)n(a)da \cdot n(b)db \\ \frac{dn(m)dm}{dt} &= \beta(a,m-a)n(a)da \cdot n(m-a)d(m-a) \end{aligned} \tag{C.12}$$

Note that the length of the interval dm is constrianed by the relation:

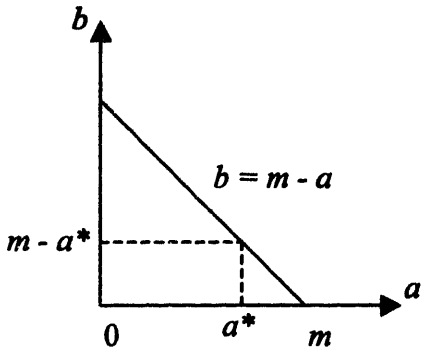

Figure C-5: Mass-conservation restriction on two coagulating particles forming a particle of mass *m*.

$$dm = da + d(m - a) \tag{C.13}$$

which is graphically depicted in Figure C-6. This constraint is derived from comparing the limits

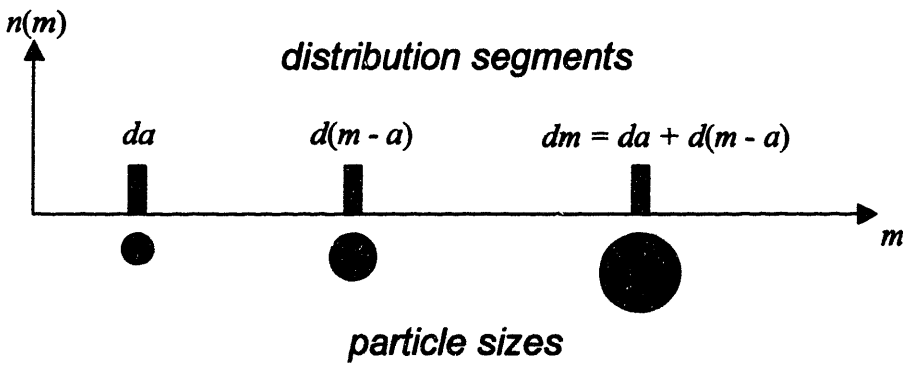

Figure C-6: Particle masses in multicomponent coagulation.

of the coagulating intervals, as summarized in Table C-3. It holds from this constraint that if *da*

Table C-3: Differential coagulation intervals

Variable	*Lower Limit*	*Upper Limit*	*Range*
a	a	$a + da$	da
$m - a$	$m - a$	$(m - a) + d(m - a)$	$d(m - a)$
m	m	$m + dm$	$dm = m - a + d(m - a) + a + da - m$ $dm = da + d(m - a)$

is held constant, then $d(m - a)/dm = 1$. This allows the conversion of Equation (C.12) to a form

describing the evolution of the number density $n(m)$.

$$\frac{dn(m)}{dt} = \beta(a, m-a)n(a)da \cdot n(m-a) \tag{C.14}$$

This expression account for the creation of particles size m by the coagulation of particles of mass a with particles of mass m - a. In order to find the total contribution, it is necessary to consider all possible combinations of a and m - a which can produce a particle of mass m. To accomplish this, integration over all possible values of a is employed:

$$\frac{dn(m)}{dt} = \int_{\Omega} \beta(a, m-a)n(a)n(m-a)da \tag{C.15}$$

Because the coagulating particles a and m - a clearly must be smaller than m, the integration limits for a are restricted to the interval (0, m). However, using these integration limits actually repeats each value of the integrand, as illustrated in Figure C-7. Table C-4 shows direcly how these inte-

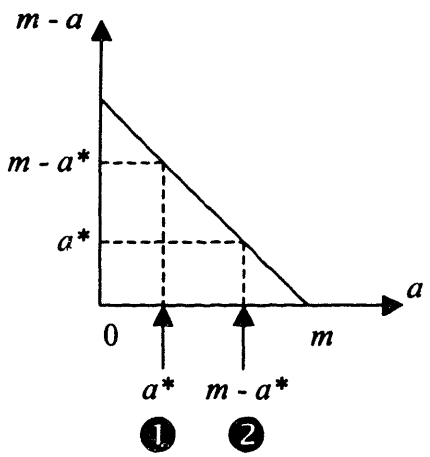

Figure C-7: Replication of integrand during coagulation production integration over the interval a = (0, m).

grand values are repeated. Clearly, the same.duplication of integrands will occur for every value $a^* \in (0, m)$. In order to correct for this double-counting, the integral can be multiplied by a factor of 1/2:

Table C-4: Duplication of integrands during coagulation production integration over $a = (0, m)$.

Point	1	2
a	a^*	$m - a^*$
$m - a$	$m - a^*$	a^*
$n(a)$	$n(a^*)$	$n(m - a^*)$
$n(m - a)$	$n(m - a^*)$	$n(a^*)$
$\beta(a, m - a)$	$\beta(a, m - a)$	$\beta(a, m - a)$
Integrand	$\beta(a^*, m-a^*)n(a^*)n(m-a^*)$	$\beta(m-a^*, a^*)n(m-a^*)n(a^*)$

$$\frac{dn(m)}{dt} = \frac{1}{2}\int_0^m \beta(a, m-a)n(a)n(m-a)da \tag{C.16}$$

Alternatively, the double-counting can be eliminated by reducing the integration limits for a, as shown in Figure C-8.

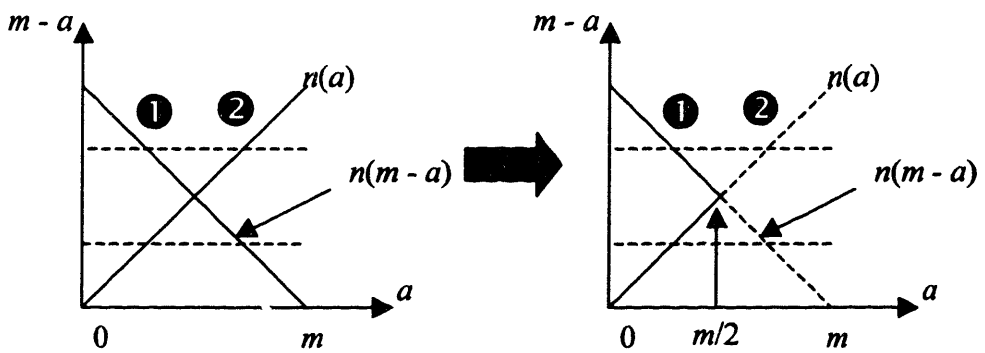

Figure C-8: Elimination of double-counting by reduction of integration range.

It the diagram at the left, the integration range covers the interval $a = (0, m)$. This double-counts the points labeled "1" and "2," which correspond to the points $a = a^*$ and $a = m - a^*$ in Figure C-7. By decreasing the integration range to $a = (0, m/2)$, the diagram at the right shows how only point 1 is counted. Point "2," is outside the integration limit and is therefore not counted. In fact, none of the points outside the integration limits are counted, which completely eliminates double-counting. The factor of 1/2 can thus be eliminated from the governing equation when the integration range for a is $(0, m/2)$:

$$\frac{dn(m)}{dt} = \int_0^{\frac{m}{2}} \beta(a, m-a)n(a)n(m-a)da \tag{C.17}$$

Equations (C.16) and (C.17) are equivalent forms of the expression for productionof particles size m due to binary coagulation of smaller particles.

C.4 Two-component Coagulation Production

In two-component systems, the number density $n(\mathbf{m}) = n(m_1, m_2)$ where m_1 and m_2 are the individual component masses. If two particles a and b of respective compositions (a_1, a_2) and (b_1, b_2) coagulate, a particle of mass (m_1, m_2) will be formed. Figure C-9 illustrates these coagulating particles and the resulting particle of composition m.

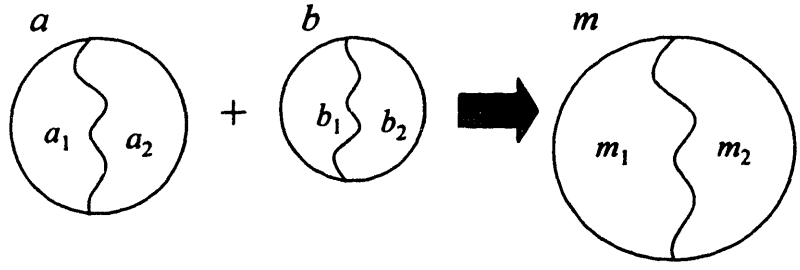

Figure C-9: Individual mass components of two coagulating particles *a* and *b*.

Note that four compositions are needed to fully define the two coagulating particles: a_1, a_2, b_1, and b_2. However, m_1 and m_2 are related to the individual component masses in the coagulating particles by their respective mass balances:

$$\begin{aligned} m_1 &= a_1 + b_1 \\ m_2 &= a_2 + b_2 \end{aligned} \tag{C.18}$$

Using this restraint, the number of degrees of freedom required to specify the coagulation rate of particles at composition $m = (m_1, m_2)$ is reduced from four to two. Thus, only a_1 and a_2 need to be specified to determine the coagulation rate:

$$\begin{aligned} \frac{dn(\mathbf{m})}{dt} &= \beta(\mathbf{a},\mathbf{b})n(\mathbf{a})n(\mathbf{b})da_1da_2 \\ \frac{dn(m_1,m_2)}{dt} &= \beta(a_1,a_2,b_1,b_2)n(a_1,a_2)n(b_1,b_2)da_1da_2 \end{aligned} \tag{C.19}$$

Of course, these expressions only account for coagulation production from one set of combinations for the coagulating particles. In order to produce the coagulation production expression for all combinations of particles, integration is performed over both of these degrees of freedom.

$$\begin{aligned} \frac{dn(\mathbf{m})}{dt} &= \int_{\Omega_2}\int_{\Omega_1}\beta(\mathbf{a},\mathbf{b})n(\mathbf{a})n(\mathbf{b})da_1da_2 \\ \frac{dn(m_1,m_2)}{dt} &= \int_{\Omega_2}\int_{\Omega_1}\beta(a_1,a_2,b_1,b_2)n(a_1,a_2)n(b_1,b_2)da_1da_2 \end{aligned} \tag{C.20}$$

Substituting the mass balance from Equation (C.19) into this expression results in the production expression for two-component coagulation:

$$\begin{aligned} \frac{dn(\mathbf{m})}{dt} &= \int_{\Omega_2}\int_{\Omega_1}\beta(\mathbf{a},\mathbf{m}-\mathbf{a})n(\mathbf{a})n(\mathbf{m}-\mathbf{a})da_1da_2 \\ \frac{dn(m_1,m_2)}{dt} &= \int_{\Omega_2}\int_{\Omega_1}\beta(a_1,a_2,m_1-a_1,m_2-a_2)n(a_1,a_2)n(m_1-a_1,m_2-a_2)da_1da_2 \end{aligned} \tag{C.21}$$

Because neither of the coagulating particles cannot contain more a component than the product particle m, the integration limits for a_1 and a_2 are restricted to the intervals $(0, m_1)$ and $(0, m_2)$, respectively.

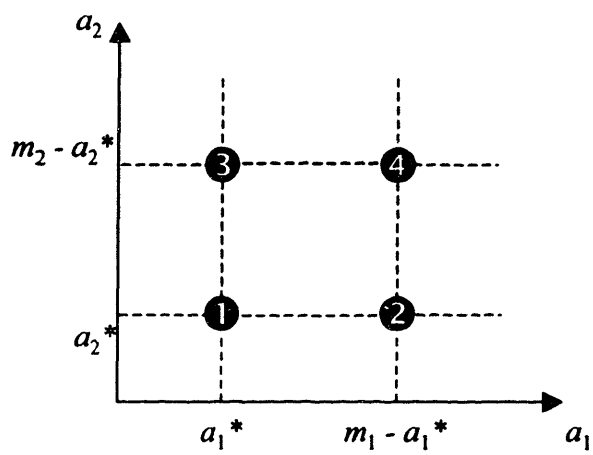

Figure C-10: Elimination of double-counting by reduction of integration range.

In order to properly analyze any possible double-counting in this two-dimensional integral, the integrand will be analyzed at all combinations of points involving mass $a_1 = a_1^*$ or $a_2 = a_2^*$. These points are summarized in Table 6. Note that the integrand for the coagulation production

Table C-5: Duplication of multicomponent coagulation production integrands over $a = (0, m)$.

Point	$n(a_1, a_2)$	$n(m_1 - a_1, m_2 - a_2)$	β
1	$n(a_1^*, a_2^*)$	$n(m_1 - a_1^*, m_2 - a_2^*)$	$\beta[(a_1^*, a_2^*),(m_1 - a_1^*, m_2 - a_2^*)]$
2	$n(m_1 - a_1^*, a_2^*)$	$n(a_1^*, m_2 - a_2^*)$	$\beta[(m_1 - a_1^*, a_2^*),(a_1^*, m_2 - a_2^*)]$
3	$n(a_1^*, m_2 - a_2^*)$	$n(m_1 - a_1^*, a_2^*)$	$\beta[(a_1^*, m_2 - a_2^*),(m_1 - a_1^*, a_2^*)]$
4	$n(m_1 - a_1^*, m_2 - a_2^*)$	$n(a_1^*, a_2^*)$	$\beta[(m_1 - a_1^*, m_2 - a_2^*),(a_1^*, a_2^*)]$

expression is the product of the three columns. Due to the symmetrical nature of the coagulation kernel β, points 1 and 4 produce the same integrand, as do points 2 and 3. These two sets of integrands are distinct, illustrating that the integral over the limits $a_1 = (0, a_1)$ and $a_2 = (0, a_2)$ still produces double-counting and requires the factor 1/2 to correct for this:

$$\frac{dn(m_1, m_2)}{dt} = \frac{1}{2}\int_0^{m_2}\int_0^{m_1}\beta(a_1, a_2, m_1 - a_1, m_2 - a_2)n(a_1, a_2)n(m_1 - a_1, m_2 - a_2)da_1 da_2 \quad \text{(C.22)}$$

It is still possible, however to reduce the integration limits while eliminating this double-counting. By reducing the integration limits in the outer integral to $a_2 = (0, m_2/2)$, only points 1 and 2 in Figure C-10 are included in the integral and no double-counting is produced:

$$\frac{dn(m_1, m_2)}{dt} = \int_0^{\frac{m_2}{2}}\int_0^{m_1}\beta(a_1, a_2, m_1 - a_1, m_2 - a_2)n(a_1, a_2)n(m_1 - a_1, m_2 - a_2)da_1 da_2 \quad \text{(C.23)}$$

C.5 Multicomponent Coagulation Production

In the general case of an s-component system, the point $a^* = (a_1, a_2, ..., a_s)$ will generate 2^s combinations of node points. This is due to the fact that the expression for $n(\mathbf{a}^*)$ can either be composed of a_i^* or $m_i - a_i^*$ for each component i. This binary set of alternatives for each compo-

nent generates a set of 2^s possible combinations and therefore 2^s node points. Each of these node points has *exactly* one other equivalent integrand, where $n(\mathbf{a}^*)$ is the "complement" of the original point. These two points produce equivalent integrands, as illustrated in Figure C-11. Because

$n(\mathbf{a}^*)$	$n(\mathbf{m} - \mathbf{a}^*)$	
$n(m_1 - a_1^*, a_2^*, ..., m_s - a_s^*)$	$n(a_1^*, m_2 - a_2^*, ..., a_s^*)$	← **original point**
$n(a_1^*, m_2 - a_2^*, ..., a_s^*)$	$n(m_1 - a_1^*, a_2^*, ..., m_s - a_s^*)$	← **"complement" point**

Figure C-11: Elimination of double-counting by reduction of integration range.

only one unique complement exists, the replication of integrands is limited to double-counting and the factor of 1/2 will correct this regardless of the number of components in the system, *s*.

$$\frac{dn(m_1, m_2)}{dt} = \frac{1}{2}\int_0^{m_s}\cdots\int_0^{m_2}\int_0^{m_1}\beta(a_1, a_2, m_1 - a_1, m_2 - a_2)n(a_1, a_2) \cdot n(m_1 - a_1, m_2 - a_2)da_1 da_2 \ldots da_s \tag{C.24}$$

Similarly, this factor of 1/2 can be eliminated by reducing the integration limits of the outer integral:

$$\frac{dn(m_1, m_2)}{dt} = \int_0^{\frac{m_s}{2}}\cdots\int_0^{m_2}\int_0^{m_1}\beta(a_1, a_2, m_1 - a_1, m_2 - a_2)n(a_1, a_2) \cdot n(m_1 - a_1, m_2 - a_2)da_1 da_2 \ldots da_s \tag{C.25}$$

C.6 Summary

Coagulation is one of the most important mechanisms in the formation of particles. However, it is also the most computationally intensive of the mechanisms influencing these processes. This paper presents a systematic and sound method for significantly reducing the computational effort required for coagulatiion calculations while maintaining the same accuracy.

The symmetry of the coagulation kernel coupled with the mass balance on coagulating parti-

cles results in double-counting over the logical range of integration for the coagulaiton production expression. This result holds regardless of the number of species in the system. This can either be corrected by multiplying the integral by a factor of 1/2 or by reducing the upper integration limit for the outermost integration variable by a factor of 1/2.

Reducing the integration range by a factor of 1/2 rougly reduces the computational cost of evaluating the coagulation production kernel by 50%. Because coagulation is the most intensive mechanism to evaluate, large reductions can be expected in the time required to solve dynamic population balance problems.

References

[1] Valentas, Kenneth J.; Amundson, Neal R. *Breakage and Coalescence in Dispersed Phase Systems,* Industrial and Engineering Chemistry Fundamentals, **5,** 533-542, 1966.

[2] Valentas, Kenneth J.; Bilous, Olegh; Amundson, Neal R. *Analysis of Breakage in Dispersed Phase Systems,* Industrial and Engineering Chemistry Fundamentals, **5**, 271-279, 1966.

Appendix D: Parameter Estimation in Population Balance Models

D.1 Introduction

Population balance models are used to describe a wide range of physical phenomena from crystallization and aerosol dynamics to granulation and milling operations. Typical population balance models are governed by a set of partial integro-differential equations. Solution of these equations requires numerous evaluations of integrals at each numerical time-step, which is computationally intensive and time-consuming, causes inversion algorithms to scale very poorly with number of model evaluations.

Inversion algorithms generally converge after many iterations, each of which requires a varying number of model evaluations depending on the algorithm. Random and grid searches as well as simulated annealing rely almost entirely on a large number of model evaluations to perform an inversion. In contrast, gradient search algorithms perform a significant amount of analysis on the results of model evaluations in an attempt to find a more optimum convergence path. The stability of gradient search algorithms is generally not known *a priori*; as a result a number of model evaluations are often required to ensure stability. The ridge regression technique, however guarantees stability by performing considerable analysis on the model evaluations at each time step and is therefore promising for population balance model inversion applications.

This work investigates the efficacy of ridge regression for population balance models by using an analytical solution describing the evolution of a population subject to particle growth and coagulation under special conditions.

D.2 Population Balances

D.2.1 Representation of population distributions

Populations are generally composed of a large size range of particles containing a large number of particles at each size. It is therefore convenient to represent the population as a distribution of particles where if $n(s)$ is the number density of particles at size s, then the number of particles between size s and $s + ds$ is:

$$N = \int_{s}^{s+ds} n(s) \tag{D.1}$$

and can be represented by the shaded region Figure D-1:

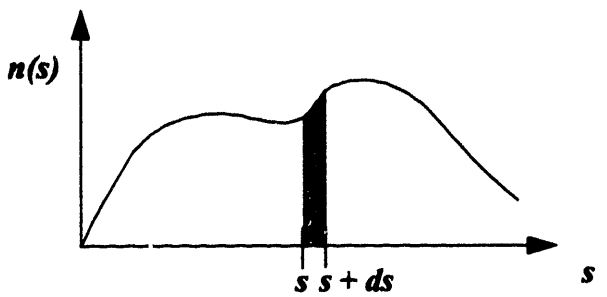

Figure D-1: Distribution Representation of Population

The number density can be converted to another basis by equating the number of particles in a differential "slice" of the distribution. For example:

$$n(s)ds = n(\log s)d(\log s) \Rightarrow n(s) = n(\log s)\frac{d(\log s)}{ds} = \frac{n(\log s)}{\ln(10)s} \tag{D.2}$$

$$n(\log s) = \ln(10)s \cdot n(s) = 2.303s \cdot n(s)$$

D.2.2 Dynamic population balance equation

Population balances are generally governed by the general dynamic equation (GDE):

$$\frac{\partial}{\partial t}n(s) = \underbrace{\frac{1}{2}\int_0^s \beta(x, s-x)n(x)n(s-x)dx}_{\text{coagulation from smaller particles}} + \underbrace{\int_s^\infty \gamma(x, s)n(x)dx}_{\text{fragmentation from larger particles}}$$

$$- \underbrace{n(s)\int_0^s \gamma(s, x)dx}_{\text{fragmentation into smaller particles}} - \underbrace{n(s)\int_0^\infty \beta(x, s)n(x)dx}_{\text{coagulation with other particles}}$$

$$\underbrace{\nabla \cdot \mathbf{v}n(s)}_{-\text{transport due to convection}} + \underbrace{\nabla K \cdot \nabla n(s)}_{\text{transport due to diffusion}} + \underbrace{f(s)}_{\text{other functions e.g., growth}} \tag{D.3}$$

The first coagulation term evaluates the rate at which particles size s are produced from particles size x and s-x by integrating the coagulation kernel $\beta(x, s - x)$ over the entire range of particles that are smaller than s. The factor of ½ results from the fact that two particles form to produce one particle - half as many new particles as old particles. The fragmentation kernel $\gamma(x, s)$ expresses the efficiency at which a larger particle size x fragments to produce a smaller particle size s. Other particles may also be produced through this fragmentation, but only that particles size s will affect $\partial n(s)/\partial t$. The expressions for fragmentation of a particle size s and coagulation of a particle size s are developed similarly. The GDE may also include terms for particle transport, diffusion, or other effects such as growth, nucleation, deposition, etc. For example, a particle growth term takes the form:

$$\frac{\partial}{\partial t}n(s) = \frac{\partial}{\partial s}(I(s)n(s)) + \text{other effects} \tag{D.4}$$

Particle size s can be represented by a variety of metrics, including mass, length, or volume.

D.2.3 Analytical solution

An analytical solution exists for a special case of the GDE for particle coagulation and growth when the coagulation kernel is constant and the growth rate is proportional to particle size:

$$\beta(x, y) = \beta_0 \qquad I(v) = \sigma v \tag{D.5}$$

As in Equation (D.5), particle size will be represented by volume, v, for the remainder of this paper. The analytical solution requires an exponential initial number density distribution based on particle volume:

$$n(v, 0) = \frac{N_0}{v_0}\exp\left(\frac{-v}{v_0}\right) \tag{D.6}$$

with an average particle size v_0 and an initial total number of particles N_0. The analytical solution is:

$$n(v,t) = \frac{N_0}{v_0(1+\tau)^2}\exp\left(\frac{-v}{v_0(1+\tau)}\exp(-\Lambda\tau) - \Lambda\tau\right) \tag{D.7}$$

where $\tau = \frac{1}{2}N_0\beta_0 t$ and $\Lambda = \frac{2\sigma}{N_0\beta_0}$

If the parameters take on the values given in Table D-1:

Table D-1: Parameter Values

Parameter	*Value*	*Units*
N_0	1.0×10^{6}	–
β_0	1.0×10^{-7}	s^{-1}
σ	1.0×10^{-2}	$\frac{\mu m^3}{s}$

Figure D-2 shows plots of the analytical solution at t=0, 20, and 200 with 35 points evenly spaced on a log scale:

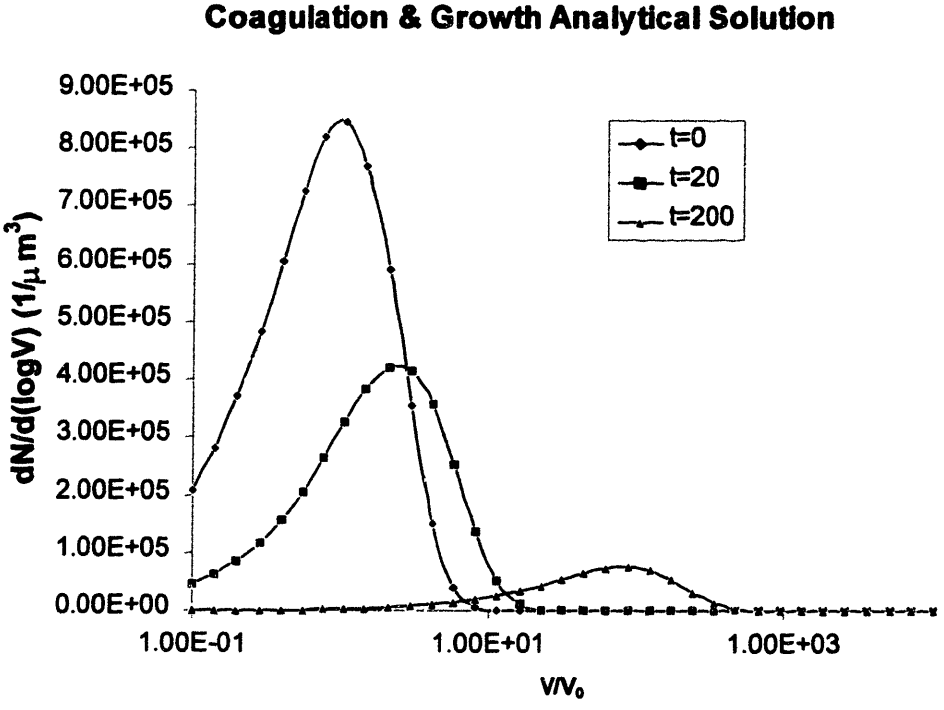

Figure D-2: Analytical results comparison.

The $dN/d(\log(V))$ notation is equivalent to $n(\log(V))$. Distributions are commonly expressed in this form, as $n(\log(V))$ is actually the change in total number of particles N with respect to change in $\log(V)$.

D.3 Parameter Estimation Techniques

D.3.1 Least squares techniques

Least squares parameter estimation techniques seek to estimate optimal parameter values by linearizing a function at the initial best parameter estimate:

$$\mathbf{n} = \mathbf{n_0} + \mathbf{A}\Delta\mathbf{p} \tag{D.8}$$

where $\mathbf{A}$ is the Jacobian with elements $a_{ij} = \frac{\partial n_i}{\partial p_j}$ if n_i is the number density at node i and p_j is the j^{th} parameter.

If $\Delta\mathbf{n}$ is defined as the vector of differences between data and model values at each point

$$\Delta n_i = n_i - \hat{n}_i \tag{D.9}$$

then the least squares solution which minimizes the length of the error vector $\Delta\mathbf{n}$ is:

$$\Delta\mathbf{p} = (\mathbf{A}^T\mathbf{A})^{-1}\mathbf{A}^T\Delta\mathbf{n} \tag{D.10}$$

The new parameter estimates are then found by $\mathbf{p}_{new} = \mathbf{p}_{old} + \Delta\mathbf{p}$ and the length of the error vector is calculated. The new $\mathbf{A}$ matrix is then evaluated at the new parameter values $\mathbf{p}$ and the next iteration of the algorithm is performed. Often, however, the $\mathbf{A}^T\mathbf{A}$ matrix is not well-conditioned, so "damping" is added to the system to facilitate the matrix inversion:

$$\Delta\mathbf{p} = (\mathbf{A}^T\mathbf{A} + \varepsilon^2\mathbf{I})^{-1}\mathbf{A}^T\Delta\mathbf{n} \tag{D.11}$$

Increased damping has the effect of limiting the magnitude of $\Delta\mathbf{p}$ and slowing the convergence rate while increasing the stability of the algorithm.

One common measure for the error vector is the root mean square (RMS) error:

$$\text{RMS} = \sqrt{\frac{\sum_{i=1}^{N}(n_i - \hat{n}_i)^2}{N}} \tag{D.12}$$

In general, least squares techniques will seek to reduce this RMS error at each iteration using a

variety of schemes which adjust damping values until the RMS error is reduced (i.e., the algorithm remains stable) at the new parameter values. For the ridge regression algorithm, a wide range of damping values are used to show the values of the new parameters as a function of damping, allowing the new parameter values to be hand-picked. Most often parameters are chosen which represent some moderate change to avoid either converging painfully slow or becoming unstable.

D.3.2 Log-rescaling

Log-rescaling attempts to rescale data the Jacobian matrix **A** such that the derivatives are normalized and dimensionless. The elements of the **A** matrix for log rescaling are:

$$a_{ij} = \frac{p_j \partial n_i}{n_i \partial p_j} \tag{D.13}$$

D.4 Results

The response surface of the error at t=200 was evaluated by:

$$\text{error} = \int_{v_{min}}^{v_{max}} \sqrt{(n(v)|_{\text{data}} - n(v)|_{\text{model}})^2}\, dv \tag{D.14}$$

Figure D-3 plots the contours of the response surface using the parameters defined in Table D-1. The optimum parameter values are in the center of the red oval at the left side of the plot; the ini-

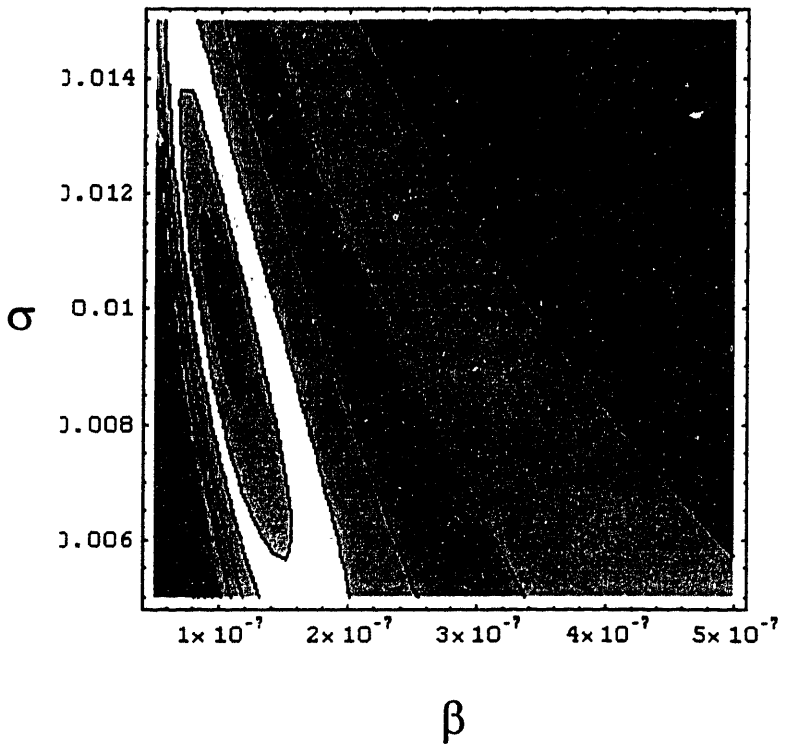

Figure D-3: Model response surface contours.

tial parameter guess for parameter estimation is marked by the **X** and listed in Table D-2:

Table D-2: Initial Parameter Guesses

β	σ
3.0×10^{-7}	7.0×10^{-3}

Data points were generated by adding Gaussian noise with a standard deviation equal to 10% of the value of each point to the analytical solution at 35 points evenly spaced along a log scale from

0.1 to $1.0x10^4$. Figure D-5 shows the response surface of the RMS error of the data points with

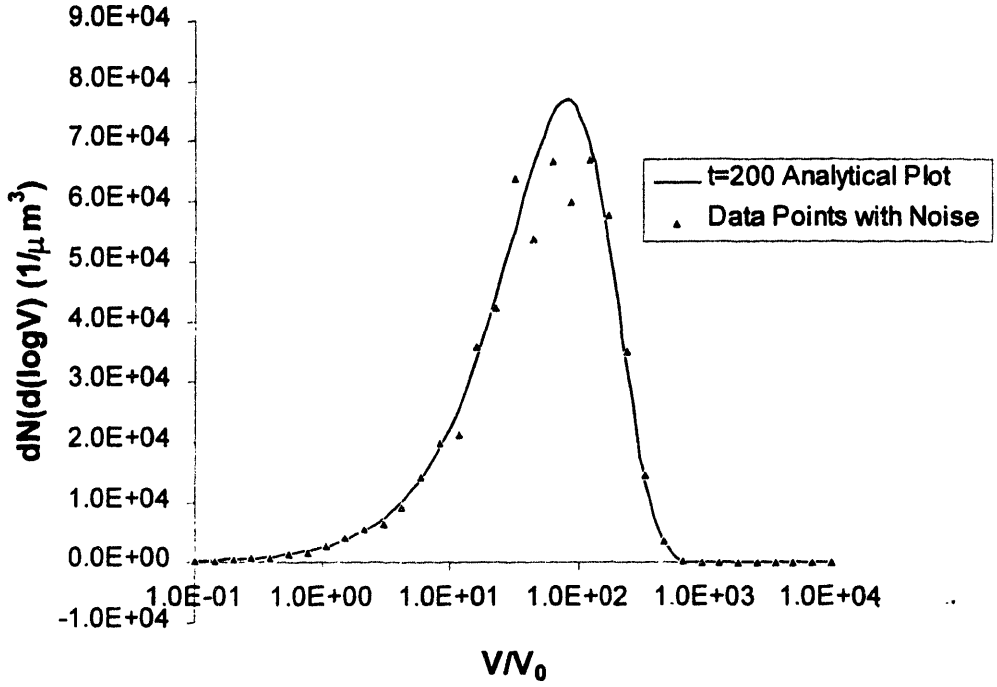

Figure D-4: Data points for parameter estimation

noise vs. model points:

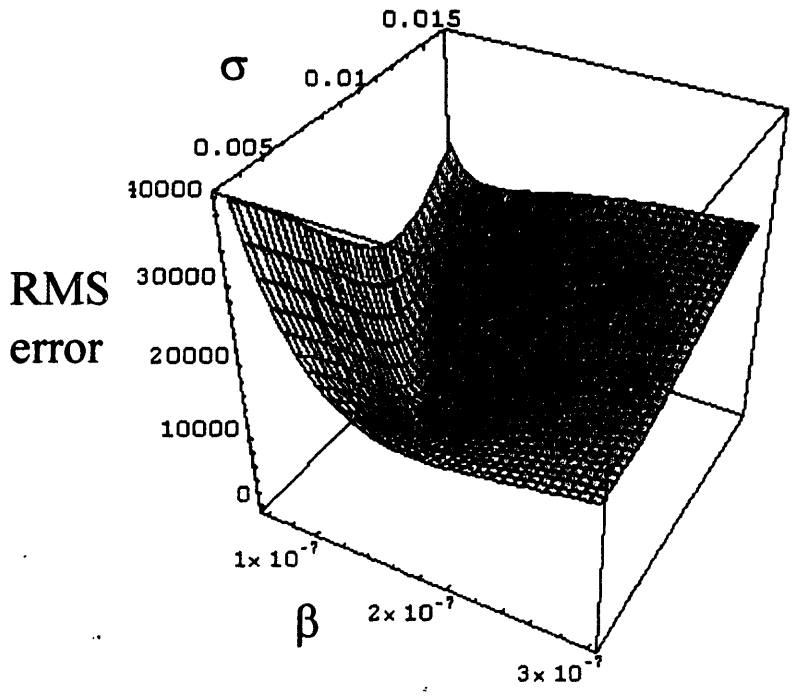

Figure D-5: RMS response surface.

Note that the contours of this surface would appear very similar to Figure D-4, indicating that the RMS response surface will take on a similar shape regardless of the noise. The following subsections review the results of variations on the ridge regression method with this data set. For all of the inversions performed, derivatives for the Jacobian matrix were estimated using a two-point finite difference formula.

D.5 Case Study: Log rescaling with low number density threshold

D.5.1 Implementation

Unlike the output from an analytical model, all numerical solutions to the GDE will employ some minimum number density threshold below which the number of particles is essentially negligible. Two undesirable effects arise from this effect:

- 1) the first derivative is discontinuous at the point where the threshold is first enforced, subjecting the Jacobian to error at this point

• 2) the sensitivity of the model to every parameter is artificially forced to zero wherever the threshold is in force

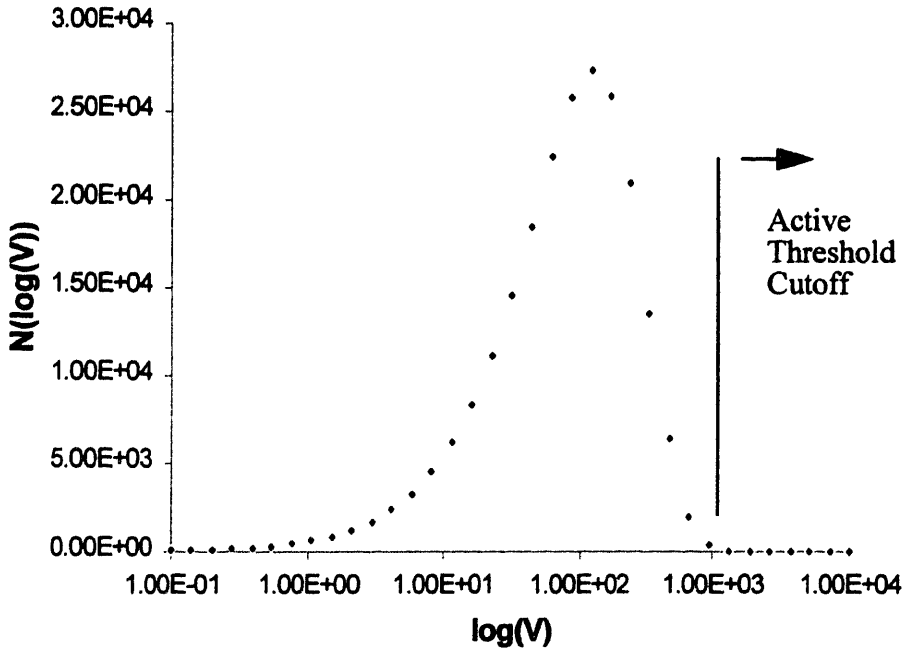

Figure D-6: Number Density Threshold

The number density threshold for this graph is 1.0×10^{-12}. Previously, an uncertainty analysis was carried out on this system which revealed that the "front" of the number density distribution is the region where the model is most sensitive to variations in the parameters β and σ, as shown

by the error bars.

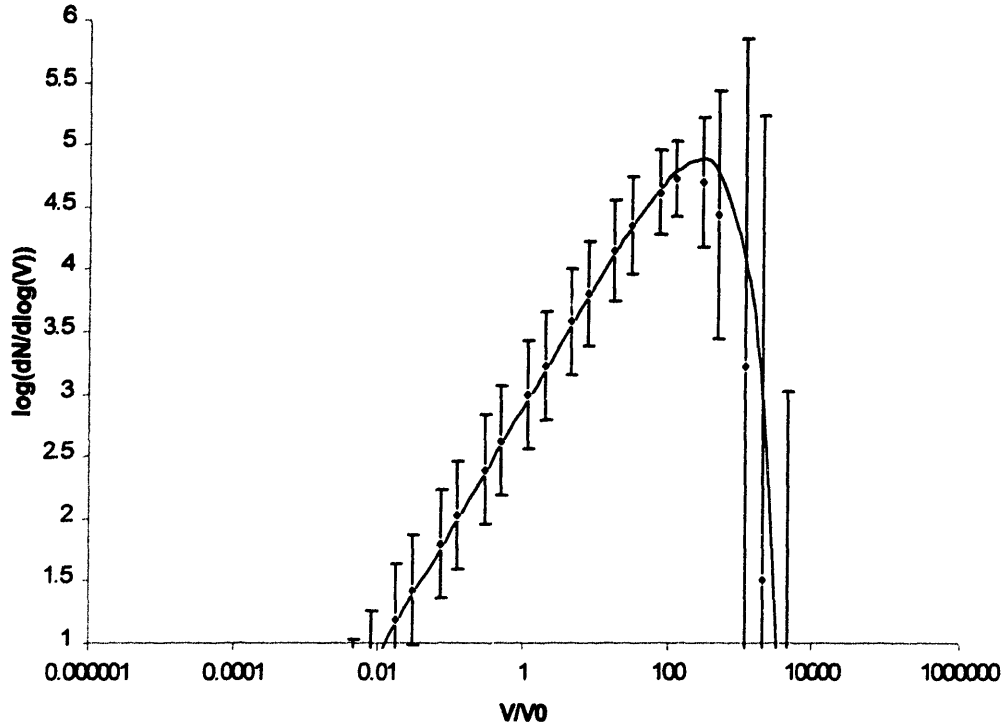

Figure D-7: Uncertainty analysis of particle size distribution.

In an effort to retain the effects of the "front" part of the distribution, the threshold was set to an extremely low value, 1.0×10^{-300}. This resulted in and $\mathbf{A}^{\mathbf{T}}\mathbf{A}$ matrix with eigenvalues in the range of 1.0×10^{50} and a completely intractable solution.

D.6 Case Study: Log rescaling using logN(log(V))

In an effort to scale down the sensitivity of the system and eliminate threshold effects, the output of the model and data was expressed as log$N$(log(V)). Note that because log rescaling uses the error vector:

$$\Delta\ln(N) = \ln(N_{\text{data}} - N_{\text{model}}) \tag{11.2}$$

whenever N_{data} and N_{model} have different signs, $\Delta\ln(N)$ will be undefined. For these cases, $\Delta\ln(N)$ is redefined as:

$$\Delta\ln(N) = \ln(|N_{\text{data}}|) + \ln(|N_{\text{model}}|) \tag{11.3}$$

The log rescaled sensitivity expression, however, has log(N(log(V)) in the denominator, so an asymptote appears where log(N(log(V))=0, as shown in Figure D-8:

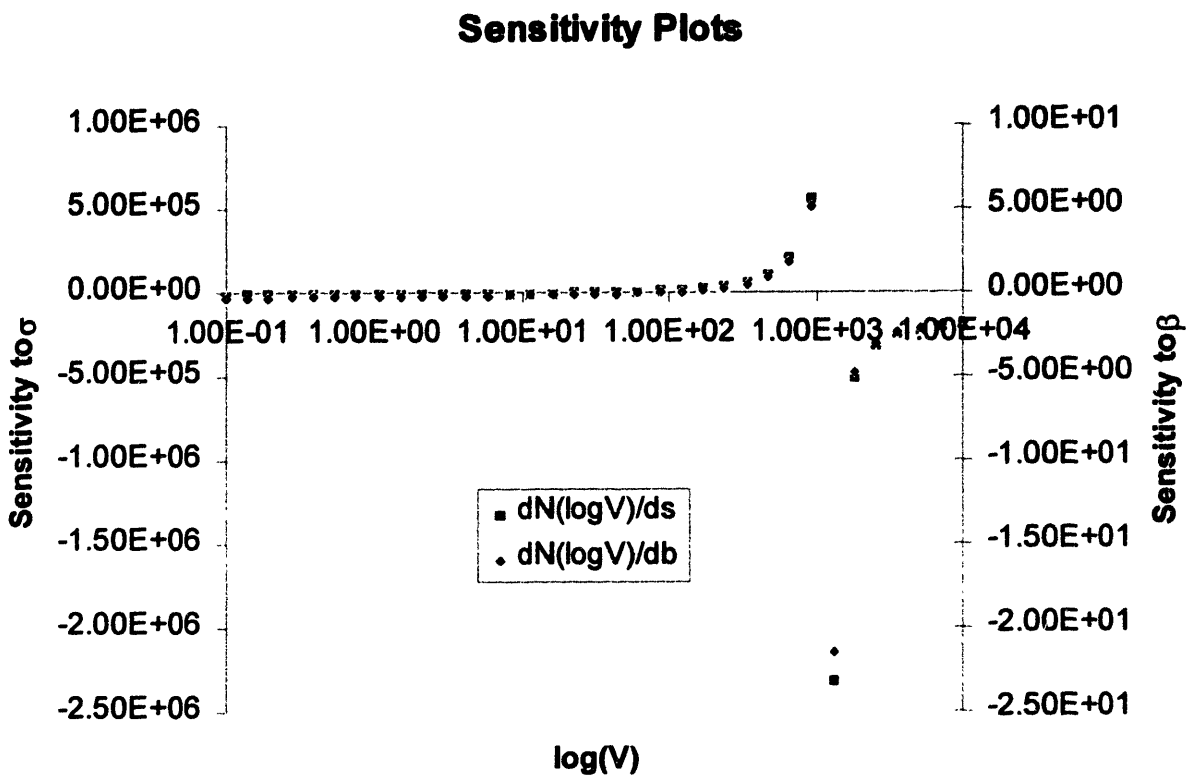

Figure D-8: Sensitivity plot of logN(log(V)) results.

D.7 Case Study: Log rescaling with data shift

Asymptotes in the sensitivity expression and the need to correct the sign of $\Delta\ln(N)$ can be eliminated by simply adding a constant to every data and model point such that all log(N)'s are

greater than zero. The resulting sensitivity plot exhibits no asymptotic behavior:

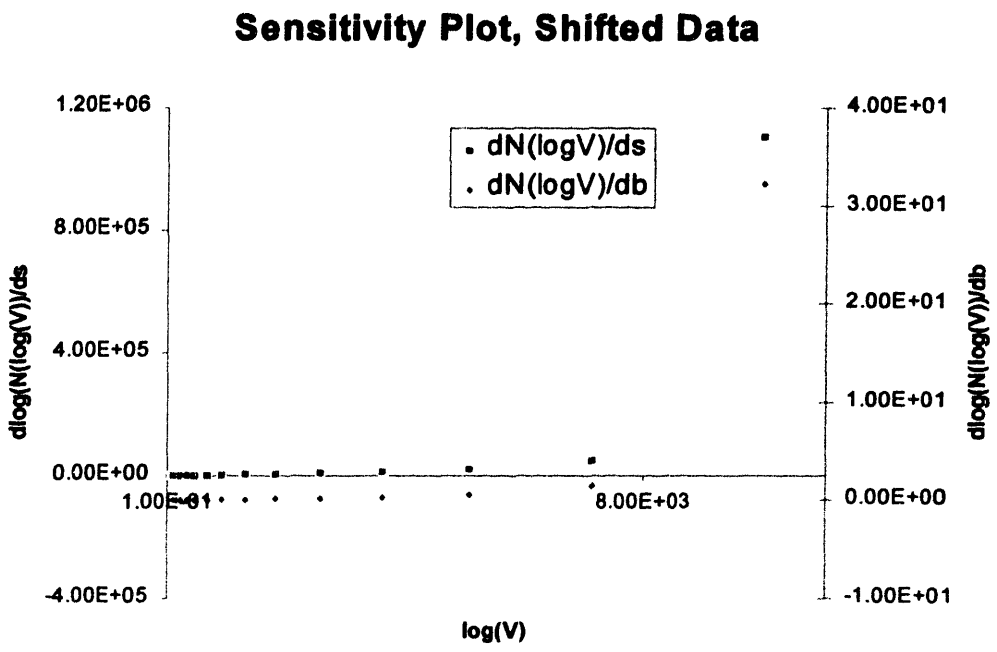

Figure D-9: Sensitivity plot with shifted data points.

However, the eigenvalues for this system make the problem no more tractable than the previous case.

Table D-3: Eigenvalues and Data Forms

Method	*Log Rescaling*	*Data*	*Eigenvalue 1*	*Eigenvalue 2*
Shifted Log	Yes	$\log(N(\log(V)))$	0.4279	8.90×10^{10}
Corrected Sign	Yes	$\log(N(\log(V)))$	2.62×10^{-4}	1.22×10^{12}
Basic Ridge Regression	No	$\log(N(\log(V)))$	4.02×10^{13}	7.28×10^{16}

D.7.1 Case Study: No log rescaling using log number density data

Ridge regression was also examined without log rescaling. As shown in Table D-3, the eigenvalues for this method suggest that this method is much more tractable than the other methods

investigated in this study. In addition, the sensitivity plot also suggested this:

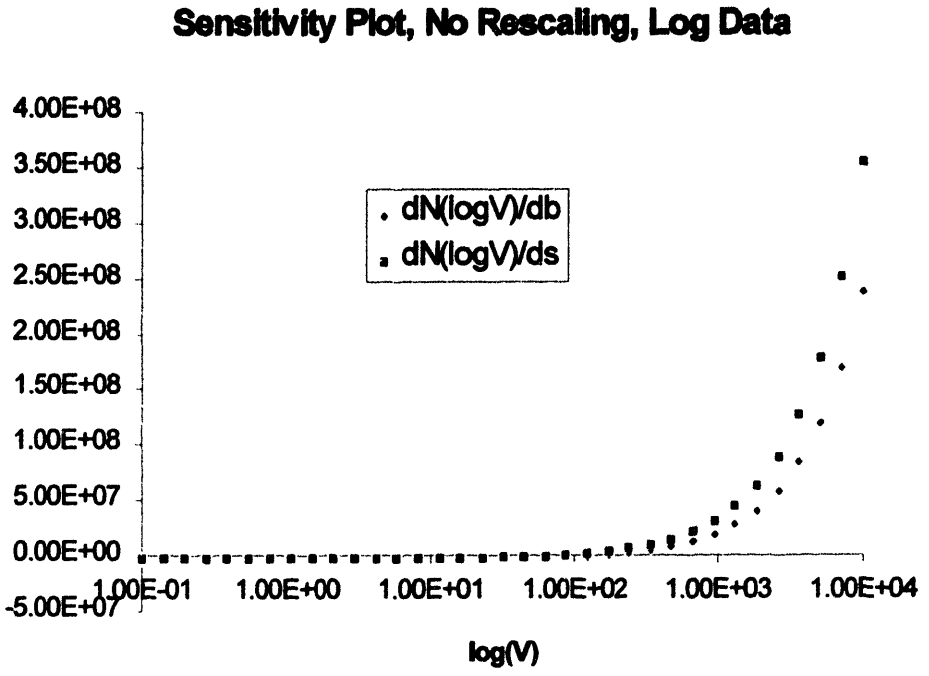

Figure D-10: Sensitivity plot for ridge regression without log rescaling.

The ridge trace for the first iteration is similarly well-behaved:

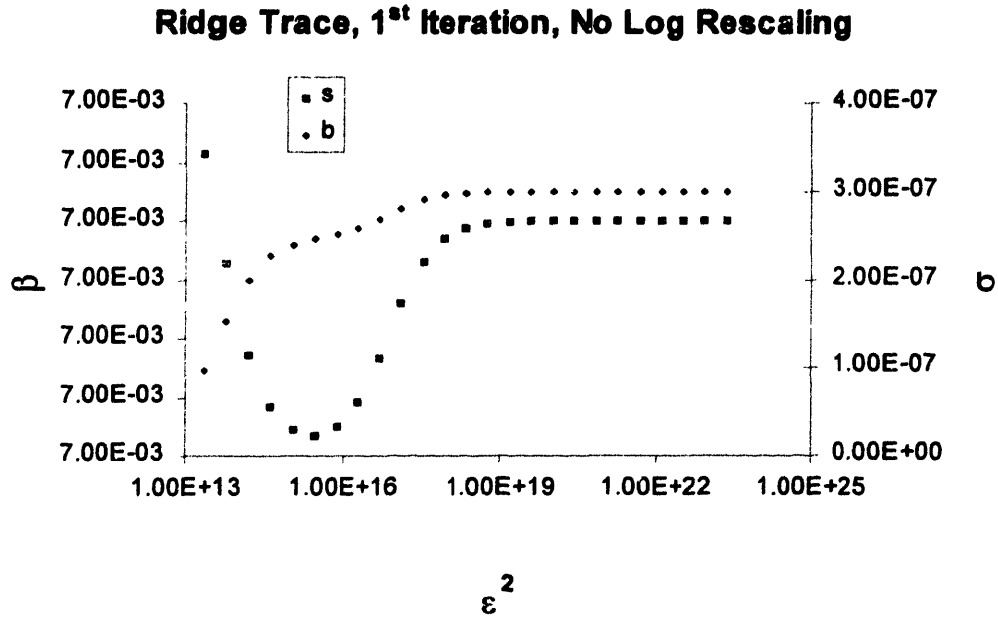

Figure D-11: Ridge trace for ridge regression without log rescaling.

Finally, the RMS error decreased monotonically with the number of iterations:

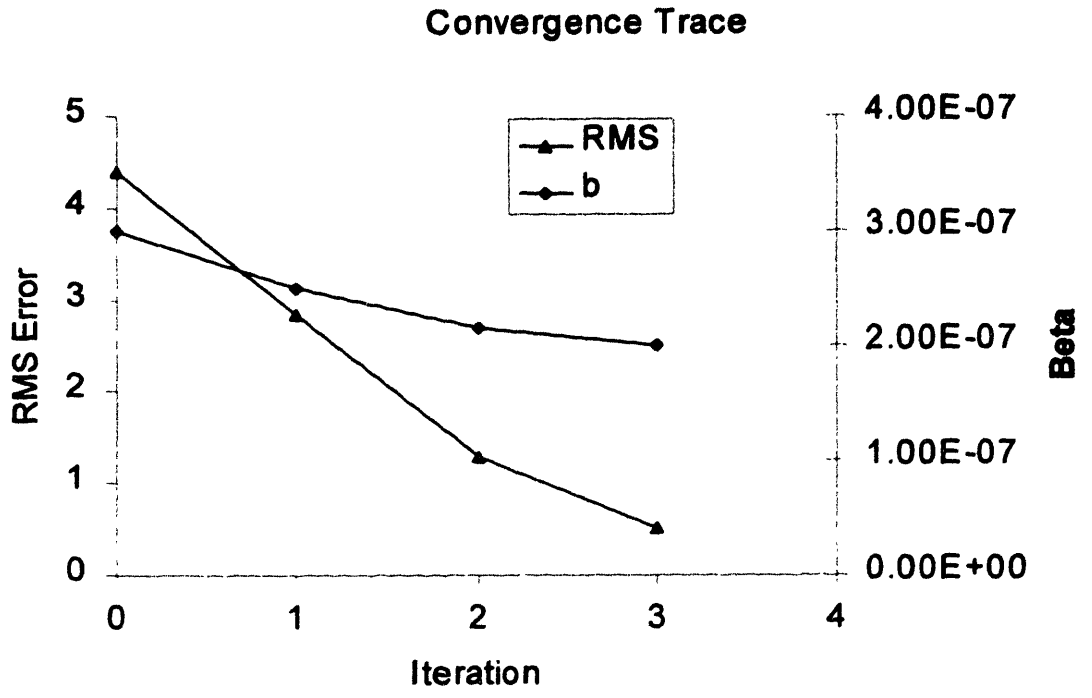

Figure D-12: RMS error and β value vs. iterations.

In addition, convergence is relatively rapid, in spite of the fact that only b changed over the first 3 iterations.

Table D-4: RMS error and Parameter Values Results

Iteration	β	σ	ε^2
0	3.0×10^{-7}	7.0×10^{-3}	7.24×10^{15}
1	2.51×10^{-7}	7.0×10^{-3}	8.26×10^{14}
2	2.14×10^{-7}	7.0×10^{-3}	1.51×10^{15}
3	1.99×10^{-7}	7.0×10^{-3}	N/A

Plotting the parameters on the RMS contour leads to the following results:

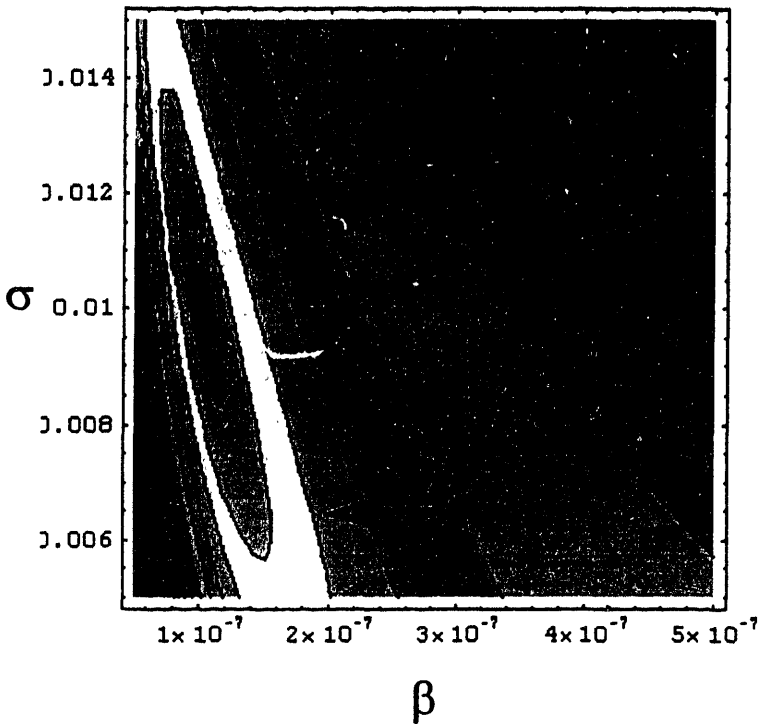

Figure D-13: Parameter evolution.

D.7.2 Conclusions

Several variations on ridge regression were investigated for inversion of a population balance problem including growth and coagulation effects. Using actual number density data as opposed to log(number density) produced ill-conditioned systems. All attempts to implement log rescaling produced ill-conditioned systems, generally due to changes in sign in the logarithm or the arguments of the logarithm. Ridge regression without log rescaling produced encouraging results. Further efforts should be made to determine an optimal convergence scheme for this method.

D.8 Definitions

D.8.1 Greek symbols

$\beta(x, y)$ The collision efficiency at which two particles size x and y coagulate to form a larger particle size $x + y$

$\gamma(x, y)$ The efficiency at which a particle size x will produce a particle size y as a result of breaking up.

Appendix E: Probability Density Functions

All probabilistic notation hinges on using some form of a *random variable* to describe the outcome of a random event. A random variable is often written in the form $x(\omega)$ where $x(\omega)$ is the outcome of a random process with ω as the input, as shown in Figure E-1.

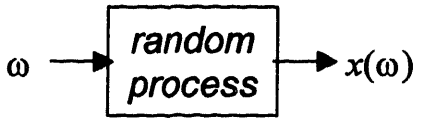

Figure E-1: Random output x(ω) from a random process with input ω.

The possible outcomes of the random event may be discrete, as in rolling a die, or continuous, as in the direction which a spinning bottle points when it comes to rest. For a discrete event, the probability of a particular outcome x_0 may be described by $p_x(x_0)$, the probability that the outcome of the random event is x_0 (Drake, 1976). This may also be expressed as $P\{x = x_0\}$ (Papoulis, 1991). For the example of rolling a six-sided die, the probability that any one side faces up is 1/6. Similarly, for a continuous event, we define the probability that the outcome lies within a range of possible outcomes. For example, the probability that the spinning bottle comes to rest between 0 and 30 degrees is 1/12. This is denoted by $p_x(0 < x < 30)$ or $P\{0 < x < 30\}$. However, what if we want to describe the probability of the outcome of a given value x_0? This is denoted in the limit:

$$f(x)dx\big|_{x_0} = \lim_{\Delta x \to 0} \frac{P\{x_0 < x < x_0 + \Delta x\}}{\Delta x} \tag{E.1}$$

and is defined as the probability density function of x. Note that this density function has units equal to $1/x$. The function $f(x)$ is a density function; therefore it does not represent an actual probability but rather a *slice* of the probability density distribution represents the probability of an event:

$$f(x)dx\big|_{x_0} = P\{x_0 < x < x_0 + dx\} = P(x)\big|_{x_0} \tag{E.2}$$

as illustrated in Figure E-2.

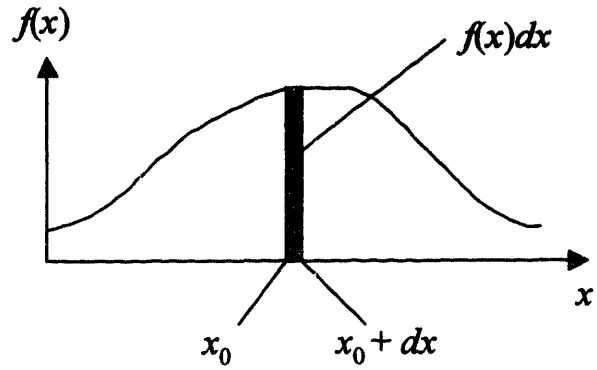

Figure E-2: Probability density function *f*(*x*) and corresponding segment ranging from x_0 to x_0 + *dx*.

Note that if we use the notation $x(\omega)$ for a random variable, this expression is slightly altered:

$$f(x(\omega))dx|_{x_0} = P\{x_0 < x(\omega) < x_0 + dx\} = P(x(\omega))|_{x_0} \tag{E.3}$$

which emphasizes the fact that the $x(\omega)$ is the outcome of a random event.

In general, several properties define probability density functions. First, probability density functions are nonnegative over their entire domain:

$$f(x) \geq 0 \qquad \forall x \tag{E.4}$$

Second, the sum of all possible outcomes must equal one. For a probability density function, this sum is expressed as an integral:

$$\int_{-\infty}^{\infty} f(x)dx = 1 \tag{E.5}$$

Often, the expression $f(x)dx$ is written as $dP(x)$ to acknowledge that the total probability $P(x)$ increases as the area under the curve expressed by the product $f(x)dx$ (see Figure E-2).

$$\int_{-\infty}^{\infty} dP(x) = 1 \tag{E.6}$$

E.1 Moments of a Probability Density Function

A number of statistics can be used to describe the characteristics of a probability density func-

tion. The most commonly used statistics are the *moments* of the probability density function. The n^{th} moment of a probability density function, written as $E[x^n]$, of the density function, is defined as:

$$E[x^i] = \int_{-\infty}^{\infty} x^i \cdot dP(x) \tag{E.7}$$

Note that the zeroeth moment is one! In general, $E[\cdot]$ is known as the expectation operator and acts as a linear operator on any arbitrary function. For example:

$$\begin{aligned} E[q(x)+r(x)] &= \int_{-\infty}^{\infty} [q(x)+r(x)]dP(x) \\ &= \int_{-\infty}^{\infty} [q(x)+r(x)]f(x)dx \\ &= \int_{-\infty}^{\infty} q(x)f(x)dx + \int_{-\infty}^{\infty} r(x)f(x)dx \\ &= E[q(x)] + E[r(x)] \end{aligned} \tag{E.8}$$

Expected value operations on the different exponents of the random variable in question are referred to as *moments*. The zeroeth moment is $E[1]$ and is equal to one for all probability density functions, the first moment $E[x]$ is the mean. Central moments are referred to as moments of the distribution less the mean. For example, the second central moment of a random variable x is $E[(x\text{-}E[x])^2]$. This moment is referred to as the *variance* of the distribution. Third and fourth central moments are referred to as *skewness* and *curtosis*, respectively.

E.2 Moment Generating Functions

Special probability density functions have well-defined standard central moments. One such example is the normal, or Gaussian probability density function. The normal probability density function is:

$$p_x(x) = f(x) = \frac{1}{\sigma\sqrt{2\pi}} e^{-\frac{x^2}{2\sigma^2}} \tag{E.9}$$

The n^{th} moment of this density function is given by the formula (Papoulis, 1991):

$$E[x^n] = \int_{-\infty}^{\infty} f(x)x^n dx = \int_{-\infty}^{\infty} \frac{1}{\sigma\sqrt{2\pi}} e^{\frac{-x^2}{2\sigma^2}} x^n dx$$
$$= \begin{cases} 0 & n = 2k+1 \\ 1 \cdot 3 \cdot \ldots (n-1)\sigma^n & n = 2k \end{cases} \tag{E.10}$$

where k is any nonnegative integer. This property is critical to the derivation of the split composition distribution method in Chapter 7.

References

[1] Drake, Alvin.W. *Fundamentals of Applied Probability Theory,* McGraw-Hill, Inc. 1967.

[2] Papoulis, Athanasios *Probability, Random Variables, and Stochastic Processes,* 3rd Ed., McGraw-Hill, 1991.

Appendix F: Orthogonal Polynomials

Unique sets of orthogonal polynomials exist on and are defined by the interval over which they are orthogonal. Table lists different sets of polynomials and their corresponding domains:

Table F-1: Summary of Orthogonal Polynomials

Orthogonal Polynomial	*Domain Type*	*Domain Example*
Hermite	Infinite	$(-\infty,\infty)$
Laguerre	Semi-Infinite	$(0,\infty)$
Legendre	Bounded	$(0,1)$

For more information on types of orthogonal polynomials, please refer to Wang (1999).

Orthogonal polynomials are uniquely defined by a recursive relationship. An n^{th} order polynomial:

$$L_n = \sum_{i=0}^{n-1} a_i r_i(x) \tag{F.1}$$

If L_n is an orthogonal polynomial of order n - 1, then the following conditions completely determine the polynomial:

$$\begin{aligned} a_0 &= 1 \\ \langle L_i, L_j \rangle &= 0 \qquad \forall i \neq j \end{aligned} \tag{F.2}$$

In the case where the polynomial is also *orthonormal*, the following additional condition applies:

$$\langle L_i, L_i \rangle = 1 \qquad \forall i \tag{F.3}$$

In the case of a Legendre polynomial over the domain (0, 1), these relations yield $L_0 = 1$, and L_1 follows from recursion:

$$L_0 = 1, L_1 = a_0 + a_1 x$$
$$\langle L_0, L_1 \rangle = \int_0^1 L_0 \cdot L_1 dx = \int_0^1 1 \cdot (1 + a_1 x) dx = 0 \Rightarrow x + \frac{a_1}{2} x^2 \Big|_0^1 = 0 \Rightarrow a_1 = 2 \qquad \text{(F.4)}$$
$$\Rightarrow L_1 = 1 - 2x$$

The $n + 1$ undetermined coefficients of an n^{th} order orthogonal polynomial are likewise determined by n inner products with all lower-order polynomials from L_0 to L_{n-1} and an arbitrary scaling condition $a_0 = 1$. In the special case of orthonormal polynomials, the condition $a_0 = 1$ is replaced by the orthonormality condition given in Equation (F.3).

Taking the example of the first Legendre polynomial L_1 from Equation (F.4), this normalization requirement results in:

$$\int_0^1 w^2 (1 - 2x)^2 dx = 1 \Rightarrow w^2 \frac{(1 - 2x)^3}{-6} \Big|_0^1 = 1 \Rightarrow w = \sqrt{3} \qquad \text{(F.5)}$$

Using this rescaling factor, the orthonormal function L_1 is:

$$L_1 = \sqrt{3} - 2\sqrt{3}x \qquad \text{(F.6)}$$

The utility of orthogonal polynomials is that they form a *complete* basis set which is capable of representing any arbitrary function $f(x)$ on the domain of the orthogonal polynomial to any desired degree of accuracy:

$$f(x) = \sum_{i=0}^{\infty} c_i L_i \qquad \text{(F.7)}$$

Furthermore, due to the orthogonality of the individual terms, this series converges at an optimal rate. When a truncated representation is used to form an n-term expansion of $f(x)$:

$$f(x) \approx \sum_{i=0}^{n} c_i L_i \qquad \text{(F.8)}$$

The optimal coefficiencts c_i for this expansion are determined by minimizing the error in the expansion over the domain of the orthogonal representation:

$$\text{Error} = \int_0^1 \left(\sum_{i=0}^{n} c_i L_i(x) - f(x) \right)^2 dx \tag{F.9}$$

This error is minimized when the derivative of this expression with respect to each coefficient c_j is zero:

$$\frac{d}{dc_j}\int_0^1\left(\sum_{i=0}^{n}c_iL_i(x)-f(x)\right)^2dx=0\Rightarrow 2\int_0^1\left(\sum_{i=0}^{n}c_iL_i(x)-f(x)\right)L_j(x)dx=0\Rightarrow\left\langle\sum_{i=0}^{n}c_iL_i(x),L_j(x)\right\rangle=\left\langle f(x),L_j(x)\right\rangle$$

$$\Rightarrow c_j\left\langle L_j(x),L_j(x)\right\rangle=\left\langle f(x),L_j(x)\right\rangle\Rightarrow c_j=\frac{\left\langle f(x),L_j(x)\right\rangle}{\left\langle L_j(x),L_j(x)\right\rangle} \tag{F.10}$$

Thus c_j is the length of the projection from of the function $f(x)$ onto the representation function $L_j(x)$ (see section 4.5.2). In the special case where orthonormal polynomials are used, c_j is simply the inner product of L_j and $f(x)$. Note that the intermediate expression:

$$\int_0^1 \left(\sum_{i=0}^{n} c_i L_i(x) - f(x) \right) L_j(x) dx = 0 \tag{F.11}$$

indicates that the optimal values of c_j are those which satisfy the condition that the *error of the representation is orthogonal to all of the orthogonal basis polynomials.* Adding a new term to the expansion results in the addition of a new expansion term which is also orthogonal to all of the previous expansion terms. Because both the error and the new term are orthogonal to all of the previous terms, this new is able to account for and capture as much of the error as possible. Thus, the expansion is optimally convergent. For more information on orthogonal basis functions, please refer to Strang (1986), Stoer and Bulirisch (1993), or Naylor and Sell (1982).

References

[1] Naylor, A. W.; Sell, G. R. *Linear Operator Theory in Engineering and Science,* Springer-Verlag, 1982.

[2] Rudin, Walter *Principles of Mathematical Analysis,* McGraw-Hill, 1976.

[3] Stoer, Josef; Bulirisch, R. *Introduction to Numerical Analysis,* 2nd edition, translated by R. Bartels, W. Gautschi, and C. Witzgall, Springer-Verlag, 1993.

[4] Strang, Gilbert *Introduction to Applied Mathematics*, Wellesley Cambridge Press, 1986.

[5] Wang, Cheng *Parametric Uncertainty Analysis for Complex Engineering Systems,* MIT Thesis, 1999.

Appendix G: Wiener Expansion

G.1 Definition

Consider following definition of Wiener expansion (also known as the polynomial chaos expansion) from Ghanem and Spanos (1991):

Let $\{\xi_i(\omega), i=1,\ldots,\infty\}$ *be a set of orthornomal Gaussian random variables. Consider the space* $\mathbf{S}(\Xi_p)$ *of all polynomials in of degree not exceeding p. Let* Ξ_p *represent the set of all polynomials in orthogonal to* $\mathbf{S}(\Xi_{p-1})$. *Finally, let* $\mathbf{SS}(\Xi_p)$ *be the space spanned by* Ξ_p. *Then the subspace* $\mathbf{SS}(\Xi_p)$ *of* Θ *is called the* p^{th} *homogeneous chaos, and* Ξ_p *is called the polynomial chaos of order p, where* Θ *is a Hilbert space of functions defined by mapping the probability space,* Ω, *onto the real line,* $\mathbf{R}$.

This scheme was pioneered in 1938 by Wiener (Wiener, 1938) and was originally referred to as the "polynomial chaos." Follow-up work was conducted by Cameron and Martin (1947).

Tatang (1995) applied this Wiener expansion to random variables to develop a new uncertainty analysis technique. The random variable $x(\omega)$ can be approximated in the space Θ with the following polynomial chaos expansion:

$$x(\omega) = a_0\Xi_0 + \sum_{i_1=1}^{\infty} a_{i_1}\Xi_1(\xi_{i_1}(\omega)) + \sum_{i_1=1}^{\infty}\sum_{i_2=1}^{\infty} a_{i_1 i_2}\Xi_2(\xi_{i_1}(\omega), \xi_{i_2}(\omega)) + \sum_{i_1=1}^{\infty}\sum_{i_2=1}^{\infty}\sum_{i_3=1}^{\infty} a_{i_1 i_2 i_3}\Xi_3(\xi_{i_1}(\omega), \xi_{i_2}((\omega), \xi_{i_3}(\omega))) + \ldots \quad \text{(G.1)}$$

When used in finite problems, a p^{th} order polynomial chaos expansion will approximate an N-dimensional random variable where N replaces ∞ in equation (G.1).

G.1.1 Example problem

As an illustration of the polynomial chaos expansion method, the following equation is considered:

$$a(\omega)x(\omega) = b(\omega) \quad \text{(G.2)}$$

Choosing the Ξ_p's of the polynomial chaos expansion to be Hermite polynomials leads to

orthogonal Ξ_p's with the representation:

$$x(\omega) \approx \sum_{j=1}^{N} x_j H_j(\{\xi_i(\omega)\}) \tag{G.3}$$

where $H_j(\{\xi_i(\omega)\})$ is a multidimensional Hermite polynomial of order j. Substituting this into equation (G.2) and re-expressing as a residual yields:

$$R_N(\underline{x}, \omega) = a(\omega) \sum_{j=1}^{N} x_j H_j(\{\xi_i(\omega)\}) - b(\omega) \tag{G.4}$$

Thus, a two-dimensional polynomial chaos expansion for $a(\omega)$ and $b(\omega)$ would look like:

$$\begin{aligned} a(\omega) &= a_0 + a_1\xi_1 + a_2\xi_2 + a_3(\xi_1^2 - 1) + a_4\xi_1\xi_2 + a_5(\xi_2^2 - 1) + \ldots \\ b(\omega) &= b_0 + b_1\xi_1 + b_2\xi_2 + b_3(\xi_1^2 - 1) + b_4\xi_1\xi_2 + b_5(\xi_2^2 - 1) + \ldots \end{aligned} \tag{G.5}$$

Expressing $a(\omega)$ and $b(\omega)$ as *independent* Gaussian random variables eliminates all cross-terms and terms of order higher than ξ_i:

$$\begin{aligned} a(\omega) &= a_0 + a_1\xi_1 \\ b(\omega) &= b_0 + b_2\xi_2 \end{aligned} \tag{G.6}$$

where the constant term is the mean and the coefficient of the ξ_i term is the standard deviation of each distribution. The corresponding polynomial chaos expansion for $x(\omega)$ will include second-order terms to account for any ξ_1-ξ_2 interactions:

$$x(\omega) = x_0 + x_1\xi_1 + x_2\xi_2 + x_3(\xi_1^2 - 1) + x_4\xi_1\xi_2 + x_5(\xi_2^2 - 1) \tag{G.7}$$

The form of the residual is:

$$\begin{aligned} R_6(\underline{x}, w) = (a_0 + a_1\xi_1)(x_0 + x_1\xi_1 + x_2\xi_2 + x_3(\xi_1^2 - 1) + x_4\xi_1\xi_2 + x_5(\xi_2^2 - 1)) \\ -(b_0 + b_2\xi_2) \end{aligned} \tag{G.8}$$

In order to solve for the six coefficients $x_0 \ldots x_5$, the residual is orthogonalized with Hermite polynomials $H_i(\xi_1, \xi_2, \ldots, \xi_j)$ where i is the order of the polynomial and j is the number of probabilstic dimensions it spans:

$$\int_{-\infty}^{\infty}\cdots\int_{-\infty}^{\infty}\int_{-\infty}^{\infty}H_i(\xi_1,\xi_2,\ldots,\xi_j)R_6(\underline{x},\omega)dP(\xi_1)dP(\xi_2)\ldots dP(\xi_j)=0 \tag{G.9}$$

where $dP(\xi_i)$ enforces that this is an integral over a probabilistic space. Recalling the analogy between probability density functions and number density functions in Chapter 2:

$$dP(\xi_i) = f(\xi_i)d\xi_i \tag{G.10}$$

where $f(\xi_i)$ is the probability density function and $d\xi_i$ is the segment of the probability density distribution. Thus, Equation (G.9) can be rewritten as:

$$\int_{-\infty}^{\infty}\cdots\int_{-\infty}^{\infty}\int_{-\infty}^{\infty}f(\xi_1)f(\xi_2)\ldots f(\xi_j)H_i(\xi_1,\xi_2,\ldots,\xi_j)R_6(\underline{x},\omega)d\xi_1 d\xi_2\ldots d\xi_j=0 \tag{G.11}$$

The H_i's are determined by an orthogonalization procedure. For the case of $i = 0$, the Hermite polynomial is constant and is chosen as $H_0 = 1$. For $i = 1$, the Hermite polynomials are determined by a routine orthogonalization algorithm with Gaussian probability density functions as weighting functions:

$$\begin{aligned}&\int_{-\infty}^{\infty}\cdots\int_{-\infty}^{\infty}\int_{-\infty}^{\infty}H_i(\xi_1,\xi_2,\ldots,\xi_j)H_k(\xi_1,\xi_2,\ldots,\xi_j)dP(\xi_1)dP(\xi_2)\ldots dP(\xi_j)=0 \qquad i\neq k\\ &\int_{-\infty}^{\infty}\cdots\int_{-\infty}^{\infty}\int_{-\infty}^{\infty}[H_i(\xi_{i_1},\xi_{i_2},\ldots,\xi_{i_j})]^2dP(\xi_1)dP(\xi_2)\ldots dP(\xi_j)=1\end{aligned} \tag{G.12}$$

The first condition in Equation (G.12) forces all of the H_i's to be orthogonal. The second condition is optional; it further requires that the H_i's are normalized. Applying Equation (G.10) to this expression yields:

$$\begin{aligned}&\int_{-\infty}^{\infty}\cdots\int_{-\infty}^{\infty}\int_{-\infty}^{\infty}f(\xi_1)f(\xi_2)\ldots f(\xi_j)H_i(\xi_1,\xi_2,\ldots,\xi_j)H_k(\xi_1,\xi_2,\ldots,\xi_j)d\xi_1 d\xi_2\ldots d\xi_j=0 \qquad i\neq k\\ &\int_{-\infty}^{\infty}\cdots\int_{-\infty}^{\infty}\int_{-\infty}^{\infty}f(\xi_1)f(\xi_2)\ldots f(\xi_j)([H_i(\xi_{i_1},\xi_{i_2},\ldots,\xi_{i_j})])^2dP(\xi_1)d\xi_1 d\xi_2\ldots d\xi_j=1\end{aligned} \tag{G.13}$$

Note that this orthogonalization scheme can be used for any given probability density function

$f(\xi_i)$. In fact, a different probability density function can be used along each coordinate ξ_i. When $f(\xi_i)$ is used to represent a normal probability density function along both coordinates of a two-dimensional Wiener expansion, the H_i's are:

$$\begin{aligned} H_0 &= 1 \\ H_2(\xi_1, \xi_2) &= \xi_1 \\ H_3(\xi_1, \xi_2) &= \xi_2 \\ H_4(\xi_1, \xi_2) &= \xi_1^2 - 1 \\ H_5(\xi_1, \xi_2) &= \xi_1 \xi_2 \\ H_6(\xi_1, \xi_2) &= \xi_2^2 - 1 \end{aligned} \tag{G.14}$$

Note that it is trivial to arrive at these functions from the orthonormal equations in Equation (G.13) using the following property which applies to the moments a normal distributions (Papoulis, 1991):

$$E\{\xi^n\} = \int_{-\infty}^{\infty} \xi^n f(\xi) d\xi = \begin{cases} 1 \cdot 3 \cdot \ldots n-1 & \text{for } n \text{ even} \\ 0 & \text{for } n \text{ odd} \end{cases} \tag{G.15}$$

For example, for the $b(\omega)$ term in the H_1 expression:

$$\begin{aligned} \int_{-\infty}^{\infty} \int_{-\infty}^{\infty} f(\xi_1) f(\xi_2)(b_1 + b_3 \xi_2) d\xi_1 d\xi_2 &= \int_{-\infty}^{\infty} f(\xi_1) \int_{-\infty}^{\infty} f(\xi_2)(b_1 + b_3 \xi_2) d\xi_2 d\xi_1 \\ &= \int_{-\infty}^{\infty} f(\xi_1) b_1 d\xi_1 = b_1 \end{aligned} \tag{G.16}$$

Thus, the system of equations reduces to the following set of matrix equations:

$$\begin{bmatrix} a_1 & a_2 & 0 & 0 & 0 & 0 \\ a_2 & a_1 & 0 & 2a_2 & 0 & 0 \\ 0 & 0 & a_1 & 0 & a_2 & 0 \\ 0 & 2a_2 & 0 & 2a_1 & 0 & 0 \\ 0 & 0 & a_2 & 0 & a_1 & 0 \\ 0 & 0 & 0 & 0 & 0 & 2a_1 \end{bmatrix} \begin{bmatrix} x_1 \\ x_2 \\ x_3 \\ x_4 \\ x_5 \\ x_6 \end{bmatrix} = \begin{bmatrix} b_1 \\ 0 \\ b_3 \\ 0 \\ 0 \\ 0 \end{bmatrix} \tag{G.17}$$

with the corresponding solution:

$$
\begin{aligned}
x_1 &= \left(\frac{b_1}{a_1}\right)\left(\frac{2a_2^2 - a_1^2}{3a_2^2 - a_1^2}\right) \\
x_2 &= \frac{b_1 a_2}{3a_2^2 - a_1^2} \\
x_3 &= \frac{b_3 a_1}{a_1^2 - a_2^2} \\
x_4 &= \frac{b_1 a_2^2}{a_1(a_1^2 - 3a_2^2)} \\
x_5 &= \frac{b_3 a_2}{a_2^2 - a_1^2} \\
x_6 &= 0
\end{aligned}
\tag{G.18}
$$

References

[1] Bender, C.; Orszag, S. *Advanced Mathematical Methods for Scientists and Engineers,* McGraw-Hill, New York, 1978.

[2] Cameron, R. H.; Martin, W. T., "The Orthogonal Development of Nonlinear Functionals in Series of Fourier-Hermite Functionals."

[3] Ghanem, Roger; Spanos, Pol D. *Stochastic Finite Elements: A Spectral Approach.* Springer-Verlag, New York, 1991.

[4] Papoulis, Athanasios *Probability, Random Variables, and Stochastic Processes,* 3rd Ed., McGraw-Hill, 1991.

[5] Stoer, J.; Bulirisch, R. *Introduction to Numerical Analysis,* 2nd Edition, translated by R. Bartels, W. Gautschi, and C. Witzgall, Springer-Verlag, New York, 1993.

[6] Tatang, Menner A. *Direct Incorporationof Uncertainty in Chemical and Environmental Engineering Systems,* MIT Thesis, 1995.

[7] Wang, Cheng *Parametric Uncertainty Analysis for Complex Engineering Systems,* MIT Thesis, 1999.

[8] Wiener, Norbert *The Homogeneous Chaos* American Journal of Mathematics, **60**, 897-936,

1938.

Appendix H: Population Statistics

This section rigorously reviews the proper techniques for calculating population statistics, including the mean and standard deviation, from multidimensional number density distributions.

In general an exponentially-distributed population with s components is defined by the following expression:

$$n_0(m_1, m_2, \ldots, m_s) = N_0 \frac{e^{\left(-\frac{m_1}{m_{10}}\right)}}{m_{10}} \frac{e^{\left(-\frac{m_2}{m_{20}}\right)}}{m_{20}} \cdots \frac{e^{\left(-\frac{m_s}{m_{s0}}\right)}}{m_{s0}} \tag{H.1}$$

For a two-component exponentially distributed population this expression reduces to:

$$.n_0(m_1, m_2) = N_0 \frac{e^{\left(-\frac{m_1}{m_{10}}\right)}}{m_{10}} \frac{e^{\left(-\frac{m_2}{m_{20}}\right)}}{m_{20}} \tag{H.2}$$

The total number of particles in the population of size $m = m_1 + m_2$ is found by integrating over all possible combinations of components m_1 and m_2 summing to m. This is accomplished by substituting $m_2 = m - m_1$ into Equation (H.2) and integrating over all possible values of m_1 from 0 to m:

$$\begin{aligned} n(m) &= \int_0^m n_0(m_1, m - m_1)\, dm_1 \\ &= \int_0^m N_0 \frac{e^{\left(-\frac{m_1}{m_{10}}\right)}}{m_{10}} \frac{e^{\left(-\frac{m_2}{m_{20}}\right)}}{m_{20}} dm_1 \\ &= \frac{N_0}{m_{10} - m_{20}} \left[e^{\left(-\frac{m}{m_{10}}\right)} - e^{\left(\frac{-m}{m_{20}}\right)} \right] \end{aligned} \tag{H.3}$$

In addition to number density, composition statistics are also of interest. The mean composition of component 1 among particles size m is calculated via the expected value of composition:

$$\overline{x_1}(m) = E[x_1(m)] = \int_0^1 x_1 p_x(x_1)\, dx_1 \tag{H.4}$$

Noting that $m_1 = x_1 \cdot m$, where m is constant and thus $dm_1 = dx_1 \cdot m$, Equation (H.4) can also be

expressed as:

$$E[x_1(m)] = \int_0^1 x_1 p_x(x_1)dx_1 = \int_0^m \frac{m_1}{m} p_x(x_1)\frac{dm_1}{m} = \frac{1}{m}\int_0^m m_1 p_x(x_1)dm_1 \tag{H.5}$$

Conversely, the linearity of the expectation operator (see Appendix E) can be applied directly to $x_1 = m_1/m$:

$$E[x_1] = E\left[\frac{m_1}{m}\right] = \frac{1}{m}E[m_1] = \frac{1}{m}\frac{\int_0^m m_1 n(m_1, M-m_1)dm_1}{\int_0^m n(m_1, M-m_1)dm_1} = \frac{1}{m}\frac{\int_0^m m_1 n(m_1, M-m_1)dm_1}{n(m)} \tag{H.6}$$

In essence, this method of calculating $E[x_1]$ is equivalent to first calculating the average m_1 per particle and dividing this by the mass of the particles, m. The average m_1 per particle, in turn, is calculated by summing the total m_1 in all particles and then dividing that by the total number of particles, as shown by the integral on the right hand side of Equation (H.6).

Comparing Equations (H.5) and (H.6) yields the expression for $p_x(x_1)$:

$$\frac{p_x(x_1)}{m} = \frac{n(m_1, m-m_1)}{n(m)} \Rightarrow p_x(x_1) = \frac{m \cdot n(m_1, m-m_1)}{n(m)} \tag{H.7}$$

In order to confirm the validity of this expression for $p_x(x_1)$, check to see that:

$$\int_0^1 p_x(x_1)dx_1 = 1 \tag{H.8}$$

This is accomplished through a simple change of integration variables, remembering that $m_1 = x_1 \cdot m$, where M is constant and thus $dm_1 = dx_1 \cdot m$:

$$\int_0^1 p_x(x_1)dx_1 \Rightarrow \int_0^m \frac{m \cdot n(x_1 m, (1-x_1)m)}{n(m)} \frac{dm_1}{m} = \int_0^m \frac{n(x_1 m, (1-x_1)m)}{n(m)} dm_1$$

$$= \int_0^m \frac{n(m_1, M-m_1)}{n(m)} dm_1 \qquad \text{(H.9)}$$

$$= \frac{n(m)}{n(m)}$$

$$= 1$$

Using integration by parts, the mean composition of the two-component exponentially distributed population is:

$$\bar{x}_1(m) = \frac{e^{\left(-\frac{m}{m_{10}}\right)}}{e^{\left(-\frac{m}{m_{10}}\right)} - e^{\left(-\frac{m}{m_{20}}\right)}} - \frac{m_{10}m_{20}}{m(m_{10}-m_{20})} \qquad \text{(H.10)}$$

Similarly, the variance of the composition can be calculated using either one of the following two expressions:

$$\sigma_{x_1}^2(m) = E[(x_1 - E[x_1])^2] = E[(x_1 - \bar{x}_1)^2]$$
$$\sigma_{x_1}^2(m) = E[x_1^2] - E[x_1]^2 = E[x_1^2] - \bar{x}_1^2 \qquad \text{(H.11)}$$

When the second expression from Equation (H.11) is used to evaluate the variance using $n(m_1, m_2)$, $E[x_1^2]$ is evaluated in a fashion similar to the evaluation of the mean $\bar{x}_1$:

$$E[x_1^2] = E\left[\left(\frac{m_1}{m}\right)^2\right] = \sum_{\text{particles}} \left(\frac{m_1}{m}\right)^2 = \sum_{\text{particles}} \left(\frac{m_1}{m}\right)^2 \frac{n(m_1, m-m_1)\Delta m_1}{n(m)} \qquad \text{(H.12)}$$

which is again evaluated using an integral to sum over all particles in the distribution.

$$E[x_1^2] = \sum_{\text{particles}} \left(\frac{m_1}{m}\right)^2 \frac{n(m_1, m-m_1)\Delta m_1}{n(m)} = \frac{\int_0^m m_1^2 \cdot n(m_1, m-m_1)dm_1}{m^2 \cdot n(m)} \qquad \text{(H.13)}$$

Such a seemingly difficult expression can easily be evaluated using a symbolic mathematics package such as Mathematica:

$$E[x_1^2] = \frac{\int_0^m m_1^2 \cdot n(m_1, m-m_1)}{m^2 n(m)} = \frac{e^{-\frac{m}{m_{10}}}}{e^{-\frac{m}{m_{10}}} - e^{-\frac{m}{m_{20}}}} + \frac{2m_{10}^2 m_{20}^2}{(m_{10}-m_{20})^2 m^2} - \frac{2e^{-\frac{m}{m_{10}}} m_{10} m_{20}}{\left(e^{-\frac{m}{m_{10}}} - e^{-\frac{m}{m_{20}}}\right) m(m_{10}-m_{20})} \tag{H.14}$$

which leads to the simplified final expression:

$$\sigma_{x_1}^2 = \frac{m_{10}^2 m_{20}^2}{m^2(m_{10}-m_{20})^2} - \frac{e^{\left(-\frac{m}{m_{10}} - \frac{m}{m_{10}}\right)}}{\left(e^{-\frac{m}{m_{10}}} - e^{-\frac{m}{m_{20}}}\right)^2} \tag{H.15}$$

Statistics for the second component in a two-component system are obtained by changing all m_1's to m_2's and m_{10}'s to m_{20}'s, and vice-versa in the above expressions.

H.1 Three-Component System

The exponential three-component population distribution is:

$$n_0(m_1, m_2, m_3) = N_0 \frac{e^{\left(-\frac{m_1}{m_{10}}\right)}}{m_{10}} \frac{e^{\left(-\frac{m_2}{m_{20}}\right)}}{m_{20}} \frac{e^{\left(-\frac{m_3}{m_{30}}\right)}}{m_{30}} \tag{H.16}$$

Integrating over all possible combinations of mass using the constraint $M = m_1 + m_2 + m_3$ gives the number density as a function of total particle mass:

$$n(m) = \int_0^m \int_0^{m-m_1} n(m_1, m_2, m-m_1-m_2) dm_2 dm_1 \tag{H.17}$$

The exponential three component population distribution is:

$$n(m) = \frac{N_0}{(m_{10}-m_{20})(m_{10}-m_{30})(m_{20}-m_{30})} \left[m_{20} m_{30} \left(e^{-\frac{m}{m_{20}}} - e^{-\frac{m}{m_{30}}} \right) + m_{10} m_{20} \left(e^{-\frac{m}{m_{10}}} - e^{-\frac{m}{m_{20}}} \right) + m_{10} m_{30} \left(e^{-\frac{m}{m_{30}}} - e^{-\frac{m}{m_{10}}} \right) \right] \tag{H.18}$$

Similarly, the average composition may be found by integrating:

$$\begin{aligned}\bar{x}_1(m) &= \sum_{\text{particles}} \frac{m_1}{m}\frac{n(m_1, m_2, m-m_1-m_2)\Delta m_2 \Delta m_1}{n(m)} \\ &= \int_0^{m(m-m_1)} \int_0 \frac{m_1}{m}\frac{n(m_1, m_2, m-m_1-m_2)}{n(m)} dm_2 dm_1 \\ &= \frac{\int_0^{m(m-m_1)} \int_0 m_1 \cdot n(m_1, m_2, m-m_1-m_2) dm_2 dm_1}{m \cdot n(m)}\end{aligned} \tag{H.19}$$

Evaluating and simplifiying this expression yields:

$$\bar{x}_1(M) = \frac{m_{10}\left(\frac{m_{20}^2 e^{-M/m_{20}}(m_{10}-m_{30})}{(m_{10}-m_{20})} - \frac{m_{30}^2 e^{-M/m_{30}}(m_{10}-m_{20})}{(m_{10}-m_{30})} - M e^{-M/m_{10}}(m_{20}-m_{30}) + \frac{m_{10}m_{20}e^{-M/m_{10}}(m_{20}-m_{30})}{(m_{10}-m_{20})} + \frac{m_{10}m_{30}e^{-M/m_{10}}(m_{20}-m_{30})}{(m_{10}-m_{30})}\right)}{e^{-M/m_{10}}m_{10}(m_{20}-m_{30}) - e^{-M/m_{20}}m_{20}(m_{10}-m_{30}) + e^{-M/m_{30}}m_{30}(m_{10}-m_{20})} \tag{H.20}$$

Using the identity from (H.11) we use the second identity to calculate the standard deviation for composition. However, the mean composition is given in (H.20) and we only need to find $E[x_1^2]$:

$$E[x_1^2] = \frac{\int_0^{m(m-m_1)} \int_0 m_1^2 \cdot n(m_1, m_2, m-m_1-m_2) dm_2 dm_1}{m^2 \cdot n(m)} \tag{H.21}$$

Evaluation of this expression leads to the result:

$$\begin{aligned}&E[x_1^2] = \\ &\left[\frac{e^{-M/m_{10}}m_{10}}{(m_{10}-m_{20})^3(m_{10}-m_{30})^3}\left\{M^2(m_{10}-m_{20})^2(m_{10}-m_{30})^2 - 2Mm_{10}(m_{10}-m_{20})(m_{10}-m_{30})\right.\right. \\ &\left.\cdot\left[m_{20}(m_{10}-m_{30})+m_{30}(m_{10}-m_{20})\right] + 2m_{10}^2\left[3m_{20}^2m_{30}^2 - 3m_{10}m_{20}m_{30}(m_{20}+m_{30}) + m_{10}^2(m_{20}^2+m_{20}m_{30}+m_{30}^2)\right]\right\} \\ &\left.+2m_{10}^2\left(\frac{e^{-M/m_{30}}m_{30}^3}{(m_{10}-m_{30})^3(m_{20}-m_{30})} - \frac{e^{-M/m_{20}}m_{20}^3}{(m_{10}-m_{20})^3(m_{20}-m_{30})}\right)\right] \\ &\overline{M^2\left\{\frac{e^{-M/m_{10}}m_{10}}{(m_{10}-m_{20})(m_{10}-m_{30})} + \frac{\left(e^{-M/m_{20}}-e^{-M/m_{30}}\right)m_{20}m_{30} - m_{10}\left(e^{-M/m_{20}}m_{20} - e^{-M/m_{30}}m_{30}\right)}{(m_{10}-m_{20})(m_{10}-m_{30})(m_{20}-m_{30})}\right\}}\end{aligned} \tag{H.22}$$

Appendix I: Scaling of the Distribution Splitting Method

The distribution splitting method for s species represents a multicomponent population as all possible combinations of pure and mixed species distributions coupled with appropriate governing composition equations for each of the mixed distributions. For instance, in a system with two components 1 and 2, there are two distributions representing each pure component and one equation to represent the distribution of mixed particles containing both components 1 and 2. One further distribution must be included to describe the composition of the mixed particles containing both 1 and 2. The total number of equations in this system are summarized in Table I-1:

Table I-1: Summary of Distribution Splitting Equations - Two Component Case

Distribution Components	*Number Distribution Equations*	*Additional Composition Distributions per Number Distribution*	*Total Equations*
One component	2	0	2
Two components	1	1	2

Similarly, for the case of three components, the total number of distribution splitting equations can be summarized as follows:

Table I-2: Three Component Distribution Splitting Equations

Distribution Components	*Number Distribution Equations*	*Additional Composition Distributions per Number Distribution*	*Total Equations*
One component	3	0	3
Two components	3	1	6
Three component	1	2	3

For instance, in the case of two components, there are three different ways of choosing two components and thus there are three number distribution equations to describe mixed distribution of

two components. Because each of these distributions contain two components, one composition distribution is necessary to define the composition each two-component mixed number distribution. For a four component system, the number of distributions needed for the distribution splitting method are summarized in Table I-3:

Table I-3: Four Component Distribution Splitting Equations

Distribution Components	*Number Distribution Equations*	*Additional Composition Distributions per Number Distribution*	*Total Equations*
One component	$\binom{4}{1} = 4$	0	$\binom{4}{1} \cdot 1 = 4$
Two components	$\binom{4}{2} = 6$	1	$\binom{4}{2} \cdot 2 = 12$
Three component	$\binom{4}{3} = 4$	2	$\binom{4}{3} \cdot 3 = 12$
Four component	$\binom{4}{4} = 4$	3	$\binom{4}{4} \cdot 4 = 4$

As shown in by the pattern revealed in Table I-3, the total number of distributions can be described by the summation:

$$\sum_{i=1}^{s} \binom{s}{i} \cdot i \tag{I.1}$$

where s is the total number of species in the system and $\binom{s}{i}$ represents a combination. Manipulating this expression slightly reveals a closed form for the number of distributions:

$$\sum_{i=1}^{s}\binom{s}{i}\cdot i = \sum_{i=1}^{s}\frac{s!}{(s-i)!\cdot i!}i = \sum_{i=1}^{s}\frac{(s-1)!}{(s-i)!\cdot(i-1)!}$$

$$= \sum_{i=1}^{s}\frac{(s-1)!}{[(s-1)-(i-1)]!\cdot(i-1)!} = s\sum_{i=1}^{s}\binom{s-1}{i-1}$$

$$= s\sum_{i=0}^{s-1}\binom{s-1}{i} \tag{I.2}$$

$$\sum_{i=1}^{s}\binom{s}{i}\cdot i = s\cdot 2^{s-1}$$

where the last equality relies on the condition:

$$\sum_{i=0}^{n}\binom{n}{i} = 2^n \tag{I.3}$$

This last relation comes from probability theory. Consider the total number of possible outcomes of a coin tossed n times. Each coin toss has two possible outcomes, so the total number of possible outcomes are the product of the number of possible outcomes of each coin toss, or 2^n. Alternatively, consider n distinct coins. The total number of different ways that i heads can be chosen from this group of n coins is $\binom{n}{i}$. This is also equal to the total number of different outcomes from flipping n coins where there are i heads. Of course, the total outcomes of flipping a coin n times is this quantity summed over all possible number of heads, or:

$$\sum_{i=0}^{n}\binom{n}{i}. \tag{I.4}$$

Thus the distribution splitting method scales as $s\cdot 2^{s-1}$ with the number of components. If each distribution has p node points, the total number of equations needed for the distribution spltting method is $p\cdot s\cdot 2^{s-1}$. This represents a considerable improvement over the scaling p^s required for a full multidimensional surface solution. However, this reduction in scaling is obtained with some limitation in the ability to truly represent all compositions. In the multidimensional case component i will always have number density at any total mass $m = m_1 + m_2 + ... + m_n$ defined for any value of $x_i = m_i/m$ as given by $n(m_1, m_2, ..., m_s)$. However, this is not true for the distribution

splitting method. For example, a two-component model is comprised of pure number density distributions for components 1 and 2, as well as one mixed component distribution with a corresponding composition distribution:

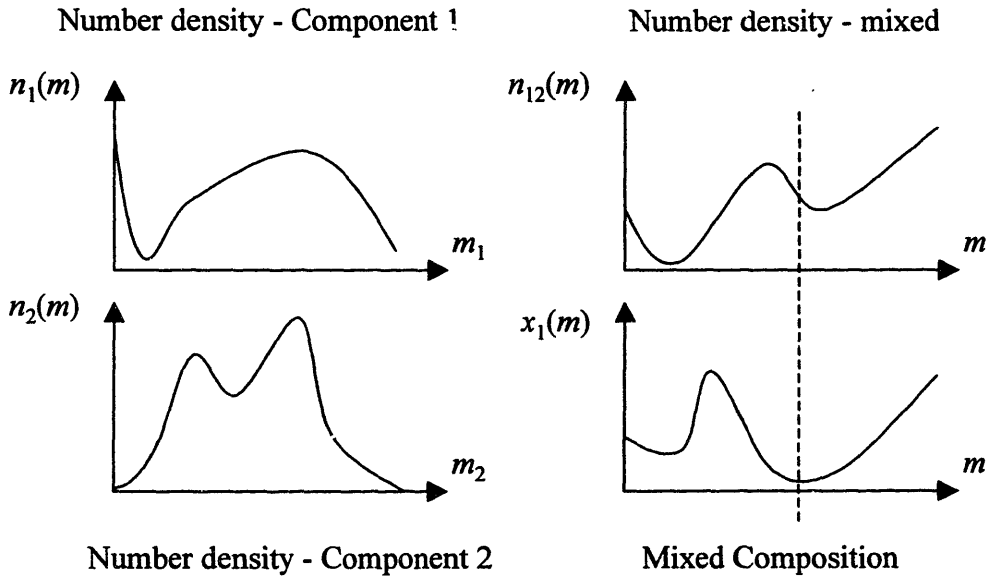

Figure I-1: Mixed composition distribution example.

At a given mass, there are only three possibilities for the composition of a particle, $x_1 = 1$, $x_1 = 0$ and x_1 as defined by the mixed composition function.

THESIS PROCESSING SLIP

FIXED FIELD: ill. ______ name ______

index ______ biblio ______

► **COPIES:** (Archives) Aero Dewey Barker Hum Lindgren Music Rotch (Science) Sche-Plough

TITLE VARIES: ► ☐ ______

NAME VARIES: ► ☐ ______

IMPRINT: (COPYRIGHT) ______

► **COLLATION:** ______

► **ADD: DEGREE:** ______ ► **DEPT.:** ______

► **ADD: DEGREE:** ______ ► **DEPT.:** ______

SUPERVISORS: ______

NOTES:

cat'r: date:

page: ► 397

► **DEPT:** Chem. E.

► **YEAR:** 2001 ► **DEGREE:** Ph.D.

► **NAME:** OBERIGKEIT, Dawn David